Imaging Physiological Brain Activity and Epilepsy with Electrical Impedance Tomography

Anna Magdalena Witkowska-Wrobel

A thesis submitted for the degree of

Doctor of Philosophy

of

University College London

Department of Medical Physics and Biomedical Engineering

University College London

September 2019

Declaration

I, Anna Magdalena Witkowska-Wrobel, confirm that the work presented in this thesis is my own. Where information has been derived from other sources, I confirm that this has been indicated in the thesis.

Signed

Abstract

Electrical Impedance Tomography (EIT) allows reconstructing conductivity changes into images. EIT detects fast impedance changes occurring over milliseconds, due to ion channel opening, and slow impedance changes, appearing in seconds, due to cell swelling/increased blood flow. The purpose of this work was to examine the feasibility of using EIT for imaging a gyrencephalic brain with implanted depth electrodes during seizures.

Chapter 1 summarises the principles of EIT. In Chapter 2, it is investigated whether recent technical improvements could enable EIT to image slow impedance changes upon visual stimulation non-invasively. This was unsuccessful so the remaining studies were undertaken on intracranial recordings. Chapter 3 presents a computer modelling study using data from patients, for whom the detection of simulated seizure-onset perturbations for both, fast and slow impedance changes, were improved with EIT compared to stereotactic electroencephalography (SEEG) detection or EEG inverse-source modelling. Chapter 4 describes the development of a portable EIT system that could be used on patients. The system does not require averaging and post-hoc signal processing to remove switching artefacts, which was the case previously. Chapter 5 describes the use of the optimised method in chemically-induced focal epilepsy in anaesthetised pigs implanted with depth electrodes. This shows for the first time EIT was capable of producing reproducible images of the onset and spread of seizure-related slow impedance changes in real-time. Chapter 6 presents a study on imaging ictal/interictal-related fast impedance changes. The feasibility of reconstructing ictal-related impedance changes is demonstrated for one pig and interictal-related impedance changes were recorded for the first time in humans. Chapter 7 summarises all work and future directions.

Overall, this work suggests EIT in combination with SEEG has a potential to improve the diagnostic yield in epilepsy and demonstrates EIT can be performed safely and ethically creating a foundation for further clinical trials.

Impact statement

Epilepsy is a major neurological disease, for which the diagnosis and treatment rates are still not satisfactory, despite the development of new diagnostic tools and modern therapeutic methods. All work presented in this thesis aimed to develop a new technique, employing Electrical Impedance Tomography (EIT), with which it might be possible to improve the diagnostic yield in epilepsy, to help in understanding it further and consequently, to improve its control in future.

EIT is an imaging technique that can be used to reconstruct internal conductivity changes into 3D images. It is already used in clinic for imaging lungs but has been proposed and showed in small-animal studies to be capable of imaging brain upon its physiological activity and in pathology. If used in epilepsy, it can be potentially integrated into already used clinical methodologies such as EEG, to provide additional information on seizure generators in patients' brains.

To start with, this work tested for the first time and proved using computer simulations that EIT could be used with intracranial human electrodes to detect simulated seizure onsets. In that setting, EIT could considerably benefit the gold-standard method currently used in epilepsy field i.e. EEG. Hence, as the next step, the work undertaken in this thesis showed it is possible to develop a new EIT imaging system that could be reliably and safely used on patients in parallel to clinically collected EEG.

Having established the theoretical basis and methodology, the described work showed that it is possible to image impedance changes due to cell swelling within the seizure onset in a large animal model of epilepsy. Then finally, the work was taken to the clinic and it was shown that fast impedance changes related to the epileptic activity in the brains of epilepsy patients could be also recorded and reconstructed into images.

As a whole, this work showed for the first time that EIT can be safely used in the clinic and has a high potential to benefit the diagnosis of epilepsy patients

implanted with depth electrodes. The work has laid foundations for further EIT optimisation, exploration, and clinical studies and hopefully, regular use of EIT in the clinic to help epilepsy patients in future.

Acknowledgements

I would like to sincerely thank to my supervisor Professor David Holder for his continuous support throughout this PhD. David, thank you for your decision to take me as your student, for giving me a chance to learn so much, even though I am only a doctor, for teaching me lots about the wiggly lines, and simply, for being a great supervisor.

Thank you to Dr Beate Diehl, my second supervisor, and Dr Fahmida Chowdhury who both gave me the access to patients and taught me about the epilepsy and EEG.

Huge thanks to neurosurgeons from NHNN, Ms Anna Miserocchi and Mr Andy McEvoy for the enormous support, finding the ways to get through, despite the obstacles, and all the positive energy during our 7am meetings.

A special thank you to Professor Gareth Barnes, for supporting the MEG-EIT study that has never reached this thesis. Thank you for the trust and letting us to push the safety boundaries of MEG.

Many thanks to Mary and Estelle for their constant moral support and teaching me the nuances of EEG. Big thanks to all the neurophysiologists at Telemetry NHNN, especially to Dolora and Ivan for helping me with accessing the patients and supporting my study. Thanks for all the help as well as the medical and non-medical conversations to the doctors and neurophysiologists at the Neurophysiology NHNN. Thank you Gareth for never-ending stories about life and research, while preparing the EIT system for its use on patients.

An amazing thank you to Mr Justin Perkins for the huge support, enormous help and all the fun we had while preparing and recording the animal studies. Big thanks to Dr Abbe Crawford for helping me with the surgeries, for being supportive, curious and open-minded. Thank you to all the RVC people for your help.

Finally, massive thanks to Dr Kirill Aristovich for all the patience with my questions, messing up and forgetting stuff. Thank you for teaching me some

basics in programming, engineering, soldering, for discussions during the coffee breaks and help throughout my PhD. Thank you to all my colleagues from my lab for sharing the EIT experience, helpful suggestions, all the support and fun I had while being at UCL.

Special thanks to my family, Mum, Dad and my brother Maciek, for their constant and never-ending love, encouragement and support. Thank you to my family-in-law who also supported me all the time. Thanks to all my friends, even if you did not understand what I was doing, you were always there to listen and try to help.

Last but not least, the most special thanks to my husband, Antoni, for your endless love, support, help and presence. Thank you for always being on my side, for listening, caring, and making my problems disappear. Thank you for always believing in me!

Table of contents

Declaration ... 3
Abstract ... 5
Impact statement ... 7
Acknowledgements ... 9
Table of contents ... 11
List of Figures ... 18
List of Tables ... 22

Chapter 1 ... 23
Overview ... 25
1.1 Epilepsy ... 27
1.1.1 Clinical introduction ... 27
1.1.2 Epilepsy treatment ... 30
1.1.3 Presurgical seizure evaluation ... 32
1.1.3.1 EEG in presurgical evaluation ... 33
1.1.3.2 Neuroimaging in presurgical evaluation ... 38
1.2 Introduction to Electrical Impedance Tomography ... 41
1.2.1 Electrical Impedance ... 41
1.2.2 Tissue bioimpedance ... 42
1.2.3 Electrical Impedance Tomography ... 45
1.2.3.1 EIT data collection ... 45
1.2.3.2 Image reconstruction ... 46
1.2.4 Neural application of EIT ... 48
1.2.4.1 Stroke and traumatic brain injury ... 49
1.2.4.2 Functional activity ... 49
1.2.4.3 Epilepsy ... 50
1.3 Injection current safety ... 54
1.4 Purpose of this work ... 56
1.5 Statement of originality ... 57
1.6 List of publications and presentations from the work described in this thesis at the moment of its publication ... 58
Chapter 2 ... 61

Overview....63
2.1 Introduction....63
2.1.1 Background....63
2.1.2 Previous studies on EIT of slow changes in the brain....64
2.1.3 Experimental design to detect slow changes based on the BOLD fMRI and PET paradigms....67
2.1.4 Improvements in the EIT technology and the reconstruction method ...68
2.1.4.1 Improvements in hardware....68
2.1.4.2 Image reconstruction method....72
2.1.5 Purpose....74
2.1.6 Experimental design....74
2.2 Methods....75
2.2.1 Subjects....75
2.2.2 Data acquisition....76
2.2.3 Paradigm....78
2.2.4 Data analysis....78
2.2.5 Image reconstruction....79
2.2.6 Statistics....79
2.3 Results....80
2.3.1 Scalp changes....80
2.3.1.1 ScouseTom (one subject)....80
2.3.1.2 SwissTom....80
2.3.2 Reconstructed images....83
2.3.2.1 ScouseTom....83
2.3.2.2 SwissTom....84
2.4 Discussion....86
2.4.1 Summary of the results....86
2.4.2 Technical issues....87
2.4.3 Is the reproducible scalp impedance change related to visual stimulation? 88
2.4.4 What are the possible mechanisms underlying the observed EIT signal changes?....89
2.4.5 If the changes are present, did they reconstruct into reliable images? ...91
2.4.6 Conclusion and future work....92

Chapter 3 ..... **95**
Overview 97
3.1 Introduction 97
3.1.1 Background 97
3.1.2 Rationale 98
3.1.3 Purpose 99
3.1.4 Experimental design 99
3.2 Materials and methods 102
3.2.1 Epilepsy cases 102
3.2.2 Mesh creation 103
3.2.2.1 MRI-CT segmentation 103
3.2.2.2 Meshing and electrode placement 105
3.2.3 Perturbations 106
3.2.4 Protocols and electrode combinations 107
3.2.5 EIT voltage simulations and image reconstruction 109
3.2.6 EEG source detection 109
3.2.7 Image quality assessment 110
3.3 Results 111
3.4 Discussion 118
3.4.1 Summary of results 118
3.4.2 Technical issues 119
3.4.3 Which electrode arrangement gives the best seizure onset localisation? 119
3.4.4 Does the best of these three methods give improved seizure onset detection compared to the current intracranial method? 120
3.4.5 Conclusions and future work 122
Chapter 4 ..... **125**
Overview 127
4.1 Introduction 128
4.1.1 Background 128
4.1.2 Serial EIT system suitable for recording in epilepsy 128
4.1.3 Parallel EIT system for recording in epilepsy 131
4.1.4 Parallel EIT system hardware 132
4.1.5 EEG amplifiers 133

4.1.6 Frequency-dependant EIT response 133
4.1.7 Criteria for the EIT system to be used on patients in the hospital 134
4.1.8 Rationale 136
4.1.9 Purpose 137
4.1.10 Experimental design 137
4.2 Methods 141
4.2.1 Protocol optimisation in a simulation study 141
4.2.2 Pre-hospital tests 143
4.2.2.1 Resistor phantom tests 143
4.2.2.2 Simultaneous EEG-EIT tests on volunteer 144
4.2.2.3 Patients 145
4.3 Results 150
4.3.1 Protocol optimisation in a simulation study 150
4.3.2 Pre-hospital tests 151
4.3.2.1 Resistor phantom tests 151
4.3.2.2 Simultaneous EEG-EIT tests on a volunteer 151
4.3.3 Patients 154
4.3.3.1 Patient 1 154
4.3.3.2 Patient 2 155
4.3.3.2.1 Raw EEG and effect of the filter box 155
4.3.3.2.2 Fast EIT change during a single spike 157
4.3.3.2.3 Fast impedance signal for averaged interictal spikes 158
4.3.3.2.4 Slow impedance signal for a quick run of interictal spikes 159
4.4 Discussion 160
4.4.1 Summary of findings 160
4.4.2 Technical limitations 161
4.4.3 What is the optimal current injecting protocol to produce the most accurate images using intracranial electrodes tested in simulation study? 161
4.4.4 Is it possible to detect expected impedance changes with the parallel system in tests with the resistor phantom? 163
4.4.5 Can EEG signal be recorded in parallel to EIT in real-time with scalp and intracranial electrodes? 163
4.4.6 Conclusion and future work 167
Chapter 5 171

Overview 173
5.1 Background 173
5.1.1 Swine model for monitoring of seizures with intracranial electrodes 173
5.1.2 Penicillin model of epilepsy 174
5.1.3 Parallel EIT system 177
5.1.4 Rationale 178
5.1.5 Purpose 179
5.1.6 Experimental design 179
5.2 Materials and methods 182
5.2.1 Animal preparation and surgery 182
5.2.2 Induction of seizures 184
5.2.3 Data acquisition 185
5.2.4 Data analysis 186
5.2.4.1 Raw ECoG/SEEG and impedance signal analysis 186
5.2.4.2 Image reconstruction 187
5.2.4.3 Analysis of correlation between ECoG/SEEG and EIT 188
5.2.4.3.1 Seizure onset 188
5.2.4.3.2 Seizure spread 188
5.2.4.3.3 Qualitative analysis 189
5.3 Results 190
5.3.1 Seizure model 190
5.3.2 Raw impedance responses during all seizures 194
5.3.3 EIT reconstructed images in focal/focal secondarily generalised seizures 196
5.3.4 ECoG/SEEG and EIT signals correlation 203
5.4 Discussion 207
5.4.1 Summary 207
5.4.2 Technical considerations 208
5.4.3 What are the EEG characteristics of this swine model of penicillin-induced seizures, recorded with intracranial electrodes? 210
5.4.4 Does EIT have the ability to image the onset and propagation of the seizures in real-time? 213
5.4.5 What are the limitations of using EIT for imaging seizures in-vivo? 214
5.4.6 Conclusions and future work 216

Chapter 6 ..... **219**
Overview 221
6.1 Introduction 222
6.1.1 Background 222
6.1.2 Rationale 223
6.1.3 Purpose 224
6.1.4 Experimental design 225
6.2 Methods 227
6.2.1 Human Study 227
6.2.1.1 Patient 1 227
6.2.1.2 Patient 2 228
6.2.1.3 Patient 3 228
6.2.1.4 Animal study 230
6.2.2 Data acquisition 231
6.2.2.1 Human study 231
6.2.2.2 Animal study 231
6.2.3 Data analysis 232
6.2.4 Image reconstruction 233
6.3 Results 235
6.3.1 SEEG 235
6.3.1.1 Patient 1 235
6.3.1.2 Patient 2 237
6.3.1.3 Patient 3 239
6.3.1.4 Switching artefact from EIT 243
6.3.1.5 SEEG during animal recordings 245
6.3.1.6 Interictal and ictal activity averaged for EIT 245
6.3.2 Raw impedance signal change 248
6.3.2.1 Human study 248
6.3.2.2 Animal study 249
6.3.3 Reconstructed images 249
6.3.3.1 Human study 249
6.3.3.2 Animal study 256
6.4 Discussion 259
6.4.1 Clinical considerations 260

6.4.2 Technical considerations 261
6.4.3 Could EIT be used to detect fast impedance changes in human subjects? 262
6.4.4 Can fast impedance changes occurring due to ictal activity be detected and imaged with EIT and depth electrodes? 264
6.4.5 Conclusion and future work 266
Chapter 7 269
Overview 271
7.1 Summary of work 271
7.2 Conclusions and future work 273
Bibliography 279

List of Figures

Chapter 1

Figure 1-1. A variety of morphologies of interictal discharges in scalp EEG 29
Figure 1-2. A cortical fold in a schematic diagram 35
Figure 1-3. The complex plane of the impedance. 42
Figure 1-4. A single cell modelled as an electrical circuit 43
Figure 1-5. Ideal Cole-Cole plot for a biological tissue. 44

Chapter 2

Figure 2-1 Impedance changes recorded in the first EIT measurements 66
Figure 2-2. ScouseTom, an overview of the system 70
Figure 2-3. SwissTom, an overview of the system 71
Figure 2-4. A visual stimulation set in a boxcar paradigm 75
Figure 2-5. EasyCap and the locations of 32 electrodes seen from the top of the head 77
Figure 2-6. ScouseTom measurements with 250 μA at 1.725 kHz current 80
Figure 2-7. Averaged recorded voltage changes for each subject 82
Figure 2-8. The instances of a significant signal from each channel in all subjects 83
Figure 2-9. EIT images of evoked activity recorded with ScouseTom 84
Figure 2-10. Reconstructed extracranial EIT images of the evoked activity 85

Chapter 3

Figure 3-1 Illustration of segmentation of one subject using Seg 3D 103
Figure 3-2. Seizure onset perturbation locations 104
Figure 3-3. Representative examples of a single perturbation reconstruction. 112
Figure 3-4. A comparison of the localisation and shape errors 113
Figure 3-5. A representative example of EEG source reconstructions of a single source 114
Figure 3-6. Comparison of the voltages detected on depth electrodes and combined location and shape errors 115
Figure 3-7. Detection accuracy with three methods 116

Chapter 4

Figure 4-1 Implantation scheme for two patients investigated in this study....147
Figure 4-2. Individual errors for each of the protocol tested....150
Figure 4-3. Examples of recordings with the resistor phantom....151
Figure 4-4. A comparison of scalp EEG....152
Figure 4-5. EEG spectrum without and with EIT....153
Figure 4-6. Averaged VEP response....154
Figure 4-7. A screenshot of the SEEG recorded with the MicroMed....155
Figure 4-8. A comparison of a single SEEG channel recorded by ActiCHamp and MicroMed....156
Figure 4-9. The beginning of the EIT recording at ActiCHamp and MicroMed 157
Figure 4-10. Single interictal spike....158
Figure 4-11. Averaged interictal spike....159
Figure 4-12. A slow impedance change after a brief run of interictal spikes....160
Figure 4-13. A comparison of SEEG recorded on one channel by the MicroMed 164
Figure 4-14. A comparison of the EEG signal when EIT system was on and off 166

Chapter 5

Figure 5-1. A comparison of the ex-vivo and MRI scan of brains from a human, rhesus monkey, pig and rat....174
Figure 5-2. Overview of surgical site....183
Figure 5-3. Reconstructed brains for all 5 animals tested in this study....184
Figure 5-4. Example of seizure epileptiform activity....191
Figure 5-5. Pattern I, a focal seizure....193
Figure 5-6. Pattern II, a focal with secondary generalisation seizure....193
Figure 5-7. Pattern III, a generalised seizure....194
Figure 5-8. Examples of raw impedance increase observed during seizures....195
Figure 5-9. Examples of a focal seizure in three pigs....195
Figure 5-10. Onset reconstruction with EIT for 16 focal seizures in pig 1....198
Figure 5-11. Example of focal seizure in pig 1....199

Figure 5-12. Onset reconstruction with EIT for 5 focal seizures in pig 2 200
Figure 5-13. Example of the onset reconstruction in pig 2 201
Figure 5-14. Onset reconstruction with EIT for 16 focal seizures in pig 3 202
Figure 5-15. Example of focal seizure in pig 3 203
Figure 5-16. Example of progression of focal seizure 204
Figure 5-17. Example of progression of focal, secondarily generalised seizure 206
Figure 5-18. Correlation between ECoG/SEEG and EIT signal 207

Chapter 6

Figure 6-1. Schematics of depth electrode implantations. 229
Figure 6-2. Background SEEG from patient 1 236
Figure 6-3. Focal and generalised interictal discharges arising from the region around the lesion. 237
Figure 6-4. Background SEEG recorded from patient 2 238
Figure 6-5. Independent interictal activity arising from precuneus and the lesion 239
Figure 6-6. Background SEEG recorded from patient 3 239
Figure 6-7. Typical representation of interictal activity 240
Figure 6-8. Three events captured during EIT measurements 241
Figure 6-9. Representative examples of the switching artefact coming from EIT 243
Figure 6-10. A representative example of seizure recorded from the pig 245
Figure 6-11 Interictal and ictal activity seen in patients 1 to 3 and in the pig 247
Figure 6-12. Spike and impedance response from the 62-channel EIT recording averaged across all interictal spikes detected in three patients respectively 248
Figure 6-13. Spike and impedance response averaged over seizures recorded from an anaesthetised pig 249
Figure 6-14. T1-MRI of patient 1 250
Figure 6-15. EIT image sequence of averaged interictal spikes in patient 1 252
Figure 6-16. MRI of the second patient 253
Figure 6-17. Reconstructed impedance changes in patient 2 253

Figure 6-18. Non-lesional MRI of the third patient 255
Figure 6-19. EIT reconstruction of the impedance change recorded during the events in the third patient 255
Figure 6-20. The centre of mass of the reconstructed change in a pig 257
Figure 6-21. Reconstruction of impedance signal in the whole porcine brain .. 258

List of Tables

Table 2-1. Significant channels in SwissTom recordings for each subject..... 81
Table 3-1 Medical background for three patients 100
Table 3-2. The approximate locations of the perturbations 105
Table 4-1 Detailed anatomical coverage 147
Table 4-2. Localisation accuracy 150
Table 5-1. Seizures types recorded in each animal 192
Table 5-2. Detailed accuracy of EIT onset reconstruction 197
Table 6-1. Sampling area of each depth electrode 229
Table 6-2. Impedance changes detected due to interictal spikes 248

Chapter 1

Introduction

Overview

Electrical Impedance Tomography (EIT) is an emerging, safe and relatively inexpensive medical imaging technique capable of obtaining 2D and 3D images of internal conductivity changes of an object from the boundary measurements. The basic principle of brain applications of EIT is that each tissue of a human head has a specific conductivity and differences between them can be employed to distinguish between one and another or to identify regions of activity and pathology. Hence, EIT could be useful for tasks such as localising seizure foci, differentiating between the ischaemic and haemorrhagic stroke, and for monitoring patient's state after a brain injury. This gives EIT a potential to become a helpful tool in the clinic during neurological diagnosis process.

EIT works by injecting very small current between two electrodes on subject's head and measuring the voltage on the remaining electrodes. This can be then used to reconstruct the pattern of impedances of the layers inside the subject's head and possibly obtain an image of the studied region. For this reason, an additional advantage of EIT over many other methods is that it uses relatively inexpensive equipment, often already implanted on the patient's head for other reasons, such as scalp and/or intracranial electrodes. Hence, the only additional equipment it really requires is the system for the injections and measurements of the current changes.

EIT can be employed to record two types of the impedance change in the brain: fast and slow changes. Slow changes occur over seconds, and a reason for the measured impedance change is explained by the haemodynamic and cerebrospinal fluid fluctuations due to functional or pathological activity. This means that brain regions that show higher activity and so an increased blood flow, e.g. upon stimulation, should exhibit potentially traceable slow EIT changes. Indeed, physiological slow impedance changes related to sensory stimulation were recorded with EIT with scalp electrodes in the past, although they have not been reconstructed into images. In brain pathology, such as epilepsy, it is hypothesized the affected tissues would

also show a distinctive pattern of slow impedance changes that could be then reconstructed into images. Previous studies in small-animal models of epilepsy seem to support this hypothesis. In contrast to slow changes, fast changes appear in milliseconds, due to impedance changes of the cell membranes occurring upon depolarization cycles in active neurones. Due to their more elusive nature and only a weak impedance signal that can be recorded upon their occurrence, fast changes are significantly more challenging to record, however, the feasibility to image fast neural activity with EIT with intracranial surface electrodes in a rat brain during evoked potentials and epileptogenic spikes have been recently reported. To this date, however, neither slow nor fast changes occurring during seizures have been recorded from a human brain. Previous attempts to record them with scalp electrodes were unsuccessful due to movement artefacts that completely masked the signal and no measurements with intracranial electrodes have been attempted.

Following the recent breakthroughs in animal studies, as well as the ultimate need to proceed with the human recordings, we set off to try to detect fast and slow impedance changes in a live human brain. Optimally, such measurements would be performed non-invasively with scalp electrodes. However, due to high resistivity of the skull, which effectively masks the impedance changes from within the brain, this is not currently possible for fast changes and yet to be tested for slow changes. Also, as the recent animal studies have indicated it is possible to record fast neural EIT images using intracranial electrodes, testing such a set up on the human brain is an obvious next step towards moving brain EIT to the clinic.

The current widespread use of intracranial electrodes in the treatment of advanced epilepsy could further facilitate EIT studies. Epilepsy patients with pharmacoresistant focal epilepsy are sometimes offered an implantation of intracranial electrodes for video-telemetry monitoring, as a part of presurgical evaluation towards the resective surgery. Invasive EEG monitoring may include using the intracranial depth electrodes, subdural grids and strips, or a combination

of all of them and even additional scalp electrodes. However, the main disadvantage of EEG, even in its intracranial version, is its limited detection of some signal sources due to their size or orientation. These detection problems could be one of the reasons why seizures reappear in approximately 50% of patients after the neurosurgery, as not all sources are being removed. Contrary to EEG, EIT is not sensitive to the dipole characteristics of the sources and could potentially provide a better resolution in comparison with the existing clinical methods. Also, EIT could be used as a supplementary tool to existing setups on telemetry wards to confirm the diagnosis. Finally, it could be potentially used without the need of any further additional complicated procedures and most importantly, with absolutely no risk of side effects for a patient.

The main aim of this work is to advance the use of EIT to measure fast and slow neural activity so that it can be used as a technique to detect and monitor the onset of a seizure and its propagation in the brain. This would especially benefit patients with intracranial electrodes, awaiting resective surgery.

1.1 Epilepsy

1.1.1 Clinical introduction

Epilepsy, affecting approximately 65 million people worldwide, is one of the most common neurological diseases of a significant burden of premature death and residual disability (Ngugi et al. 2010; Beghi et al. 2019). Yet, the detailed pathophysiology is still not completely understood. Currently, it is assessed that nearly 3% of people will experience a seizure at some point in their life. However, the cause of the epilepsy is unknown for at least 50% of patients suffering from seizures, and more than 30% of the patients continue to have seizures despite the treatment (Bell et al. 2014; Neligan et al. 2012). These numbers clearly indicate a substantial need for further epilepsy research.

Epilepsy has many possible presentations and causes. Overall, it is manifested by unpredictable and recurring seizures caused by abnormally synchronised and/or excessive firing in the neuronal networks. It is likely however that the increased recruitment of neurons is only a secondary effect to a combination of various phenomena, such as expanded connectivity and neuronal transmission, reduced inhibitory mechanisms, and also some fundamental changes in the biochemical properties of neurons (Duncan et al. 2006; Elger and Schmidt 2008; Bell et al. 2017). Seizures can be manifested by quick attacks of distorted consciousness, disrupted motor, sensory, autonomic and cognitive activity – all depend on where the hyperexcitability originates and how far it propagates over the brain. However, even a normal healthy brain can overreact in response to an adequate stimulus, such as, for example, fever, hypoxia, hypoglycaemia, ethanol intoxication, or lack of sleep, and discharge excessively producing seizures. Thus, the diagnosis of epilepsy, in order to be recognised clinically, requires at least two unprovoked seizures that appeared within a period of more than 24 hours apart (Duncan et al. 2006; Schuele and Lüders 2008; Fisher 2015; Fisher et al. 2017; Scheffer et al. 2017).

The clinical definition of epilepsy and its classification system is established by the International League Against Epilepsy (ILAE). The classification is constantly evolving, and it is often used as a guidance for selecting the right antiepileptic treatment. The most recent update was published in 2017 (Scheffer et al. 2017; Fisher et al. 2017). Currently, the basic classification starts with defining the onset of the seizures, i.e. focal, generalised or unknown. In focal epilepsies, where the onset can be located in a particular region of the brain, the resulting seizures start within a limited area, but they can spread further over the entire brain. In some cases, when a focal discharge spreads rapidly, a seizure can generalise before the focal manifestation is clinically recognised. In generalised epilepsies, there is an overall reduced threshold for seizures thus they can affect both hemispheres equally all over the cortex (Duncan et al. 2006; Fisher et al. 2017). For seizures with unknown onset,

other characteristics, such as motor or non-motor presentations, can be used for expanded classification. Following defining the onset, the seizures can be further described using other scales, such as a level of subject awareness, their responsiveness, or associated syndromes and deficits that occur in parallel to the seizure (Fisher et al. 2017).

The clinical diagnosis of epilepsy is usually supported by appropriate tests, including electroencephalography (EEG), magnetic resonance imaging (MRI) with a specific epilepsy protocol to detect anatomical lesions and gyri abnormalities, and blood tests for serum levels of glucose and ions for any malfunctions (Moshé et al. 2015). Interictal EEG is recorded between the seizures and it plays a crucial role in the diagnosis and management process. EEG is relatively easy to apply, a convenient and cheap technique to determine the physiological and abnormal activity coming from the brain. There are several patterns seen in EEG but, in fact, only interictal epileptiform discharges (IED, Figure 1-1) are associated with seizure disorders (Smith 2005; Pillai and Sperling 2006). Other abnormalities, such as fluctuations of background rhythms, focal slowing or regional attenuation are commonly indications of some sort of structural pathology or diffuse cortical dysfunction underlying the seizure disorder rather than clinical epilepsy itself.

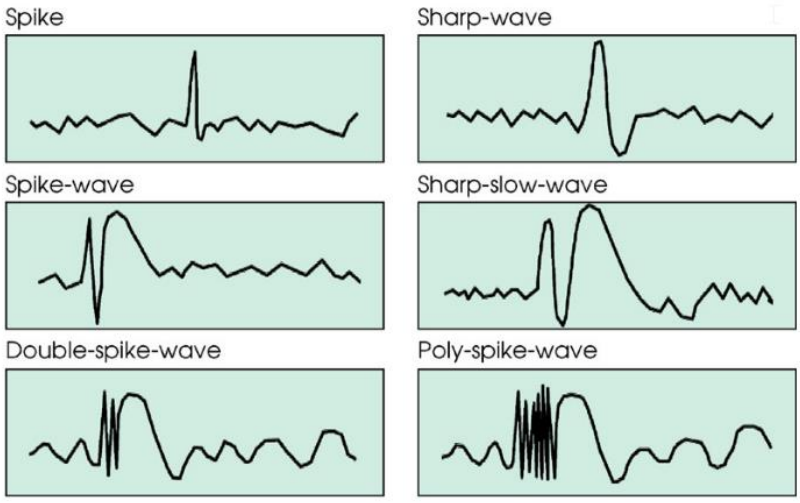

Figure 1-1. A variety of morphologies of interictal discharges in scalp EEG: spikes have a maximal duration of 80 ms, slow waves last between 80 and 200 ms (Elger and Schmidt 2008).

Still, a normal interictal EEG does not exclude a possible diagnosis of epilepsy. It is estimated that at least 30% up to 50% of the first EEG tests in patients later diagnosed with epilepsy do not show obvious abnormalities (Elger and Schmidt, 2008; Smith, 2005). In such cases, repetitions, of up to four times, of the EEG recording are usually suggested, including a sleep deprivation EEG study that usually show abnormalities in a half of the patients with a normal first recording (Duncan et al., 2006; Elger and Schmidt, 2008; Smith, 2005).

Epilepsy patients have an increased risk of the concomitant medical conditions, injuries, accidents and premature death (Gaitatzis et al. 2004; De Tisi et al. 2011; Elger and Schmidt 2008; Duncan et al. 2006; Neligan et al. 2012; Wrench et al. 2011; Moshé et al. 2015). Diseases affecting cardiovascular, cerebrovascular, respiratory, gastrointestinal, and musculoskeletal systems are common conditions coexisting with chronic epilepsy. Epilepsy patients also often show issues of psychiatric and psychological nature, such as anxiety, migraines, depression, suicidal thoughts, and psychogenic nonepileptic diseases. Epilepsy patients have also an increased risk of sudden death (SUDEP, sudden unexpected death in epilepsy), the mechanism of which is still unclear (Moshé et al. 2015).

Overall, the diagnosis of epilepsy can influence person's quality of life, morbidity, and mortality, especially when seizures are frequent. In addition, epilepsy can significantly increase the costs of the treatment and rehabilitation for both, individuals and the healthcare system and hence, development of new methods to improve the diagnostic yield in epilepsy is of utmost importance.

1.1.2 Epilepsy treatment

An initial seizure treatment usually starts with antiepileptic pharmacotherapy (antiepileptic drugs, AED). However, current AEDs are only a palliative step in epilepsy treatment, as they can only suppress the seizures without actually affecting

their real, underlying source. As a result, the best AED for a person can only be chosen on a clinical basis, after a detailed assessment of the seizures and general condition, taking also the financial factor into account. The crucial issue is to balance the benefit of becoming seizure-free, with the potential risks and side effects due to AEDs therapy. Although modern AEDs have a relatively little risk of adverse effects in comparison to the previous generations, side effects, such as central nervous toxicity, overall hypersensitivity, and metabolic problems can still appear, even if the treatment is strictly monitored (Moshé et al. 2015; Elger and Schmidt 2008). An important advantage of current AEDs is however, a lower risk of interactions with other drugs (Elger and Schmidt 2008; Duncan et al. 2006), especially crucial for elderly patients, who are often treated for other diseases such as hypertension or diabetes.

In total, it is estimated that the AED therapy is effective for 60-70% of patients (Moshé et al. 2015; Schuele and Lüders 2008). Approximately 50% of patients with the new onset of epilepsy will remain seizure-free with AEDs only, and in about 20% of cases seizures will be significantly reduced. However, the remaining 30% will not respond at all to the drug treatment and will require another form of therapy (Regesta and Tanganelli 1999; Duncan et al. 2006; Moshé et al. 2015), most often a resective surgery or palliative procedures such as vagus nerve stimulation, as other approaches, for instance radiotherapy or deep brain stimulation, still remain somewhat experimental (Elger and Schmidt 2008; Schuele and Lüders 2008; Nowell et al. 2014; Moshé et al. 2015).

A resective neurosurgery is a preferable therapy for patients with refractory epilepsy and a focal seizure onset, in which the region generating the ictal discharges can be localised and removed. This procedure is commonly used for the mesial temporal epilepsy but it can be also offered for other focal epilepsies (Nowell et al. 2014; Duncan 2011). It is estimated that about 50% of all non-responders to AED are viable candidates for the focal resection (Nowell et al. 2014). The outcome of the

surgery strictly depends on the onset of location accuracy. For example, in temporal lobe epilepsies, a resection of the epileptogenic tissue can significantly improve the brain function in about 50-60% of patients. It is estimated that approximately a half of these cases would not require any continuous pharmacotherapy, while the other half would only require an additional AED treatment to become completely seizure-free or almost seizure-free (Elger and Schmidt 2008; Kelley and Theodore 2005; Schmidt and Löscher 2003). The resective surgery can offer a life-changing cure, but it is always associated with neuronal deficits and cognitive impairment. Hence, it is crucial not only to assess the onset accurately but also to evaluate the impact of a possible resection on patient's daily functioning. This assessment is based on a detailed investigation, which in a majority of cases includes all of the following: a clinical examination, imaging (MRI, ictal-SPECT, and interictal-PET), prolonged interictal scalp EEG with video telemetry, usually during a period of reduced anticonvulsant therapy, psychological and psychiatric assessments, and, as the last step, an invasive intracranial EEG using depth electrodes, subdural strips and grids (Duncan 2011; Moshé et al. 2015; Schuele and Lüders 2008; Jackson and Badawy 2011). Despite the intense diagnostic procedure and prolonged multidisciplinary assessments, the seizures remain unaffected in at least a third of all surgically treated patients (Bell et al. 2017; De Tisi et al. 2011). The reason for such an outcome remains unclear, but a likely explanation seems to be the resected area had not been properly matched with the actual onset zone (Lesser et al. 2011). This demonstrates a crucial clinical need for a more precise method to localise the onset, which could potentially be addressed by Electrical Impedance Tomography.

1.1.3 Presurgical seizure evaluation

The success of a surgery in epilepsy treatment depends on how accurately a resection or disconnection strategy can yield full seizure control. Therefore, many factors must be assessed during the presurgical evaluation, including the clinical

context of the seizure occurrence, the definition of the ictal events in EEG and a presence of structural abnormalities in the brain.

1.1.3.1 EEG in presurgical evaluation

EEG is widely used to obtain information on the functional abnormalities and fast changes in neuronal activity. The EEG signal is describing functional brain activity at different frequency bands, i.e. delta (1-4 Hz), theta (4-8 Hz), alpha (8-12 Hz), beta (12-30 Hz) and gamma (up to 100 Hz). It can reveal epileptiform discharges, such as spikes, sharp waves, and spike-wave discharges that taken together indicate the spread of the so-called irritative zone. Also slowing of this signal can be related to a localised structural pathology or diffuse cortical dysfunction.

The diagnostic yield of EEG can be improved by simultaneous video-EEG recordings, for which the onset and the initial spread of the seizure can be captured and combined with the observed semiology. Video-EEG can be also helpful to distinguish the epileptic seizures from other paroxysmal clinical events that would manifest in the patient.

Scalp EEG has a high temporal resolution of 1 millisecond but has a poor spatial resolution (Burle et al. 2015). The most of the EEG waveforms are a result of the current flow from and to the neurones, due to a summation of the inhibitory and excitatory postsynaptic potentials (IPP and EPP respectively), as the gradient in the electrical potential is generated in the extracellular cortical space (Tatum et al. 2008). The postsynaptic potentials build up from local changes of membrane potentials, so-called action potentials; however, they can be measured for longer than the latter. The summed postsynaptic potential emerging as result of simultaneous activity of a number of neurons gives rise to a larger volume current that can be measured in EEG (Lüders, 2008). Due to the nature of postsynaptic potentials, which arise from flows of positive and negative ions corresponding respectively to EPP and IPP, the EEG sources are also dipoles.

There are three main factors that can influence the signal detection by the EEG electrodes: the size of the cerebral source, its orientation and location (Ebersole 1991; Teplan 2002; Smith 2005; Schuele and Lüders 2008; Beghi et al. 2019; Ramantani et al. 2013; Tatum et al. 2008). If the size of the source is not large enough, it will not be detected because the signal will be attenuated by the tissues before it reaches the recording electrodes. It is estimated that approximately a few square centimetres of the cortex area has to be active simultaneously to become detectable with EEG, although such estimations are highly speculative (Benbadis et al. 2005; Benbadis and Lin 2008). One of the first studies performed on an artificial head phantom with no background EEG signal suggested that the minimum size of 6 cm^2 of the cortical area must be involved before it becomes visible for scalp EEG (Cooper et al. 1965). In studies based on the comparison between the intracranial and scalp EEG recordings the numbers vary. It was estimated that spikes might be recorded by the scalp EEG from the activated cortical area of a range between 6 cm^2 (Tatum et al. 2008), 8 cm^2 (Ebersole 1991), 10 to 20 cm^2 (Tao et al. 2005), 19 cm^2 (Tao et al. 2007), or between 6 to 24 cm^2 (Kobayashi et al. 2005). It has been also suggested that detection of interictal discharges requires a wide area of at least 10 cm^2 (Tatum et al. 2008). Based on the realistic source modelling for epilepsy spikes of amplitude 1.5 times bigger than the background activity, cortical sources of at least 3 cm^2 size were detected by the intracranial recordings. This size had to be increased to at least 7 cm^2 for the scalp measurements, (Cosandier-Rimele et al. 2008). The orientation of the source also affects the voltage field maxima detected by EEG, and in some cases the EEG electrodes will be completely blind. If the cortical generator is in parallel to the scalp electrode and produces the orthogonal and radial field, the maximum voltage is recorded on the electrodes. Sources oriented tangentially (e.g. bank of the sulcus or lobar fissure, Figure 1-2) will produce no voltage change, as the recording electrodes above lie in the isopotential line (Schuele and Lüders 2008; Smith 2005; Scherg 1990).

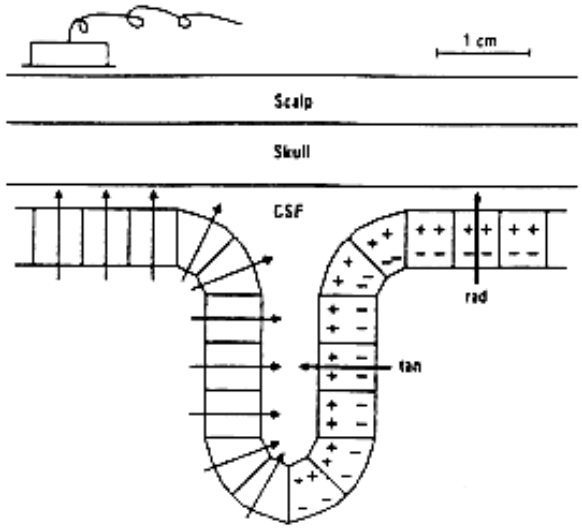

Figure 1-2. A cortical fold in a schematic diagram. Two single dipoles are marked to illustrate different source orientation (described in the text). One source is tangential (*tan*), for which no voltage will be recorded on the electrode above it. Another signal generator is radial (*rad*) and maximum voltage can be recorded by the electrode (Scherg 1990).

Due to the above limitations of extracranial EEG, sometimes the intracranial monitoring, which allows recording directly from the cortex, is required in order to improve the detection of the seizure onset location prior to resective surgery. The seizure onset is usually characterised by various diverse discharge patterns, but it is the focal fast activity that has been found to be a specific marker for the postsurgical outcome in epilepsy (Jiménez-Jiménez et al. 2015). Intracranial EEG is a method with the highest spatiotemporal resolution and, hence, the best signal to noise ratio among the methods currently used for seizure monitoring (Schindler et al. 2016). The submillisecond temporal resolution of the intracranial EEG is the main reason for its use to measure the neural activity (Lachaux et al. 2003). Unfortunately, the spatial sampling of the method is limited only to the adjacent region of the cortex covered by the electrodes. Invasive EEG (iEEG) recordings include subdural and depth electrodes (Diehl and Lüders 2000; Lesser et al. 2010).

Subdural electrodes (electrocorticogram, ECoG) includes grids and strips. They can be useful for the detection of the cortical onset, but they are especially helpful for mapping the extent of the epileptogenic and irritative zone, for instance over a wide cortical dysplastic area (Zijlmans et al. 2019). ECoG is also commonly used for the functional localisation studies, to map the cortical physiological functions prior to the resective surgery (Lachaux et al. 2003; Wellmer et al. 2012). Subdural electrodes allow recording the signal directly from the brain and they can be placed in a variety of locations, including fissures between the hemispheres and the shape and size of the ECoG array can be customised for each patient's individual needs. However, their efficiency is limited when sampling from highly vascularized regions or depth structures (Lesser et al. 2010, 2011) and the electrodes have fixed separated positions on the array. If the epileptogenic activity occurs in the midway from one electrode to another, it can potentially be not accurately localised. Also, the usage of the ECoG arrays comes with many dangers for the patient. They have an associated increased risk of infection (almost 12% for grids and about 1% for strips), a concurrent risk of cerebrospinal fluid (CSF) leakage, and the strip position can potentially be affected by patient's movements during the fit. Other complications related to subdural electrodes include oedemas and haemorrhages, but these are relatively rare (Benbadis et al. 2005; Lesser et al. 2010; Nowell et al. 2014).

Stereotaxically-implanted multicontact depth electrodes (stereo-EEG, SEEG, stereo-electroencephalography) resemble very thin needles that can be inserted deep into the brain structures. They can only sample a limited brain area directly adjacent to them, but their usage has several advantages over the ECoG arrays. In general, being planted deeper they offer a better coverage of the depth structures, as they are located closer to the source generator. Hence, they might help to clarify the location of the seizure onset and its spread more accurately, when the extracranial EEG results are incoherent (Zijlmans et al. 2019). Also, the implantation procedure of depth electrodes is less invasive than that of ECoGs, as it is done through burr holes

and does not require craniotomy. This lowers the infection risk very significantly, when compared with ECoG, to just ~0.5%. This number can however increase up to 5%, when a prolonged SEEG monitoring during telemetry is required. Furthermore, a modern computer-assisted stereotaxic implantation method simplified and significantly improved the precision, as well as the speed of a placement of this type of electrodes under local or general anaesthesia (Benbadis et al. 2005; Nowell et al. 2014; Nowell et al. 2015; Zuluaga et al. 2014). Similarly, SEEGs can be also removed relatively quickly, under local anaesthesia only (Nowell et al. 2014). In the past, SEEG electrodes were considered harmful and potentially damaging to the cortical tracts during their implantation; this, however, has been proven incorrect (Benbadis et al. 2005). The histology tests showed the areas of gliosis, cystic degeneration, and microabscesses in the affected areas where the electrodes were implanted but further studies have shown no functional impact on the brain function and, therefore, depth electrodes are now regarded as safe (Benbadis et al. 2005). The main risk related to SEEG electrodes is a haemorrhage occurring during the implantation in 0.5% to 5% of cases (Benbadis et al. 2005). In order to avoid this complication, a safety margin of at least 3 mm from the vascular structures is recommended when planning the SEEG implantation (Nowell et al. 2015; Zuluaga et al. 2014).

Even though EEG is the gold-standard method in epilepsy diagnosis, there is currently no widely accepted method for 3D image reconstruction of the neuronal activity propagation based on the EEG signal. Such an imaging technique is called the electrophysiological source imaging (ESI) and it is used to try to estimate the brain sources activities based on EEG. However, the inverse solution for EEG is ill-posed, not unique and it is unstable (Grech et al. 2008). The signal localisation is found not to be reliable, due to the errors in head and source modelling, as well as the biological and instrumental noise. For these reasons, the method is rarely applied and of little

clinical importance and hence, there is still a need for employing existing and developing new alternative techniques to find the seizure onset and image it in 3D.

1.1.3.2 Neuroimaging in presurgical evaluation

Neuroimaging plays a crucial role in the field of epilepsy diagnosis. It is necessary for detecting structural lesions, especially in the refractory cases that could benefit most from the resective surgery. It has been found that an absence of the structural abnormalities in MRI reduces by half the likelihood of positive outcome of the epilepsy surgery (Kuzniecky et al. 1987; Cendes et al. 2016; Mosewich et al. 2000). Hence, optimising structural imaging to identify any potential lesions is essential for accurate pre-surgical assessment. The adaptation of the epilepsy protocol for MRI facilitated the substantial progress observed in this field recently. The current protocol includes a whole-head, high-resolution 3D T1-weighted and T2-weighted imaging, fluid-attenuated inversion-recovery (FLAIR) sequence, and sensitive for haemosiderin and calcification sequences. The hippocampal volume is estimated from the coronal T2 and FLAIR. The scan should be then assessed by at least one the neuroradiologist specialising in epilepsy imaging and reviewed by another neuroradiologist (Duncan et al. 2006; Jackson and Badawy 2011; Zijlmans et al. 2019).

In addition to the structural assessment, a further evaluation towards indirect abnormalities can be performed with the functional magnetic resonance imaging (fMRI). fMRI is commonly used for the hemispheric lateralisation and domination assessment and to evaluate potential deficits due to a resective surgery, instead of the previously used and invasive method, the carotid amytal test (Duncan et al. 2006). The intensity of the fMRI signal changes, depending on the magnetic properties of deoxygenated and oxygenated haemoglobin resulting in a so-called blood-oxygenation-level-dependent (BOLD) response (Ogawa and Lee 1990). Hence, the BOLD response could be hypothetically used in epilepsy to differentiate slow haemodynamic fluctuations related to the seizure onset zone in the brain. The

temporal resolution of fMRI is currently estimated as above 1 second but it is possible to lower the spatial resolution to less than 1 mm (Koretsky 2004), so it would be potentially a very valuable technique for the onset localisation. Unfortunately, measuring the BOLD response is very severely affected by any movements and so its potential use is very limited to rare cases such as absence seizures. Even in such cases, a logistic problem of preparing the patient for fMRI straight before the potential seizure occurs still remains, making the method currently unviable for any direct ictal imaging.

Haemodynamic fluctuations can be also assessed using nuclear imaging methods, the costs of which are although relatively high in comparison with CT or MRI. In positron emission tomography (PET), a radio-labelled biological molecule is administered, and its fate followed with a scan. The decaying isotope emits positrons that hit electrons from tissues and form photons to be detected with a gamma camera in PET (Ollinger and Fessler 1997). The detector is the limitation for the spatial resolution of PET, which is approximate 4-5 mm (Robinson et al. 1999) but it can potentially be decreased to less than 2.5 mm (Moses, 2011). The temporal resolution of PET and the exposure to radiation depends on the radioactive tracer distribution (Robinson et al. 1999), for instance, for the commonly used in epilepsy ^{18}F labelled fluorodeoxyglucose (FDG-PET), the radiation dose is about 6 mSv. A PET scan is performed interictally so that the hypometabolism on FDG-PET indicates the dysfunctional cortex that could point to a presence of the seizure focus (Zijlmans et al. 2019).

Regional cerebral perfusion can be also monitored with single-photon emission computed tomography (SPECT). SPECT produces images from gamma rays emitted by radioisotopes administered in tracer compounds, with ^{99m}Tc-hexamethylpropyleneamineoxime (^{99m}Tc-HMPAO) being the most commonly used in epilepsy. The spatial and temporal resolution of SPECT is comparatively low (7 mm and 15 min respectively). The tracer can be injected ictally and interictally so

that the findings from both phases can be compared to each other, and with the outcomes of other methods, such as EEG, MRI and PET. SPECT is preferred to use as an accompanying tool to these, especially for non-lesional and extratemporal epilepsies (Zijlmans et al. 2019). The local ictal hyperperfusion of the radioactive isotope, with the hypoperfusion of the surrounding area, is usually related to the onset zone.

In addition to the commonly used clinical methods for diagnosing seizures, there are several new experimental developments proposed for localising seizure onsets. They include magnetoencephalography (MEG), with the recent development of optically pumped magnetometers (OPM) that enable portable recordings (Boto et al. 2018), spike-triggered EEG-fMRI (Salek-Haddadi et al. 2006), and intrinsic optical imaging (Haglund and Hochman 2004). Even though potentially very promising, they all currently remain research-only methods and their accuracy and outcome measures are still quite difficult to compare with the clinical gold-standard techniques.

Finally, electrical impedance tomography is a method that has a potential to produce images of physiological brain activity and pathologies such seizures. Changes in the conductivity of the brain tissues due to a rise in the cerebral blood volume and blood flow during cognitive activity in humans (Tidswell et al. 2001), and due to interictal and ictal discharges in the rat brain (Vongerichten et al. 2016; Hannan et al. 2018) can be measured with EIT. Currently, EIT can detect and localise changes related to the interictal and ictal activity with epicortical arrays with a resolution 200 μm and 2 ms in rat cortex giving a promise for future clinical application for patients with epilepsy. This thesis focuses on future developments of the method to apply it in the clinical setting.

1.2 Introduction to Electrical Impedance Tomography

Electrical Impedance Tomography is a relatively new imaging method, which was proposed for clinical application in chest imaging for the first time by Henderson and Webster (1978). The main advantages of EIT, when it is used to record functional activity, are low price, portability, high temporal resolution, and minimal invasiveness, that all are not characteristic of any other single imaging method, which is currently available in the clinic. With EIT, a tiny and safe current is injected, and voltages are recorded by an array of the electrodes placed on the body surface so that the recorded voltages can be reconstructed into images (2D or 3D). EIT is limited by low spatial resolution, due to the coverage of applied electrodes, and high sensitivity to errors in the reconstruction methods.

1.2.1 Electrical Impedance

Electrical impedance (Z) can be defined as an opposition in an electrical circuit. In a direct current environment (DC), the impedance is equal to the resistance (R), whereas, with alternating current (AC), where the capacitance (C) is involved, the measured voltage lags after the injected current by the phase angle (the lag phase). Thus, the impedance has to be defined in a complex plane (Figure 1-3), in which the absolute impedance (Z) is represented by the relation $Z=R + iX$ where R is the real component, the resistance. The imaginary part (the reactance of the circuit, X) with the imaginary unit i is inversely proportional to the frequency (f) and stays in relation $X=1/\omega C$, where $\omega=2 \pi f$.

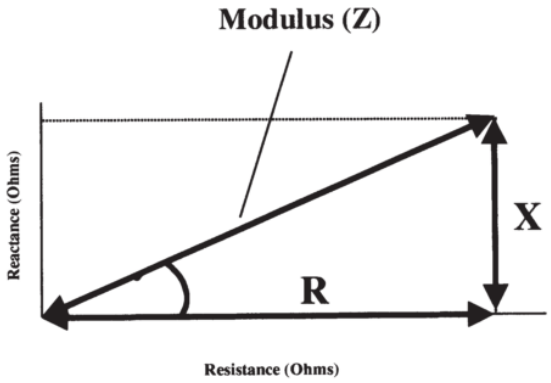

Figure 1-3. The complex plane of the impedance shows the relation between the real (R) and imaginary (X) part of the impedance with the phase angle (Holder 2005).

1.2.2 Tissue bioimpedance

All tissues in the human body have particular electrical characteristics that can be determined in response to an externally applied current and that can be described as bioimpedance. Those characteristics depend on the tissue type, its condition, and the frequency of the current applied. Hence, measuring those characteristics could theoretically allow one to differentiate the tissue types and their conditions. This is the basic concept for the EIT recordings. In brain applications of EIT, changes in blood volume and blood flow, neuronal cell size (e.g. during cell swelling) and local concentrations of ions in the extracellular space, which all may be a result of healthy functional brain activity, such as evoked sensory stimulation, or pathologies, like a seizure, stroke or regional brain injury, are all expected to modify the recorded impedance.

Biological tissues can be modelled as an electrical circuit combined with a set of capacitors and resistors. The impedance of a tissue is characterised by its resistive features composed of the extracellular and intracellular spaces (R_e, R_i), which are very conductive due to high concentrations of various ions in them, and a capacitive component (C_m) that is created by a lipid cell membrane, which has the properties of

the electrical insulator and prevents low frequency current to get through (Figure 1-4).

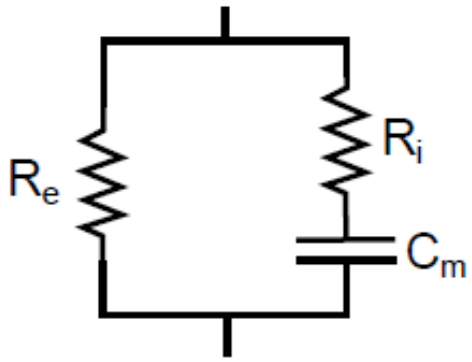

Figure 1-4. A single cell modelled as an electrical circuit. The resistance is modelled by the intracellular (R_i) and extracellular (R_e) space and the capacitance (C_m) is created by the lipid cell membrane (Holder, 2005).

At low frequencies, such as below 100 Hz (alpha dispersion), current cannot pass through the cell membrane and it spreads within extracellular space, whereas with an increase in frequency (e.g. at beta dispersion, between 10 kHz and 10 MHz), the membrane can be crossed by the current, up till the highest frequencies (gamma dispersion, at around 10 GHz), in which this capacitive feature of the membrane can be neglected again, and the measurements are purely resistive. With an increase in frequency, the resistive component of the impedance falls and the reactive one initially rises. At the highest frequencies, more current is transmitted to the intracellular space and the reactance becomes insignificantly small (Holder, 2005). This typical reaction of the biological tissue to the change in frequency is usually described on a Cole-Cole plot (Cole and Cole, 1941) (Figure 1-5).

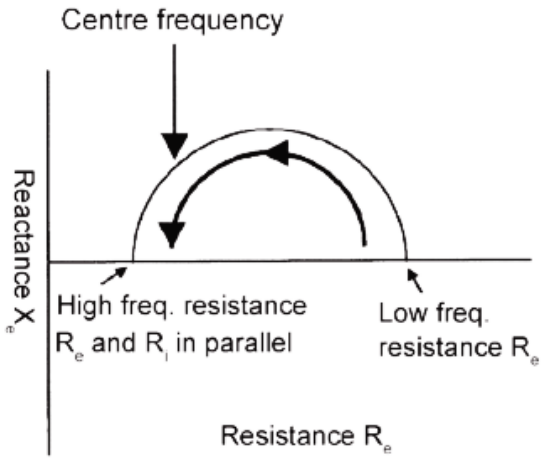

Figure 1-5. Ideal Cole-Cole plot for a biological tissue (Holder, 2005).

The resistivity of a tissue is closely related to a number of charged species that can conduct the current within it. Knowing several features of these species, such as their mobility and size, one is able to predict how easily the current will flow in a given tissue. Smaller ions, like Cl^-, Na^+, Ca^{2+} and K^+, are more mobile, so then they can carry current easier compared to larger molecules such as proteins (Ochs and Van Harreveld 1956). In addition, cell membranes also influence the current flow, for example, the resistivity of blood rises with an increase in a number of red blood cells and so increased density of cell membranes (Geddes and Baker 1967). In the brain, the plasma membrane of neurones is highly resistive, whereas that of glial cells is much more penetrable (Lux et al. 1986). A current injected through scalp or intracranial electrodes will flow through several sections including glial and neuronal layers, blood, and extracellular fluid and thus any changes in at least one of these compartments will modify the current flow and so the overall brain impedance, and eventually the recorded boundary voltage measurements (Holder, 2005). Such changes can be a result of a healthy neuronal activity and regional blood changes related to it (e.g. during evoked activity) or pathologies like a seizure and haemorrhagic or ischaemic strokes. The increased blood volume during functional brain activity causes a few percents decrease in impedance, as blood has a lower

resistivity than averaged brain tissues (approximately 125 Ω.cm and 350 Ω.cm respectively at 50 kHz (Holder, 2005)), which overall allows more current to flow through the area. In some pathologies like seizures, ischaemia and spreading depression, an increase in impedance arises due to cell swelling. Water and ions enter neurones and glial cells causing cell enlargement with simultaneous reduction in the volume of the extracellular space and thus increasing the overall resistivity (Holder, 2005).

1.2.3 Electrical Impedance Tomography

In principle, EIT is capable of generating images of changes in the internal body impedance from the surface voltage measurements made with EEG or ECG electrodes that are placed directly on the skin (Bayford, 2006). The boundary voltages measured in an EIT experiment are then combined with the prior information on the electrical properties of the tissues and used to compute a conductivity change inside the studied body part. Then, these changes can be visualised on a tomographic image.

1.2.3.1 EIT data collection

A typical instrument set up for EIT consists of electronics to inject the current and record voltages, a current source to apply alternating current, a voltmeter to measure voltages, a switching network to connect the equipment to electrodes, the electrodes (scalp or intracranial, the same EEG electrodes that are used in clinics), and a computer to store and process the data.

The boundary voltage changes that are measured in EIT are generated by injecting a tiny and medically safe (IEC 60601-1) current between a given pair of electrodes spanning the largest distance and recording resulting voltages with all the other electrodes. EIT is most commonly used as a sequential (serial) method, so that the current injection is switched from one electrode pair and then performed by another electrode pair, up until all electrodes are used forming a full current injection

protocol necessary for imaging. Such a protocol specifies the number and order of electrode pairs, the amplitude and the frequency of the current. This usually covers injections between 16 to 32 scalp electrodes (Tidswell et al. 2001; Fabrizi et al. 2009, 2006) or even more in measurements with the intracranial electrode arrays (Hannan et al. 2018; Vongerichten et al. 2016; Faulkner et al. 2018; Aristovich et al. 2016). However, it is also possible to use parallel current injections, during which current is injected at multiple frequencies at the same time between pre-set electrodes (Dowrick and Holder 2018; Avery et al. 2017). Such system uses frequency division multiplexing, so that there is no switch between the pairs as full imaging protocol is collected constantly. Such system has been recently proposed to use and work described in chapter 4 was focused on improving the system for its further use on patients and in large animal brain.

Further information on EIT systems is provided in chapters 2 and 4.

1.2.3.2 Image reconstruction

Image reconstruction in EIT is based on calculations of the forward and inverse problems, in which the current path inside a studied part of the body has to be modelled. The most common way to solve the forward problem is to use the finite element method (FEM), in which a final model of a body part is formed of multiple small elements, for instance, as a tetrahedral or hexahedral elements mesh so that the current flow can be calculated for each element separately. This solution has been recently significantly aided by novel methods of mesh creation that take into account the real head shape and tissue distribution of a patient derived from MRI and CT scans (Jehl et al. 2016). Previously used methods for segmentation have several limitations, which decreased the accuracy of EIT images. When meshes were based simply on CT scans, only the shape and size of the skull were reproduced, while all tissues inside the skull were represented as a single layer. Conversely, meshes based just on MRI scans suffered from poor reconstruction of the skull layer (Vonach et al. 2012). Because of that, a segmentation from joint CT-MRI scans is now

a preferred method to create realistic head meshes, as it models all layers of the actual head accurately (Jehl et al. 2016). Joint CT-MRI segmentation is also advantageous for epilepsy cases with intracranial electrodes, as the exact location of electrodes can be extracted directly from the scans. Nevertheless, even now, the obtained mesh is still far from perfect due to errors in the accurate prediction of the conductivities of real tissues, while the contact impedance from the electrode placement adds further artefacts to the method. The resulting voltages are linearly dependent on the applied current, which is modelled in the forward problem and generated in the sensitivity (Jacobian) matrix. The inverse problem is used to inverse the sensitivity matrix to calculate the conductivity for image reconstruction. For a unique inverse problem, a whole boundary has to be known, which for the EIT is not true as only a part is covered with the electrodes. Thus, the inverse problem in EIT is ill-posed and small modelling errors might grow significantly in the reconstruction. In order to stabilise the problem, prior information and regularisation procedures have to be applied. Alternatively, the inverse problem is commonly solved by linearizing it around the forward model with the Jacobian matrix and removing some errors with the time difference images.

There are three different types of imaging in EIT: absolute, time difference, and frequency difference. Absolute imaging is, in theory, the most straightforward transformation of measured voltages into a conductivity distribution without a reference and at any time point (Vauhkonen et al. 1999). This method, however, is the most sensitive to modelling and reconstruction errors. To avoid them a majority of EIT measurements are dynamic time difference imaging methods i.e. they compare the baseline conditions with a change in the system over time. An example of this could be imaging of a stomach filled with a saline solution. Here, an empty stomach of a subject before they drink the liquid forms a baseline (Mangnall et al. 1987). Analogously, in cardiac imaging, a heart emptied of blood in a diastole makes the baseline (Metherall et al. 1996), whereas in the ventilation cycle imaging, the

baseline is the end of expiration, when lungs are relatively empty (Harris et al. 1987). With this dynamic approach, it is possible to minimise reconstruction errors, however, it limits the potential application of the EIT to the events that occur only within a short period of time. If the changes show up in a longer time course, the artefacts from the electrode impedance drift appear and therefore more noise is introduced into the images. The possible solution to overcome the limitations of absolute and time difference imaging is to employ the frequency difference imaging with multi-frequency EIT. This is possible because the conductivity of all tissues in the human body is frequency-dependant, so a characteristic impedance response with EIT can be obtained by passing currents with different frequencies in a single experiment. Such procedure can achieve anatomically correct images at one time point (Grimnes and Martinsen 2015).

Nowadays, EIT has a range of clinical applications in studying lung ventilation in the healthy state and in pathologies (Frerichs, 2000), as well as potential clinical applications still in development (Holder, 2005) for screening for the breast cancer (Cherepenin et al. 2001; Zou and Guo 2003) and cardiac and circulatory diseases (Noordegraaf et al. 1996), measuring normal and pathological gastrointestinal activity (Nour et al. 1995), and monitoring brain function (Holder 2005). Our work in the UCL group is focused on this last application.

1.2.4 Neural application of EIT

The main applications of brain EIT are monitoring pathologies such as seizures (Fabrizi et al. 2006; Vongerichten et al. 2016; Hannan et al. 2018) and stroke (Romsauerova et al. 2006; Goren et al. 2013; Holder 2005; McEwan et al. 2006) but also functional activity during evoked responses (Tidswell et al. 2001; Faulkner et al. 2018; Oh et al. 2011; Aristovich et al. 2016, 2014). In each application, the underlying mechanism of the physiological response or the pathology leads to conductivity changes and therefore can be potentially detected, differentiated and imaged in 3D with EIT.

1.2.4.1 Stroke and traumatic brain injury

In principle, EIT has a capability to differentiate between the haemorrhagic and ischemic stroke that can be instrumental in providing the relevant treatment in the early stages of medical intervention. Depending on the current frequency, a normal healthy brain has a conductivity of approximately 0.1 S/m at <100 Hz, when a current mainly passes through extracellular space, that further increases to 0.18 S/m at >1 MHz, when current can pass through cell membranes and into cell lumens. In the haemorrhagic stroke, the conductivity rises to 0.7 – 0.82 S/m at <100 kHz due to lower resistance of blood than of the brain tissue. In principle, such large differences between the impedance of stroke-affected tissues should be detectable using EIT.

In a similar way, EIT can be used to detect a developing delayed or secondary onset of a haematoma after traumatic brain injuries (TBIs) but before any clinical symptoms appear. In TBI, the clinical progression of patients can be assessed using the Glasgow Coma Scale (GCS) and CT scans. However, there are limitations to the intervals at which CT imaging can be performed and thus, there is a great need for a safe and non-invasive method for monitoring TBI and theoretically, EIT could be used for this application.

Unfortunately, recent studies on EIT application in stroke in rats and humans were not completely successful (Dowrick et al. 2015; Goren et al. 2018) and so further work is necessary to obtain reliable images.

1.2.4.2 Functional activity

Slow and fast impedance changes can be recorded with EIT during the physiological functional activity of a healthy brain. Slow changes can be explained by the fluctuations in blood flow in activated regions, whereas fast changes arise from variations in the membrane potential of neuronal membranes during brain activity. EIT has been proved capable of measuring impedance changes in activated areas of

the brain (Faulkner et al. 2018; Aristovich et al. 2016; Gilad and Holder 2009; Holder et al. 1996; Tidswell et al. 2001; Adey et al. 1962). Although in theory, a regionally increased blood flow evoked by repetitive sensory stimulation should evoke local decrease in the impedance signal, in all studies both, an increase and a decrease in impedance were observed in the activated areas. This was explained by linking the observed rise in impendence to the changes in the cerebrospinal fluid (CSF) distribution and cell swelling (Tidswell et al. 2001).

The first human study aimed at imaging the cortical activity evoked by sensory stimulation (Tidswell et al. 2001) employed scalp electrodes. The authors of this study reported changes in the impedance signal, which were both reproducible and related to the stimuli, but could not be reconstructed into reliable images. Authors reported problems arising from physiological factors, which likely disrupted the image reconstructions, such as cell swelling, temperature changes in the activated region, and the flow of the CSF as well as from technical issues including a possibly oversimplified reconstruction algorithm, which modelled a human head as a homogeneous sphere, and other potential reconstruction artefacts arising e.g. from erroneous electrode positioning. Several of these factors have been addressed in the recent developments in hardware, software, and image reconstruction for EIT and have been already showed to significantly improve the precision of imaging the functional brain activity with EIT in computer modelling and animal studies (Bagshaw et al. 2003; Dowrick et al. 2014; Aristovich et al. 2014). Chapter 2 of this thesis addresses using EIT to image functional activity and contains more details on this topic.

1.2.4.3 Epilepsy

Imaging impedance changes related to the focal ictal discharges and their spread in the brain have been attempted for many years and proved challenging (Holder, 2005). EIT has the potential to image areas of both synchronous neuronal firing and changes in extracellular space that both are characteristic in the epileptogenic zone.

These phenomena are the principles of the two types of changes in brain impedance that can be referred to as “fast” and “slow”.

The “fast changes” occur over the range of milliseconds. They are caused by synchronous depolarization in a local neurone network, such as the one in neuronal depolarization or during interictal and ictal discharges, that leads to a direct transient decrease in impedance of the cell membrane when the depolarization wave propagates. The change occurs due to ion channels opening and follows the current flow through the conductive intracellular space. Fast changes have already been recorded in evoked potentials (EP) in animals with an intracranial array of electrodes (Klivington and Galambos 1967; Oh et al. 2011; Faulkner et al. 2018). Recent work in our group showed that imaging fast changes in the rat brain during ictal and interictal activity can be also achievable (Vongerichten et al. 2016; Hannan et al. 2018).

During the study aimed at recording the interictal activity (Vongerichten et al. 2016), seizures were triggered with a subcortical injection of the chemoconvulsant, either 4-aminopyridine (4-AP) or picrotoxin or penicillin, in a rat brain. The ECoG and impedance change was recorded with a 30-contact epicortical array placed on the exposed cortex. There was a quick fall of the impedance signal recorded approximately 12ms before (in 4-AP and picrotoxin model) or during (penicillin model) the interictal spike, followed by a rise within the subsequent 120 ms afterwards. The observed negative change had a magnitude of -0.26% and -0.93%, whereas the positive change was within 0.61 to 2.34%. These changes were also reconstructed into images with accurate location and propagation of approximately 1mm deep into the rat’s cortex. The recorded drop in the signal could be explained by the synchronised neuronal depolarisation of local network, whereas the follow-up increase was likely to occur due to the shrinkage of the extracellular space caused by increased neuronal activity. This study, however, was reconstructing only the changes coming from the interictal activity, that can arise from a larger irritative

zone, not only from the onset zone. The study that followed (Hannan et al. 2018) aimed to record the fast impedance changes occurring during ictal events and employed an electrical model of seizures in a rat brain. Here, seizures were triggered on-demand, while ECoG and EIT signals were recorded directly from the rat cortex with a 57-electrode epicortical array. There was a consistent negative change of a magnitude of -0.31 ± 0.06% observed, correlating with the ictal spike and wave discharges and reconstructing onto early onset in the whisker barrel cortex, with a spread over the adjacent somatosensory cortex over the following 20ms. Both studies clearly showed that EIT is a valuable neuroimaging tool that can help to understand epilepsy better. However, both studies required averaging multiple spikes, either interictal or ictal, and therefore, repeated epileptiform activity. Such approach has a limited application for clinical usage, as it might not be possible to record enough data to average during clinical monitoring. In addition, both studies were performed with epicortical arrays that are currently less commonly use in humans. Finally, these recordings were performed on a flat surface of a rat brain, which is completely different from the folded, gyrated human brain and with seizures triggered artificially. The work described in chapters 3 and 6 of this thesis tried to address these limitations and further advance EIT as a tool for imaging fast changes during seizures.

The “slow changes” in neuronal impedance are associated with a redistribution of fluids and a decrease in the volume of the extracellular space that follows a period of increased neuronal activity. These are due to a decrease in the extracellular space as neurones are unable to maintain the osmolality of the intra- and extra-cellular environments and water moves into their lumen over seconds. As almost all the applied current for measuring impedance travels in the extracellular space, this causes an increase in resistance. Slow changes, of a magnitude up to 12% in impedance signal could be detected within 10 seconds after the onset in various animal models of epilepsy. The maximum reported impedance increase was 10-12%,

recovering within the following 30 seconds, was measured with two cortical surface electrodes at 1 kHz with seizures induced with Metrazol (Harreveld and Schade 1962). Analogous changes, lasting 20-25 seconds, were measured at 1kHz with depth electrodes and seizures induced with a tungsten acid gel (Elazar et al. 1966). When seizures were provoked electrically (10-20 μV at 1 kHz), a 2.5-3% impedance increase was detected with a system injecting a sine wave at 1kHz on chronically implanted depth electrodes located in an animal limbic system (Adey et al. 1962). A similar system was used to measure impedance changes in patients with temporal lobe epilepsy, for whom impedance changes of up to 7% and a 9-10 minutes latency were recorded at 1 kHz (Porter et al. 1964). In preliminary experiments performed by Rao et al. (1997), a ring of electrodes was placed directly on exposed cortex of a rabbit, whereas seizures were triggered artificially with an electric stimulus. The observed cerebral impedance changes have risen by 7.1 ± 0.8% during the seizures. however, the study suffered from poor spatiotemporal resolution due to technical limitations.

The aforementioned animal studies were carried out using intracranial epicortical electrodes, while the only epilepsy study completed to date in human subjects (Fabrizi et al. 2006) was performed using a scalp-electrode-based system. In scalp measurements during seizures, the expected EIT signal has a magnitude of approximately 0.1% - 1%, because of the signal attenuation by tissues shielding the brain, mainly the skull. Also, the magnitude of the signal varies depending on the size and depth of the source generator.

The first pilot human study on patients of a telemetry EEG ward (Fabrizi et al. 2006) was performed with the UCLH-EIT Mark 1b system (Yerworth et al. 2002) with 32 standard EEG cup scalp electrodes placed according to the 10-20 Electrode Placement System (Oostenveld and Praamstra 2001) on top of a standard EEG montage used for clinical monitoring. The study failed to measure any reproducible raw impedance changes related to seizure, and consequently, no image

reconstruction was attempted (Fabrizi et al. 2006). The entire EIT signal observed by the authors was attributed completely to multiple movements and systematic artefacts that reached up to 54% voltage change from the baseline. Nevertheless, the authors managed to prove the feasibility of a parallel EIT and EEG recording on patients, where the EEG signal could be clearly recovered from the switching artefacts caused by changes of current-injecting pairs of electrodes in EIT by employing filtrations on both software and hardware level. The authors concluded that further work is required to advance the hardware used to measure the basic EIT signal (Fabrizi et al. 2006, 2010). In spite of the number of studies on slow changes in seizures, there have been no worked described that would employ depth electrodes. This need is addressed in chapters 3 and 5 of this thesis.

In summary, the recent developments in the brain EIT with intracranial arrays have improved the resolution of the method significantly, allowing recording both fast and slow impedance changes related to discharges in the rat brain. Currently, EIT can reach temporal resolution of 2 ms and spatial resolution of below 0.2 mm when measured with 30-electrode mat during the somatosensory evoked responses in a rat brain (Aristovich et al. 2016). However, no one has managed to record similar changes in humans yet. Patients with focal refractory epilepsy already undergo the intracranial electrodes implantation and such electrodes could be used for EIT. As the recent results from the animal studies are encouraging, EIT should be expanded towards human recordings and potentially proceed towards clinical applications. This thesis tries to address this need.

1.3 Injection current safety

The injections of current in EIT have to meet strict safety criteria, no matter what type of electrodes is used (scalp or intracranial): the method must not alter the brain function or cause any pain sensation while delivering the maximum permitted current. The two major documents, the International Electrotechnical Commission (IEC 60601-1, 2005) and the British Standard Institute (BS5724, 1979), specifies the

safety limits to be safely injected into a human head as 100 μA at 1 kHz, then above that frequency to f *100 μA, where f is the frequency used (in kHz) up to the maximum of 10 mA at above 100 kHz. These limitations are set as 10% of the mean sensation threshold.

The additional safety criterion is the risk of neural injury due to current injections. Such a risk was assessed during an extended electrical stimulation in animal studies. A current density of up to 250 A/m^2 at 50 kHz was injected via intracranial electrodes in cats without any apparent, pathological effect on neural tissue even after over 7 hours of constant stimulation (McCreery et al. 1990). An additional safety study on rats was also performed in our group (Hannan, 2016), which showed the current density of 254 A/m^2 at 2 kHz injected for 60 minutes via intracranial electrode array did not cause any damage to the brain tissue, as tested with histology. Also, such current levels had no discernible effect on cortical evoked responses in rats (Aristovich, et al., 2016).

As for the intracranial recordings using the human electrodes (AdTech, Severn Healthcare Technologies, UK), the electrodes have a standard electrode diameter of 1.1 mm and 2.4 mm length, giving the total surface area of 8.29 mm^2. For this surface area, it is possible to inject up to 2.1 mA at kHz frequencies within the 250 A/m^2 safety criterion. For all studies presented in this thesis, the proposed amplitudes are within 50-60 μA at <11kHz, corresponding to a current density near the electrodes of c. 6.03 A/m^2, which rapidly falls off away from the electrodes and is completely safe. This was furthermore tested as having no effect on somatosensory cortical evoked responses in pigs (author's unpublished data although see chapter 5 for details of the study set up).

An additional standard for the total charge injection was provided by the depth electrode manufacturer (Ad-Tech Medical Instrument Corporation, USA). The stimulation parameters (the latency of the pulse duration and the amount of injected current) were specified in the instructions for use mentioning the threshold of

0.5 A/cm^2 as being completely safe for a stimulated tissue (manufacturer information sheet attached to depth electrodes). For example, for the electrodes used during the clinical cortical mapping simulations at Telemetry Ward NHNN, it is safe to inject current up to 10-15 mA if it is injected for a short period (0.2 ms).

1.4 Purpose of this work

The research described in this thesis has been focused on developing EIT as a method that can be used to localise seizure onset and follow its propagation in a gyrated brain. The diagnostic methods currently available for epilepsy are not powerful enough to sufficiently perform this task, as demonstrated by only 50% seizure-free effectiveness of a resective surgery in epilepsy patients. In addition, none of the clinical tools available now can image changes occurring during seizure onset and its propagation inside the brain in 3D.

Electrical Impedance Tomography (EIT) is an imaging technique detecting fast and slow impedance changes. In rats, EIT has been shown to image regions of increased brain activity and pathology. The purpose of the work described in this thesis was to extend EIT to be used for imaging a large and gyrencephalic brain as that of the human. The main focus of the work was to examine the feasibility of using EIT for imaging seizures in a large brain with depth electrodes, as SEEG is currently the method of choice for intracranial monitoring in the clinic. The idea of using EIT with SEEG is appealing, as patients with focal refractory epilepsy are investigated with multiple intracranial depth electrodes prior to the potential resective surgery, allowing employing the already existing setup on the ward for EIT measurements. If achieved, this would be the first time to record such changes in humans offering a great potential to benefit patients in future, as EIT would provide additional information to the ECoG/SEEG in localising the seizure onset. Also, when established, the method could potentially help in better understanding epilepsy as a disease, the mechanisms that are causing the seizures, as well as help to propose an alternative for the treatment currently used.

1.5 Statement of originality

All work presented in this thesis is my own work that has been undertaken as a part of my PhD in the Department of Medical Physics and Biomedical Engineering at the University College London. However, as EIT requires multidisciplinary knowledge and expertise, I have received guidance and help from many people throughout.

In chapter 2, Dr Kirill Aristovich advised me on data analysis and helped with technical issues during experiments. In chapter 3, Dr Michele Rizzi provided anonymised patient MRI and CT scans. Dr Kirill Aristovich, Dr Mayo Faulkner and Dr James Avery helped me to establish an effective method for simulations. I also used a method developed by Dr Kirill Aristovich for EEG inverse source modelling. In chapter 4, Dr Mayo Faulkner, Dr James Avery and Dr Thomas Dowrick assisted me with preparing an EIT system and advised me on appropriate ways of testing it. Dr Mayo Faulkner prepared the protocol maximising the current density on a perturbation for a simulation study. Dr James Avery developed the 0.1 Hz filter-box and helped me with the initial data collection on patients. In chapter 5, I obtained invaluable help during the surgery from Dr Abbe Crawford and Mr Justin Perkins. Dr Thaleia Stathopoulou and Dr Jamie Viscasillas maintained the anaesthesia. Dr Kirill Aristovich helped me preparing the EIT system and with technical issues during the recordings, as well as advised me on the data analysis. In chapter 6, Dr Kirill Aristovich helped me preparing the EIT system and Dr Roman Rodionov prepared tissue layers parcellation in EpiNav™ software.

All the other work was undertaken solely by myself. This comprised all the data collection and analysis.

1.6 List of publications and presentations from the work described in this thesis at the moment of its publication

Chapter 2

Witkowska-Wrobel A, Aristovich K, Avery J, Holder D (2015) "High-resolution imaging of evoked activity in humans recorded with electrical impedance tomography (EIT) and scalp electrodes." Proceedings of the 16th International Conference on Biomedical Applications of Electrical Impedance Tomography. Zenodo. http://doi.org/10.5281/zenodo.17752 (Poster presentation).

Chapter 3

Witkowska-Wrobel A, Aristovich K, Faulkner M, Avery J, Holder D (2018). "Feasibility of imaging epileptic seizure onset with EIT and depth electrodes." NeuroImage. 173. 10.1016/j.neuroimage.2018.02.056.

Witkowska-Wrobel A, Aristovich K, Avery J, Faulkner M, Holder D (2018). T15. "Imaging fast neuronal depolarization in 3D during seizures with electrical impedance tomography and scalp and intracranial depth electrodes." Clinical Neurophysiology. 129. e7. 10.1016/j.clinph.2018.04.016.

Witkowska-Wrobel A, Aristovich K, Avery J, Faulkner M, Holder D (2017). "Feasibility of recording epilepsy changes with EIT and depth electrodes." Proceedings of the 18th International Conference on Biomedical Applications of Electrical Impedance Tomography. Zenodo. http://doi.org/10.5281/zenodo.55709 3 (Conference talk).

Witkowska-Wrobel A, Aristovich K, Avery J, Holder D (2016). "A method for imaging epilepsy with EIT and depth electrodes." Abstracts of the 16th International Conference on Electrical Bio-Impedance and 17th International Conference on Electrical Impedance Tomography. Zenodo. http://doi.org/10.5281/zenodo.55753 (Conference talk).

Chapter 4

Avery J, Dowrick T, **Witkowska-Wrobel A**, Faulkner M, Aristovich K, Holder D (2019). "Simultaneous EIT and EEG using frequency division multiplexing." Physiological measurement. 10.1088/1361-6579/ab0bbc.

Faulkner M, Jehl M, Aristovich K, Avery J, **Witkowska-Wrobel A**, Holder D (2017). "Optimisation of current injection protocol based on a region of interest." Physiological measurement. 38. 10.1088/1361-6579/aa69d7.

Chapter 5

Witkowska-Wrobel A, Aristovich K, Faulkner M, Avery J, Holder D (2019). "Imaging the seizure onset zone and trajectory with Electrical Impedance Tomography." ECR 2019: Book of Abstracts. Insights into Imaging 2019 10 (Suppl 1):22 https://doi.org/10.1186/s13244-019-0713-y (Conference talk).

Witkowska-Wrobel A, Aristovich K, Crawford A, Viscasillas J, Stathopoulou T, Perkins J, Holder D (2019). "Imaging slow impedance changes in focal epilepsy model in porcine brain with EIT and depth electrodes." Proceedings of the 20th International Conference on Biomedical Applications of Electrical Impedance Tomography. http://doi.org/10.5281/zenodo.2691705 (Conference talk).

Witkowska-Wrobel A, Aristovich K, Crawford A, Viscasillas J, Stathopoulou T, Perkins J, Holder D (2019). "Imaging slow changes in focal model of epilepsy in pig's brain with Electrical Impedance Tomography (EIT)" International IEEE EMBS Conference on Neural Engineering, NER'19 (Poster presentation).

Chapter 2

Imaging evoked activity recorded with electrical impedance tomography and scalp electrodes

Overview

Electrical Impedance Tomography carries the potential to produce non-invasive functional images of brain activity with scalp electrodes. The measured signal is a slow impedance change, of approximately 1-second latency. The estimated magnitude of a signal change is 1%, if recorded with intracranial electrode mats, and 0.1% when recorded with scalp electrodes. Such change was measured in humans for the first time almost 20 years ago in our group in the study by Tidswell et al. However, this change could not be reconstructed into reliable images with consistent localisations in the brain. Back then, the measurements were performed with the HP 4284A impedance analyser, injecting up to 2.5 mA at 50 kHz current and collecting the whole dataset at every 25 seconds. Over the following years, significant improvement has been made in the temporal (200 μm) and spatial (2 ms) resolution of EIT. Although the level of noise is similar, the method is now quicker and image reconstruction has been significantly improved. Thus, we set out to again record the slow changes during functional brain activity in healthy subjects with scalp electrodes and EIT and attempt to reconstruct accurate images of such activity.

2.1 Introduction

2.1.1 Background

As introduced before in chapter 1, the functional activity of the brain measured with EIT can be detected at two levels, fast and slow. The former occurs in the range of milliseconds during the action potentials and is intrinsically difficult to measure due to the low amplitude of the signals, the extremely fast latency of their manifestation, and a very limited area where they occur. The slow change is relatively easier to detect and arises from increased blood flow (cerebral blood flow, CBF) and volume (cerebral blood volume, CBV) occurring as a response to the rise in the metabolic demand during neuronal activity. This signal has a larger amplitude, slower time of

occurrence, and it appears in wider regions of the brain than the fast changes and thus, it is easier to detect even with scalp electrodes.

Although both types of change can be detected with EIT, the study described in this chapter was focused on recording slow changes with non-invasive scalp EEG electrodes, due to higher probability of detecting changes arising due to sensory stimulation.

2.1.2 Previous studies on EIT of slow changes in the brain

Measurements of the slow impedance decrease related to the increased blood flow in the brain have been undertaken previously on animal and human subjects. In the first study on animals, the observed impedance signal decreased in the measurements performed with chronically implanted coaxial electrodes in the hippocampus and septum of the cat's brain upon visual, auditory, olfactory, and gustatory stimuli (Adey et al. 1962). Similar, reproducible results were obtained in rabbits during visual and somatosensory stimulation, in which declines of 2.7 ± 2.4% and 4.5 ± 2.7% (mean ± SD) respectively in the impedance signal were noted. The recordings were measured with a ring of 16 Ag/AgCl electrodes on the exposed cortex (Holder et al. 1996). Interestingly, the authors have also reported a corresponding increase in the impedance of 2.9 ± 2% and 1.7 ± 1.1% (for visual and somatosensory stimulation respectively) in the brain regions adjacent to the ones stimulated. They proposed to explain this increase by either physiological in origin, i.e. regional cell swelling and fluctuations of the cerebrospinal fluid (CSF) or artefactual, due to employed reconstruction algorithm, and further work was suggested to explain this phenomenon. However, the main advantage of animal over human recordings was the possibility to use intracranial electrodes, and therefore to benefit from direct recordings, without the resistive barrier of the skull. The skull is known to attenuate the signal significantly, decreasing it by an order of magnitude when compared with the cortical measurements (Holder, 2005).

The first experiment to image slow impedance changes with scalp electrodes in humans was described by our group (Tidswell et al. 2001). It aimed at imaging cortical activity evoked by sensory stimulation with EIT and EEG electrodes. Reproducible impedance changes were recorded, however, none of them could be reconstructed into images with accurate localisation in the brain. The study was performed on 39 people, during visual, somatosensory and motor stimulation, using a Hewlett-Packard 4284A impedance analyser attached to 31 Ag/AgCl EEG electrodes. The sensory stimulation set was repeated at least 6 times per subject. A full, one EIT data set from all scalp electrodes was recorded every 25 seconds, and an image was created with the data from 258 measurement channels, averaged for a subject. 1 to 2.5 mA amplitude current at 50 kHz frequency was injected between two diametrically opposed scalp electrodes, while the voltages were measured on two other electrodes. Authors reported both, decreases and increases in the recorded impedance signal (Figure 2-1). A significant change, defined as more than 2 standard errors of the mean, from the baseline (SEM) was observed in 25% of the channels for the visual and motor stimuli and in 12% of the channels for somatosensory stimulation. The recorded impedance increases of $0.62 \pm 0.19\%$ (mean ± SEM) for visual, $0.63 \pm 0.14\%$ for motor and $0.19 \pm 0.02\%$ for somatosensory stimulation were observed. The recorded decreases in impedance were: $-0.46 \pm 0.07\%$, $-0.44 \pm 0.20\%$ and $-0.22 \pm 0.03\%$ respectively.

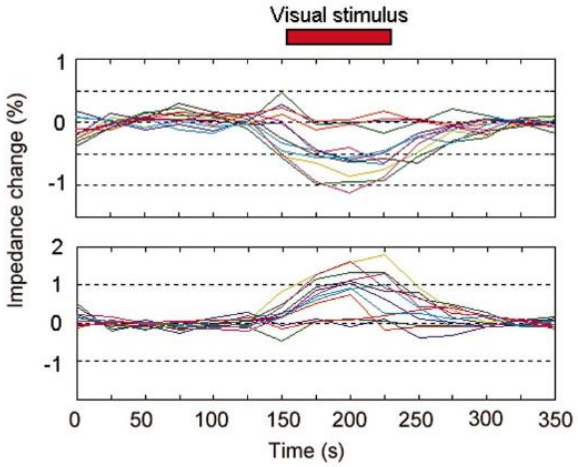

Figure 2-1 Impedance changes recorded in the first EIT measurements of the slow changes in humans. The results show both, the decrease (top) and the increase (bottom) in the impedance signal observed in one selected electrode combination. The x-axis is the timescale expressed in seconds; y-axis shows the percentage impedance change from baseline. Stimulus onset and duration are shown in the red rectangle at the top of the graph (Tidswell et al. 2001).

However, the reconstructed images were noisy, and the impedance change was spread all over the brain that globally made it impossible to localise the measured changes accurately in any of the stimulated regions. The authors explained these results as a mixture of physiological and technical issues that happened at the same time, making it impossible to obtain reliable images. Physiological mechanisms occurring during the sensory stimulation and affecting the reconstruction included the parallel cell swelling, changes in the local temperature and in the CSF distribution. The technical problems that could contribute to these results involved the use of a simplified reconstruction algorithm, in which human head was modelled as a homogeneous sphere, misrepresentation of the image because of the layers in the structure of the head, other reconstruction artefacts, and/or errors in electrode positioning or, very likely, a combination of several factors. Overall, authors suggested that the low temporal resolution of EIT with scalp electrodes and high occurrence of reconstruction artefacts are first problems that would require fixing

in the nearest future to set up EIT as a useful functional neuroimaging tool for accurately imaging evoke activity.

2.1.3 Experimental design to detect slow changes based on the BOLD fMRI and PET paradigms

The most commonly used method to image perfusion changes in neurosciences is functional magnetic resonance imaging (fMRI), although similar paradigms have been also tested with positron emission tomography (PET). Therefore, the experimental paradigm to detect slow impedance changes with EIT has been based on previous findings from fMRI and PET that measured brain activity during visual stimulation.

The intensity of the fMRI signal depends on the magnetic properties of deoxygenated and oxygenated forms of haemoglobin that can be visualised as the blood-oxygenation-level-dependent (BOLD) response to a particular stimulus (Ogawa and Lee 1990). When a subject performs a cognitive task, the increased neuronal activity in a stimulated brain region is followed by a local rise in the cerebral blood flow, volume and metabolic rate of oxygen exchange that all produce the BOLD signal. Simultaneously, the hemodynamic state of non-stimulated areas of the brain remains stable over time. Hence, the observed BOLD signal is interpreted as regional neuronal activation when compared to baseline conditions. A paradigm aiming to study such local changes is called the “block paradigm” aka the “boxcar paradigm” (Ogawa and Lee 1990). The paradigm contains a period of a set time of the stimulation (ON) to arouse the activity in a particular region of the brain that is then followed by a no-stimulation period (OFF), during which all detected changes are expected to recover, and the signal is back at the baseline level. It is estimated that during visual stimulation under fMRI, the cerebral blood flow increases in 1 to 2 seconds after the onset of the stimulation, reaches a peak at 5 to 7 seconds, and then remains stable until 6 to 10 seconds after the stimulus has been stopped (Belliveau et al. 1991; Kwong et al. 1992; Tootell et al. 1995). Very similar activity patterns have

been reported in PET studies (Fox et al. 1986; Zeki et al. 1991; Ito et al. 2001) and they were repeatable with other sensory stimulation paradigms, such as a motor or somatosensory stimuli.

It has been established in fMRI experiments that a good visual stimulation can be achieved by showing a checkerboard, in which black and white squares reverse over time. Such a visual stimulation was performed in a quiet, darkened room with only a small amount of ambient light present in order to minimise the noise and maximise the signal. A stimulation rate of 16 reversals of checkerboard per second has been shown to give the highest signal in the BOLD fMRI experiments (Brigell et al. 1998; Odom et al. 2004, 2010; Parkes et al. 2004). Usually, a fixation point is placed in the middle of the screen during the fMRI experiments in order to keep the subject's eyes focused and hence maintain a good signal (Uludag et al. 2004; Odom et al. 2010). We propose to employ the protocol for visual stimulation, as well as the blocking paradigm optimised in the fMRI studies for our studies with EIT.

2.1.4 Improvements in the EIT technology and the reconstruction method

The instrument performance is a major factor that determines, whether the reconstruction of EIT images is successful. Over past several years, our group has made significant advances in the EIT hardware, software, and algorithms to develop a reliable method to image brain activity with EIT (Aristovich et al. 2014; Vongerichten et al. 2016; Dowrick et al. 2015; Aristovich et al. 2016).

2.1.4.1 Improvements in hardware

The early EIT system used in the first human study to measure slow, BOLD fMRI-like, changes (Tidswell et al. 2001) was based on the HP 4284A impedance analyser, used as a balancing bridge circuit, that was highly accurate but slow. Data collection in EIT comes from a different combination of four electrodes in a polar drive montage, hence two electrodes inject current and another two record voltage changes. To allow EIT measurements, the system was modified with a multiplexer.

Multiplexer, controlled by a computer, switched the injecting current electrodes. The system sampled at 50 kHz from 31 electrodes and 258 measured electrode combinations. The main drawback of this EIT system was a relatively low temporal resolution, as the HP EIT required 25 seconds to acquire each image dataset. Therefore, only slow impedance changes, related to the blood flow, could be recorded. The experimental protocols were modified to match the system capabilities with significantly longer visual stimulation when compared with the BOLD fMRI paradigms.

In order to improve the resolution and noise levels, a new EIT system, called the 'ScouseTom', has been recently developed in our lab (Dowrick et al. 2014). In addition to significant improvements in resolution and noise levels, it has been made as easy to use or transport, and is stable across different current amplitudes applied and hence, it is now commonly used by our group in a variety of neural EIT applications (Dowrick et al. 2015; Aristovich et al. 2014, 2016; Faulkner et al. 2017; Goren et al. 2013; Hannan et al. 2018).

ScouseTom EIT system consists of a combination of commercially available and custom-made instruments (Figure 2-2). The commercially sourced parts include a Keithley 6221 current source (Tektronix Company, Beaverton, USA) and an isolated, battery-powered BioSemi ActiveTwo EEG amplifier (BioSemi, Amsterdam, The Netherlands) connected with an optic cable to laptop with Matlab and BioSemi ActiView software used to control the quality of data collected or current injection protocol and to store data. The custom-made equipment includes a headbox with a switching board controlled by an Arduino Controller through a code running in the Matlab. A switch network is used to programme the electrode injection protocol. The electrodes and connecting cables complete the kit.

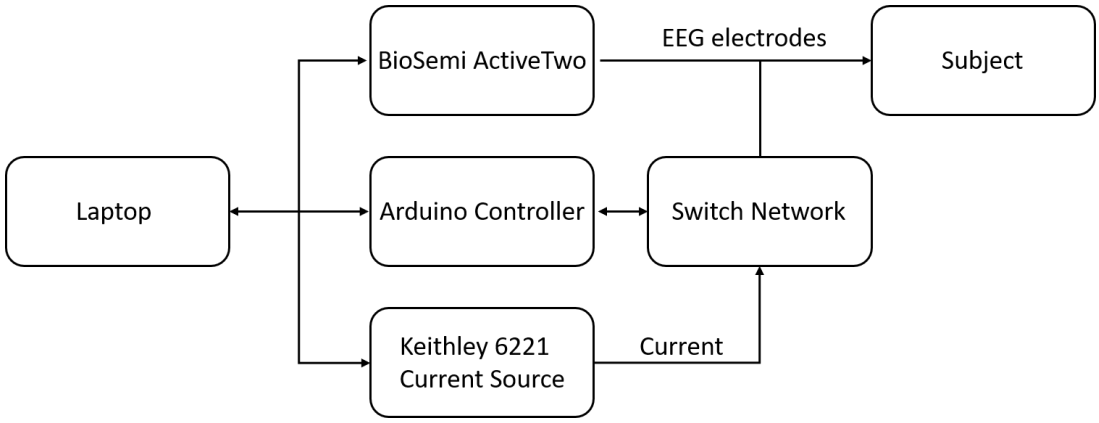

Figure 2-2. ScouseTom, an overview of the system. The equipment commercially available is Keithley 6221 current source, BioSemi ActiveTwo EEG amplifier, laptop with BioSemi and Matlab software and EEG electrodes. The remaining elements were developed in our group (Dowrick et al. 2014).

ScouseTom has a relatively low noise of 0.06% of the mean voltage. It is able to accurately source AC current at 100 kHz and up to 100 μA amplitude. Depending on individual needs, it can be configured to use at 16, 32 or 128 channels at 16 kHz sampling rate and signal bandwidth between DC and 3.2 kHz. The frequency of the injected current is currently limited by the BioSemi amplifier bandwidth to <2 kHz. Data processing must be done offline, due to the BioSemi amplifier capable to store the unprocessed voltage data for all the channels only.

Therefore, when measurements at higher frequencies, above 2 kHz, are required, yet a different EIT system, capable to acquire the data at the higher sampling frequency, has to be used. Current injected at higher frequencies is beneficial for EIT measurements, as it influences the ease, through which current passes through tissues. When frequency increases, charges can pass backwards and forward faster, so that a higher amplitude of the current can be used safely and, hence, better signal-to-noise ratio can be achieved (Holder, 2005). In addition, contact impedance decreases if current density increases at higher frequencies, thus also reducing the noise levels.

One of the EIT systems that are capable to inject at higher frequencies is the commercially available SwissTom (SwissTom AG, Switzerland). This EIT system was used in most of the experiments described in this chapter. SwissTom is available to use in respiratory system diagnosis and monitoring physiology and pathology of lung activity (Wolf et al. 2013). SwissTom is capable to produce up to 50 images per second, so it is much faster than the old HP EIT. The operating software is clear and easy to use, and the device is light and easy to move for clinical applications. To accelerate EIT applications, a new product, the EIT Pioneer Set, has been developed by the SwissTom AG Company for research purposes, and in further description in this chapter, whenever used the SwissTom system name, it always refers to the EIT Pioneer Set. EIT Pioneer Set is a plug-and-play package of software and hardware, designed to run and collect datasets without engineering qualifications or training. It has an internal ground and reference, consists of a Sensor Belt (Belt Bus) with 32 clips, a Sensor Belt connector, and software to process the data and show the results via the Ethernet cable connection (Figure 2-3).

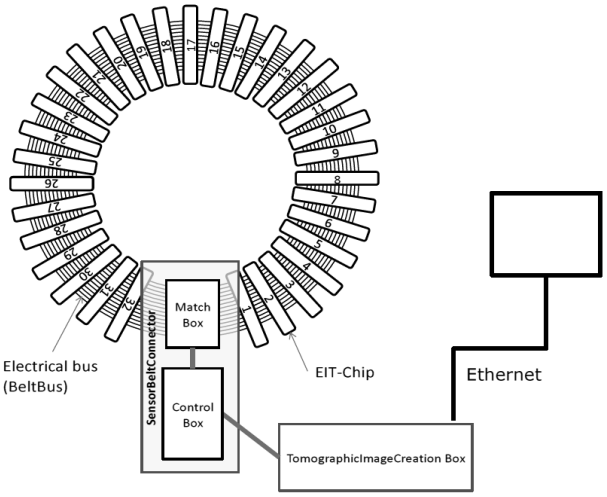

Figure 2-3. SwissTom, an overview of the system. The Belt Bus has built-in electrode clips for chest electrodes connection. Inside the Sensor Belt Connector, a Match Box and a Control Box with Tomographic Image Creation Box set current injections, demodulate the signal and remove the artefacts (EIT Pioneer-Set hardware overview provided by SwissTom AG).

The Sensor Belt connector injects current, but it is also used for data demodulation and artefacts removal during the recordings so that real-time images could be produced. However, the last setting can be only used for lung applications, for which SwissTom was initially developed and is currently clinically approved. The main advantage of using SwissTom over ScouseTom is its ability to apply a current of up to 10 mA amplitude and 250 kHz frequency. It is advantageous for measured signal-to-noise ratio and it would not have been possible with the BioSemi amplifier in ScouseTom. However, the main drawback of using SwissTom is the design of the Sensor Belt. It was developed to use for lung activity monitoring so that the belt is constructed to surround the human chest, not the head. In order to perform brain EIT, we had to adjust the belt with additional connections, via crocodile clips to the EEG box, for scalp electrodes. Such connection will cause additional noise in the recordings and might produce various technical artefacts.

2.1.4.2 Image reconstruction method

The reconstruction algorithm in EIT is used to transfer the raw voltages measured from the surface of the head into the conductivity changes inside the brain. The reconstruction process involves two major steps. First, a forward model is used to predict a current flow and voltage measurements based on the current injection protocol and internal conductivities of the head, which results in the generation of the sensitivity, Jacobian, matrix. Then, the matrix is inverted to get the approximate internal conductivity distribution. Inverse problem for EIT is ill-posed, so the image reconstruction needs to be regularised.

The first problem, involving prediction of the current flow, requires an accurate representation of the 3D head geometry in order to precisely incorporate the conductivities of different regions. However, a very detailed and realistic representation of the head geometry makes the computational process of a forward solution very complex and time-consuming, as described in detail in the following chapters. If a simple geometry model, such as a sphere, is assumed, the voltage

distribution and current flow can be calculated analytically, whereas, for more complex structures, a numerical method has to be applied. In the previous EIT experiments, including Tidswell's study (2001), a simplified version of the algorithm was used, in which the head was modelled as a homogeneous sphere of uniform conductivity for all layers. This was clearly an oversimplification, as all tissues, including those forming a human head, have different conductivity and anisotropy properties. Hence, an implementation of more accurate head model has already been shown to produce better images (Bagshaw et al. 2003; Tizzard et al. 2005). Furthermore, a new way to create subject-specific, realistic meshes of human head from CT or/and MRI images has been recently developed in our group to improve EIT reconstruction (Jehl et al. 2016).

Forward solution for more sophisticated meshes is calculated using the finite element method (FEM). FEM is a numerical method, in which the total volume of a head is divided into many small elements of known geometry, for instance, tetrahedrons or hexahedrons, and then the potential for each of them is calculated individually in order to provide the distribution for the whole head. These calculations for brain EIT are now made with a newly developed Parallel EIT Solver (PEITS) programme (Jehl et al. 2014). The sensitivity matrix contains the voltages for each combination of independent measurements of given electrode pairs from the boundary recordings in each voxel. To get approximate conductivity distribution, this matrix has to be inverted. Inverse problem for EIT is ill-posed, due to a difference between a number of elements in the mesh and electrode combinations that measure changes. In practice, this means that small changes in the measurements can affect the reconstruction and show up as large changes in the image (Holder, 2005). Hence, in order to reconstruct the image, the method is normally stabilised through regularisation. The common methods used for this purpose are truncated singular value decomposition (Bagshaw et al. 2003) or Tikhonov regularisation (Vauhokonen et al. 1998). The most recently developed regularisation method, which is currently

used in our lab, is the zeroth-order Tikhonov regularisation with which cross-validation is used to set the hyperparameter (Aristovich et al. 2014). Once the optimal parameter is set, the Jacobian matrix can be inverted. In addition to this regularisation method, a novel approach to optimise image post-processing has been also recently developed in our lab. This method is based on a noise *t-score* correction, in which the standard deviation of conductivity changes in each hexahedron is computed using an inverted Jacobian matrix (Aristovich et al. 2014).

2.1.5 Purpose

The purpose of this chapter was to produce images of visually evoked activity using EIT and scalp electrodes in humans.

The questions that we set out to answer were:

Are there reproducible scalp impedance changes in the raw EIT signal that can be related to the visual stimulation?

If there are reproducible changes, can they be reconstructed into physiologically plausible images?

2.1.6 Experimental design

The experiment was conducted on 10 healthy subjects. Recordings obtained from the first three subjects were used to optimise the paradigm and then, the data from the following seven subjects were further analysed and described in detail. A contrasting black and white checkerboard was used in a boxcar paradigm for the visual stimulation and repeated to average the signal (Figure 2-4).

All EIT measurements were performed with 32 EEG electrodes clipped to the adaptors on a nylon elastic cap. Using the elastic cap and fitting the electrodes to the cap is helpful to ensure the consistent placement between the subjects and aids localisation of the electrodes in the data post-processing. Such a setup has been proved beneficial over the conventional EEG electrodes for the prolonged

recordings, and it is now successfully used in our lab for human recordings in previous studies (Goren et al. 2013; Avery et al. 2017; Goren et al. 2018).

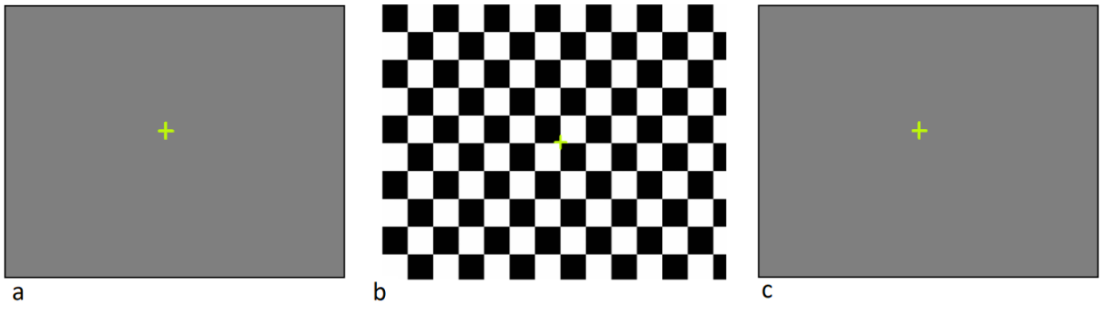

Figure 2-4. A visual stimulation set in a boxcar paradigm. Visual stimulation (a reversing checkerboard at screen 'b') was presented for a limited time to locally increase the blood flow and volume in the activated brain region. A baseline period without the stimulation was set before and after the checkerboard (screen 'a' and 'c'). Such a stimulation set was repeated several times, between 20 and 60 depending on a subject, to average the signal. Green cross in the middle of the screen kept subjects' gaze and attention focused during the experiments.

Two EIT systems were tested during experiments; ScouseTom and SwissTom. The former was used for the initial data collection on one subject, however using low-frequency current resulted in relatively noisy data and possible errors related to the skin impedance (Rosell et al. 1988) and hence, to maximise the signal-to-noise ratio, only SwissTom was used for further measurements.

2.2 Methods

2.2.1 Subjects

Overall, the measurements analysed further were performed on 7 healthy subjects, between 18 and 33 years old (median 25), with no history of neurological disorders and who had given informed consent to participate in the study. The study was approved by the local ethics committee; the volunteers were recruited from people working in the Medical Physics department at the UCL and they did not receive any award for the participation. Data from one subject were collected with the ScouseTom EIT system; the remaining six with the SwissTom. During the

experiments, the subjects were sitting on a comfortable office chair, with their back fully supported and a travel air pillow around their neck used to reduce head movements and subsequent muscle artefacts.

2.2.2 Data acquisition

The experimental set was in a block paradigm. It comprised of an initial baseline period, a stimulus, and a final baseline. For the ScouseTom recordings, these phases were 40-75-40 seconds respectively; repeated 20 times to average the signal. For the SwissTom measurements, the scheme was 20-20-40 seconds, so that the initial baseline and the stimulus was set for 20 seconds, except a single case when the initial baseline was measured for 10 seconds, each followed by a 40-second final baseline; the measurement was then repeated 30 to 60 times to average.

Regardless of the system used, all measurements were made with 32, 12 mm-radius, Ag/AgCl EEG ring electrodes secured on the elastic EasyCap (EasyCap ® Germany, Figure 2-5 for the montage). To minimise the electrode-skin impedance, remove any potential dirt or grease from the skin surface and the external, *stratum corneum* layer of skin cells subject skin was pre-prepared prior the electrode placement (Rosell et al. 1988). The skin was rubbed with ethanol and cleaned with an abrasive gel (NuPrep, Weaver and Company, USA), using a fresh cotton bud at each stage. Next, the electrodes were clipped to the cap and a conductive EEG paste (Elefix, Nihon Kohden, Japan) was applied with a syringe to fill the space between the skin and each electrode. The maximum accepted contact impedance of an electrode was 500 Ω and, in case the contact impedance was too high, the electrode was reapplied. Once all electrodes were placed, the cap was secured with a chest belt to reduce movements of head and neck. Even though such preparations were time-consuming and required more effort than a standard EEG electrode placement in clinic, they were necessary to maintain a good contact impedance and collect reliable data. However, as the montage was designed by the EEG Company (EasyCap® Germany) to match the modified International 10-20 Electrode Positioning System (Oostenveld and

Praamstra 2001), hence no expert technical knowledge was required when applying the electrodes. In the ScouseTom measurements, two additional electrodes for ground and reference were placed on the forehead (10 mm radius Ag/AgCl EEG cup, Micromed Electronics Ltd, England).

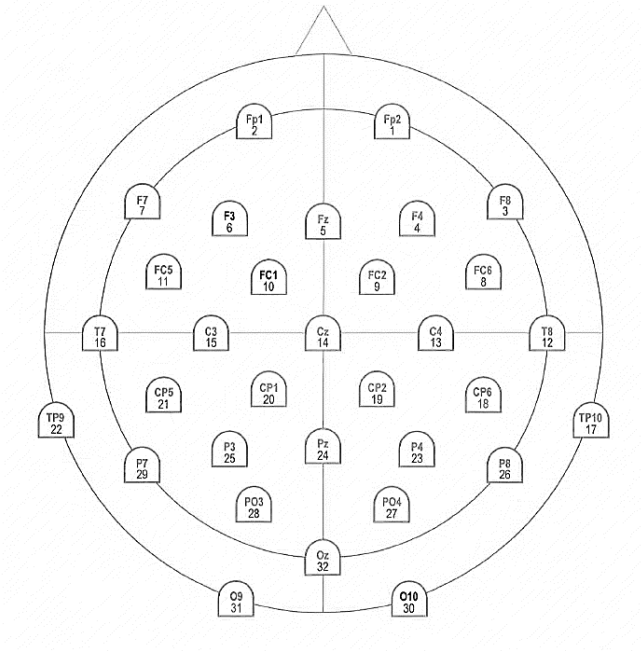

Figure 2-5. EasyCap and the locations of 32 electrodes seen from the top of the head; the nose of the subject is at the top of the picture. The montage corresponds to the modified 10-20 International System (Oostenveld and Praamstra 2001).

In total, there were 31 polar drive injections of 250 μA at 1.725 kHz current per each measurement cycle (a frame), each lasting 50 ms. During each cycle, the signal was measured by 930 individual channels. All the measurements were made with respect to the reference electrode. The recordings with SwissTom were collected with the current of 10 mA amplitude at 195 kHz injected for 20 to 60 ms through a pair of electrodes. The voltages were recorded at all of the other 30 electrodes, forming 928 measuring channels per cycle.

The recording period for the whole stimulation set was 155 seconds (ScouseTom) and 80 seconds (SwissTom) with 5 to 95 frames (full image data set) per second and repeated for averaging up to 60 times per subject.

2.2.3 Paradigm

Visual responses were evoked with a 0.6° black and white checkerboard reversing at 8 Hz presented 70 cm in front of the subject on a laptop screen. The sensory stimulation was controlled by Matlab code using the PyschToolbox (http://psychtoolbox.org/) to adjust the check size, focusing point, green cross, and the stimulation latency. All subjects sat at rest in a darkened room and they kept their eyes opened and focused their gaze on a cross in the middle of the screen during the whole experimental period. This setup was very similar to the one used by Tidswell (2001).

2.2.4 Data analysis

When an experiment was finished and the data downloaded, the impedance signal in both voltage and percentage changes from the mean of the baseline was calculated in Matlab. Then, image reconstruction was attempted. This followed data analysis described in the only previous study on this topic (Tidswell et al. 2001).

In SwissTom hardware, the signal was already bandpass-filtered with a bandwidth of 10 kHz (± 5 kHz each side of the carrier), with a further high-pass filter (cut-off 40 kHz) and anti-aliasing low-pass filter (cut-off 1.4 MHz) before the analogue-to-digital converter (ADC). At the data reading stage, all injecting electrode combinations, which included the current conveying channels, were excluded due to high voltages on the recording electrodes. As the aim of this experiment was to record slow changes in the brain, a software filter of 1 Hz was applied (3^{rd} order Butterworth). The linear drift was then removed using a linear correction for each channel. Once these preliminary preparation steps were finished, all recorded trials from a subject were grouped together to average over the epochs and in a form of

one file. Then, all the channels were assessed for a significant change. Once the significant channels had been found, they were then divided into two groups representing either, a positive or a negative change, for which the mean of the signal was greater or smaller than zero respectively, in order to calculate the maximum change and plot the change with respect to the sensory stimulation.

2.2.5 Image reconstruction

For all subjects, the same 3.5 million tetrahedron head mesh was used to model the tissues of the human head in order to compute the forward solution and generate the sensitivity matrices. The resolution of the mesh was very fine (0.5 mm size) over the electrode sites and become coarser (up to 4 mm) deep in the head. Conductivities were set to 0.3 S/m grey matter, 0.15 S/m white matter, 1.79 S/m cerebrospinal fluid, 0.018 S/m skull, 0.44 S/m skin and other tissues and 0.0001 S/m air. To reconstruct changes, a separate 10 mm and 3392 hexahedral element mesh was generated. In order to stabilise the reconstruction process, the zeroth-order Tikhonov regularisation was applied and noise-based image post-processing.

2.2.6 Statistics

In order to find out whether the recorded change is significant in a sample and if it can be related to the visual stimulation, the average and the standard deviation of the impedance signal samples across trials were computed at each time point for each subject and expressed in both voltage and percentage change from baseline.

A significant change was defined as a response across trials when the mean of the channel was greater than 3 standard errors. In addition, the response after averaging had to be significant with respect to the baseline ($T<0$) $p<0.001$ (one-sided). The employed statistical analyses were analogical to the method used in the previous study (Tidswell et al. 2001) and consistent with the approach currently used in the brain EIT. The signal to noise ratio (SNR) was calculated for the averaged signal during stimulation and noise being the standard deviation from the baseline voltages

for a subject for all experimental trials and all electrodes. The SNR was calculated for positive and negative channels separately. All results are expressed as mean ± 1SE unless otherwise stated.

2.3 Results

2.3.1 Scalp changes

2.3.1.1 ScouseTom (one subject)

Both, an increase and a decrease of the recorded impedance signal was noted. 15 (1.6%) out of 930 recording channels, had a significant impedance change, with a positive change in 10 channels, negative change in 5 channels. The recorded increase in the impedance signal was 0.4 ± 0.02 µV (0.1 ± 0.05%) and the decrease was -0.3 ± 0.02 µV (-0.1 ± 0.05%) (Figure 2-6).

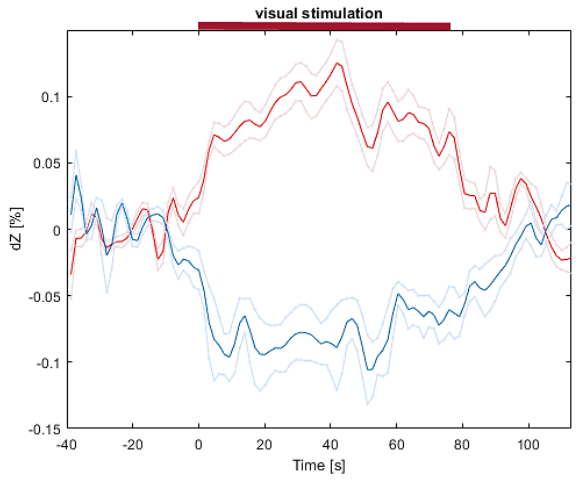

Figure 2-6. ScouseTom measurements with 250 µA at 1.725 kHz current. The figure shows a time course of the peak increases and decreases in the percentage impedance change (dZ) during visual stimulation (red line at the top of the graph). The impedance change is expressed as mean ± 1SE for significant channels.

2.3.1.2 SwissTom

Significant impedance changes, as well as both, the increases and decreases in impedance signal were recorded for all six subjects. Significant changes were

recorded on 8.5 ± 3.3% (mean ± SD) of all 928 measuring channels. The increase and decrease in impedance during the stimulus period were 0.2 ± 0.07 µV (0.2 ± 0.08%) and -0.2 ± 0.09 µV (-0.2 ± 0.07%), respectively (Table 2-1, Figure 2-7). The SNR was 7.6 ± 0.8 for positive and 0.7 ± 0.3 for negative channels.

	All channels	**Positive dZ change**		**Negative dZ change**	
	(*) channels	(*) channels	Mean ± SE [%]	(*) channels	Mean ± SE [%]
1	100	72	0.1±0.01	28	-0.2±0.2
2	72	34	0.1±0.04	38	-0.2±0.07
3	78	49	0.1±0.04	29	-0.2±0.16
4	78	14	0.1±0.03	64	-0.04±0.02
5	26	25	0.1±0.04	1	-0.1
6	117	45	0.3±0.1	72	-0.2±0.02

Table 2-1. Significant channels in SwissTom recordings for each subject respectively. The total number of 928 channels was recording signal. (*) marks number of significant channels, 'dZ' is for impedance change.

Then, a comparison if the significant channels were consistent among the subjects, i.e. whether the same channels were significant for more than one subject (Figure 2-7). Seven pairs of electrodes showed a significant signal among three different subjects and many more pairs showed a significant change in two subjects. However, when the location of these 7 channels was investigated further, it did not appear to align with the occipital area in the brain, where the activity was expected.

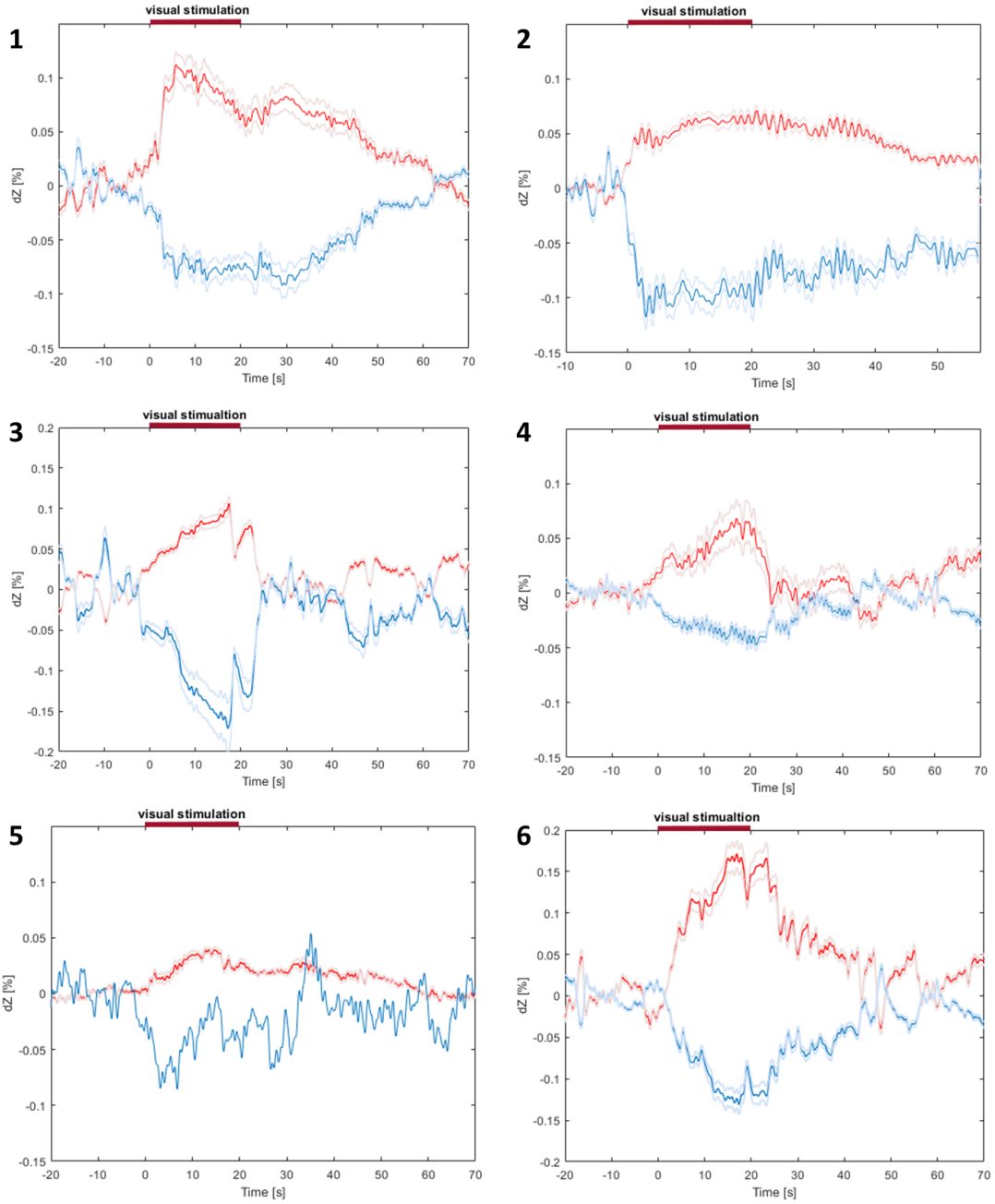

Figure 2-7. Averaged recorded voltage changes for each subject. In each graph, the bold lines show the mean of the signal (dZ; red line – positive, blue line – negative) from the significant channels ± SE (lighter lines). Averages for the subjects were 40, 40, 30, 45, 45, 60 for subjects 1, 2, ,3, 4, 5, 6, respectively. The red bracket at the top of each graph indicates when the visual stimulation occurred.

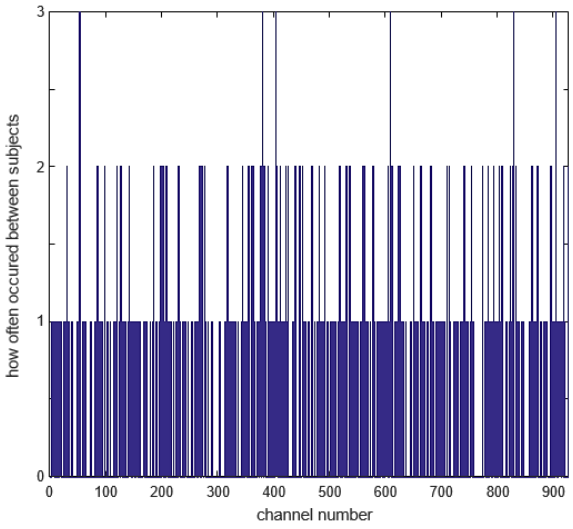

Figure 2-8. The instances of a significant signal from each channel in all subjects. The x-axis shows, whether a significant signal was measured in a given channel (one of 928) for any of the subjects, the y-axis represents for how many subjects a particular channel recorded a significant change.

2.3.2 Reconstructed images

2.3.2.1 ScouseTom

The images generated were very noisy and no significant impedance change could be reconstructed in the occipital area of the brain, where the response to the visual stimulation was expected (Figure 2-9).

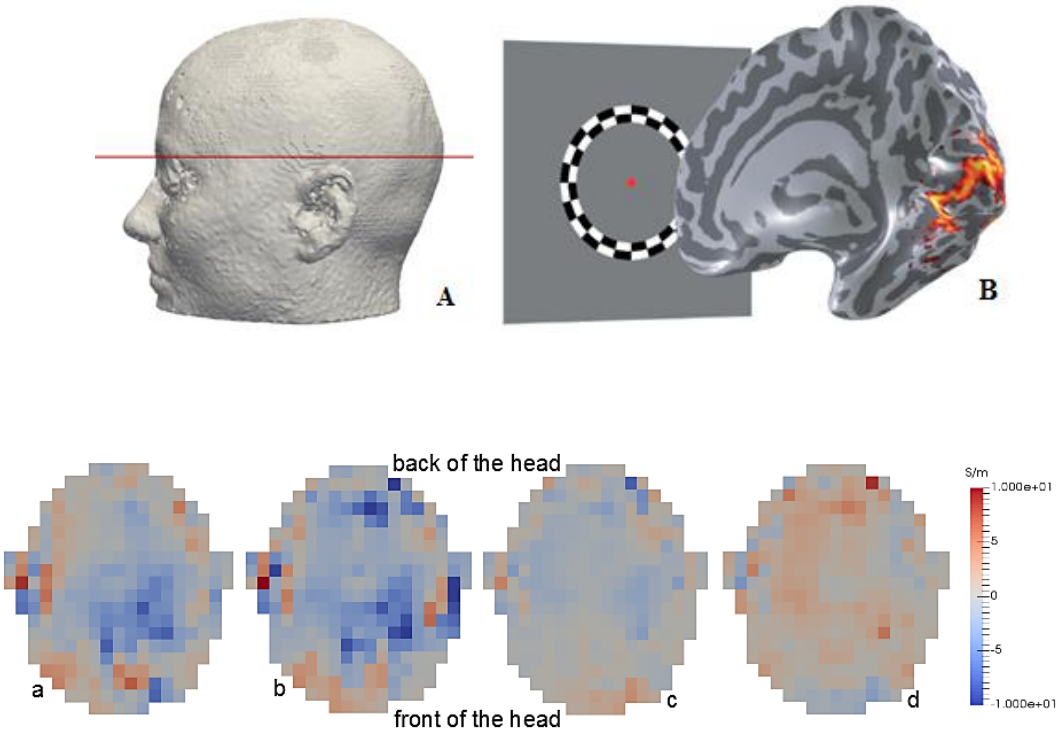

Figure 2-9. EIT images of evoked activity recorded with ScouseTom as axial sections of the reconstructed images. Top panel: (A) The human head mesh used for the reconstruction of the data for all subjects, recorded with ScouseTom and SwissTom. The red line shows the level of an axial section for images presented below. (B) shows where the expected activation due to a visual stimulation should be placed in the brain (occipital cortex, mainly the calcarine sulcus region, here one hemisphere) (Wandell et al. 2010). Lower panel: EIT reconstruction. Picture 'a' and 'd' show the images during the baseline period (in the middle of the baseline), before and after visual stimulation set respectively, 'b' image is 20 seconds after stimulation started and 'c' is after 40 seconds of the stimulation. The scale shows impedance increase (red) and decrease (blue) in standardised units (S/m, t-score based noise correction). All images are noisy and there is no significant activity in the occipital region reconstructed.

2.3.2.2 SwissTom

Similarly, the data reconstructed only as very noisy images for all 6 subjects - there was no significant impedance change over the occipital cortex that would correspond to the known region of visual stimulation (Figure 2-10).

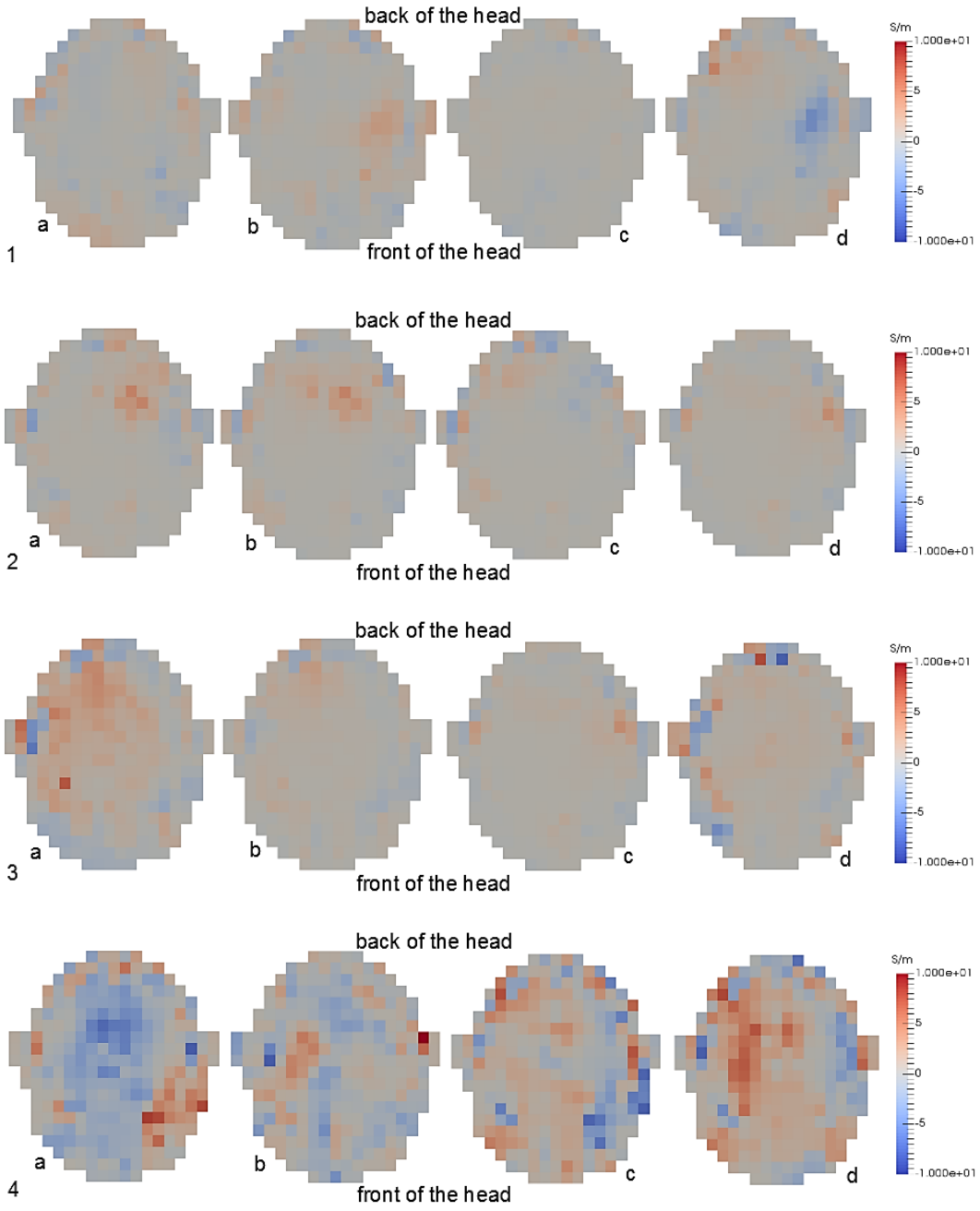
back of the head
front of the head
a
b
c
d
1
2
3
4
S/m
1.000e+01
5
0
-5
-1.000e+01

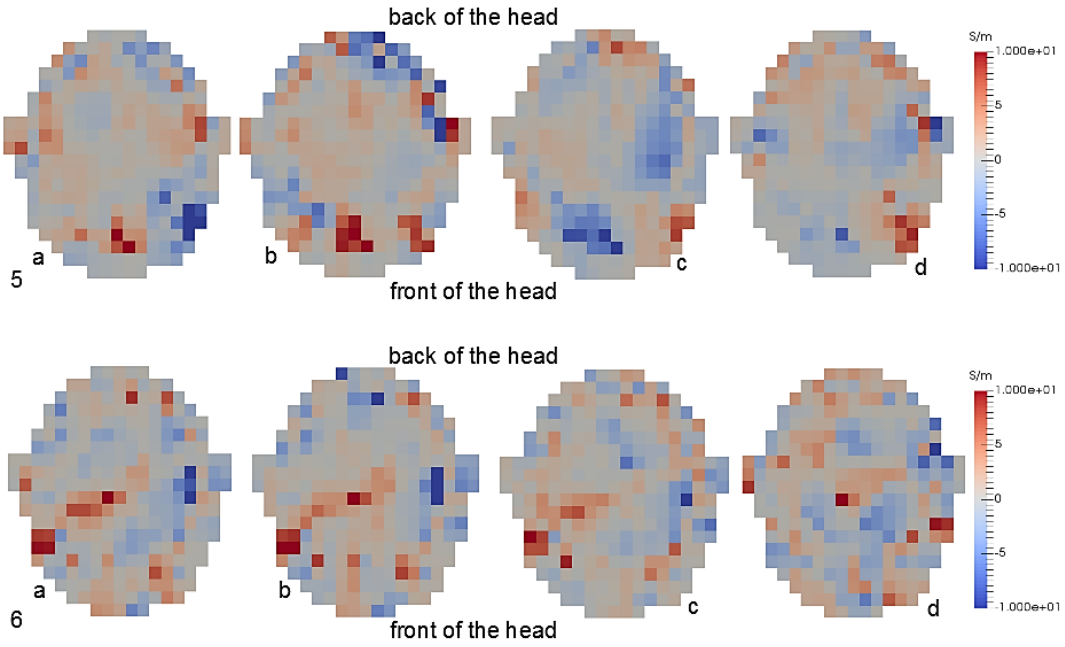

Figure 2-10. Reconstructed extracranial EIT images of the evoked activity. The images present 4 sections for each subject during a visual simulation: 'a' is a baseline before the stimulation (half time of baseline), 'b' is 10 seconds after the stimulation started (the expected maximum change point), 'c' is 20 seconds after stimulation started, which is the moment when the checkerboard switched to blank screen and 'd' is the baseline after the stimulation (half time of baseline). Images were noisy with both positive and negative changes that were spread all over the head, without any clear localisation over the occipital lobe. The scale shows impedance increase (red) and decrease (blue) in standardised units (S/m, t-score based noise correction).

2.4 Discussion

2.4.1 Summary of the results

This study demonstrates that it is possible to record significant impedance changes of a few tenths of a percent above the noise level in the raw signal. These observed changes were both negative and positive. The shape of the response was relatively similar to the one reported before by Tidswell et al. (2001). However, the obtained images were noisy and did not show accurate localisation of the change with respect to the stimulation. This is also in line with the previous human studies with extracranial electrodes by Tidswell et al. (2001).

2.4.2 Technical issues

Although the higher levels of current injected with the SwissTom might have improved the strength of the observed signal, the system itself could be the main reason for the failed reconstruction attempt. In contrast with ScouseTom EIT system, the design of the SwissTom does not allow the end-user to implement any modification to what or to combine it with another computer to measure the impedance changes and show the visual stimulation simultaneously. Also, due to the system limitations, the paradigm presented in this study, the checkerboard used as a visual stimulus, had to be activated manually by the experimenter, in parallel to the current injections start point, but outside of the sight of a subject. As a potential mismatch between the starting point of the measurements and stimulation cannot be measured accurately, the first repetition of stimulation set was removed, and thus, more repetitions of the set had to be performed for signal averaging. Also, subjects complained that the visual stimulation was quite monotonous and hence, breaks were required that prolonged the experiment and increased the boredom and tiredness of the subjects. Tidswell et al. (2001) reported similar problems in their study. In comparison for ScouseTom, it was possible to implement current injections paradigm into the code controlling the checkerboard, which was definitely an advantage.

The SwissTom EIT system is also limited by its designed application for chest imaging. It has a fixed number of 32 electrodes and the internal ground and reference that make the system less flexible for the scalp measurements. For our purposes, it was necessary to modify the connection to the system, to adjust electrode belt for the recordings with EEG electrodes. The SwissTom Company provided a specially designed sensor belt with EIT clips for the chest measurements, which filters and demodulates the signal automatically. In this study, it was impossible to connect the belt directly to scalp electrodes on the head but the measurements without this belt were not possible either, due to the design of the system. Hence, the EIT clips had to

be attached to the EasyCap electrode connector indirectly via the crocodile clips. This additional connection, however, might have caused artefacts and increased the noise of the recordings.

2.4.3 Is the reproducible scalp impedance change related to visual stimulation?

The detected changes in the raw impedance signal are significantly affected by the artefacts. Although the size of the changes we observed is smaller in general when compared with previously described (Tidswell et al. 2001), a close look at the response shape shows the major differences between the subjects. Based on the literature review on BOLD fMRI and PET response, we expected the peak of the signal to be recorded roughly at 5 to 7 seconds after the stimulation started and return to the baseline within 10 seconds without any stimuli (Fox et al. 1986; Belliveau et al. 1991; Zeki et al. 1991; Kwong et al. 1992; Tootell et al. 1996; Ito et al. 2001). This is not consistent with the result from this study, where for some subjects the peak appeared by the end of the visual stimulation i.e. after 20 seconds from the stimulation onset, and returned to the baseline within approximately 10-15 seconds (n=4 subjects), whereas for others, the signal was recovering for approximately 40 seconds or even, was masked by the following simulation set (n=2).

In addition, we would expect that the electrode pairs recording significant impedance change would have been consistent between the subjects and also, align with the occipital area of the brain. However, for all 928 measuring channels, there were only total seven electrode pairs that reported a significant change in three different subjects and no pairs that would have shown a significant change in four or more subjects. Furthermore, none of these seven pairs was consistent in localisation with the occipital cortex. The vast majority of the channels reported as significant had a change only in a single subject. Taken together, these observations suggest that the recorded change is probably largely random and affected by factors of unknown nature, rather than the actual real response of the brain to the stimulation.

Finally, the comparison between the obtained SNR ratios between the positive and negative channels confirms that the signal recorded is highly affected by various artefacts. Previous studies on evoked activity in animals and humans showed that both types of change can be recorded with EIT; i.e. an impedance decrease related to regionally increased blood flow in a stimulated area of the brain, and an impedance rise probably appearing due to other physiological changes happening in the brain at the same time (Holder et al. 1996; Tidswell et al. 2001). The comparison between the SNR ratios for positive and negative change recorded in this study suggests that the measured decrease in the signal is significantly noisier than the positive change. The SNR measured for the negative significant channels was very low (0.7 ± 0.3) in comparison to the positive channels (7.6 ± 0.8). Hence, the expected physiological change upon stimulation associated with the negative change in the impedance is likely dominated by artefacts. This makes accurate reconstruction impossible at this point.

2.4.4 What are the possible mechanisms underlying the observed EIT signal changes?

In general, an increased regional blood volume and a blood flow are the main mechanisms responsible for the impedance change related to a periodical sensory stimulation in a healthy brain (Holder, 2005). In comparison with the surrounding brain cortex, blood has significantly lower resistivity, thus the regional impedance decrease is expected as a result of the sensory stimulation. However, there are also other physiological factors, appearing in the other regions of the brain, that can influence a recorded EIT signal causing either its rise or its decline.

One of the most likely physiological sources of the observed artefacts can be related to the movement of CSF (Holder, 2005; Vollmer-Haase et al. 1998). With a total volume of up to 150 ml, CSF can be found outside and inside the brain and in the spinal cord. CSF surrounds the subarachnoid space and fills the ventricular system and brain sulci. In a healthy brain, CSF is a clear liquid with the high ionic

concentration, which makes it extremely conducive in comparison to other tissues of the head. All these features lead to a significant impact of CSF on the voltages recorded through the head. In our study, CSF was segmented as a separate layer; however, its flow all over the brain could still have had an important impact on the raw impedance measurements and have introduced artefacts and location errors into images.

The less likely reason for the high noise levels observed in our study might be the local change in the temperature of the activated region of the brain. When the temperature rises, the impedance decreases (Holder, 2005). This influence was assessed as about 2-3% change for a 1˚C (Li et al. 1968). Also, some *in-vivo* and functional imaging studies suggest that the prolonged sensory stimulation can lead to a local rise in the temperature, of a value up to 1˚C (McElligott and Melzack, 1967; Yablonsky et al. 2000). However, even if the heat is produced by the regionally increased oxygen consumption, it is probably relatively quickly cooled by the after the flow of blood and CSF due to the general tendency of the brain to maintain homoeostasis. Hence, the influence of temperature on the observed EIT signal is likely negligible.

There are also non-physiological factors that can be detected with the EIT system and that might have contributed to the increased noise. The measurements in our study were made with the standard EEG electrodes, which are designed to record cortex activity but that can also catch other electrical activities from the surroundings. Artefacts in the EEG recordings might occur either due to physiological signals such as cardiac, ocular, and muscle activity as well as sweating or as a result of technical issues including a possible influence of external electric fields and electrode artefacts (Urigüen and Garcia-Zapirain 2015). Since the same electrodes are used for EEG and EIT boundary voltages measurements, the same artefacts can affect both types of equipment. For example, it has been demonstrated before, that the movement artefacts during seizures can significantly obscure the

expected EIT signal, making the measurements practically impossible (Fabrizi, et al., 2006). In addition, the local skin-electrode impedance, which is influenced by various factors, such as the biological activity of skin, like sweating, significantly affects the recorded EIT signal (Holder, 2005). As described before, in this study the contact impedance was checked and electrodes reapplied, if necessary, before each round of stimulation in order. This, however, could not rule out possible contact impedance artefacts resulting from increased skin activity after the experiment was started. Furthermore, the recorded signal can also be disturbed by the movements of other people in the same room (Tidswell et al. 2001) but again, this source of the artefact was reduced to a minimum, as the only person in the room was experimenter, who sat still over the entire experiment.

In order to eliminate potential sources of artefacts, all EIT recordings were conducted in the same darkened room; the electrodes were fixed with the EasyCap and a chest belt to an additional reduction of any potential movements, and all subjects were instructed, how to behave during the experiment, i.e. they were required not to move or talk and to keep their jaw relaxed, in a slightly opened position, during the whole session. Subjects were also asked to focus on the small cross in the middle of a screen during the experimental session in order to reduce eye movements. Experimental conditions were checked and controlled all the time and, if problems had arisen, e.g. subject closed eyes for longer than an eye blink, the trial was rejected from further analysis. Despite these preventive measures, the study still experienced the artefacts of various nature that significantly affected the results.

2.4.5 If the changes are present, did they reconstruct into reliable images?

In a similar way as in the previous study (Tidswell et al. 2001), it was not possible to reconstruct the recorded significant changes in the measured raw impedance signal to accurate images for any of the subjects. The obtained images failed to demonstrate

a reliable localisation of impedance change in the areas expected to be stimulated by the visual stimuli. There are several possible explanations for these results.

First, the problems with image reconstruction could have been expected due to the low signal to noise ratio in the raw data. The main barrier, which obstructs recording an accurate impedance signal above the noise level, remains the skull (Tidswell et al. 2001). According to the literature, the skull resistivity takes considerably different values for a dry skull (6.7 kΩ/cm to 7.5 kΩ/cm) and a skull immersed in 0.2% saline (approximately 20.5 kΩ/cm) (Pant et al. 2011; Tidswell et al. 2003). For a living skull, the saturating solution that changes its total resistivity is composed of blood, bone marrow and connective tissue, likely resulting in resistivity significantly higher than 20 kΩ/cm. The mean resistivity of a scalp (after removing the capacitive *stratum corneum* layer, Holder 2005) is 2.5 to 3.3 kΩ.cm (Yamamoto and Yamamoto 1976) and the total combined brain, i.e. CSF plus white and grey matter, resistivity is approximately 0.35-0.39 kΩ.cm (Lattikka et al. 2001). All these values show that the skull clearly has the largest impact on the head resistivity and it is a matter of question, whether it will be possible to overcome this problem and maximise the flow of current inside the brain with only scalp EEG electrodes for EIT recording in future.

2.4.6 Conclusion and future work

There were significant changes in impedance signal above the noise level measured with the scalp EEG electrodes and either of the EIT systems; ScouseTom and SwissTom. However, not only an expected decrease in the signal was recorded, but also an increase, suggesting that some other physiological mechanisms or artefacts could have influenced the EIT recordings. Furthermore, it was not possible to reconstruct the recorded impedance signals into reliable images.

In this project, the slow impedance changes caused by increased regional blood flow and blood volume were probably obscured by other phenomena of both

a physiological and technical nature. Further development of the system, which will allow injecting safe levels of current at higher frequencies with low noise, seems to be a necessary step to overcome these obstacles. However, it is possible that the high resistivity of a human skull might still remain an impenetrable barrier to accurately record and image impedance changes with scalp EIT during physiological activity. Therefore, an important next step would be to test the method with intracranial electrodes, and this is what the next chapters of this thesis are devoted to.

Future work on improving scalp EIT should be focused on further improvements to the EIT system itself. Development of the system so it can inject higher levels of current, a wider spectrum of amplitudes and which is also flexible enough to change a number of electrodes or implement any additional software, such as sensory stimulation, can be beneficial. Potentially, a system, which allows injecting current at a wide frequency spectrum at the same time, could improve such recordings also.

Overall, the study described in this chapter indicates that imaging evoked activity recorded with EIT and scalp electrodes is currently impossible and cannot be used as a sufficient and competitive non-invasive method to image healthy brain activity in humans at least until very significant improvements in hardware are made. Hence, further improvements of the method from the physiological rather than technical perspective should be focused on intracranial studies.

Chapter 3

Feasibility of imaging epileptic seizure onset with EIT and depth electrodes

Overview

Imaging ictal and interictal activity with Electrical Impedance Tomography using epicortical electrode mats has been demonstrated in animal models of epilepsy in rats. In human epilepsy subjects undergoing presurgical evaluation, intracranial depth electrodes are often preferred for video-telemetry monitoring. The purpose of this work was to evaluate the feasibility of using such electrodes with EIT to localise epileptogenic zones in humans in a modelling study prior to the recordings in patients. The accuracy of the method was compared for seizure onsets simulated in several locations, for both types of impedance changes, i.e. 1% expected for neuronal depolarization over milliseconds (fast changes) and 10% for cell swelling over seconds (slow changes). The EIT outcome was then compared with the EEG source modelling and with visual spike detection as for SEEG reporting.

The positive outcome of this study had been crucial for the work presented in this thesis, providing a solid base to pursue EIT towards clinical recordings and using it in parallel with SEEG.

3.1 Introduction

3.1.1 Background

Patients with focal drug-resistant epilepsy can potentially benefit from resective surgery if the epileptogenic zone is clearly identified (Duncan et al. 2006). This identification process is performed with prolonged scalp EEG with video telemetry, epilepsy protocol neuroimaging, neuropsychology and neuropsychiatry (De Tisi et al., 2011; Duncan, 2011; Elger and Schmidt, 2008; Moshé et al. 2015; Noachtar and Borggraefe, 2009). It is estimated that scalp EEG, the current gold-standard method in epilepsy diagnosis, can sample only from a limited area of approximately 10-20 mm underneath the electrodes, and its sensitivity decreases significantly for deep sources (Merlet and Gotman 1999; Yvert et al. 1997; Cuffin et al. 1991; Cohen et al. 1990). Improved localisation can be obtained with intracranial EEG, using subdural

grids, strips (ECoG) or depth electrodes (stereo-EEG, SEEG) that have the highest spatiotemporal resolution among current clinical methods for seizure monitoring (Schindler et al. 2016; Benbadis et al. 2005). However, the main drawback of intracranial EEG is limited spatial sampling to the cortical regions adjacent to the recording contacts. The ability to detect the seizure source depends on the distance of the source from the nearest contact. The sampled area for each contact is approximately a 5 mm-radius sphere around the contact boundary (von Ellenrieder et al. 2012; Lachaux et al. 2003). It also depends on the orientation of the source, as described in chapter 1, a dipolar source will not register if oriented tangentially to electrodes, and the amplitude of the generator (Burle et al. 2015; Ramantani et al. 2013; Smith 2005; Teplan 2002; Ebersole 1991). Out of all invasive intracranial monitoring techniques, depth electrodes have been shown to carry the least risk for patients (Mullin et al. 2016). Hence, when possible, SEEG has recently been favoured over ECoG (Jayakar, et al., 2016). Still, the rates for post-surgical seizure freedom vary between 49% and 83% for temporal lobe epilepsy (De Tisi et al., 2011; Murphy et al., 2010) and 14.7% and 66% in extratemporal lobe epilepsy (McIntosh et al. 2012; Jehi et al. 2009). One of the reasons for early seizure re-occurrence is an incomplete or inaccurate localisation of the onset (Ryvlin and Rheims 2008) and so improvements in the localisation method could yield considerably better patient outcomes.

3.1.2 Rationale

The motivation for this work was the idea that EIT could be used with existing intracranial electrodes placed for SEEG. In such setting EIT could be used as a complementary tool to the existing EEG recording equipment on the clinical ward, with no additional risks for the patient. EIT is not sensitive to dipole orientation and could potentially provide better resolution compared to existing clinical methods. However, if only depth electrodes are used, the injected current might be too localised, and hence, the real onset may be missed. We therefore also evaluated the

advantages of concurrent use of scalp electrodes to improve coverage. If successful, the method could thus not only improve the onset localisation but also reduce the number of depth probes implanted.

Potential applications for EIT in epilepsy clinics could be lateralising the onset, such as a mesial temporal lobe onset in patients with bilateral hippocampal abnormalities or differentiating the lobe in patients with a fronto-temporal onset in scalp EEG. EIT could aid the localisation of onset in situations where scalp EEG can be misleading, such as in patients with a previous resection. Finally, identifying the onset in multifocal abnormalities or imaging interictal discharges and their propagation could be a useful tool in clinics.

3.1.3 Purpose

The purpose of this work was to determine if EIT could offer improved accuracy in localising the seizure onset zone in human subjects with epilepsy who had intracranial electrodes implanted for onset detection. This was examined in computer simulation for both fast and slow impedance changes known to occur during seizures. Specific questions to be addressed were:

Which electrode arrangement gives the best seizure onset localisation? 3 combinations were assessed – i) Intracranial depth electrodes only ii) Intracranial electrodes and 32 scalp electrodes iii) A reduced selection of available depth and scalp electrodes with enhanced sensitivity for a defined region of interest

Does the best of these three methods give improved seizure onset detection compared to the current intracranial method with a visual inspection of SEEG voltages or EEG inverse source localisation?

3.1.4 Experimental design

Patient-specific detailed Finite Element Method (FEM) head models were created from combined T1-weighted MRI and high-resolution CT scans for three epilepsy patients (Jehl et al. 2016). The three epilepsy cases considered had 7-12 depth

electrodes. Realistic conductivities of head tissues obtained from published literature were used (Malone et al. 2014; Romsauerova et al. 2006; Horesh et al. 2006). Conductivity changes imitating seizure onset were inserted into each mesh. These were spheres, 5 mm in radius (approximately 3cm^2 area), with -1% or +10% conductivity changes, representing the "fast" and "slow" impedance changes during seizures respectively (Vongerichten et al., 2016; Rao et al. 1997; Elzar et al. 1966). At least 90% of their elements were in grey matter with the rest being in the white matter, which is representative of the real onset zones (Concha et al. 2009). The size of the perturbations was chosen as a trade-off between a tissue volume which would realistically proceed to resective surgery and offering a more stringent test of the method than perturbations used in previous brain EIT studies. It represents the smallest tissue volume, which would be considered, and involves the destruction of the minimum anatomy important in the pathophysiology during epilepsy surgery. The FEM tetrahedral meshes were used in the forward calculation, while coarser hexahedral meshes were used for image reconstruction and to avoid the 'inverse crime' (Holder, 2005). Images were reconstructed using zeroth-order Tikhonov regularization with noise-based image post-processing (Aristovich et al. 2014). The regularisation hyperparameter was chosen automatically using leave-one-out cross-validation for each reconstruction (the forward solver https://github.com/EIT-team/PEITS, the reconstruction software https://github.com/EITteam/). The method has been developed at our lab specifically for brain EIT image reconstruction and it is now in standard use and the most efficient (Aristovich et al. 2016; Vongerichten et al. 2016; Faulkner et al. 2018; Hannan et al. 2018).

Specific terms used in the further part of this chapter can be defined as follows: "an electrode set" refers to the electrodes used in simulations – either depth, scalp or both. "A protocol" refers to an electrode addressing protocol. EIT images are generated from multiple transfer impedances, each collected from four electrodes: a constant current is injected to two and voltages are recorded differentially from two

others. Several hundreds such combinations are usually collected sequentially in order to give the largest set of independent measurements. The protocol is a list of such successive measurements. The protocol may be arranged so that the maximum current density is focused on a particular region of interest or spread over a wider area.

Three different EIT configurations were simulated: clinically implanted depth electrodes only (Depth Only), a mixture of depth and scalp electrodes (Depth+Scalp) and reduced number of depth and scalp electrodes (ROI-focused). The main aim of the third protocol was to test whether a considerably reduced number of injections could still provide useful information if focusing on maximum current density only on the pre-identified region of interest. This could be potentially helpful in the lobe or hemispheric differentiation (Benbadis et al. 2005). The validity of each EIT protocol was assessed by the location and shape errors of reconstructed conductivity changes in a simulation study.

The EIT results were compared to those obtained using EEG. To investigate the dependence upon source orientation, in each location, seizure sources were modelled as current dipoles, which were rotated through 190 different solid angles to cover the 360^0 range. The magnitude of the simulated sources was set such that a voltage of 2 mV was produced at an electrode 6 mm away, as this is a typical value encountered in clinical practice (Hufnagel et al. 2000). The source detection was evaluated in two different ways. The first was to simulate visual detection of a spike as undertaken by clinicians. A 250 μV threshold was set based on an assumption of 100 μV peak-to-peak background noise, equivalent to a significance of $p<0.01$, as a reasonable approximation for acceptance visual recognition of a spike against the background signal (Alarcon, 1996). Secondly, image metrics were calculated for EEG source modelling. In this model, the same meshes, conductivities and stabilisation methods were used to calculate lead-field matrices and for image reconstruction in the EEG inverse source modelling.

3.2 Materials and methods

3.2.1 Epilepsy cases

The study was based on the datasets obtained from three patients suffering from prolonged pharmacoresistant focal epilepsy. All patients underwent the procedure of depth electrode implantation, which was followed by seizure monitoring over days at the Telemetry Ward at the National Hospital for Neurology and Neurosurgery (NHNN), London (Table 3-1). In all three cases presented, findings from scalp EEG telemetry suggested frontotemporal epilepsy. There were 7, 11, and 12 depth electrodes implanted, with 48, 82, and 71 recording contacts in total respectively for cases one to three (Figure 3-2). Although in each case the onset zone was clearly recognised during telemetry, none of the patients proceeded with the resective surgery, due to a possibility of acquiring significant neuropsychological deficits.

Case	**1**	**2**	**3**
Gender	male	male	male
Age	39	46	29
EEG	right frontotemporal	right frontal	left frontotemporal
Depth electrodes	7 electrodes (48 contacts)	11 electrodes (82 contacts)	12 electrodes (71 contacts)
After SEEG	Right mesio-frontal	Right orbito-frontal	Insula
Proceed with resection?	No, neuropsychological deficits risks	No, neuropsychological deficits risks	No, focus close to anterior language area

Table 3-1 Medical background for three patients from whom imaging data were used in this study.

3.2.2 Mesh creation

3.2.2.1 MRI-CT segmentation

Realistic head meshes were segmented from joint T1-weighted MRI and CT scans using open source software (Seg3D, http://www.seg3d.org, 2015, MIPAV, http://mipav.cit.nih.gov/, 2015, CGAL http://www.cgal.org/, 2015, MedInria https://med.inria.fr/, 2015). The segmentation included 7 layers: SEEG contacts, grey and white matter, CSF, skull, air and scalp tissues. The segmentation method implemented was adapted from creating meshes in stroke EIT (Jehl et al. 2016).

First, both MRI and CT scans were uploaded into the Seg3D to assess the rotation mismatch between the images and, if necessary, the MRI scan was rotated with respect to the CT scan using the MIPAV software. The resolution of the scans was rescaled to 512x512x512 in order to get more pixels while smoothing the surfaces of the final mesh. The skull layer was segmented from the CT scan only (*thresholding* and *filling holes* tools in Seg3D). Depth electrodes were segmented with the *thresholding* and *connected component* tools from the CT scan. In some cases, there were severe artefacts coming from the EEG contacts in CT scans that masked and overlapped the adjacent electrodes, if observed, such contacts were separated manually. Electrodes were also separated from their entry point on the skull surface so that only recording contacts were included into an electrode layer (the *paint brush* tool). This step was more time-consuming, when many electrodes were located in a small region of the brain (e.g. orbitofrontal cortex) or when there were many contacts on one electrode, as it was more likely to generate the CT artefacts. All the layers that formed soft tissues were generated from the MRI scans. This stage was the most time-consuming and it significantly depended on the quality of the T1-weighted MRI scans. At first, all tissues that were inside the head were separated as an individual brain mask with the *Polyline* tool. White matter was selected with the *thresholding, filling holes* and *remove* from the surroundings and the same strategy

was used to segment the grey matter. The white and grey matter layers were inspected and corrected manually with the *paint brush* tool if needed. The CSF was subtracted with the *threshold* tool from the MRI scans and then with removing the other already created layers from a brain mask. In order to fill the holes between layers inside the brain with the CSF and prevent the overlapping of layers, the *dilating* and *removing* tools were applied. An additional layer of air inside sinuses and airways was created with the *thresholding*. All the other voxels in the head that did not belong to the skull, electrodes, air, white matter, grey matter or CSF made up a scalp layer but with respect to the location. Then, layers were smoothed with the *smooth binary dilate-erode* and *Boolean remove* tools. Seg3D software saved each layer under a number, which can later be unified if segmentation from imaging data for many cases is created and used for specifying the conductivity of tissues. The mesh creator required a different format of the file, so the final *.nrrd* format from Seg3D was changed to *.inr* format with MedInria software. In addition, the coordinates of the depth electrodes were exported as a Matlab file to locate each of the contacts in the mesh. The same method was then repeated for the imaging data of two other patients (Figure 3-1).

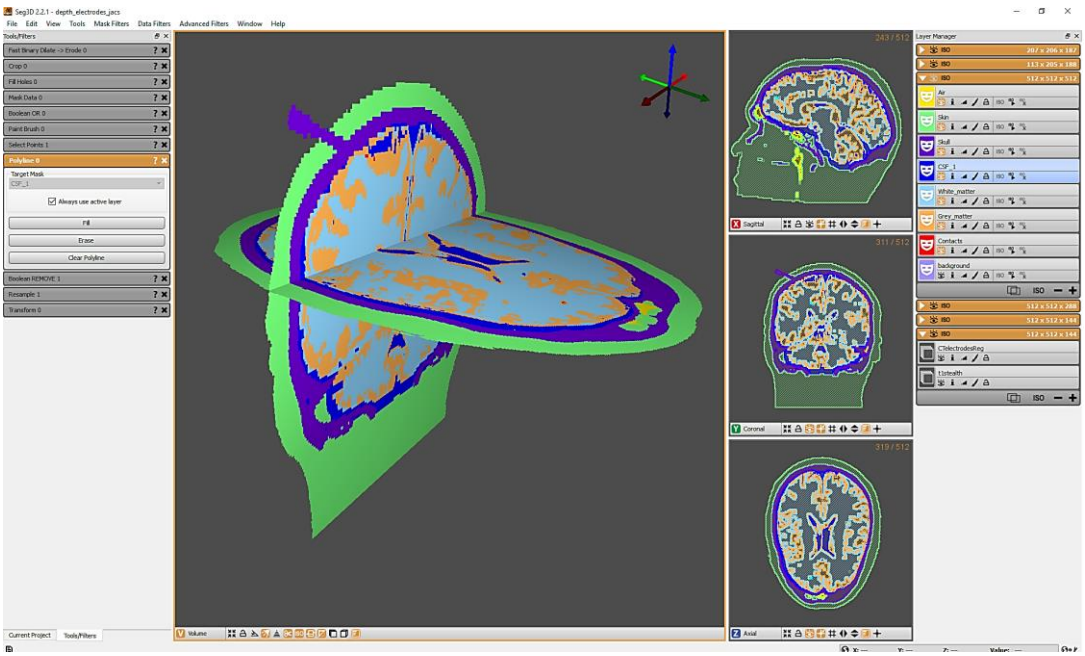

Figure 3-1 Illustration of segmentation of one subject using Seg 3D. The left-hand side shows the tools used for segmentation, the right-hand side shows created layers, the sagittal, coronal and axial sections of the segmented brain are in the middle.

3.2.2.2 Meshing and electrode placement

All three meshes were generated from the layers segmented from the joint CT-MRI scans using the CGAL open-source C++ software (http://www.cgal.org/, 2015). This mesh creator allows the specification of the size of the elements within the mesh. Meshes contained 0.7 mm size elements, which were refined to 0.3 mm in the vicinity of the electrodes (Aristovich et al. 2014). The resulting meshes comprised 8.9, 9.1 and 9.6 million tetrahedral elements for patients 1 to 3 respectively (Figure 3-2). The realistic geometry of depth electrodes was modelled from CT scans. Each electrode contact was 2.4 mm long and 1.1 mm in diameter (Ad-Tech, Spencer Probe depth electrodes). Additional 1 cm diameter scalp electrodes were simulated in two-electrode protocols; their location was according to the modified International 10-10 EEG System (Oostenveld & Praamstra, 2001). For the reconstructions, hexahedral meshes with 5 mm elements were created which resulted in 39 000, 36 104 and 35 529 elements for patient 1, 2, and 3 respectively.

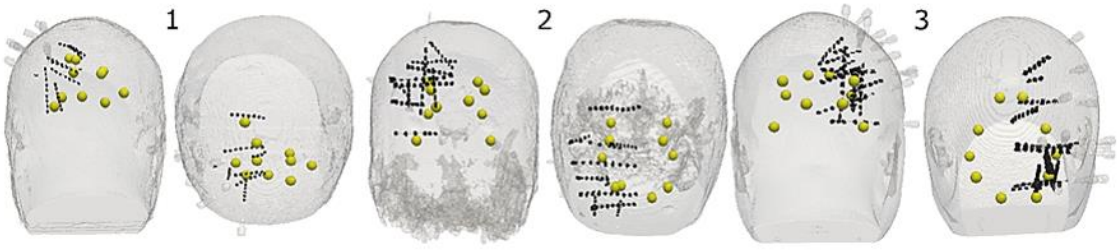

Figure 3-2. Seizure onset perturbation locations (yellow spheres) inside each mesh with respect to the SEEG depth electrodes and their recording contacts (black dotted lines). Coronal (left) and axial (right) for each patient 1 to 3.

3.2.3 Perturbations

For EIT simulations, 10 seizure onset perturbations were tested (Figure 3-2, Table 3-2): five were located within a volume enclosed by the SEEG contacts (Ipsilateral Group) and the other 5 placed in the opposite hemisphere, outside the enclosed volume (Contralateral Group). An additional group (Mixed Group) consisted of five perturbations preselected from both groups, Ipsi- and Contralateral. This group was proposed to assess the protocol with a reduced number of electrodes (ROI-focused). All perturbations in this group were placed in a line between the current injecting electrodes (depth and scalp).

For EEG modelling, the source was defined as a dipole field generator oriented in the angle most radial with respect to the closest electrode i.e. optimally for source detection.

Patient	**Ipsilateral Group** (mm)	**Contralateral Group** (mm)
1	Right superior frontal gyrus (14)	Left middle frontal gyrus (25)
	Right cingulate gyrus (mid. part) (11)	Left cingulate gyrus (27)

	Right frontal lobe (9)	Left sup. frontal gyrus (ant. part) (35)
	Right insula (8)	Left insula (13)
	Right cingulate gyrus (post. part) (10)	Left inferior frontal gyrus (45)
2	Right orbital gyrus (13)	Left orbital gyrus (22)
	Right frontal lobe (7)	Left frontal lobe (31)
	Right middle temporal gyrus (15)	Left middle temporal gyrus (54)
	Right insula (27)	Left insula (55)
	Right middle frontal gyrus (19)	Left middle frontal gyrus (29)
3	Left middle frontal gyrus (9)	Right middle frontal gyrus (25)
	Left cingulate gyrus (18)	Right cingulate gyrus (35)
	Left insula (22)	Right insula (44)
	Left middle temporal gyrus (8)	Right middle temporal gyrus (54)
	Left orbital gyrus (6)	Right orbital gyrus (17)

Table 3-2. The approximate locations of the perturbations. Distances in mm are measured to the closest depth electrode from the perturbation.

3.2.4 Protocols and electrode combinations

Three current injection protocols were tested for EIT simulations. Current injection electrodes were chosen such that the distance between electrodes was maximised

while acquiring the maximum number of independent measurements (Malone et al. 2014). Measurements on all electrodes were taken with respect to a single reference electrode placed in white matter, the same as used for clinical recordings. Across recordings, all available depth contacts were used. These comprised 7 to 12 SEEG electrodes with 48 to 82 contacts, and 32 additional scalp electrodes, placed according to the 10-10 International System (Oostenveld & Praamstra, 2001).

Protocol 1 ('depth only'): comprised all depth electrodes, which recorded with respect to a reference depth contact used for the SEEG recordings in the clinic. The set combined 48, 82 or 71 contacts, depending on the mesh. There were 47 independent current injections giving 2070 measured voltages, 81 giving 6320 and 70 injections yielding 4692 measurements for cases 1, 2, and 3, respectively. 50 μA at 10 kHz was injected.

Protocol 2 ('depth and scalp'): included all depth electrodes and additional 32 scalp electrodes. The forward solution was superimposed on the results from Depth Only Protocol, to reduce the processing time. Both sensitivity matrices were combined for image reconstruction. There were 31 additional injections between scalp electrodes resulting in 2418, 3472 and 3131 measurement lines, for subjects 1, 2, and 3, respectively. 250 μA current was injected between scalp electrodes.

Protocol 3 ('ROI-focused') had a reduced number of current injection sites: three contacts on a single depth electrode (the top, middle and the bottom contact) and less than 10 scalp electrodes on the opposite side of the head, giving up to a maximum total of twelve electrodes. The scalp electrodes were chosen to maximise the current density in perturbation regions. The measurements were made with all available SEEG electrodes. Here, there were 1560, 1680 and 2020 measured voltages for cases 1, 2, and 3, respectively. The current level was 50 μA. This protocol was used to test whether a considerably reduced number of injections can still provide useful information on a potential onset when the maximum current density was focused only on a preselected area.

EEG source modelling: all available depth probes and additional 32 scalp electrodes were used in the simulations.

3.2.5 EIT voltage simulations and image reconstruction

The conductivities were set to: 0.3 S/m for the grey matter, 0.15 S/m for the white matter, 1.79 S/m for the CSF, 0.018 S/m for the skull, 0.44 S/m for the scalp tissues and 0.0001 S/m for air as specified in the literature for frequencies around 10 kHz (Malone et al. 2014; Romsauerova et al. 2006; Horesh et al. 2006). The conductivity changes inside the seizure onset perturbations were set to 0.003 S/m and 0.03 S/m equivalent to 1% and 10% for the fast and slow impedance changes. The forward solution was calculated using PEITS on the fine tetrahedral meshes (Jehl, et al., 2014). Reconstruction was performed on hexahedral meshes with zeroth-order Tikhonov and noise-based image post-processing (Aristovich et al. 2014). The realistic additive noise of zero mean and a standard deviation of 1μV was added to all simulated voltage changes, which matched the noise in animal experiments with intracranial electrodes (Avery et al. 2017; Vongerichten et al. 2016), resulting in a mean SNR of 19.6.

3.2.6 EEG source detection

EEG source imaging was accomplished using the same realistic head meshes and conductivity properties of elements as for EIT simulations. The forward lead-field matrix was calculated using the adjoint field theorem and electrical reciprocity principle (Vallaghé et al. 2010) on the tetrahedral head mesh created for all patients. To generate realistic sources, single dipoles were placed in the same 10 locations as the perturbations in the EIT study. The dipoles were represented as spherical perturbations with the same dimensions as for EIT. The elements within the perturbation were assigned a constant current density vector computed on the basis of the detection criterion described by Hufnagel (2000), while the rest of the elements were assigned 0 current density vectors. The voltages were generated on

each electrode by multiplication of the lead field matrix by the resulting current density vector and adding Gaussian random noise with the same parameters as in the EIT case. The source with the most radial (*the max angle,* the highest detected voltage) and the most tangential (*the min angle*, the lowest detected voltage) orientation were reconstructed into images. These were produced by first computing the inverse source problem solution, then using the resulting electrode voltages combined the lead-field matrix obtained by projection of the forward tetrahedral lead-field matrix into the same hexahedral mesh as used for each EIT. Inversion was performed using linear zeroth-order Tikhonov regularisation (Grech, et al., 2008), resulting in the current density vector distribution within the entire hexahedral domain. The current density vectors were then weighted using the same noise-based t-scoring approach as for EIT for a consistent comparison. Finally, the magnitude of the resulting vectors was used for image display.

3.2.7 Image quality assessment

The quality of the reconstructed images was evaluated using two metrics: localisation and shape errors (Jehl et al. 2016; Malone et al. 2014). The localisation error was defined in millimetres, as the ratio between the distances of the centre of mass of the reconstructed perturbation (at the maximum conductivity change) from the actual location of the perturbation placed within a head mesh. The shape error was defined as the mean of the difference in each axis of the reconstructed perturbation to the perturbation's actual width, expressed as a percentage of the mesh's dimensions. In this case, the reconstructed perturbation contained all voxels with at least 75% (significance defined as 1 standard deviation for 1 degree of freedom Student's t-distribution) of the maximum conductivity change. The average localisation and shape errors were calculated for each of the EIT protocols separately for perturbations from Ipsilateral, Contralateral Groups and for the EEG sources with the best and the worst source orientation.

The difference between the localisation error for Protocol Depth Only and Depth+Scalp in EIT, and Depth+Scalp and EEG source detection were compared with a two-sided t-test, p-value <0.05 or p<0.01.

To simulate the clinical procedure of visual inspection for a spike, the generated voltage amplitude for the *max* and the *min* angle of a dipole source were found for each location. This was done to ascertain if the generated voltage was large enough to exceed the 250 μV detection threshold on the closest SEEG contact. In order to compare these results with EIT images, an arbitrary clinically acceptable accuracy was set as shape and localisation errors of <10% and 10 mm respectively. The comparison was only made with Depth+Scalp Protocol, as this gave the best results of EIT.

3.3 Results

The Depth and Scalp EIT Protocol resulted in better accuracy for both 1% and 10% impedance changes (Figure 3-3 and Figure 3-4). For a 1% impedance change, the localisation errors were improved from 26.5±26.8 mm to 5.2±1.8 mm (p<0.05) for the Ipsilateral Group or 83.1±22.9 mm and 29.6±38.7 mm (p<0.01) for the Contralateral Group, for Protocols Depth Only and Depth+Scalp respectively. For a 10% impedance change, the localisation errors similarly were 66.1±37.2 mm or 26.1±36.2 mm in the Contralateral Group (p<0.05). For a 10% ipsilateral change, both protocols resulted in localisation errors of 4.3±0 mm. The accuracy of the ROI-focused Protocol was severely affected by artefacts (observed especially in the first mesh), which impeded satisfactory localisation of the seizure onset. There was no significant difference in the shape errors between the two protocols (Figure 3-4).

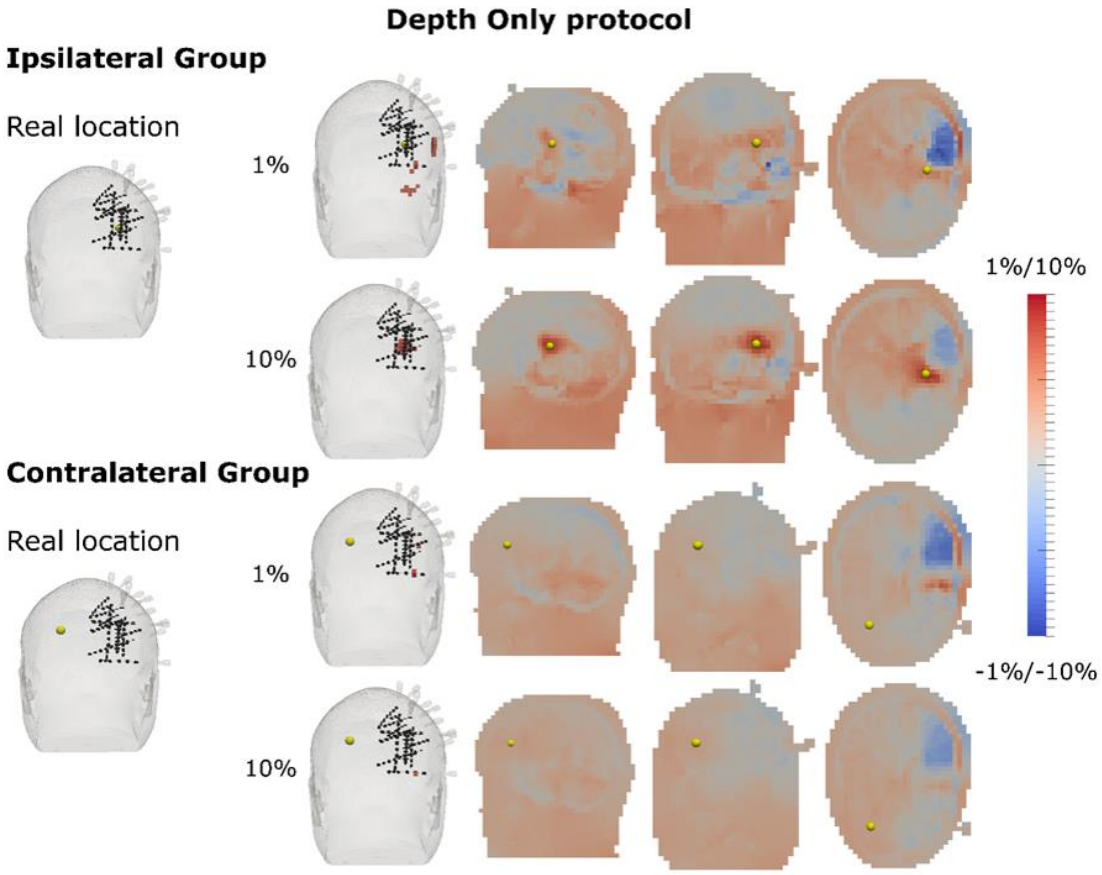
Depth Only protocol
Ipsilateral Group
Real location
1%
10%
Contralateral Group
Real location
1%
10%
1%/10%
-1%/-10%

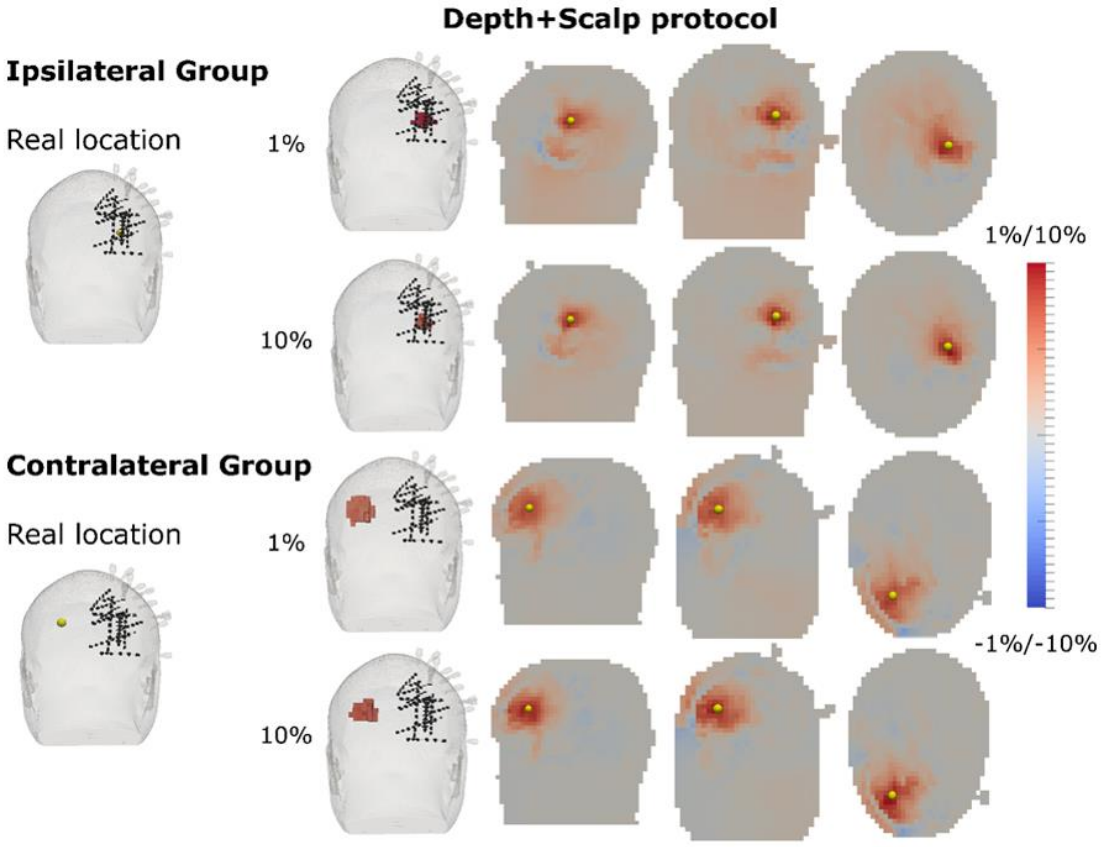
Depth+Scalp protocol
Ipsilateral Group
Real location
1%
10%
Contralateral Group
Real location
1%
10%
1%/10%
-1%/-10%

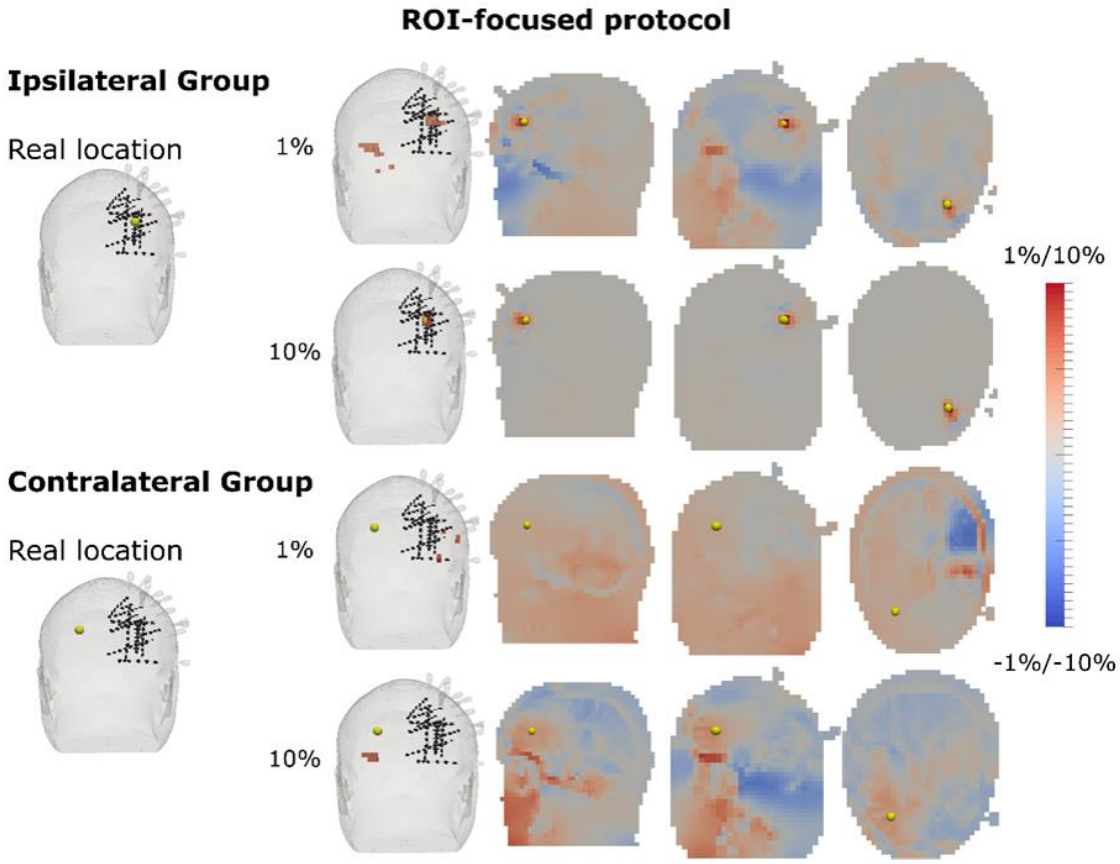

Figure 3-3. Representative examples of a single perturbation reconstruction; simulations of 1% and 10% impedance change in both hemispheres for all three protocols tested. The Ipsilateral Group represents perturbations located within SEEG electrodes coverage; the Contralateral Group is in the opposite hemisphere. Each reconstruction is shown in four sections, front view of a whole mesh with SEEG electrodes, and sagittal, coronal and axial planes. The 'Real location' shows the actual placement of the perturbation (yellow sphere) with respect to the SEEG contacts (black dotted lines). The reconstructed change is presented as a change at 75% threshold of maximum conductivity in the mesh. The scale corresponds to the impedance increase (red) and decrease (blue) in conductivity change (%, t-score based noise correction). It may be seen that the perturbation was reconstructed accurately in all cases for the Depth+Scalp Protocol and only for the Ipsilateral Group 10% case for Depth Only Protocol. In case of the ROI-focused Protocol, reconstructions were only accurate within close proximity to recording contacts.

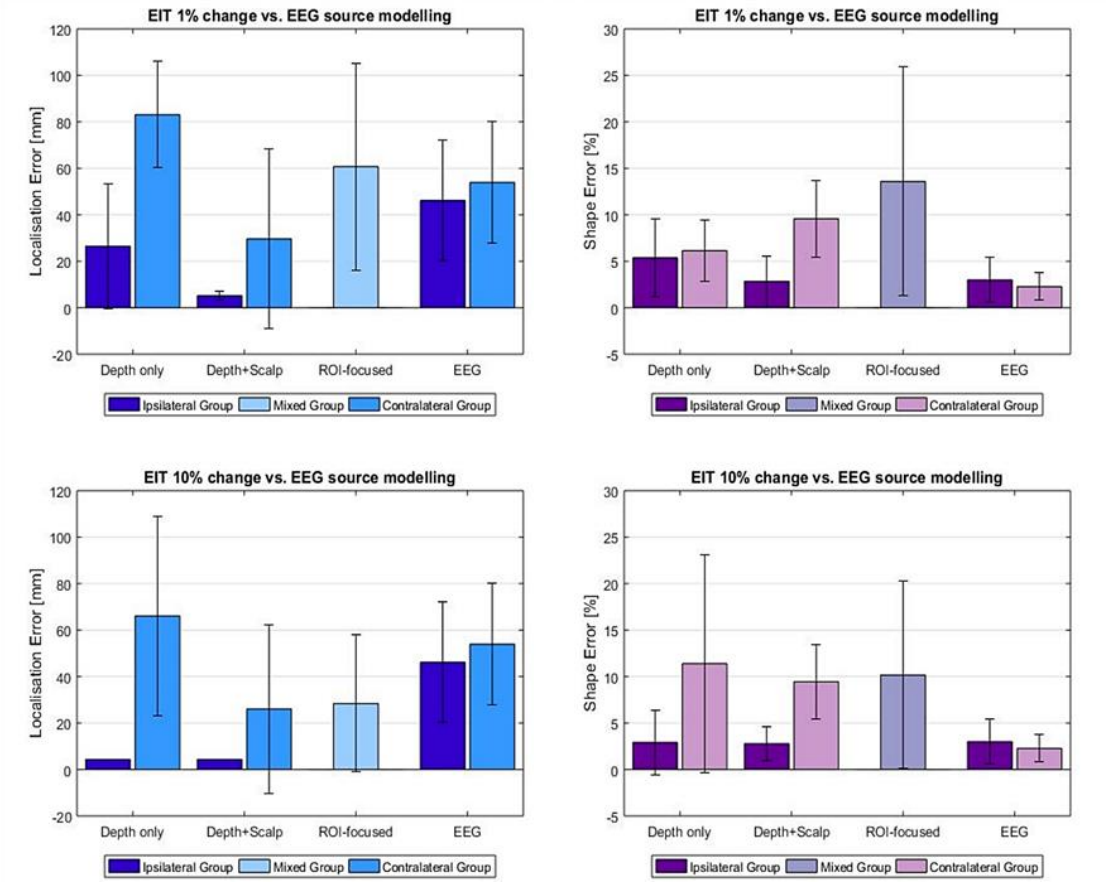

Figure 3-4. A comparison of the localisation and shape errors for all protocols tested overall in three meshes for fast (1%) and slow (10%) conductivity changes in EIT with EEG source modelling. The Ipsilateral Group represents perturbations placed within the coverage of SEEG electrodes, the Contralateral Group is in the opposite hemisphere, and Mixed Group is formed from both groups, selected for ROI-focused protocol. EEG source presents the max angle orientation of the source. Overall, protocol Depth+Scalp improved the localisation error significantly when compared with Protocol Depth Only (t-test, two-sided, n=15 in each group). For EEG modelling, localisation errors were significantly larger for both groups, Ipsi- and Contralateral, when compared with the EIT Protocol Depth+Scalp. Shape error was improved in the Contralateral Group in EEG.

EEG inverse source modelling resulted in worse localisation accuracy. Localisation errors were 46.2±25.8 mm (Ipsilateral Group) and 54.0±26.2 mm (Contralateral Group) for the *max* angle, which was significantly worse than with EIT Protocol Depth+Scalp ($p<0.01$ for ipsilateral group, $p<0.05$ for contralateral group), although

the EEG shape error was improved in the Contralateral Group, when compared with EIT ($p<0.01$) (Figure 3-4). The quality of the reconstructed images was considerably better for the *max* angle as opposed to the *min* angle reconstructions (Figure 3-5); however, it was qualitatively a larger reconstructed region than with EIT.

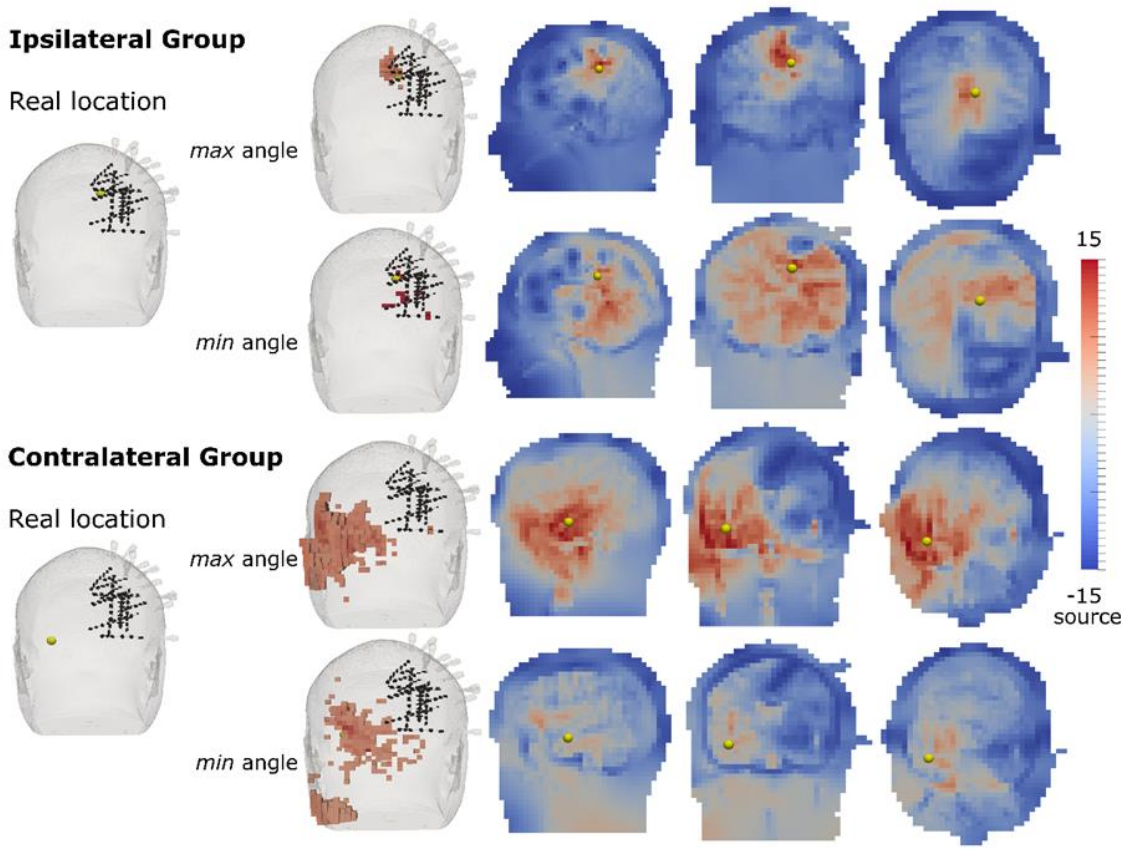

Figure 3-5. A representative example of EEG source reconstructions of a single source from Ipsilateral Group (top panel) and Contralateral Group (bottom panel). For each group, two examples are presented, the reconstruction of the highest voltages detected (the max angle) and the lowest voltages detected (the min angle). Each reconstruction is shown in four sections, front view of a whole mesh with SEEG electrodes, and sagittal, coronal and axial planes. The 'Real location' shows the actual placement of the perturbation (yellow sphere) with respect to the SEEG contacts (black dotted lines). The reconstructed change is visualised as a change at a 75% threshold of maximum conductivity in the mesh. The scale corresponds to the impedance increase (red) and decrease (blue) (source as corrected current density, t-score based noise correction).

With visual spike recognition, 8 out of 15 ipsilateral, and zero contralateral sources generated a field above the detection threshold (Figure 3-6). In general, sources closer than 11 mm to contact produced voltages greater than the arbitrary threshold of 250 μV and spike amplitude varied with the distance from the recording contact (Figure 3-7). In contrast, the EIT Depth+Scalp Protocol detected 15/15 for either 1 or 10% changes ipsilateral, and 8/15, 9/15 contralateral respectively (Figure 3-6, top and bottom row, middle and right columns) up to a maximum distance of 27 mm.

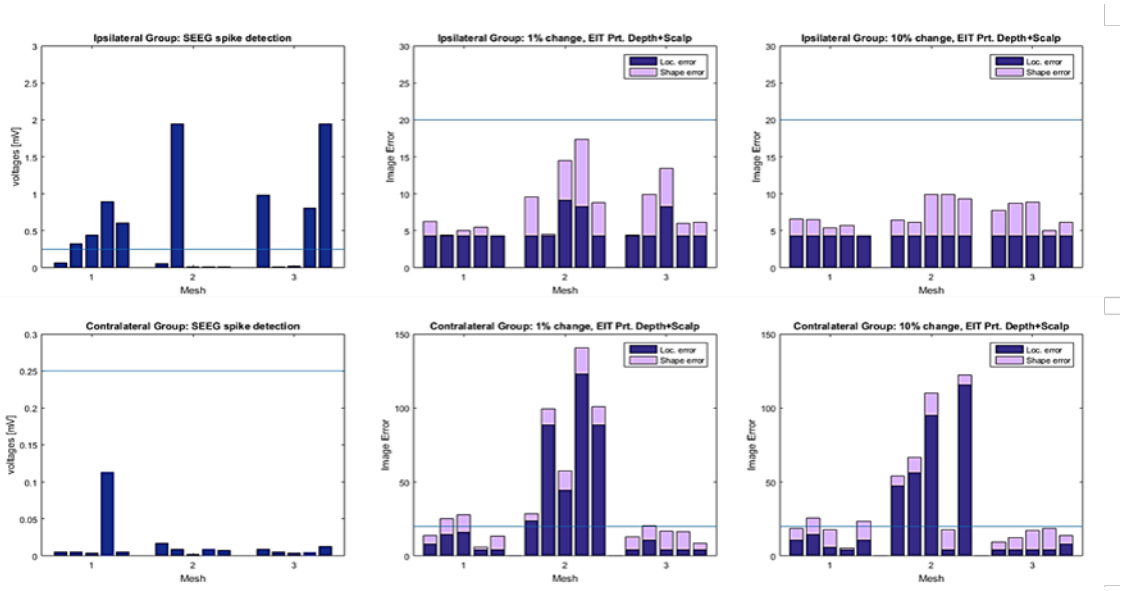

Figure 3-6. Comparison of the voltages detected on depth electrodes (SEEG spike detection, left column, the max angle) and combined location and shape errors measured with EIT Protocol Depth+Scalp for Ipsi- and Contralateral Group for 1% (middle column) and 10% (right column) impedance change in all three meshes. The horizontal line represents either a 250 μV detection threshold for SEEG spikes or the acceptable combined EIT error (shape and localisation errors of <10% and <10 mm respectively)

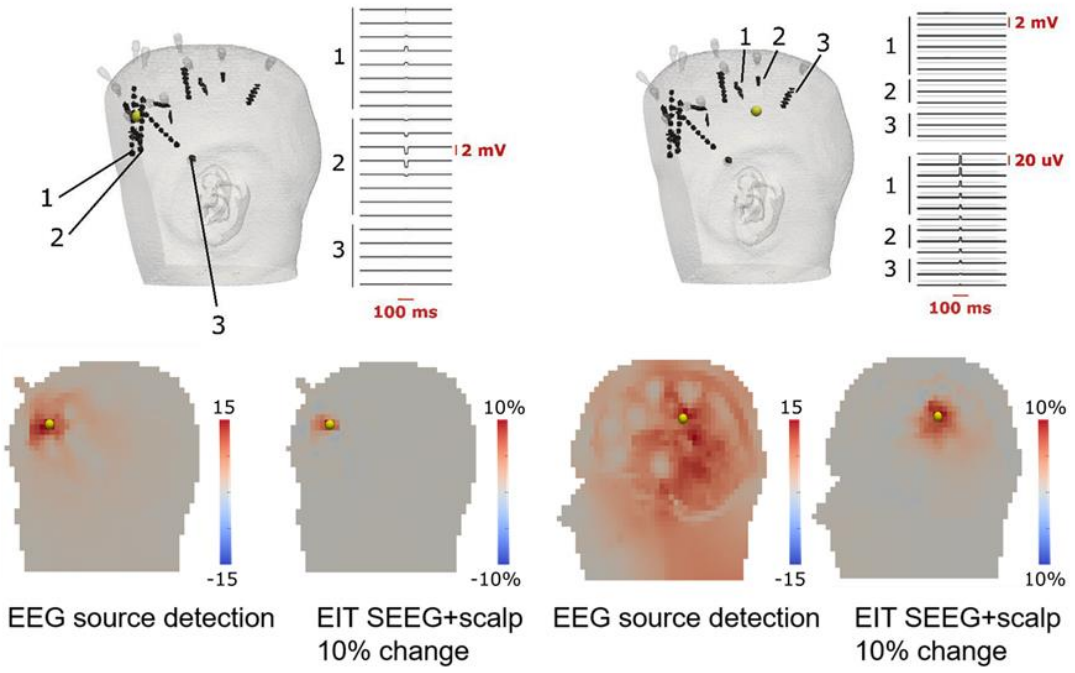

Figure 3-7. Detection accuracy with three methods: model of clinical spike detection (top, SEEG on respective contacts presented as horizontal lines), the reconstruction with EEG inverse source (source as corrected current density, t-score based noise correction) and the best protocol for EIT (Protocol Depth+Scalp, described as conductivity change in %, t-score based noise correction) (bottom). The real location of the source is shown as a yellow sphere. Visual detection of a dipole spike shows that sources close to contact (~7 mm distance, left panel) produced spikes above the threshold (the highest amplitude was ~1.5 mV) and the spike amplitude changes with respect to the distance and orientation. A more distant source still within SEEG coverage (~ 18 mm distance, right panel) produced a significantly lower voltage (~16 μV) on the closest SEEG contact, below the detection threshold of 250 μV. In this case, the perturbation was not successfully localised with inverse source modelling but was located within 5 mm using EIT.

3.4 Discussion

3.4.1 Summary of results

This study demonstrates the feasibility of imaging 1% and 10% conductivity change with EIT and depth electrodes in computer simulations. EIT resulted in better accuracy than either SEEG spike detection or EEG inverse source modelling and the

accuracy of detecting distant and fast impedance changes was further improved when scalp electrodes were added to the protocol.

3.4.2 Technical issues

The overall computation of the reconstruction procedures for ~9 million tetrahedral- and ~35 000 hexahedral-element meshes involved ~6000 lines of protocol and took up to 240 hours of CPU time for a single patient with the Jacobian matrix taking up to ~500 GB of memory in the case when all depth and scalp electrodes were used. This might raise difficulties in the proposed application of EIT for telemetry and continuous monitoring. However, for each patient, the described method requires only a single time-consuming computation of the forward problem and inverse Jacobian for a given geometry and measurement protocol. It is therefore feasible for prolonged recordings on the ward, as the necessary scaling of the calculations for long-term monitoring is only a matter of simple offline signal processing. Moreover, the reduction of time and memory taken for the calculations could be achieved by lowering the number of SEEG/EEG contacts for EIT protocol and/or applying coarser meshes, although such modifications would affect the sensitivity of the method. Future work on protocol optimisation in EIT to find out the minimum required number and locations of depth electrodes for accurate EIT images is in progress.

3.4.3 Which electrode arrangement gives the best seizure onset localisation?

Three arrangements of electrodes were tested in this study. Among them, the one utilising all depth probes and additional 32 scalp electrodes resulted in the most accurate localisation of the seizure onset.

In clinical practice, it may not always be possible to apply this number of scalp electrodes in a broad 10-20 montage, as there is a potential risk of infection if scalp electrodes were to be located in very close proximity to the craniotomy and burr

holes for depth electrodes. Infections are the second main cause of SEEG complications, although they were reported in only 0.8% of patients undergoing depth electrodes implantation and were well controlled with antibiotics (Mullin, et al., 2016). Furthermore, it has not been thoroughly investigated, whether scalp electrodes could affect the risk of infection in clinics. Applying a limited number of scalp electrodes during intracranial monitoring is not a standard clinical procedure but it is sometimes proposed to improve the diagnostic yield. It seems likely that applying scalp electrodes should pose a negligible risk if the scrupulous aseptic technique is used. Ideally, they should be placed during the same operation as the depth electrodes and with a margin of >2 cm from any surgical site. Although these constraints may somewhat reduce the accuracy of the EIT Depth+Scalp protocol described in this study, the use of as many scalp electrodes as possible and safe appears to be a valid recommendation for any future clinical studies.

3.4.4 Does the best of these three methods give improved seizure onset detection compared to the current intracranial method?

The localisation accuracy was significantly better with the best EIT protocol than with EEG inverse source in presented models. Also, by its nature, EIT was not sensitive to the dipole orientation, whereas EEG detection varied with the field angle and was severely compromised in sub-optimal dipole orientations.

In the presented models, EIT detected the 10%-conductivity-change sources overall better than EEG modelling (Figure 3-7). Sources placed within 5 mm distance from the electrodes were reconstructed accurately in both EEG inverse source and EIT (Figure 3-7, left side). When the distance between the perturbation and the nearest recording electrode was extended above 11 mm, the recorded voltage dropped below the EEG detection threshold (Figure 3-7, right side). Consequently, the inverse source modelling could not accurately locate the source in these instances, while EIT was able to provide reconstructions with an accuracy of 4.3 mm.

Imaging the slow 10% impedance changes presented here is likely to be of less clinical impact, as these changes are likely representative of the propagation of the seizure and could be detected through other methods such as EEG-fMRI or SPECT. Nevertheless, this might still be of value in locating the seizure onset zone. Future work should focus on the detection of the fast, 1% changes, as they have the highest clinical utility, and are the most challenging to detect with existing methods due to their low SNR and short time course.

It is also worth noting that EIT offers immediate image reconstruction, while the inverse source modelling, even though it is capable of the same, is not routinely used in the clinical setting. There are several further considerations when reconstructing seizure-related changes with EIT. The inverse problem in EIT is ill-posed and ill-conditioned, therefore; it is crucial to minimise modelling errors in the forward problem. In this modelling study, the component head tissues were treated as isotropic and homogenous. This appeared to be reasonably valid in this study, as the brains of the patients showed no observable abnormalities on neuroimaging. In some cases of epilepsy, there could be local pathology which could influence local tissue impedance. In such cases, the assumption of homogenous conductivity values across the brain tissues should be modified. Such lesions, though, could be visualised in MRI prior to the SEEG implantation and built into the mesh as a separate layer with a different conductivity value. The same procedure can be applied to various post-operative tissue abnormalities following the implantation of electrodes such as haemorrhages, infarcts, oedemas, etc., which can be easily visualised in post-operative CT imaging (Schmidt, et al., 2016). Furthermore, it was recently reported by Koessler et al. (2017) that non-lesional epileptogenic zones can have different conductivity values than the surrounding healthy tissue. Even in such cases, time-difference EIT minimises the impact of such aberrant impedances, as modelling errors are attenuated when the difference between two time points is taken (Holder, 2005) and hence, it may still be possible to achieve acceptable source localisation.

Finally, it is important to note that this study represents only a subset of cases, and therefore it is limited to unilateral intracranial electrode coverage. However, it will be beneficial to extend the method to study cases with bilateral electrode placement, as it may offer some insight into seizure progression from deep onset to cortical regions.

3.4.5 Conclusions and future work

The feasibility of a new method of combining Electrical Impedance Tomography with depth electrodes implanted for clinical monitoring prior to the resective surgery in epilepsy was tested in computer simulations. EIT improved the onset detection with localisation accuracy compared to EEG inverse source modelling and was sensitive to sources not visible with visual spike detection.

There are multiple directions for further studies. Most importantly, the study should be tested *in-vivo*, in order to compare the simulation results with the actual physiological data. This could be done in two steps, in animals and then followed by the human study. Ideally, both types of recordings use the same type of intracranial electrodes to represent the clinical situation accurately. Furthermore, investigating the regional limitations to particular cortical or subcortical areas would be similarly beneficial for the development of the method. A rigorous investigation of the relation between the number of depth electrodes and the accuracy of source localisation would demonstrate if EIT has the potential to reduce the number of SEEG electrodes implanted in the future. The method could also be easily extended within the current setup to test the possibility to differentiate multiple seizure foci at the same time.

The presented results suggest that EIT could aid epilepsy diagnosis when combined with existing methods. It is crucial to emphasize that this study suggests that EIT could assist in clarifying the location of seizure onset, if other methods, such as extracranial and intracranial localisation and imaging data, remain unclear. Hence, a combination of EIT and SEEG could improve the diagnostic yield and help in better

understanding of epilepsy, with no additional costs or risks for patients. These results support the use of EIT on patients, which should be the first stage of the follow-up work after this study.

Chapter 4

Method development for parallel EIT recordings

Overview

Currently, the EIT system used at our lab for all neuro applications is a serial or sequential method. Thus, it injects current between a pair of contacts and then switches to the following, as defined by the imaging protocol. Such a system has several limitations if applied for epilepsy imaging. It requires multiple seizures to average the signal and it produces a switching artefact in clinically collected EEG signals. The latter is a significant problem for the clinical team, and, therefore, an alternative EIT system is required. This work was thus focused on preparing a parallel EIT system, which would overcome the previously mentioned obstacles. The new system injects current at separate frequencies on multiple electrodes at the same time, so can benefit in quicker data collection and no switching artefact in the clinical setup. However, a completely new EIT design requires accurate and detailed testing to define the system performance. Optimally, such a system should perform reliably, be portable, and completely independent from the external power supply if used in clinics and would need to pass all the safety tests performed by the medical engineering department in a hospital. EIT performance can be tested with a resistor phantom, modelling the ideal environment of recording the data without any external and physiological sources of noise, so that the internal noise of the device can be described. The tests should also include the recordings with scalp EEG electrodes and intracranial EEG electrodes so that the influence of EIT recording could be described on healthy and epileptic background EEG signals. Finally, the optimal current injection protocol when using parallel EIT system on patients should be established. This chapter summarises the tests and advances completed towards the development of the parallel EIT system that is safe and suitable to use on patients for long-term EIT-EEG recordings.

4.1 Introduction

4.1.1 Background

Usually, a standard EIT system comprises a current source, a voltage-measurement component, an EEG amplifier, a switching board addressing all electrodes and a controller to set the measurement and injecting processes. A current of pre-set amplitude and frequency is injected for a defined period between a pair of electrodes with all electrodes measuring the voltages. All electrode pairs used for current injections and the injection order form the EIT imaging protocol. A complete dataset comprises all voltage measurements, of n number equal to the number of injection pairs multiplied by the total number of electrodes connected. A single measurement is a demodulated voltage amplitude recorded from a pair of electrodes, which can be then averaged for several periods of the sine wave. These measurements can be completed in two different ways, serial and parallel, i.e. applying time-division or frequency-division multiplexing.

4.1.2 Serial EIT system suitable for recording in epilepsy

The typical and most commonly used EIT system for brain imaging applications, such as both systems described in chapter 2, injects current in a serial or sequential pattern (Vongerichten et al. 2016; Aristovich et al. 2016; Hannan et al. 2018; Faulkner et al. 2018). Current injection is set between a pair of electrodes for a fixed time, which is then switched to the second pair in a sequence defined in the imaging acquiring protocol. A single frequency operation is routed to all injection pairs through a switch network. Such approach allows addressing of arbitrary pairs of electrodes, controlled by the software, and consistent averaging of the signal. The optimal current frequency, maximising the signal-to-noise (SNR) ratio, can be defined by a frequency sweep. Finally, such a single-frequency approach allows manipulation of a filtering bandwidth around the carrier, so that both fast and slow impedance changes can be extracted from the data.

Despite these advantages, serial EIT has several limitations that can be problematic for epilepsy applications in patients. Seizures are rather unpredictable events that might appear without an external trigger or even a sign or a symptom for a patient, and they can be very brief. The nature of seizures makes coherent averaging of the signal for a full EIT imaging protocol difficult. Serial EIT does not allow for continuous current injections on multiple electrode pairs at the same time. Electrodes chosen in the protocol to inject current, are typically set in pairs of a maximum distance, so that, they could cover a wider area of the brain. In case of a seizure, there is a theoretical risk that the ictal event occurs exactly during the time when EIT injects current on a distant pair of contacts from the onset zone. In such case, EIT would have significantly lower sensitivity over the ictal region. That was established as not problematic for planned experiments on animals, for which evoked activity or even seizures were triggered on demand (Faulkner et al., 2018; Hannan et al., 2018), but it can likely limit the long-term use of EIT in epilepsy patients, for which the onset zone is unclear and has to be recognised during video-telemetry. One way to overcome such a limitation is to decide on the injection protocol beforehand so that to focus all injections in and around the predicted epileptogenic zone. This, however, requires prior knowledge on the boundaries of the seizure onset zone and so limits the proposed benefit of using EIT in epilepsy imaging in the first place.

The second drawback of serial EIT is related to the switching between the electrodes. Such switching produces a significant artefact seen in the EEG signal, lasting up to 0.5-1.5 sec. The switching transient can be seen on the EEG traces despite using a separate set of electrodes for EEG and EIT (Fabrizi et al. 2006). It does, however, depend on the EIT recording frequency, as described below. Again, if the measurements were performed only on animals, for which a continuous and unaffected EEG is not required, a serial EIT system is perfectly suitable. However, once the system is proposed to be used in human subjects, as in the telemetry setting

in a hospital, no artefacts in the EEG signal related to research activity can be accepted by the clinical team.

This switching artefact problem has been previously addressed after the initial clinical study on imaging epilepsy with EIT and scalp EEG (Fabrizi et al. 2006). The authors did not manage to image seizures with EIT, due to movement artefacts blurring the signal completely, which is also a well-known problem during scalp EEG recordings of seizures. However, the authors have challenged the issue with the EIT artefact seen on the simultaneously acquired EEG (Fabrizi et al. 2010). In theory, EIT and EEG signals should not interfere with each other, due to the difference in frequencies used for EIT (tens of kHz) and EEG bandwidth (usually up to 100 Hz if scalp EEG and <1000 Hz if intracranial EEG). However, in practice, EIT had an obscuring effect on EEG detected by the clinically used equipment and despite independent electrodes used for EIT, because of switching artefact. Therefore, as two isolated sets of electrodes were used, an individual filtering method could be applied on each set, i.e. a hardware low-pass and high-pass filters. The low-pass filtering was set between the EEG system and the subject, so that high-frequency noise generated by EIT could be cut-off, whereas the high-pass filtering was applied between the EIT and the subject to cut off the low-frequency switching between the pairs of electrodes in EIT. In practice, a 1^{st} order passive high-pass filter at 72 Hz was inserted on each EIT electrode and 2^{nd} order low-pass filter at 48 Hz was on each EEG electrode. In addition, software filtering extracting the remaining switching EIT artefact from the continuous EEG recording was also tested. Such switches had similar appearances of very sharp and high amplitude spikes. Therefore, they could be used as triggers for the software to recognise them from the background scalp EEG signal and remove, however, the removal of artefact required further time corrections for each electrode. Several correction methods were investigated; the best performance was found if a single EEG channel was used for time processing. The software took approximately 3.5 min to process 15 minutes of data. Overall, the

subtraction of EIT from EEG reduced the occurrence of the switching artefacts but did not completely remove them. An occasional low-frequency artefact at the EIT imaging rate still occurred, possibly because spike artefacts expressed an unusual shape that could not be automatically distinguished by the software. It was also likely that electrodes used for current injection retained charge and discharge after use; this created transient signals at the switching frequency so there was still a significant artefact within the EEG bandwidth. Nevertheless, the remaining EEG was possible to read and report, as assessed by the professionals (Fabrizi et al. 2010).

Unfortunately, as it is crucial to correlate accurately the video findings with the EEG traces during EEG video-telemetry in clinical setting, such a delay makes it impossible to look at the data in real-time. In theory, it is still possible to apply artefact filtration afterwards, especially given that many clinicians assess the video EEG offline rather than in real-time. However, in our case, the signal delay, together with the remaining artefact seen on the EEG, were not accepted by the clinical team that we currently collaborate with and so using a serial system for recordings on patients would require further engineering work on optimising the filtering method. In addition to the EEG problems but most importantly for EIT imaging, the switching artefact would also very likely be problematic for measuring slow impedance changes especially if such a switch occurs during the ictal event, as it is impossible to filter it out while retaining the data necessary for reconstructing the impedance change.

4.1.3 Parallel EIT system for recording in epilepsy

For all aforementioned reasons and in order to pursue EIT imaging of epilepsy further, a new system has been developed in our group at UCL, the so-called “parallel EIT system” (Avery et al. 2017, 2019). This EIT system offers a possibility to record the EIT signal in parallel to clinical EEG while avoiding the various artefacts caused by the serial system described above. It might be also used for imaging nerve compound action potentials, for which single-shot data might be collected without

averaging. The parallel EIT system uses frequency division multiplexing, so it injects current at several frequencies on different electrode pairs at the same time. The major benefit of a parallel over serial EIT system is avoiding the switching artefact seen in EEG and thus also avoiding the potential risk of a switch occurring during the unpredictable ictal event. This, in theory, allows recording EIT in parallel to EEG telemetry for long times, without affecting the medical workflow at a ward and offers a possibility of constantly collecting full imaging protocol in real-time. However, due to significant complexity in designing the circuits and hardware for a parallel current source, as well as in processing of the signal, the current version of the parallel EIT system is capable of injecting only at a maximum of six different frequencies at the same time (Dowrick and Holder 2018). However, despite this limitation, it has already been shown using a tank with saline that an imaging protocol reduced to six injection pairs could still produce quite accurate images (Avery et al. 2019) although, it requires considerably more preparations prior to starting the EIT recordings, such as choosing the adequate electrodes to inject current and its frequency. Unfortunately, in epilepsy applications, preparation of such a protocol involves analysing the EEG findings first, so that all the injecting electrodes cover the area with the majority of interictal and ictal discharges, highly limiting the potential advantage of EIT over EEG in the clinic. Finally, a limitation of a number of injection pairs to only six can often significantly decrease the spatial resolution of EIT, if used with depth electrodes in humans, because each depth electrodes has very many contacts (usually over 60-80) and so, it is very hard to select the optimal ones for the recording protocol. It is, therefore, desirable that parallel EIT system is upgraded to inject with more pairs, ideally through all available contacts.

4.1.4 Parallel EIT system hardware

The parallel EIT system is built in a similar way as the serial EIT system and so it uses the ActiCHamp EEG system (Brain Products GmbH) to record the EEG signal as well as the EIT voltages at up to 100 kHz sampling rate (Dowrick and Holder 2018;

Avery et al. 2019). The Keithley current source in the serial EIT system was replaced with a custom-made six-channel current source printed circuit board (PCB) and the frequency on each current source is set individually using an Arduino Pro Micro, while the amplitude is controlled by a jumper on the output stage. The current design of the parallel system allows choosing between following amplitudes: 12, 30, 60 and 120 μA. All these levels are safe to inject through human depth electrodes if the kHz frequency is set (as described in chapter 1), but 60 μA is the most commonly used setting for the intracranial electrodes used at the collaborating hospital. The current source is powered by a 3V battery, which, once charged, makes the system completely independent from the external power supply. The detailed description and design of the current injecting boards are open-source available online https://github.com/EIT-team/Parallel_CS_Altium. Such a design makes the system suitable for use on patients but also improves the portability if compared with serial EIT that have the Keithley current source that had to be powered from the mains.

4.1.5 EEG amplifiers

The clinical EEG system, MicroMed SD LTM 32/64 Express system (MicroMed, Italy) comprised 64 channels simultaneously sampled at 1024 Hz, with a hardware anti-aliasing filter cut-off frequency set to 340 Hz. Whereas the research EEG amplifier used in EIT, ActiCHamp data acquisition system (Brain Products GMBH, Germany), comprised 64 channels simultaneously sampled at 50 kHz, with a hardware antialiasing filter (cut-off frequency 12.5 kHz). No software filters are commonly used during data acquisition.

4.1.6 Frequency-dependant EIT response

The frequency of current influences significantly the recorded impedance response. Depending on which impedance changes, fast or slow, are measured, a different setup has been found as optimal. As it is expected that the response would drop if

the frequency of current increased (Holder 2005), it is crucial to find the optimal frequency characteristics for an application.

For fast impedance changes, this relation has been described in modelling, suggesting a fall from approximately 1% when applying direct current (DC) to 0.01% at 10 kHz (Liston et al. 2012). The maximum signal recorded during epileptiform discharges in cortical tissues of a rat brain was observed between 1 kHz and 3 kHz, with the highest SNR at 1.355 kHz and measured change of a maximum of -0.4% from the cortex (Hannan et al. 2018). Between 3 kHz and 10 kHz the signal remained stable, but the SNR increased due to lower noise recorded at higher injection frequencies. Similar results have been measured during evoked brain activity in a rat brain, with the highest SNR obtained at 1.475 kHz. (Faulkner et al. 2018).

The slow impedance signal may be explained by the cell swelling and an overall decrease in volume of the extracellular fluid due to seizure. As the majority of current applied within a range of 1 to 10 kHz is conducted through the extracellular fluid, an impedance increase is expected. An increase of almost 5% was observed during a seizure. However, as such a change lasts longer and is a secondary effect of the excessive neuronal firing, the obtained SNR remains stable across the frequencies within the 1 to 10 kHz bandwidth (Hannan et al. 2018).

Therefore, the authors concluded that the optimal current frequencies for measuring an epilepsy-related impedance signal would be 1.355 kHz if a serial system is used for fast, or 3 to 10 kHz separated by 500 Hz if a parallel system is used for slow impedance changes (Hannan et al. 2018).

4.1.7 Criteria for the EIT system to be used on patients in the hospital

There were several criteria to be fulfilled for the parallel EIT system to be used in the hospital environment with patients. These included safety regulations for the circuits and hardware, aseptic rules to minimise the infection risk and clinical regulations for the system to be used in parallel with standard medical workflow.

Work equipment used in hospitals in the UK must meet the safety criteria defined by the Safety Health and Welfare at Work (General Application) Regulations (2018). All equipment must be safe and compliant with the correct documentation in English, and have the CE mark. This, however, does not apply to the research equipment. As a part of the ethical approval procedure in the UK, Health Research Authority allows using a non-CE marked and custom-made equipment for research activity, if tested by the medical engineering department on site. The tests are based on the safety regulations defined by the International Electrotechnical Commission (IEC 60601 2012) and the British Standard Institute (BS5724, 1979). The main aim of such tests is to check whether there is a current leakage at any point of the equipment, and how it behaves in case of a failure, to make sure the patient is not at risk if the kit malfunctions. In the current design of the parallel EIT system all its parts, i.e. the current source, EEG amplifier and laptop are battery-powered making the safety tests relatively straightforward to pass.

Additional requirements are set for the potential infection risk. All parts of the system that are in contact with a patient must be easy to clean with ethanol. This includes all parts of the system that could be touched by the patient, such as the main box, cables, the laptop and the connector box between the hospital EEG headbox and EIT. In addition, if any of the elements need to be 3D-printed, they must be reprinted for each patient separately, as it is not possible to clean 3D-printed boxes well enough due to their porosity. The latter requirement was set by the hospital engineers, as a hospital policy to limit the infection risk. This set a requirement of making the system neat and portable, with almost all hardware hidden in one, easy-to-clean box.

Finally, the hospital engineers also defined the minimal frequency at which we could inject current. They specified that if we wanted to measure EIT in parallel to SEEG, we must not inject below 1.5 kHz, to be over the SEEG bandwidth.

The final criteria were set by the medical team and could be defined in two categories, the practical and medical. The former required the system to be portable and easily movable to the side if another clinical procedure needed to be performed on the patient. The system had to be simple to unplug and plug in but at the same time, connected securely enough so it does not disconnect during a seizure or any similar event. Finally, the medical conditions required by the team were focused on maintaining the collected EEG data unaffected and avoiding causing any ill effects, triggering ictal or interictal discharges or altering any other monitored parameters such as e.g. ECG or breathing pattern.

4.1.8 Rationale

The proposed application of EIT for imaging epilepsy requires simultaneous recordings of EEG and EIT during clinical EEG video-telemetry assessment. In such a case, however, EIT must not alter the clinically collected EEG signal. There are several sources of artefacts that EIT can introduce, such as for instance the switching artefact at the EIT image acquisition rate, and their impact would vary depending on the carrier frequency used. Work has been done before towards removing these artefacts, clearly demonstrating that EEG could be reported, if adequate filtering was applied. Still, as the residual EIT artefact was maintained on EEG traces, some clinical teams could not accept that, and would not allow for long-term EIT recordings. Therefore, further work to minimise the EIT influence on EEG was desirable. This can be achieved by developing a new parallel EIT system that does not switch between the injecting current electrodes but can collect a whole imaging dataset continuously while injecting current on multiple electrodes at the same time. However, as previous studies have been done with the serial EIT, the performance of the new system must be described in greater detail. It also requires a formal assessment of its influence on clinically recorded EEG, allowing further studies. The parallel EIT system at its current design could only inject up to 6 frequencies. It is a significant limitation for the spatial resolution of the system. Therefore, work should

have been also done to define the optimal current injection protocol, so that to maximise sensitivity of the method and by so, the odds for the successful outcome of EIT measurements.

4.1.9 Purpose

The aim of this chapter was to assess the performance of the newly developed parallel EIT system prior to starting recordings on patients and to identify the optimal protocol for this system used in epilepsy application. Then, the clinical safety tests were pursued to obtain approval for long-term recordings on the telemetry ward. The final purpose was to record EIT with depth electrodes in epilepsy patients for the first time.

The specific questions to be answered in this work were:

What is the optimal current-injecting protocol to produce the most accurate images using intracranial electrodes?

Is it possible to detect the expected impedance changes with the parallel system as tested with a resistor phantom?

Can a faithful EEG signal be recorded in parallel to EIT in real-time with scalp and intracranial electrodes?

4.1.10 Experimental design

In this chapter, the extent to which parallel EIT and EEG recordings are possible and feasible was investigated.

A simulation study aiming to check whether a reduced electrode protocol could still produce a clinically valuable reconstruction is described. The current design of the parallel EIT system limits the use of electrodes to only 32, which might theoretically be a too small number to achieve accurate image reconstruction. In order to test this, three protocols were proposed: the maximum distance (‘md’), the maximum current (‘mc’), and the white matter protocol (‘wm’). In the ‘md’ protocol, commonly used by

our group in the past, the injecting electrodes are spread inside the brain in a maximum spanning tree (Malone et al. 2014; Jehl et al. 2016; Goren et al. 2013; Witkowska-Wrobel et al. 2018). The 'mc' protocol was recently developed and proved beneficial for cortical recordings during evoked activity in rats (Faulkner et al. 2017). The aim of this protocol is to maximise the current on the region of interest. Such an approach, however, requires knowing precisely where the area of interest lies. Although it is practicable for imaging physiological activity, for which it is known which structures are activated but the protocol has limited applicability for localising a previously unmapped seizure onset in epilepsy. The third protocol was proposed as a solution to the potential problem that recording EIT might affect the SEEG signal on current-injecting electrodes. In this approach, the SEEG contacts set to inject EIT current were selected only from the contacts placed in white matter. This was possible as depth electrodes, inserted into the brain tissues through the burr holes, usually had the recording contacts spread evenly throughout the whole length, so that they could sample areas difficult to reach with scalp EEG, such as the orbitofrontal cortex or deep structures of amygdala or hippocampus. All clinically important information in SEEG came from the grey matter structures, but due to electrode geometry and brain sulci, some of the contacts ended up in the white matter. These contacts could be clearly distinguished while looking at the SEEG recording, as well as confirmed with the brain imaging acquired after the electrode implantation. Clinicians could use some of these contacts for grounding and reference of the SEEG. Therefore, the procedure used for this protocol was to manually find all available contacts within the white matter and combine them empirically in pairs within a maximum spanning tree, to increase EIT coverage. The main limitation of such an approach was that there could be only relatively few contacts available in the white matter, as neurosurgeons are constantly trying to improve their electrode placement including finding the way to maximise the number of contacts in the grey matter. It is thus possible that in some cases there were few contacts in white matter and not sufficient for the EIT imaging protocol.

That was indeed a case for one of the presented simulations, for which only four contacts could be set to inject current. An additional theoretical concern could be that the white matter contacts might be spread in a too far distance from each other to provide a reasonable EIT coverage, but this was to be tested in the described study.

These three protocols were then tested in a simulation study aimed at measuring the accuracy of imaging the seizure onset on the three intracranial epilepsy cases described in the previous chapter.

Subsequently, the parallel EIT system was tested with a resistor phantom to find out and define its noise levels without the influence of external sources, and while doing so, make sure the internal noise of the equipment is low enough to detect the expected small impedance changes. In order to do so, a phantom was used to simulate various levels of impedance signal change, while the EIT system was injecting current and measuring the voltages. The resistor phantom was connected instead of the EEG electrodes. While injecting current, as of during the actual in-vivo experiments, the phantom created the pre-set resistivity levels, without the addition of physiological noise coming from neuronal activity.

Further measurements were undertaken on a healthy volunteer with scalp EEG electrodes so that the impact of EIT injections on EEG signal could be assessed. A subject was recorded with EEG and EIT under resting conditions to define the spectrum of the background EEG signal, and during the sensory stimulation to get visual evoked potentials (VEP). It was expected that within similar conditions, the background EEG remained within the same spectrum and distribution of the detected frequencies, despite EIT injections. Similarly, the VEP response, as a standard clinical test with a very strict description of the amplitude and latency of the response, should provide a similar outcome, if neuronal activity was not altered.

Finally, the system was tested in clinical conditions on the telemetry ward, while recording the EIT signal together with the intracranial EEG (SEEG) from two epilepsy patients. All recordings were performed in epileptic patients producing frequent interictal activity after clinical telemetry was completed. The first patient was recorded for approximately 20 minutes with the initial design of the parallel EIT system and 32 contacts connected. The aim of the recording was to assess the SEEG signal picked up by the hospital EEG system, MicroMed, during EIT injections. This showed a saturation of the SEEG signal on the injecting channels and therefore required further developments to filter out observed DC offset artefact on hospital system due to EIT. Hence, we developed a high-pass filter to reduce the DC offset in real-time. A 0.1 Hz filter was installed on a connection between the SEEG electrodes and the MicroMed EEG amplifier. This was then placed on the split between EIT and SEEG on the channels set for injecting EIT current. Upon above and some further improvements of the EIT system so it was able to record on 64 channels, a second patient was measured for approximately 3 hours. None of this work aimed to reconstruct the images, and all of the measurements were undertaken to improve the EIT system and to adjust it, so it could meet clinically acceptable standards. This work was partially successful and so allowed later performance of EIT recordings with intracranial patients described in chapter 6.

Unless otherwise stated, the hospital system relates to the MicroMed EEG recorder and amplifier, used at Telemetry Ward at NHNN for clinical monitoring. This is to differentiate from the ActiCHamp, a system that records EEG in EIT that is currently approved for research but does not have the CE mark and so cannot be routinely used in the clinical setting. The details of the hardware of both systems are found under introduction section of this chapter.

4.2 Methods

4.2.1 Protocol optimisation in a simulation study

Three 3D anatomically accurate and subject-specific head meshes were used for this study, the same ones as those used previously to test the feasibility of recording EIT with depth electrodes described in chapter 3. Meshes of approximately 9 million tetrahedral and 37 000 hexahedral elements were created from joint CT-MRI. For each case, 32 SEEG contacts were selected from all available ones, so that then number of contacts matched the current capabilities of the parallel EIT system. The selection criterion was to cover the brain regions from where the majority of interictal and ictal activity came from, information about which was already available from telemetry monitoring, as this study was retrospective. The accuracy of the method was tested with five perturbations imitating a seizure onset per mesh. Their locations were ipsilateral to the depth electrodes, repeated from those previously described in chapter 3. The perturbations were placed within 6 to 27 mm distance from the closest SEEG contact used for EIT. All perturbations were 5-mm-radius spheres and had two levels of conductivity change, 1% and 10%, mimicking the fast and slow impedance change. The additive noise of a zero mean and a standard deviation of 1 μV was used to match the noise levels measured during the animal experiments (Avery et al. 2017; Vongerichten et al. 2016).

As introduced above, three protocols were proposed: maximum current (‘mc’), maximum distance (‘md’) and white matter (‘wm’). For each, five different electrode pairs were set to inject current of 60 μA at 10 kHz, and 32 other electrodes were set to record the voltages. In total, that resulted in 150 measurement lines for each protocol.

The ‘maximum current’ (‘mc’) protocol aimed to choose to inject electrodes based on delivering maximum current density to the region of interest, in this case, to the epileptic perturbation (Faulkner et al. 2017). In this approach, the average current

density was calculated for a given perturbation for an every possible injection pair. Then, all injection pairs for this perturbation were ranked within the maximum spanning tree, in order to find pairs that were weighted the highest. For this simulation study, five electrode pairs per perturbation were set to form a protocol. The 'maximum current' approach was, however, limited by the priors, as it was necessary to know the coordinates of the region of interest, i.e. the seizure focus, before selecting the protocol for EIT.

The 'maximum distance' ('md') was a protocol, in which identifying the injecting current electrodes was based on the maximum distance between them, i.e. the maximum spanning tree, so that the method was sensitive to the whole volume (Malone, et al., 2014). This protocol could find the minimum orthogonally independent set of pairs of electrodes, i.e. the smallest number of pairs that could cover all possible combinations and were farthest apart. This protocol has been already used for the study described in chapter 3, above however, in order to match the parallel EIT system, it was here limited to five pairs of electrodes injecting current only.

The 'white matter' ('wm') approach was a heuristic protocol proposed to address the problem of saturation of the SEEG chains, seen on injecting channels during preliminary recordings on the Telemetry Ward in the NHNN. For that, the contacts that do not provide valuable clinical information, i.e. in white matter, were manually selected for current injection.

The quality of the reconstructed images was evaluated using three metrics: localisation, shape and noise errors (Jehl et al. 2016; Malone et al. 2014). The reconstructed perturbation contained all voxels with at least 50% of the maximum conductivity change. Image quantification was assessed with respect to the ideal reconstructed image. The localisation error was defined in two units: millimetres and percentages of the mesh's dimensions, as the ratio between the distances of the centre of mass of the reconstructed perturbation (at the maximum conductivity

change) from the actual location of the perturbation placed within a head mesh as in chapter 3. The shape error was defined as the mean of the difference in each axis of the reconstructed perturbation to the perturbation's actual width, expressed as a percentage of the mesh's dimensions. The noise image error was defined as a standard deviation of the conductivity changes that are not in the reconstructed change expressed as a percentage of the mean conductivity change in the reconstructed perturbation. 95% confidence limit was used to compare the obtained errors for localisation, shape and noise, for each protocol.

4.2.2 Pre-hospital tests

All measurements in this section were made using the 32-channel version of the parallel EIT system (as described in the introduction to this chapter). The system consisted of one board able to inject 5 frequencies in parallel. For all tests described below, a current of 60 μA was set on all of them. The frequencies used were within the range of 4 kHz to 11 kHz in steps of 1 kHz. The 8 kHz frequency was skipped, due to the additive ActiCHamp noise at that level. The detailed frequencies used are stated under relevant sections below. This EIT system was approved and ready to use on patients, so that the recordings can mimic the real situation of EIT measurements in the hospital setting.

4.2.2.1 Resistor phantom tests

The EIT system performance was tested on a 32-electrode resistor phantom that could be switched between specific resistivity levels. The phantom was programmed to test three levels of impedance change, 0.1%, 1% and 10%, as this is the expected range of the impedance signal change for fast and slow changes, with the 0.1% change being an expected threshold of a detectable change. All electrode pairs available to inject current were tested, injecting 60 μA current at five frequencies at a time, within a range of 6 kHz and 11 kHz in 1 kHz steps, except the value of 8 kHz.

4.2.2.2 Simultaneous EEG-EIT tests on volunteer

Simultaneous EEG and EIT recordings were performed on one volunteer who signed a written consent prior to the experiment and in accordance with the approval we obtained for this study from the local Research Ethics Committee. 21 scalp Ag/AgCl cup EEG electrodes (10 mm radius, Micromed Electronics Ltd, England) were placed on the subject's head in accordance with the International 10-20 positioning system (Oostenveld and Praamstra 2001). Additional ground and reference electrodes were placed adjacent to the midline. Skin preparation was the same as described in chapter 2, using ethanol, an abrasive gel (NuPrep, Weaver and Company, USA) and a conductive EEG paste (Elefix, Nihon Kohden, Japan). The contact impedance was kept below 500 Ω. All electrodes were additionally secured with tape.

Awake, spontaneous EEG was recorded in 30-second sets of eyes closed and opened, resulting in a total of 10 minutes of the recording. Such series was recorded twice so that the spectrum of the EEG signal could be compared with and without EIT. The "eyes closed" period was used to enhance the alpha frequency in EEG and then to check its attenuation with the eyes opening. The EEG signal was filtered using Butterworth filter (2^{nd} order) with 0.5 Hz and 70 Hz cut-off frequencies, which are typical settings used during the clinical reading of scalp EEG. EEG recorded without and with EIT was compared qualitatively same as during the clinical assessment of EEG in the reporting sessions. The EEG spectrum was calculated using the power spectral density (PSD) estimate for each 30-second period using Welch's method for 1 Hz bins between 0 and 50 Hz. To identify the significance of the EIT influence on the EEG spectrum during eyes opened and closed, the t-test (two-tailed paired, $p<0.01$) was performed.

The visual evoked simulation (VEP) is a clinical test, which can provide information on signal conduction in the visual pathway (Odom et al. 2010; Hashimoto et al. 1999). It is commonly used to identify various neuropathologies while assessing a response delay. In a healthy person, there is a clear and very consistent positive peak at 100

ms after the stimulation (P100). The stimulation can be either a light flash or reverse of the checks in the checkerboard (American Clinical Neurophysiology Society 2006). The VEP paradigm was employed, using a reversing black and white checkerboard (a pattern-reversal VEP), with 0.6° black and white checks reversing at 2 Hz for 2 minutes, controlled with the Matlab extension PsychToolbox (http://psychtoolbox.org/). In the middle of the screen, a focusing gaze point (green cross) was presented during the whole experiment. A laptop screen showing the checkerboard was set on a distance of 70 cm in front of the subject. The subject was sitting on a comfortable chair, which was supporting the back and neck, in a darkened room.

4.2.2.3 Patients

Two epilepsy patients were recorded in this study. They were implanted with multiple intracranial depth electrodes and monitored on the Telemetry Ward of the NHNN. The patients gave informed and written consent to participate. The local ethics committee (London-Harrow Research Ethics Committee, 15/LO/0092) approved the study. The recordings were performed at the end of the clinical monitoring periods and both patients were on full dosage of previously taken antiepileptic drugs, so no ictal events were captured. The recordings took place in patients' hospital rooms, while the participants were in bed. SEEG was recorded with both systems, the hospital MicroMed EEG (Micromed S. p. A.) and EIT by the ActiCHamp (Brain Products GmbH).

Patient 1: a 43-year old male with a 30-year history of pharmacoresistant epilepsy. Currently, presents frequent focal seizures impairing awareness that arise without a significant warning and despite the medications. Based on EEG video telemetry, imaging data and clinical seizure assessment, the semiology was consistent with seizures possibly arising from the left temporal pole, orbitofrontal/mesial frontal, or insula regions. Therefore, he was subjected to an extensive intracranial implantation (11 electrodes, Figure 4-1, Table 4-1) to cover the left frontal and temporal areas and

to map the anterior language area. The interictal activity presented as independent sharp waves in the left frontotemporal, region of various frequency, usually every two minutes or so.

EIT was recorded for approximately 20 minutes. The preparation to connect EIT between the headbox and the MicroMed EEG system took another 20-30 minutes. EIT was connected to 32 electrodes, covering the contacts going to the amygdala, orbitofrontal, mesial pre-frontal and insula regions, as in these areas the majority of interictal activity was detected (Table 4-1). EIT injected 60 μA at three frequencies in parallel: 6, 7 and 9 kHz. The ground and reference were shared with those selected for clinical SEEG.

Patient 2: a 31-year old male, with a 15-year history of seizures, occurring daily. The seizure onset localisation was uncertain, with a rapid propagation over both hemispheres, semiology suggesting frontal lobe epilepsy, not clearly lateralising non-lesional MRI, and multifocal PET. EEG-video telemetry indicated the right hemisphere, which was not consistent with the psychometry, suggestive of the left dominant hemisphere dysfunction. Therefore, he was subjected to an extensive frontal and parietal exploration with SEEG. The implantation of 13 depth electrodes covered both frontal lobes (orbitofrontal cortex, inferior frontal, prefrontal), the supplementary motor and cingulate areas (Figure 4-1 and Table 4-1). Due to an unclear diagnosis, further two depth electrodes were implanted later during the presurgical investigation at telemetry, to cover the right mesial frontal and superior/medial frontal gyrus regions. The interictal spikes usually occurred about every two minutes or less frequently, occasionally forming the polyspikes.

The parallel EIT system recorded on 63 contacts for 3 hours. It was connected to the channels with the highest frequency of interictal activity (details in Table 4-1), sharing the ground and reference with the clinical system. There were five injections of 60 μA in parallel at 6 to 11 kHz, in steps of 1 kHz, skipping the 8 kHz frequency. 32 channels, including all those injecting current, were connected through a 0.1 Hz

high-pass filter junction box, which was added in attempt to avoid the saturation and reduce the DC offset artefact of the input channels on the MicroMed EEG system.

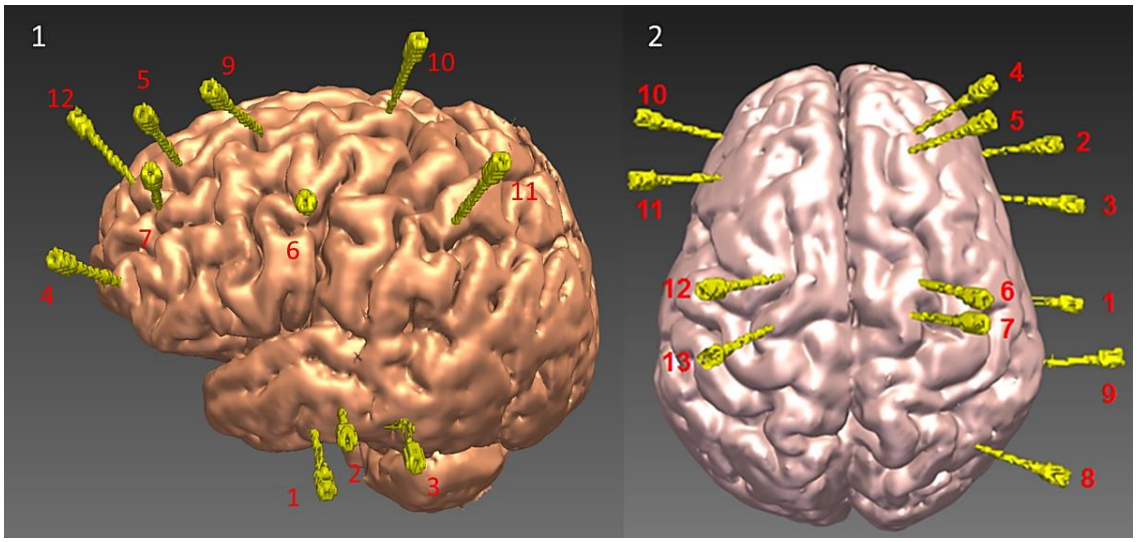

Figure 4-1 Implantation scheme for two patients investigated in this study. Patient 1 (left) was recorded with EIT on 32 channels, covering contacts on electrodes 1, 4, 5, 6 and 12; patient 2 (right) was recorded with EIT on 63 channels on electrodes 2, 3, 4, 5, 9, 10 and 12. In patient 2, two additional electrodes implanted after two weeks of telemetry (not shown here, both placed between 5 and 6) were also used for EIT. The coverage of each electrode is described below in the table (Table 4-1).

	Patient 1		**Patient 2**	
	SEEG	**EIT**	**SEEG**	**EIT**
1	Amygdala	2	R Anterior Hippocampus	
2	Anterior Hippocampus		R Orbitofrontal	10
3	Posterior Hippocampus		R Inferior Frontal Gyrus	7

4	Orbitofrontal	10	R pre-frontal	8
5	Mesial pre-frontal	9	R Superior Frontal Gyrus	6
6	Middle Cingulate	G+R	R Ant. Supplementary Motor Area	
7	Anterior Cingulate		R Supplementary Motor Area	
8	-		R Superior Parietal	
9	Ant. Supplementary Motor Area		R Posterior Cingulate	4+ G+R
10	Supplementary Motor Area		L Orbitofrontal	10
11	Posterior Insula		L Anterior Cingulate	
12	Anterior Insula	9	L Ant. Supplementary Motor Area	8
13	-		L Supplementary Motor Area	
			Two additional electrodes implanted later, not shown: R Mesial Frontal R Medial Frontal gyrus	 6 4

Table 4-1 Detailed anatomical coverage of the regions where the intracranial electrodes sampled (SEEG column) and the details on which contacts were connected to EIT (EIT column). The numbers in the first column correspond with the models presented in the figure above (Figure 4-1).

The recordings from the patient 1 were performed only to qualitatively assess the influence of EIT on the MicroMed EEG signal as the time slot assigned to us by the clinicians for EIT measurements was too short to capture interictal activity that could be correlated with EIT signal in this patient. In case of the patient 2, who was recorded for approximately three hours, this time was enough not only to assess the influence of EIT on EEG but also to capture interictal activity on some intracranial contacts. Before recording the latter, an additional 0.1 Hz high-pass filter junction box was developed and connected between EIT and hospital EEG. Preliminary tests with human depth electrodes in 0.2% saline showed that such a filter reduced the DC offset artefact on one electrode in an injection pair, so that one contact recovered, while the other one remained still saturated in the injection pair.

The impedance signal during interictal activity was processed for single injection pairs at each carrier frequency individually. EEG recorded with both systems, MicroMed and ActiCHamp, was filtered with a 1 Hz and 200 Hz bandpass filter (6^{th} order). The ActiCHamp data were re-referenced to create a bipolar montage, same as used in the clinical assessment of SEEG. The EEG signal recorded by both systems was combined to assess the EEG match. To assess fast impedance changes, a 200 Hz bandpass filter (30^{th} order Butterworth) was applied around each carrier frequency and demodulated using Hilbert transform. To assess slow impedance changes, a 20 Hz bandpass filter (30^{th} order Butterworth) was applied. The data were analysed in three ways in order to: (I) check fast impedance change during a single spike, (II) average fast impedance response from all interictal spikes during 3-hour recording appearing on one channel (rSFG4, electrode 5 on implantation plan) and (III) assess slow impedance change after a run of interictal spikes observed with a maximum on a single SEEG contact. To average the signal, the data were segmented into 480-ms epochs around each spike. These epochs were then averaged for each frequency

separately, yielding a mean impedance change to express the results. The SNR of the signal was computed by dividing the mean impedance change during the expected change by the standard deviation of the baseline. Unless otherwise stated, all data are presented as mean ± 1SD.

4.3 Results

4.3.1 Protocol optimisation in a simulation study

There was no statistical difference in described protocols in any of the image error metrics (n=15 perturbations, Figure 4-2) for both 1% and 10% impedance changes.

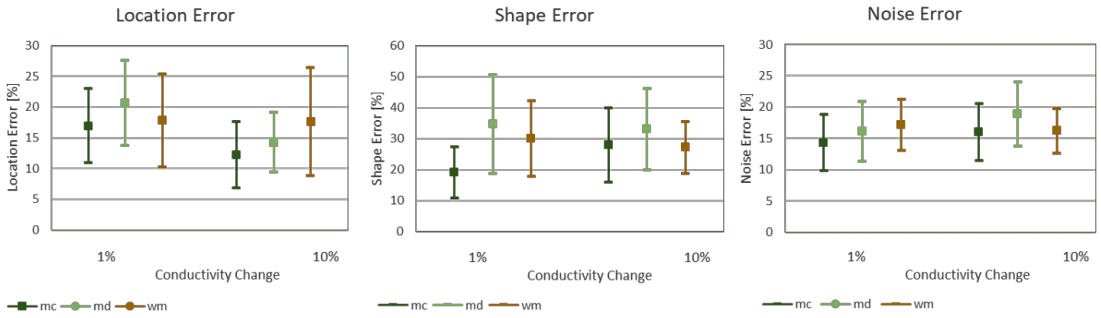

Figure 4-2. Individual errors for each of the protocol tested for both, fast, 1%, and slow, 10%, impedance change as represented by mean with 95% confidence limits. No statistical difference was noted between the protocols in any of the error metrics.

Similarly, the difference in localising the change as assessed in millimetres was not statistically significant. As expected, the 10% change was localised more accurately than 1% change (Table 4-2).

Protocol	**1% conductivity change**	**10% conductivity change**
mc	27.0±20.5 mm	18.6±17.6 mm
md	37.5±25.1 mm	20.3±19.2 mm
wm	40.0±34.1 mm	23.6±21.7 mm

Table 4-2. Localisation accuracy expressed in mm for each of the protocols tested (mean ± SE) in 1% and 10% conductivity change. Overall, the protocol maximising current density on perturbation resulted in the best localisation accuracy for both conductivity changes. However, none of these results was statistically significant.

When the outcome was compared qualitatively, the 'mc' protocol, maximising the current on the region of interest resulted in the smallest mean error for almost all metrics and for both 1% and 10% conductivity change, except for the shape error for 10% change.

4.3.2 Pre-hospital tests

4.3.2.1 Resistor phantom tests

A change of a maximum 15±3 μV (0.1% change), 100±8 μV (1% change) and 1300±9 μV (10% change) was observed in the resistor phantom tests (Figure 4-3). The measured noise across channels was 1.87±1.12 μV (0.014±0.012%).

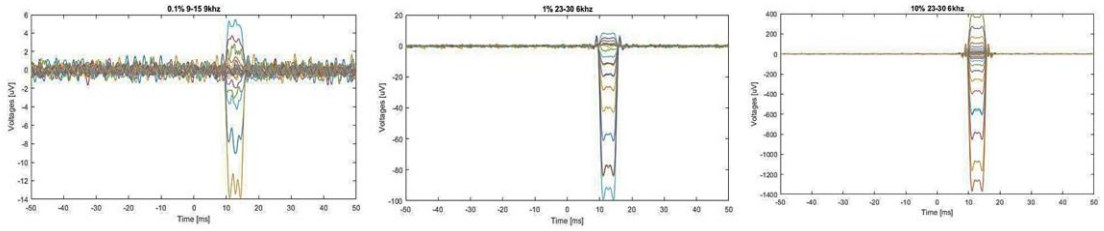

Figure 4-3. Examples of recordings with the resistor phantom at three levels of impedance change, 0.1%, 1% and 10% (left to right) between different pairs of electrodes. Various frequencies were tested with 60 μA current.

4.3.2.2 Simultaneous EEG-EIT tests on a volunteer

The noise in the EIT measurements on the volunteer was 1.51±0.85 μV. The raw EEG signal showed a well-formed alpha background rhythm (9-11Hz, up to 50 μV amplitude) with a normal attenuation to eyes opening. Similarly, a well-formed background rhythm (8-11 Hz, up to 50 μV amplitude) with a normal attenuation on eyes opening was seen when the parallel EIT system was injecting current (Figure 4-4). There was no significant difference in the spectrum for EEG during eyes opened

and eyes closed with and without EIT, as seen in PSD (Figure 4-5). The addition of EIT increased the 50 Hz noise (from 1.03±1.06 μV to 1.65±2.18 μV), requiring using further 50 Hz notch filter for VEP analysis. This is likely a result of additional EIT cabling, but it did not influence the latency and the amplitude of P100. The P100 averaged response amplitude was 6.62±1.7 μV and 8.85±2.3 μV respectively (n=220 repetitions, Figure 4-6). There was no statistical difference in the peak voltage or the latency with the EIT was or was not injecting current.

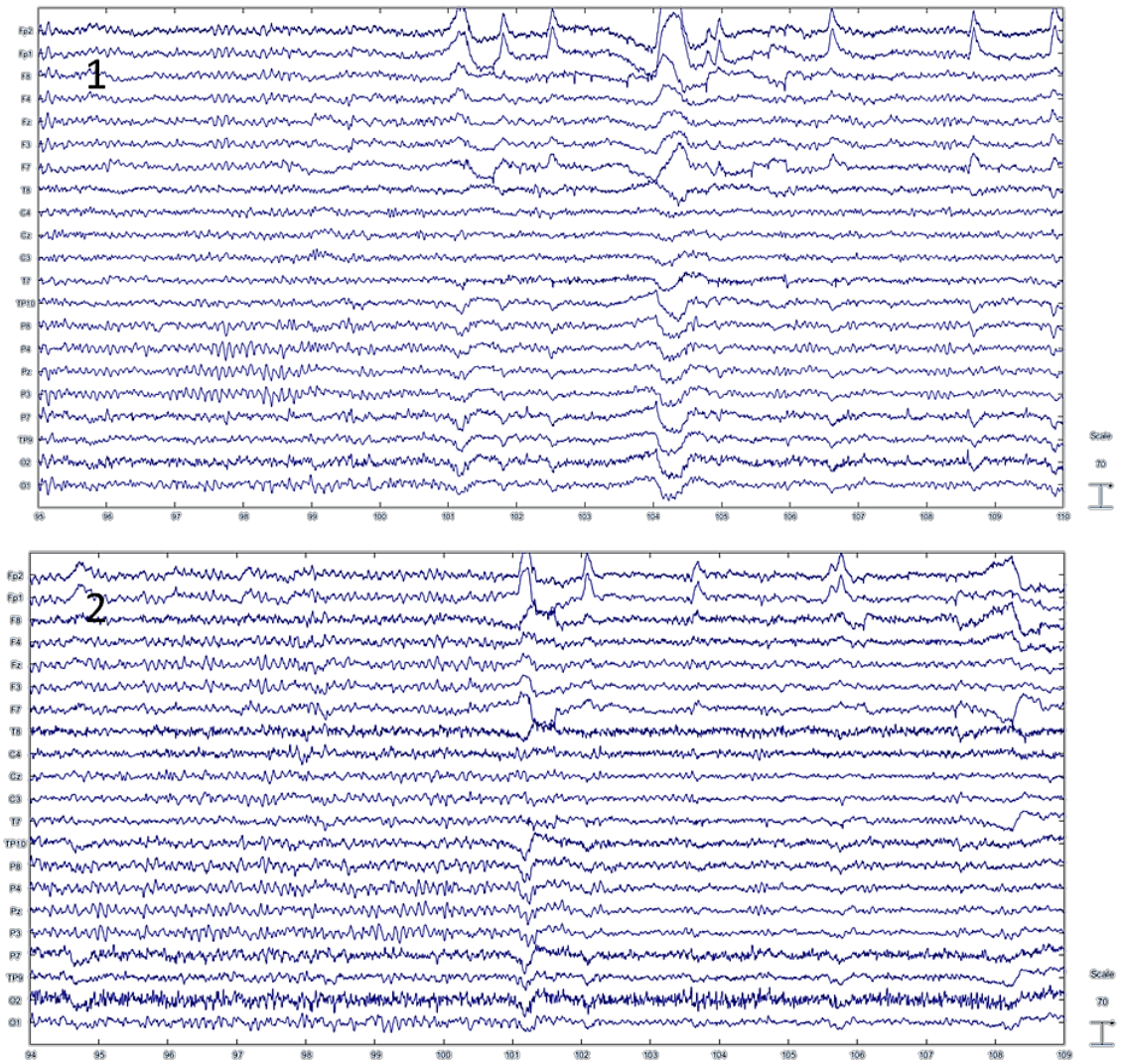

Figure 4-4. Comparison of scalp EEG recorded for 15 seconds on 21 electrodes in a common average montage, with 0.5 Hz and 70 Hz cut off. Top (1) shows EEG recorded without EIT when a subject was

asked to open eyes at around 101st second displaying a clear signal attenuation, together with eye-blinks artefacts over the frontal leads. Bottom (2) shows EEG when EIT was injecting 60 μA current between the electrodes Fp1 – O1 (4 kHz) and T7 – P8 (5 kHz). Again, a clear attenuation of alpha rhythms, as well as the amplitude of the signal is seen once subject opened eyes at around 101st second. 50 Hz notch filter was not used for either of these recordings. The scale of Y-axis is in μV.

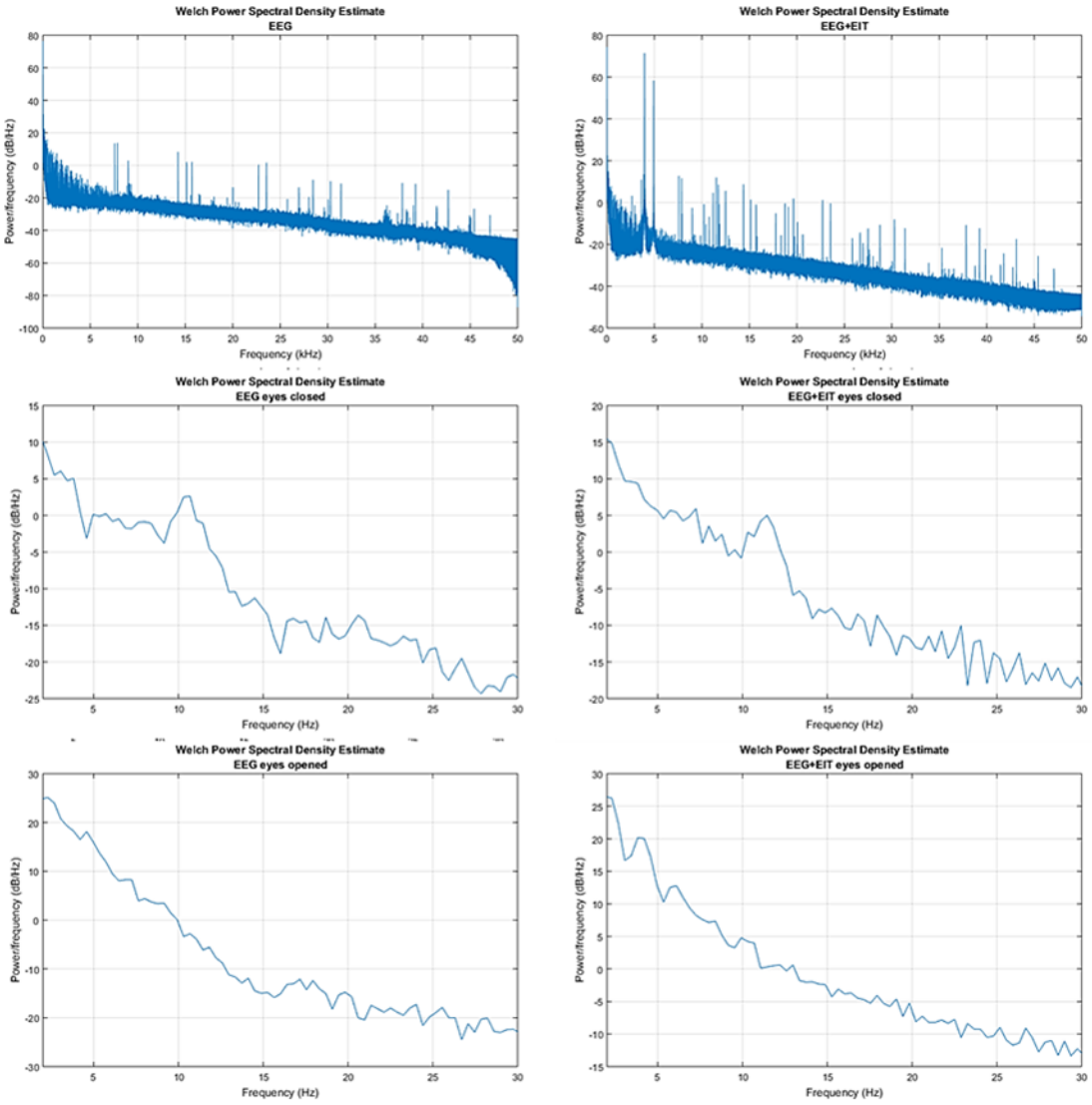

Figure 4-5. EEG spectrum without (left) and with (right) EIT injecting current at 4 kHz and 5 kHz in parallel. Top two graphs show the whole spectrum of the signal up to 50 kHz, for which there are two additional peaks for 4 kHz and 5 kHz, the injecting frequencies of EIT system (right). Middle and bottom rows show the enlarged spectrum between 0 and 30 Hz for eyes closed and opened

respectively. There is a clear peak at around 10 Hz for alpha rhythm when the subject had eyes closed, which disappeared with eyes opening for both recordings.

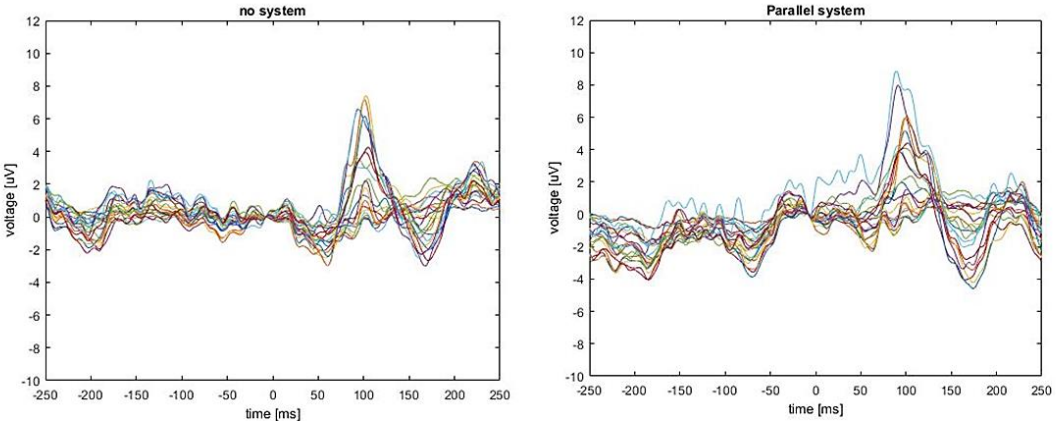

Figure 4-6. Averaged VEP response recorded on all scalp electrodes with EEG only (left, no EIT system), and when EIT was injecting current (right, the parallel system) from one subject. There was no difference in amplitude or latency of VEP response. Clear P100 peak is seen for both at 100ms with an amplitude of 6.62±1.7 μV and 8.85±2.3 μV respectively.

4.3.3 Patients

4.3.3.1 Patient 1

Saturation of all EEG channels set to inject current with EIT was observed throughout the recording on patient 1 (Figure 4-7) and all the other channels connected to EIT captured additional noise of 18±2 μV magnitude. The expected switching artefact was seen on the EEG traces, once the EIT injections were switched on but it disappeared in the initial seconds of the recording. All channels that saturated in the MicroMed were recorded with the ActiCHamp EEG in EIT without disruption, showing unaffected EEG.

Figure 4-7. Screenshot of SEEG recorded with MicroMed showing only the electrodes connected to the EIT system over a 20-second page. The switching artefact could be seen on contacts OF4, OF6, mPF2 and aIN3, when a pair OF4 – mPF2 was switched on to inject current. Following this artefact, these two chains became flat, as they were saturated during current injection. Similarly, the pair OF6 – aIN3 was already flat before this artefact, as it was injecting current before.

4.3.3.2 Patient 2

4.3.3.2.1 Raw EEG and effect of the filter box

The addition of EIT increased the background noise of EEG during recording patient 2 by 12±4 µV, which however could be considered negligible when compared with the millivolt magnitude of intracranial EEG and the observed amplitude of interictal activity (Figure 4-8).

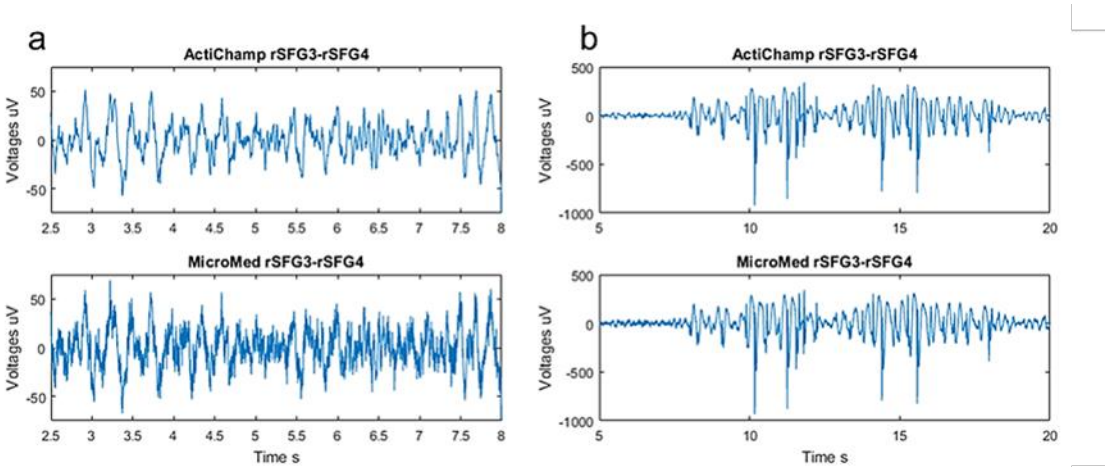

Figure 4-8. A comparison of a single SEEG channel recorded by the ActiCHamp (top for both figures) and MicroMed (bottom). There was a clear increase in noise seen on the MicroMed recording, coming most likely from additional cabling with EIT (a, no interictal activity captured), which can be considered negligible when assessing interictal activity (b, interictal activity captured). The noise could be further minimised with the addition of the 50 Hz notch filter.

The addition of a high-pass filter junction box removed the saturation of one channel in a pair injecting 11 kHz as seen on the MicroMed trace (Figure 4-9). The second channel remained still saturated, as expected from initial tests in saline. The filter box did not help with recovering the signal at lower frequencies, of 10 kHz, 7 kHz and 6 kHz (example for 6 kHz and 11 kHz on Figure 4-9).

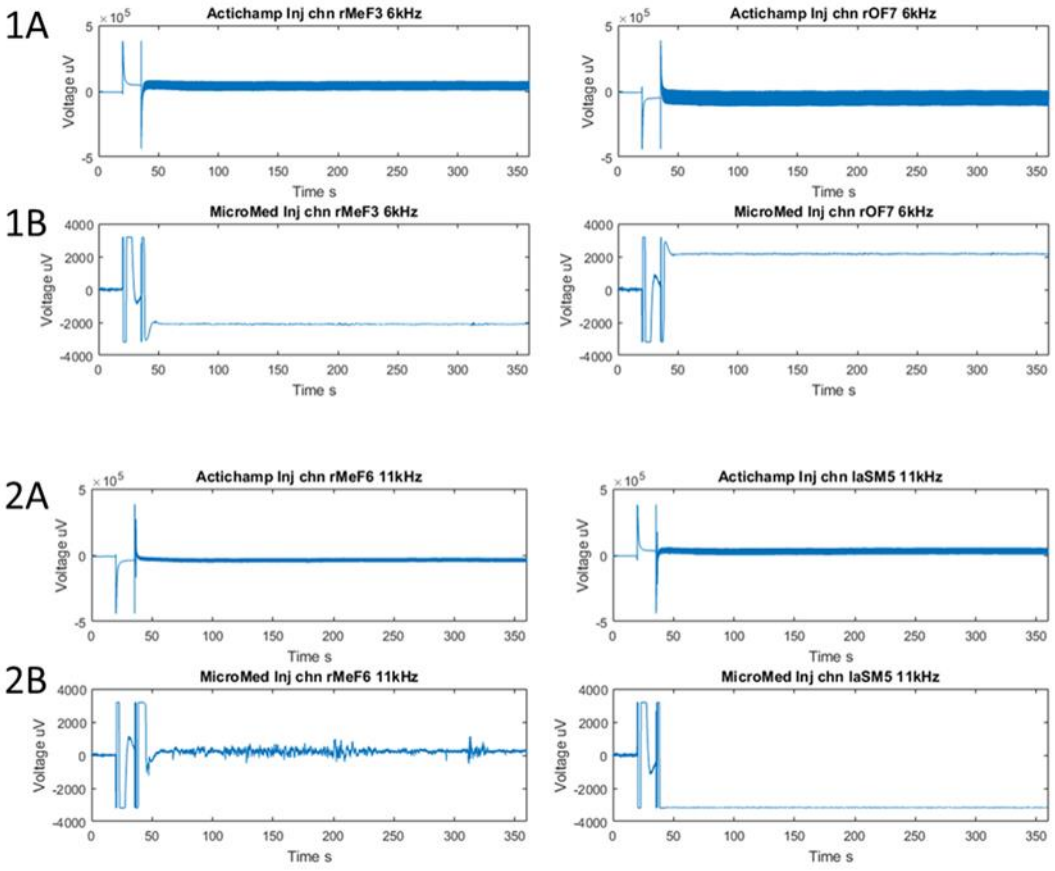

Figure 4-9. Beginning of the unfiltered EIT recording as seen by the ActiCHamp EEG amplifier (1A and 2A) and MicroMed (1B and 2B) on two pairs of contacts injecting 60 μA at 6 kHz (1A and 1B, injection pair rMeF3-rOF7) and at 11 kHz (2A and 2B, injection pair rMeF6-laSM5). There are expected artefacts related to switching on the EIT system seen on all channels at around 25 to 50 seconds, disappearing afterwards. After that, all channels recorded by ActiCHamp recovered, showing the SEEG signal coming from the respective contacts, whereas the signal on MicroMed saturated, except for rMeF6 at 11 kHz. The EEG signal seen on the ActiCHamp is raw and unfiltered, so the EEG component is masked with the sine wave coming from injecting EIT. This, however, is filtered out during the data processing.

4.3.3.2.2 Fast EIT change during a single spike

There was no impedance change detected during a single interictal spike at any frequency injected (example at 11 kHz in Figure 4-10) during the EIT recording of patient 2.

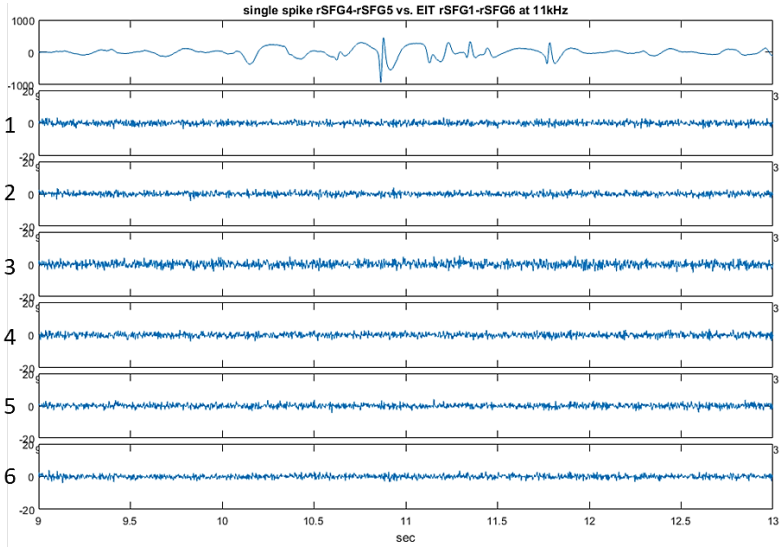

Figure 4-10. Single interictal spike with the maximum at channel rSFG4- rSFG5 (SEEG, top graph) and impedance signal observed on contacts around that spike, i.e. rSFG1 to rSFG6 (channels 1-6). No impedance change was detected.

4.3.3.2.3 Fast impedance signal for averaged interictal spikes

Averaging 50 interictal spikes coming from one SEEG channel did not yield a significant impedance change from the baseline at any frequency used (Figure 4-11). The baseline noise was 2±0.8 μV at 6 kHz, 1.8±0.3 μV at 7 kHz, 1.7±0.4 μV at 9 kHz, 1.5±0.2 μV at 10 kHz, and 1.1±0.2 μV at 11 kHz. The SNR was 0.002±0.4 to 0.01±0.05 for these frequencies.

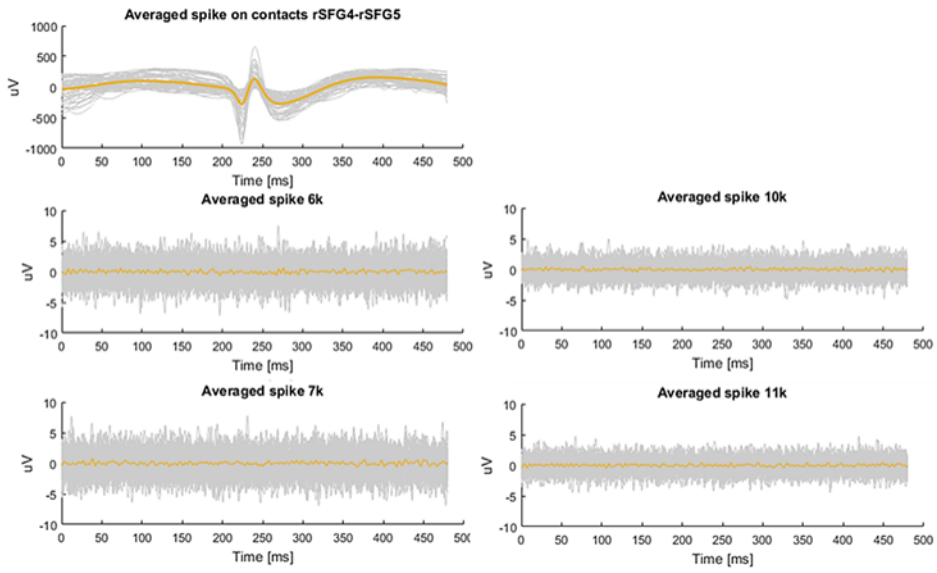

Figure 4-11. Averaged interictal spike seen on one SEEG channel over the 3-hour recording time (n=50) compared with averaged fast impedance signal observed at each frequency measured. No EIT response could be seen with respect to the interictal spike after averaging the signal.

4.3.3.2.4 Slow impedance signal for a quick run of interictal spikes

Inconsistent in direction (increase and decrease or only decrease) slow impedance changes of a maximum of 0.005±0.001% were recorded at 6-10 kHz frequencies after a quick run of interictal spikes (n=9, example on Figure 4-12). A single spike did not produce specific slow changes.

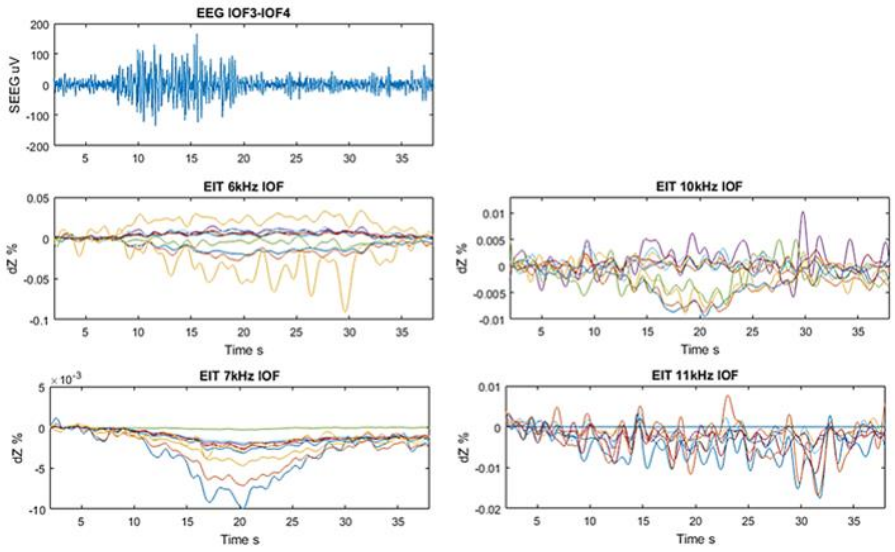

Figure 4-12. A slow impedance change arising in seconds after a brief run of interictal activity (n spikes = 9). The impedance change presented on graphs is seen on the adjacent contacts to the SEEG contact with interictal spikes (IOF). There is a positive and negative change at 6 kHz, negative change at 7 kHz and 10 kHz and no change at 11 kHz.

4.4 Discussion

4.4.1 Summary of findings

Overall, this work shows that it is possible to record an impedance signal with the parallel EIT system. As expected, it also indicates that EIT does not disturb normal brain activity as measured with EEG and evoked potentials if recorded with the ActiCHamp EEG amplifier. However, due to several limitations of the hospital system, EIT injections affected the EEG recorded with the MicroMed. It was also shown that it is possible to obtain similar accuracy of the reconstructed images with all three protocols tested in the simulation study so that even using the contacts placed only in the white matter could be a potential short-term solution for simultaneous EEG and EIT recordings in the hospital. Preliminary results collected from one of the intracranial patients are promising for detecting impedance changes in future, if longer recordings allowing for detecting more interictal activity, or seizures became possible.

4.4.2 Technical limitations

Although further work on finding out the limitations of the EEG amplifier used in the hospital could be desirable, it is beyond the scope of this thesis. Upon contacting, the company producing the MicroMed EEG system (Micromed S.p.A.) was unable to explain the reason for the saturation or recommend a potential solution. Unfortunately, due to the company privacy policy, they were not able to share the detailed design of the MicroMed amplifier, either making it impossible to overcome the problem within a timeframe reasonable for this study. A potential solution could be to find a spare or buy the MicroMed system externally, not for clinical use, and try to deconstruct it and thoroughly test it to further understand its design. This, however, is not possible to perform with the clinically used MicroMed at NHNN, to which we have access, as it would lead to losing the licence and technical support from MicroMed in the hospital. In addition, the engineers from the MicroMed Company suggested that the filter we used should have worked, and they are currently unable to suggest any way of fixing the issue. This suggests the problem might be not obvious and so very hard to solve and so other solutions, such as using alternative amplifiers, seem like the best way to advance the study.

4.4.3 What is the optimal current injecting protocol to produce the most accurate images using intracranial electrodes tested in simulation study?

The results of the simulation study described in this chapter indicated that it should still be possible to obtain EIT images of the onset despite the limitation of only 32 contacts being connected, and 6 electrode pairs injecting the current. However, as expected, the accuracy of such a method has been significantly reduced when compared with the optimal protocol described in chapter 3.

There was no statistically significant difference in the performance of any of the three protocols. When assessed qualitatively, they all performed similarly well,

slightly favouring the protocol focusing current on the region of interest ('mc'). However, the main drawback of 'mc' is that it requires some known priors on where the epileptogenic activity occurs. Potentially, for epilepsy patients with intracranial electrodes, it could be possible to prepare the injection protocol based the findings from scalp EEG and adjust it after recording the first ictal event. Still, such an approach is not optimal as some patients will have seizures rather rarely, and so their intracranial video-telemetry will be finished after recording only two ictal events or so. In such case, there would be little, if any, time to adjust the initial protocol, so, for such patients, it will be necessary to use one of the alternative protocols.

Another important outcome of this study was to show that the protocol using only contacts in white matter to inject current resulted in a similar accuracy, as the other protocols established before as 'optimal'. Contacts placed in white matter are already commonly used for the reference and ground during the clinical recordings, as they do not show SEEG signal. However, even the physiologists working at the Telemetry Ward of NHNN can sometimes struggle to find just two contacts being in white matter for that purpose. Therefore, it is possible that there would be not enough number of contacts in white matter to form a reasonable EIT imaging protocol in all cases, especially given that the current clinical approach is to limit the number of contacts in white matter to enhance the sampling from the grey-matter regions of interest. For example, at NHNN, the sampling from the orbitofrontal regions has been improved by implanting depth electrodes laterally, rather than from the top of the head. This resulted in almost all contacts being in grey matter, in comparison with having 4-5 contacts in white matter achieved often with the previous implantation approach.

Overall, the results from this study suggest that it is possible to use the EIT system with 32 contacts; however, it is desirable to improve the coverage over a wider area of the brain, as well as to inject the current on more channels. Choosing only 32

contacts to connect to seems a very low number if compared with how many contacts are actually used for SEEG recordings in intracranial patients. For these reasons the most recent work described in this chapter, i.e. EIT recordings of the patient 2, were made with a 64-channel EIT system.

4.4.4 Is it possible to detect expected impedance changes with the parallel system in tests with the resistor phantom?

The noise characteristics measured in the resistor phantom and with scalp electrodes were similar to the performance of the serial EIT system used by our group for brain applications: the ScouseTom EIT system (Avery et al. 2017; Goren et al. 2018). Also, these values met the criteria for recordings in scalp recordings during seizures (Fabrizi et al. 2006). The study has hence shown that the parallel EIT system is expected to produce optimal results for proposed application.

4.4.5 Can EEG signal be recorded in parallel to EIT in real-time with scalp and intracranial electrodes?

Data collected with scalp EEG and during VEPs demonstrated that EEG signal is not significantly affected by EIT, and so can be collected in parallel to EIT measurements, if recorded by the ActiCHamp EEG amplifier. In such case, EEG can be recovered and displayed on a screen in real-time using the in-built software filters or afterwards, by applying the external filters in Matlab software. The unaffected recording on both, injecting and recording EIT electrodes during scalp measurements, clearly supports the notion to further advance the EIT system, so that it can inject at every electrode. Depending on the montage, that can be 16 injecting pairs for stroke applications (Goren et al. 2013) or up to 64 if the system is used for intracranial recordings (Witkowska-Wrobel et al. 2018).

However, as further studies with the intracranial epilepsy patients showed, the type of the EEG amplifier used for the EIT study can pose a significant limitation. The clinically used EEG amplifiers are CE-marked and their setting flexibility is

minimised to maintain stable clinical recordings. For instance, they usually sample on significantly lower rate when compared with the non-CE marked amplifiers, such as BioSemi, ActiCHamp or g.tec. For EIT that means that an additional EEG amplifier, requiring higher sampling rates, has to be used to collect the impedance data. Then, the MicroMed has a dynamic range of several millivolts (±3.2 mV) when compared with 0.5 V of the ActiCHamp. Thus, the input can be easily saturated by the DC offset coming from EIT injection channels and affecting the respective EEG traces (Figure 4-13 A). As the inputs of the clinically used amplifiers are easier to saturate, they require custom-made hardware filters or DC blocking (Figure 4-13 B). This was overall what was observed during the preliminary recordings with SEEG on patients, as the injection channels were saturated on the MicroMed straight after the injection was started, whereas ActiCHamp showed clearly that the EEG could be easily recovered. Still, when recording SEEG on the patient, the addition of an external 0.1 Hz high-pass filter junction box did not help to solve this problem, resulting in only one electrode out of 10 frequencies recovered. This is believed to be caused most probably by some additional MicroMed settings that are not yet understood.

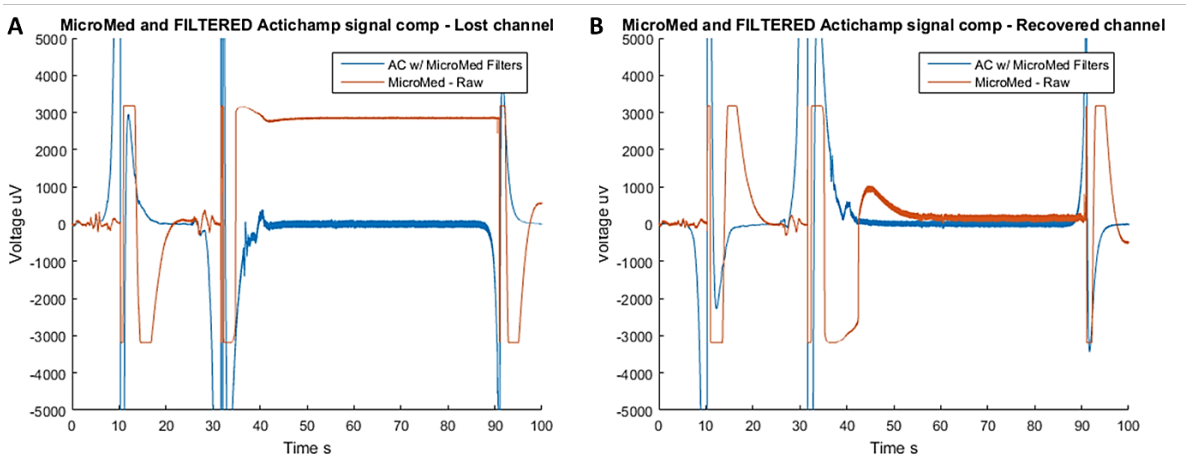

Figure 4-13. A comparison of SEEG signal recorded on one channel by the MicroMed (orange trace) and ActiCHamp (blue trace), when EIT injection of 60 μA at 7 kHz was started on that channel. Figure A shows the raw recordings, there are several expected artefacts related to turning on EIT and switching the injection on, lasting up to almost 40 sec into the recording. However, after that, the EEG

signal recorded with ActiCHamp recovered, in contrast to MicroMed, for which the signal remained saturated until the injection was stopped. Figure B shows that if the signal recorded with MicroMed goes through a hardware high-pass filter of 0.1Hz cut-off. Filter removed the DC offset so that the main reason for saturating the MicroMed channels. Hence, EEG could be recovered on both amplifiers.

Finally, considering that the main reason for the saturation seems related to the internal settings of the MicroMed, preliminary recordings with a different EEG amplifier were proposed. Currently, there are two hospitals in London performing presurgical evaluation with intracranial electrodes in adults with epilepsy, National Hospital for Neurology and Neurosurgery (NHNN) and Kings College Hospital (KGH). All EIT measurements were recorded in collaboration with the Telemetry Ward at NHNN, where MicroMed EEG system is used. However, different EEG system, with the Natus Quantum LTM EEG Amplifier, is used at KCH. This amplifier has slightly different settings, for instance, has an input signal range of ±20 mV, which could be beneficial for overcoming the channel saturation observed with MicroMed. For this reason, further preliminary tests were proposed at KCH.

Towards the very end of all the studies described in this thesis, a new collaboration was established at KCH and some initial, very preliminary recordings were performed using the scalp Ag/AgCl EEG electrodes on a volunteer connected to the headbox used for intracranial patients at KCH. Five electrodes were placed on T5, O1, O2, T6 and Pz according to international 10-20 Positioning System (Oostenveld and Praamstra 2001) and they were connected through the split to EIT, without additional filters (channels 1 to 5 respectively on Figure 4-14). A current of 60 μA at 10 kHz was injected on electrodes 1 (T5) and 3 (O2). There was no saturation observed on the KCH Natus EEG system (Figure 4-14). EIT added noise of up to 40 μV on all electrodes connected and required the use of the 50 Hz notch filter, which is usually not applied for the clinical EEG reading at KCH but after discussion with the local staff it was agreed that the clinicians could potentially accept it. The major limitation of these tests, however, was that they were performed with scalp, not intracranial electrodes. It is expected though that the outcome of such tests should

be similar, as generally the EEG recorded with intracranial electrodes has fewer external artefacts and the contact impedance in case of depth electrodes is much smaller than that of the scalp ones.

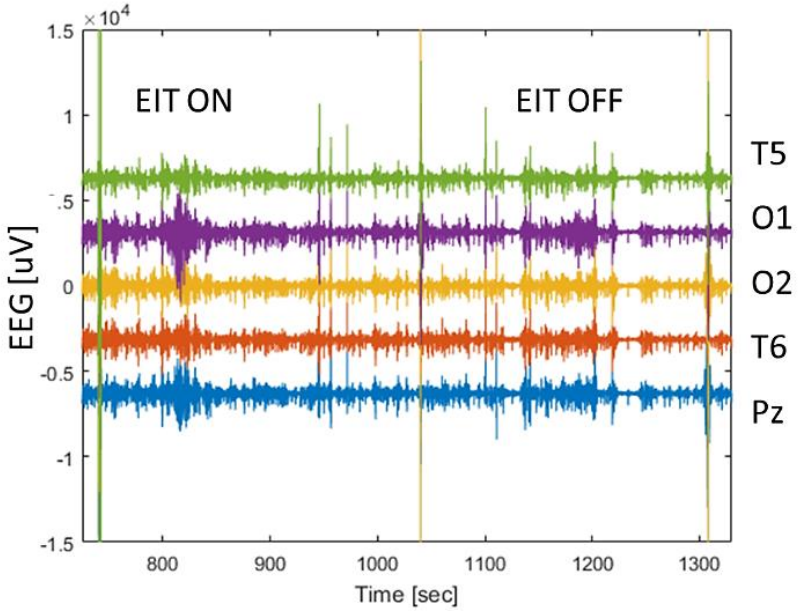

Figure 4-14. A comparison of the EEG signal recorded with the Natus Quantum LTM EEG Amplifier at KCH, when EIT system was on and off (switching on at ~740 sec, off at ~1040 sec, on at ~1305 sec, all visible with the artefact). The current was injected between electrodes T5 and O2. There is a clear artefact when the system was switched but no additional noise is seen during the injection.

However, it was also noticed that a careful selection of the frequencies used for EIT should be studied further to maximise the impedance signal recorded. When several frequencies are injected at the same time, it seems possible that the signal coming from different frequencies gets contaminated. In order to overcome this issue, the spacing between the frequencies should be at least twice as the filter bandwidth used in the signal processing. On the other hand, if the frequencies used for injections are spaced too wide within a division, the harmonics of lower frequencies will affect the higher ones. Hence, it is anticipated to set all frequencies within one octave of the fundamental. The injected frequencies must be also balanced against the bandwidth of the EEG signal recorded, which for intracranial EEG is set at up to 1 kHz, and the

medical engineer from the hospital required us to inject above 1.5 kHz. Finally, the recording ability of the currently used EEG amplifier is 20 kHz, which sets the upper limit of the frequency injected. Overall, such limitations in injected frequencies can affect potential applications of the parallel EIT system. For slow changes, such as cell swelling during seizures or blood flow in physiological activity, wide frequency range can be used, up to 10 kHz and 20 Hz bandwidth (Hannan et al. 2018). However, fast impedance signal can only be detected within a significantly smaller range, up to 3.5 kHz and with a bandwidth requiring 2 kHz spacing between the frequencies (Hannan et al. 2018; Faulkner et al. 2018). This makes our current parallel EIT system much better suited for recording the slow changes than the fast in possible epilepsy applications in the clinic.

4.4.6 Conclusion and future work

Overall, the work presented in this chapter shows the development of a new parallel EIT system, which is reliable, has similar noise levels as the serial EIT system normally used on animal experiments, is completely independent of the external power supply, and crucially which is safe. The system was tested by the medical engineers at NHNN and is now ready to use in a clinical environment for long-term telemetry recordings. We showed for the first time it is possible to use the parallel EIT system on intracranial patients and proved that EIT does not trigger ill effects and can be safely used, even if injections are within close proximity from the onset zone.

During the time required to finish this work, the system was significantly improved, allowing connecting 64 channels to record the EEG/EIT data. It has been shown that EEG can be easily recovered on all channels if assessed with the ActiCHamp EEG amplifier. However, there was an increased noise, requiring 50 Hz-notch filter, and saturation on injection current channels when assessing the signal recorded with MicroMed. The additional noise observed probably comes from the extra cabling from the EIT connection. The results have been to some extent improved with the

high-pass filter junction box, but it did not completely fix the problem. Further communication with the company producing the system has not helped either. Although this issue has remained unsolved at this moment, some successful preliminary tests performed with an alternative EEG amplifier, the Natus, at the KCH telemetry ward suggested that the easiest way to overcome the problems would be to change the site of the study from one that uses MicroMed to one that has the Natus.

Future work should be focused on further developments of the parallel EIT system so that the injection protocol combines more electrode pairs and hence leading to increased EIT sensitivity. This likely could be achieved by combining several current-injecting PCB boards into one large system. While improving the parallel EIT system, it is also worth considering how it is connected to a patient aiming at reducing the length of the cables and using shielded cabling if possible, in order to reduce the interference.

When it comes to further clinical work, there seem to be two ways to continue with the study. First is to continue it with the MicroMed at NHNN, using the protocol for which contacts only in white matter inject current or recording is performed at the end of clinical assessment, during which no ictal events can be captured but the interictal activity might produce reproducible impedance changes. Given the timescale of the whole study and the aims of this thesis, this is what was done, and the results of this work are described in chapter 6. The other solution would be to move the study to the Kings College Hospital, or to another hospital that uses an amplifier compatible with our system and performs further measurements with intracranial electrodes there. Even though the second option is beyond the scope of this thesis, as it would require extending the ethical approvals to external hospital, which would take a very long time, it seems to be the better way to optimally and conveniently advance the study in future.

Chapter 5

Imaging slow impedance changes in a focal model of epilepsy in the porcine brain with Electrical Impedance Tomography

Overview

It was shown in chapter 3 that EIT has the potential to significantly improve the localisation of the onset over SEEG or inverse source modelling but experimental confirmation of these findings is needed. The original aim was to extend the results obtained in the simulation study in human clinical studies in patients with depth electrodes. Unfortunately, access to patients was limited due to clinical caution relating to the problems described in chapter 4. Therefore, I decided to undertake empirical studies in a porcine model of epilepsy and implant human intracranial electrodes. The porcine brain closely resembles the human brain and was chosen as a model. I employed the same depth electrodes as those used in human clinical studies. Recurrent seizures were produced with a focal intracranial injection of chemoconvulsant.

5.1 Background

5.1.1 Swine model for monitoring of seizures with intracranial electrodes

Pigs have been widely used for multiple biomedical applications, such as transplantation, cardiovascular and metabolic diseases, drug and neurotransmitters metabolism, models of neurodegenerative diseases, stroke or brain injury (Sauleau et al. 2009). There has also been an increasing interest in their use in neuroimaging and neurosurgery studies (Van Gompel et al. 2011).

A porcine model for intracranial monitoring has several benefits over the other large animal species. The swine brain is relatively large, weighing approximately 180 g in an adult animal. The brain resembles that in a human to a considerable extent (Figure 5-1). It is gyrencephalic, has similar vascularisation, histology, and myelinisation. It is comparable to that of the human and the primates in gross anatomy, cortical convolutions, shape, and the total number of cortical neurons (Sauleau et al. 2009; Lind et al. 2007). Functional studies have mapped the detailed

somatotropic representations of the body surface (Craner and Ray 1991). In addition, pigs are far less expensive to procure and maintain than primates.

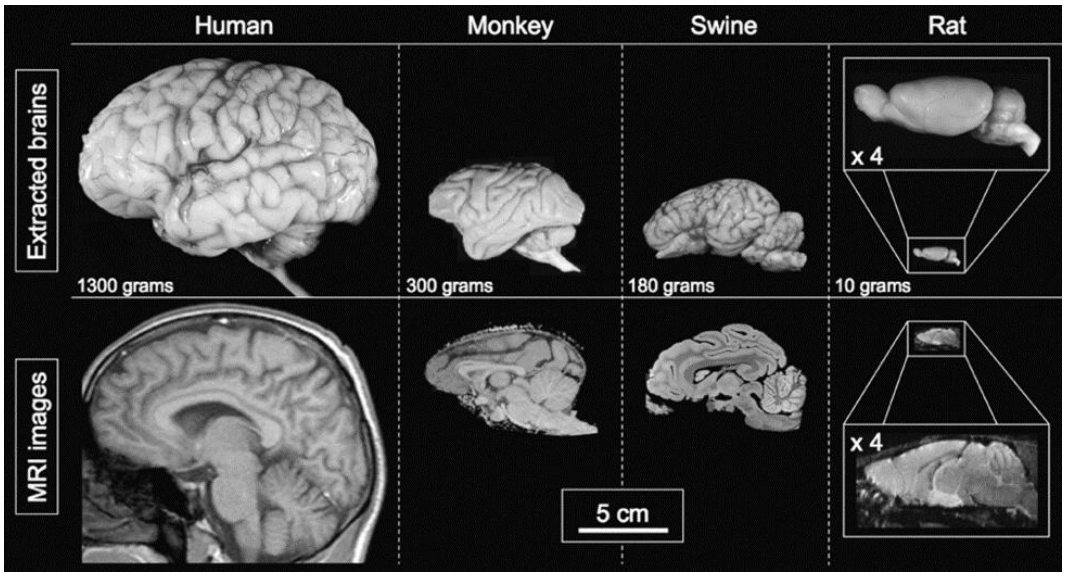

Figure 5-1. A comparison of the ex-vivo (upper) and MRI scan (lower) of brains from a human, rhesus monkey, pig and rat. Gross anatomy and geometry of human, monkey and swine brains are relatively similar, including the gyrencephalic structure. The rat brain is not only significantly smaller, with overall differences in anatomy but it is also lissencephalic. These comparisons show clearly an advantage of swine brain when compared to the rodent model for imaging or for the use of intracranial electrodes (Sauleau et al. 2009).

5.1.2 Penicillin model of epilepsy

Chemical models of epilepsy are commonly used in various animal species. Chemical convulsants are easy and quick to use, usually result in rapid seizure-induction and are relatively easy to adjust, depending on the experimental paradigm. They are often used for acute models of seizures, as most chemoconvulsants do not produce chronic epilepsy (Kandratavicius et al. 2014). Convulsant drugs can be administered systemically, such as cocaine, lidocaine, and pentylenetetrazol (Nakao et al. 2004; MacDonald and Barker 1977; Buckmaster 2004). They may also be applied locally either subcortically or intracranially, such as carbachol or penicillin (Fisher 1989;

McNamara 1984; Wagner et al. 1975). Most of the drugs have been tested and described for rodent models; the literature available for larger animals is limited.

Penicillin has been established across species and its epileptogenic effect on the mammalian cerebral cortex is well-studied. Topical, intracortical or systemic administration of penicillin leads to paroxysmal activity that may result in seizures. The seizure-inducing potential of penicillin derives from the reduction of GABA-dependent inhibition; excitatory cortical afferents then trigger epileptiform bursts (Fisher, 1989). A single cortical injection induces a focal epileptic lesion, with a dose-dependent response from a single ictal event up to status epilepticus (Akdogan et al. 2008). Most of the literature available for large animals describes an acute focal cortical model of epilepsy with penicillin injected between 1 mm to 5 mm below the dura. The model was also tested once for hippocampal injection in an ovine brain. There do not appear to be other studies on the use of penicillin models with deep, below cortical injection of penicillin in a large animal brain.

In pigs, the model was tested on several age groups of animals and for both focal and generalised seizures. In 13 piglets, 6000 IU of penicillin were injected 5 mm below the dura mater over the somatosensory cortex (Mäkiranta et al. 2005). Brain activity was monitored with fMRI and two scalp electrodes placed ipsilateral and contralateral to the injection site. The epileptic spikes were recorded over the burst suppression brain activity, due to deep isoflurane anaesthesia. Initial epileptic spiking activity started within 1 minute after penicillin induction, increased in amplitude over the following 8 to 13 minutes, but remained stable or decreased throughout the recordings. After the experiments, the animals were euthanised. Generalised seizures were induced in piglets with repetitive injections of 100000 IU of penicillin 2 mm (Leaming et al. 1999, n=19) or 3 mm (Terndrup et al. 1999, n=13) below the temporal cortical surface and recorded with the epidural electrode array. Both studies measured the respiratory effect of seizures rather than seizure development. However, despite its common use in a pig brain, the first and the most

detailed description of the focal seizure model induced with penicillin was published in 2011 (Van Gompel et al. 2011). Initial experiments were performed on 14 animals (2011). The model was later used on 45 adult pigs (Van Gompel et al. 2014). The authors tested several anaesthesia setups, including the isoflurane, fentanyl, morphine, ketamine and lidocaine, concluding that maintaining the fentanyl anaesthesia resulted in the best outcome. EEG was recorded with a 64-channel epicortical grid placed over the hemisphere. 5500 IU of penicillin were injected 4 to 5 mm below the brain surface. The animals were euthanised at the end of the recordings. The authors categorised the observed activity into the four grades. Grade I was defined by a normal background brain activity, during which no spikes could be distinguished. Grade II was represented by the high-voltage spikes, arising at less than 1 Hz frequency from the background. During grade III, spikes tended to occur more often. Grade IV was defined as a seizure, during which synchronised polyspikes or paroxysmal sharp waves were seen at >3.5 Hz frequency. This stage usually lasted more than 6 seconds, with an average duration of 46 seconds. Further analysis of whether the seizures were focal or generalised or their spread over the EEG contacts was not approached by the authors. However, based on the variability of the epileptiform activity observed, their repetitive occurrence and overall EEG progression, authors concluded that the model offers important benefits. It could be used to monitor the epileptiform propagation with the multiarray devices. Importantly, they concluded that the model was relevant enough that it could be used for investigating problems that could not be addressed in human subjects at this time.

The first study describing the use of penicillin as epilepsy model in a sheep brain showed that intracortical injection creates focal seizures with ipsilateral and secondary spread (Opdam et al. 2002). 8000-10000 IU of penicillin was injected 1 mm beyond the cortex, through the pre-prepared ports over the frontal cortex. EEG was recorded with the epidural electrode strips extending posteriorly towards the

parietal cortex in 10 sheep. The authors distinguished 5 relatively predictable and reproducible phases of epileptic activity. Several seconds after the induction, regular 0.5 Hz spikes started, and their frequency spontaneously increased to 1 Hz and then above 1 Hz. Spike morphology then changed into the 3-second bursts of multiphasic polyspikes, followed by the focal seizures. Once the seizure occurred, the epileptic activity was repetitive and consistent with the status epilepticus. Seizures were always recorded at port electrodes with the ipsilateral spread. In this study, the animals were euthanised within 2 hours after developing a seizure.

Finally, the only known study with deep brain injection of the penicillin in the large animal brain was described in sheep (Stypulkowski et al. 2011). The purpose of the study was to test the influence of the thalamic deep brain stimulation on the evoked activity and seizures. The minimum of 8000 IU of penicillin was injected through a catheter into the hippocampus. The authors observed an increase in amplitude and frequency of spikes over the initial minutes after the penicillin administration; this activity remained stable afterwards at approximately 1 Hz frequency. Increased doses of penicillin did not lead to bursts of higher frequency spikes. The spiking activity started at the closest contact to the injection site, it was then followed by the spread over the adjacent contacts. However, the brain activity was only monitored with one depth electrode with 4 contacts placed in the hippocampus. No extensive EEG monitoring was performed.

5.1.3 Parallel EIT system

The parallel EIT system used to record slow impedance changes used frequency division multiplexing, FDM-EIT (Avery et al. 2017). In a parallel system, current can be injected between different electrodes and at different frequencies at the same time simultaneously. Voltages are recorded on all of the electrodes. It enabled acquisition of all current injection pairs needed simultaneously and so produced real-time images, without the need to average the signal in post-processing. It allowed performing single-shot imaging of an ictal event. The details of the hardware

of the parallel EIT system have been covered in relevant sections of the introduction in chapter 4.

5.1.4 Rationale

The aim of the work in this chapter was to undertake an experimental study to determine if EIT could localise seizure onset as suggested in Chapter 3.

The model was chosen according to the following considerations. The aim was to use a model, which simulated human focal epilepsy.

i) Species. In order to imitate the human brain accurately, the modelled brain needed to have gyri, as in humans, and be sufficiently large to accommodate human intracranial electrodes. In order to avoid the use of primates but to keep the size and anatomy of the brain comparable to a human, a pig was the species chosen for the study.

ii) Method to produce seizures. Focal cortical injection of the chemoconvulsant, benzylpenicillin, creates a lesion, which generates focal seizures. Until now this has been described in detail for intracortical injection and cortical seizure generation, with to date one example of hippocampal seizure induction in a sheep brain. This, however, was only monitored with a 4-contact intracranial electrode. For this study, to test the ability of EIT to detect deep focal seizures similar to those in human mesial temporal epilepsy, a deeper seizure focus was desired. I, therefore, employed a model with a deep intracranial injection of penicillin, in the hope that this would produce similar cyclic and repetitive epileptogenic activity similar to the cortical grades described in the introduction. My aim was to test that EIT could provide images of seizure onset and propagation. I decided to generate images in real-time and so used a parallel EIT system with frequency division multiplexing, which produced images of slow changes during seizures without the need for averaging. This work, i.e. recording and reconstructing impedance changes appearing during

seizures with EIT and depth electrodes in a large animal brain, is the first attempt to extend EIT to a system suitable for clinical use.

5.1.5 Purpose

The purpose of this study was to determine if a real-time parallel EIT system could produce accurate images of the seizure onset and its spread in the brain. This was evaluated in a chemical model of epilepsy in the anaesthetised pig using intracranial electrodes and focal injection of benzylpenicillin. A secondary aim was to characterise the epilepsy model for intracranial, not cortical injections of the chemoconvulsant.

The specific questions to be addressed with this work were:

What are the EEG characteristics of this swine model of penicillin-induced seizures, recorded with intracranial electrodes?

Does EIT have the ability to image the onset and propagation of the seizures in real-time?

5.1.6 Experimental design

EIT was performed on a large animal brain during an acute focal model of chemically induced seizures using depth electrodes under deep anaesthesia. In order to recreate the clinical situation accurately, human depth electrodes were implanted into a porcine brain and brain activity was then monitored with electrocorticography (ECoG) and intracranial depth electrodes (SEEG). The EEG and EIT signal were collected with intracranial electrodes, 3 or 4 depth probes with a maximum of 10 recording channels each (SEEG, stereotaxically implanted depth electrodes) and a 32-contact epicortical array. Overall, the total number of 64 channels was used to record the signal in all animals. Four contacts on the epicortical array were removed in order to create entry points for depth electrodes. The array was reused between the animals increasing the consistency of the electrode placement between them. Seizures were triggered with a focal intracranial injection of procaine

benzylpenicillin (BPN). Epileptiform activity occurred in grades and spontaneously cycled between one to another, as expected from previous studies described in the introduction.

The cyclic epileptic activity could be distinguished in all animals on ECoG/SEEG, switching between stable background activity (grade I), interictal spikes (grade II and III) and finally seizures (grade IV). The interictal activity started 3 to 22 minutes following the initial injection, except two animals for which an additional dose of BPN was needed, as no seizures occurred within 60 minutes of the initial dose. Overall, the amplitude and spread of the epileptogenic changes seen in ECoG/SEEG evolved over time of the experiment, with lower amplitudes and more regional changes at the beginning, followed by a steady increase in both amplitude and generalisation of the interictal and ictal discharges over time. Total of 205 seizures were recorded in five animals, with 20 to 82 per animal. Three patterns could be distinguished in ECoG/SEEG: i) focal, ii) focal with secondary generalisation and iii) generalised, which started as such without any obvious focus. Both focal types of seizures presented a clear onset on SEEG, which then spread regionally among the adjacent intracranial contacts (pattern I, focal, n=17 in two pigs) or generalised over the majority of the intracranial and epicortical contacts (pattern II, focal generalised, n=34 in three pigs). This trend was observed after a single injection of BPN. The SEEG electrodes detecting the onset remained similar within one animal. This, however, later transpired to result in creating another epileptic zone, and produced only generalised seizures in these two cases (overall recorded n=154 generalised seizures in five pigs).

The EIT signal was recorded with the parallel EIT system, measuring slow impedance changes occurring over seconds. There were 32 injection pairs at frequencies ranging between 8 kHz and 10 kHz.

The resulting raw impedance signal was analysed for all 205 seizures recorded in five animals. Image reconstruction was only performed for a combined group of focal

and focal secondary generalised seizures (n=37 in three pigs), as these could be compared objectively with the ECoG/SEEG for the onset and seizure spread. The final number of reconstructed seizures (n=37) is lower than the total number of recorded focal/focal secondary generalised seizures (n=51). This is due to the recording method performed during the experiments. In order to minimise the size of the data and therefore ease the further loading and analysis process, the EIT/EEG recordings were manually stopped and restarted with some minor delay between the files. As seizures were spontaneously occurring, such step resulted with cutting some seizures at files edges. Therefore, such seizures did not account for image reconstruction.

Data collection started approximately 2 to 3 hours after the necessary surgical preparations have begun. A post-mortem CT scan was taken for all animals in order to obtain accurate positions of the electrodes and the BPN injection site. Data analysis was performed offline. Subject-specific Finite Element Method (FEM) head models with approximately 7-million elements were created from CT scans for five pigs (Jehl et al. 2016). Detailed FEM meshes were used in the forward calculation, while coarser hexahedral meshes with up to 1 million elements were used for the image reconstruction. Images were reconstructed using zeroth-order Tikhonov regularisation with the hyperparameter chosen automatically and noise-based image post-processing (Aristovich et al., 2014). In this way, an imaging data set was created for each of 37 seizures. This comprised EIT 3D images with a millimetre resolution of every second for a period of up to 100 seconds from 20 seconds before until 80 seconds after the seizure onset. A significant impedance change was set to be with respect to the baseline. The location of the onset and spread of the impedance change during seizures were evaluated by comparing to electrophysiological findings.

5.2 Materials and methods

5.2.1 Animal preparation and surgery

All experimental procedures and investigations performed during this study were ethically approved by the UK Home Office and undertaken under its regulations, as described in the Animals (Scientific Procedures) Act 1986.

Five pigs (70-75 kg, 4-months old) were used for simultaneous SEEG-EIT recordings. For all animals, the anaesthetic protocol included induction with ketamine and midazolam. All pigs were then intubated and mechanically ventilated; anaesthesia was maintained on sevoflurane. Respiration and heart rate, invasive arterial blood pressure, SpO_2 and rectal body temperature were monitored regularly. All animals were given pancuronium (initially 0.1 mg/kg and up to 0.08 mg/kg as needed) to maintain muscle relaxation after seizures were triggered.

The pig's head was then fixed in a stereotaxic frame (Model 1430 Stereotaxic Frame, Kopf Instruments, 7324 Elmo Street, Tujunga, CA 91042). Lidocaine was injected subcutaneously within the region of the craniotomy prior to the first skin cut. The scalp over the left hemisphere was cut using a scalpel and a bipolar coagulation unit to expose skull sutures. A craniotomy was performed using an air drill. The craniotomy window was approximately 5 cm length and 2 cm wide, extending 1 cm caudally from the frontal-parietal suture (lambda) with a lateral boundary of around 0.5 mm from the edge of the orbit, forming a trapezoidal opening. Due to already quite significant thickness of the pig skull at this age (20-30 mm), additional grooves were drilled at the posterior edge of the opening to adjust the array connecting leads (Figure 5-2 A). A bone wax was used to stop bleeding from the periosteum. The dura was incised to expose the cortex. Prior to opening the dura, a bolus of mannitol (0.5 g/kg) was injected intravenously to ease the epicortical array placement.

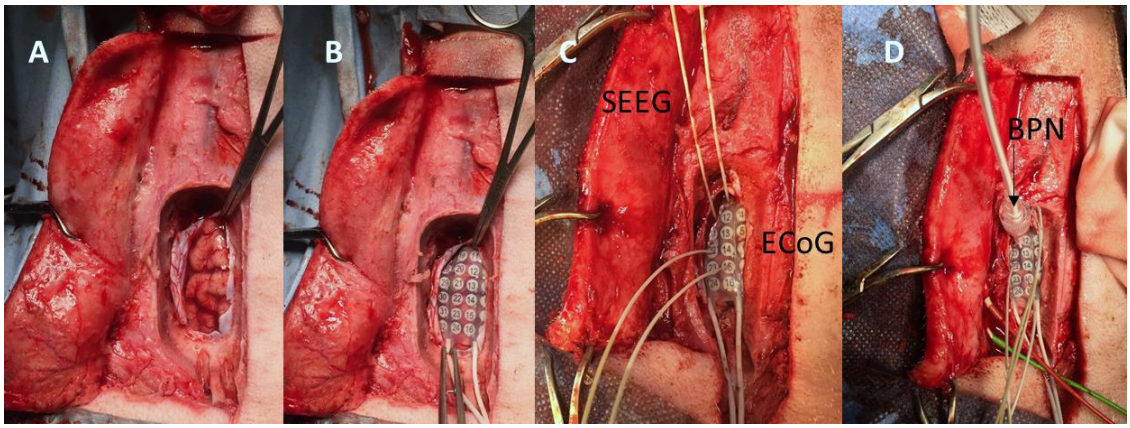

Figure 5-2. Overview of surgical site. (A) Finished craniotomy window with exposed cortex and removed dura mater. Grooves for cable leads are seen posteriorly. (B) Implanted 32-contact epicortical array (ECoG). (C) Implanted four depth electrodes (SEEG) showing their entry points on the array. (D) Final setup with a cannula for benzylpenicillin injection (BPN).

A subdural grid electrode (AdTech, Severn Healthcare Technologies, UK) with 4x8 platinum contacts, 10 mm spacing, 4 mm diameter, 2.3 mm exposure, 2 tail LTM grid was manually placed over the cerebral cortex with its edges secured under the edges of the craniotomy. Four holes in the array were pre-prepared in advance to create the entry points for depth electrodes (Figure 5-2 B and C). Depth probes were implanted manually, aiming towards the midline, hippocampus, amygdala and thalamus. Between three to four depth electrodes were used in different animals, according to brain size and geometry. Depth electrodes were platinum, 10-contact grids of 0.86 mm diameter and 2.29 mm recording length per contact, with 5 mm spacing (AdTech, Severn Healthcare Technologies, UK). A 20 G catheter for seizure induction was inserted through the array, aiming towards the midline, keeping in line with the depth electrodes (Figure 5-2 D and Figure 5-3).

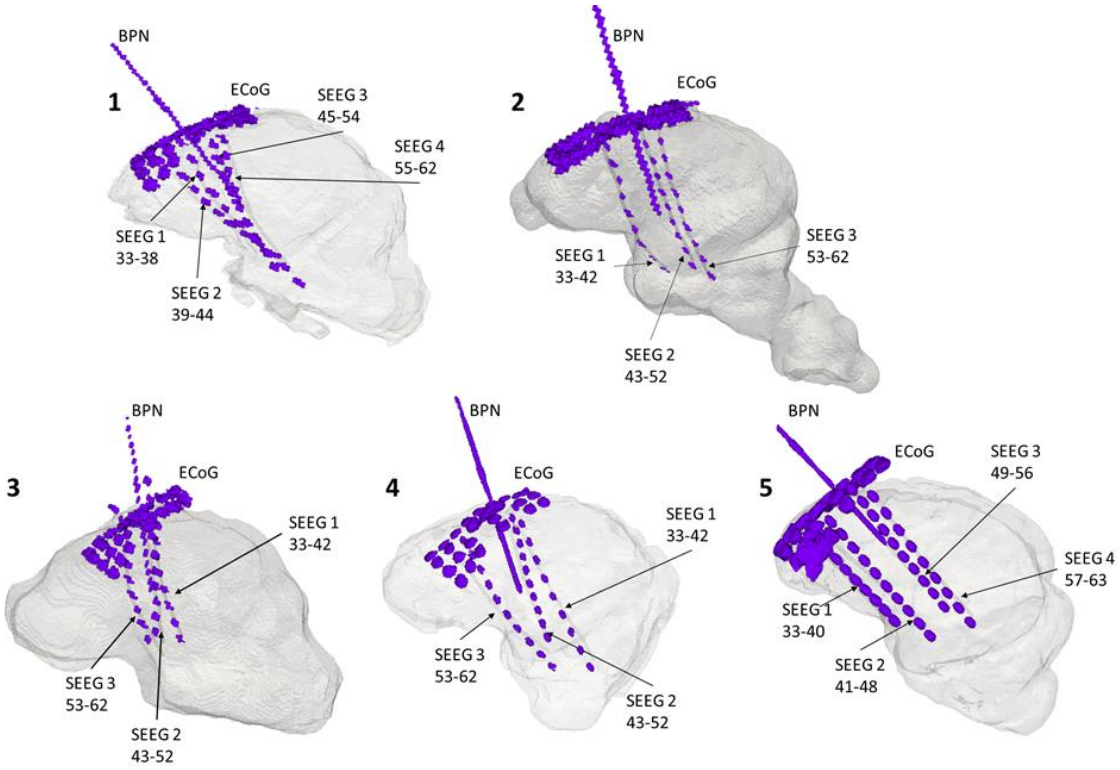

Figure 5-3. Reconstructed brains for all 5 animals tested in this study. All meshes, electrodes and cannula were obtained from animal-specific CT scans taken at the end of the recordings. Labels: ECoG – recorded from the epicortical array with 32 contacts; SEEG – recorded with depth electrodes with the respective numbers specifying how many contacts were recording the data on each probe; BNP – the site where cannula for benzylpenicillin injection was placed with respect to the electrodes.

Two-plane X-rays (posterior-anterior and left lateral) were taken after the implantation to verify the position of the electrodes. If necessary, they were re-adjusted to avoid bending and intersecting. At the end of each experiment, animals were euthanised with an overdose of pentobarbital and a post-mortem, non-contrast head CT was collected.

5.2.2 Induction of seizures

Seizures were induced with an intracranial injection of a single injection of 6000 IU (20 µl) of procaine benzylpenicillin (BPN, Depocillin, 300 mg/ml, Intervet). BPN was delivered by an injection pump through a 20-gauge plastic catheter placed through

a hole in the epicortical array over the somatosensory cortex in all experiments. After the BPN bolus, the catheter was left in place. This triggered cyclic epileptiform activity in three pigs; an additional 10 or 30 µl was required in two pigs. If further doses were necessary, they were given within the following 60 min from the initial BPN dose. Cyclic epileptic activity continued spontaneously for the following three hours until the pigs were euthanized. ECoG/SEEG was recorded, until all four grades of the epileptogenic activity were repeated at least three times. EIT recordings were then started. A detailed description of the seizures was undertaken on the simultaneous ECoG/SEEG and EIT recordings only.

5.2.3 Data acquisition

EIT was recorded with a modified version a frequency division multiplexing EIT system (Avery et al. 2019; Dowrick and Holder 2018). This was an extended experimental version of the EIT system developed in chapter 4, not yet safety tested for use on patients. The parallel EIT used for these experiments comprised six PCBs, with a six-channel current source on each board and recording frequency up to 20 kHz with the ActiCHamp EEG system (Brain Products GmbH). In this study, 60 µA was injected at 32 electrode pairs in parallel, over 8.5-10 kHz range, separated in 50 Hz steps. Independent voltage measurements were made on all electrodes at the same time. There were 28 independent current injections yielding 1548 measured voltages.

Simultaneous ECoG/SEEG and EIT recordings were made from 63 channels at a sampling frequency of 50 kHz at 128-channel ActiCHamp EEG system (Brain Products GmbH), with a hardware antialiasing filter (cut-off frequency 12.5 kHz). No software filters were set during data acquisition. The recording was undertaken with all 32 contacts on the ECoG array and 30-32 channels on SEEG.

The ECoG/SEEG was filtered at 300 Hz (low pass, 3rd order). EIT images were generated from the modulus of the complex impedance, filtered at 1 Hz (low pass,

30th order) and demodulated with a bandwidth of ±10 Hz around each carrier frequency (30th order). After filtering, the signal sampling rate was reduced 50 and 500 times for EEG and EIT signal respectively. An additional cut-off frequency filter of 0.01 Hz and 1 Hz (1st order) was used for the EIT data prior to the image reconstruction.

5.2.4 Data analysis

5.2.4.1 Raw ECoG/SEEG and impedance signal analysis

The raw ECoG/SEEG was plotted against the impedance change (dZ) on the same time scale to compare the signals. The data were then divided into blocks of one seizure, with a bin size depending on the length of a seizure but with a minimum of 30 seconds before and 60 seconds after the ictal event. The dZ baseline for each channel was defined as the mean amplitude of the signal over the first 20 seconds prior to each seizure. For each seizure, the onset and the number of contacts involved in the seizure were defined by visual assessment of all traces, in the same way as it is done during clinical EEG reporting.

The significance of the dZ change was defined by comparing the dZ value with the baseline dZ at each time point using a paired t-test, at the 0.01 significance level. Excessively noisy channels, defined as having a standard deviation of the baseline above 5 μV, were rejected from further analysis. Usually, 90% of the total number of dZ channels remained across all seizures. Similarly, noisy ECoG/SEEG channels were defined as those of a standard deviation of the baseline above the 50 μV and were then removed. The quality of recording contacts on the epicortical array tended to slowly degrade with use over time. In the initial experiments, 85% of the ECoG/SEEG channels were kept for further analysis, which then decreased to approximately 65-70% due to losing the channels at the epicortical array (increased contact impedance >2000 Ω).

The maximum impedance change was defined as the maximum voltage change across all significant channels per seizure. The onset of the dZ change was defined as the time at which the change at the channel with maximal dZ change reached double the baseline noise on this channel and this was followed by a dZ increase lasting longer than 5 seconds. Impedance changes were analysed for all 205 seizures in five animals.

A focal seizure was defined as a local ictal discharge, originating within limited networks, for which a clear onset on regional SEEG electrodes could be distinguished from the background. A clear onset was expressed by synchronised polyspikes or paroxysmal sharp waves at >3.5 Hz frequency, occurring at fewer than 10-12 contacts in total, but only at a maximum of 2 to 4 contacts of a single depth probe. In the described experimental setup, depth electrodes were surrounding the BPN cannula, so that it was possible to detect the focal onset on all SEEG electrodes but only at the contacts adjacent to the penicillin injection level. Such activity was standing out from the previous background activity and could later spread over the majority of ECoG and SEEG contacts ('focal secondary generalised') or stay within a small area of the local 8 to 12 contacts ('focal seizure').

5.2.4.2 Image reconstruction

EIT images were produced with realistic animal-specific head meshes, segmented from CT scans taken at the end of each experiment. The segmentation included two layers, brain tissue and electrodes (Jehl et al., 2016). Tissue conductivity was assumed to be isotropic and was modelled as a homogenous section of 0.22 S/m conductivity of for the whole brain (Horesh 2006). The realistic geometry of intracranial electrodes and BPN cannula were modelled from CT. The resulting meshes comprised 6.8 to 8.2 million 0.3 mm tetrahedral elements. The forward solution was calculated using the PEITS forward solver (Jehl et al., 2014). The inverse problem was solved using coarser hexahedral meshes of 500 µm element-size and 0.5 to 1 million hexahedral elements. The reconstructed conductivity changes for

each hexahedral voxel were regularised with zeroth-order Tikhonov, corrected with a noise-based correction and expressed with t-score (s, sigma) for imaging (Aristovich et al. 2014). The reconstructed conductivity values were divided by the standard deviation of the estimated conductivity change for each hexahedron, because of Gaussian noise in the voltage measurements, to yield noise correction units. Image reconstruction was only analysed for 37 seizures that presented a clear onset and spread on SEEG, focal and focal secondary generalised. As described in experimental design, seizures that occurred at the edge of recorded files were not used for image reconstruction.

The quality of the reconstructed images was assessed with a localisation error of the onset of focal seizures. The localisation error of the reconstructed EIT onset was calculated with respect to three separate points. These points were the tip of BPN cannula, the mean position of all SEEG electrodes detecting the onset and the closest SEEG contact, on which the onset could be detected. The localisation error was defined in millimetres, as the distance between the distances of the centre of mass of the reconstructed change at the maximum dZ increase from the coordinates of the three points.

5.2.4.3 Analysis of correlation between ECoG/SEEG and EIT

5.2.4.3.1 Seizure onset

For the ECoG/SEEG onset, the detailed specification of the number and position of the contacts detecting the onset was assessed visually, same as during the clinical EEG reporting, using the above criteria. The resulted number of ECoG/SEEG contacts involved in onset was then correlated with the maximum amplitude of impedance change for a seizure (the so-called ‘peak dZ’).

5.2.4.3.2 Seizure spread

Similarly to seizure onset, the seizure spread over the ECoG/SEEG (‘ECoG/SEEG spread’), so that the number and position of the contacts detecting the seizure at the

most generalised time, were also assessed visually. The 'ECoG/SEEG spread' was defined as the maximum number of channels involved at a one-time point for a seizure. This was correlated with the 'EIT spread', the number of channels to which the EIT change spread, defined as those that were covered by the reconstructed change thresholded at 65% of the maximum reconstructed value.

The ECoG/SEEG correlation with EIT was also performed for the magnitude of the signal ('peak SEEG') with the maximal amplitude of dZ change ('peak dZ'). The peak SEEG, the magnitude of ECoG/SEEG signal, was calculated from the electrographic spiking activity, using the RMS (root mean square) of the ECoG/SEEG signal on the contact on which the seizure started. The signal spectrum was obtained from the spectrogram of that channel, using a short-time Fourier transform of the input signal. The peaks of spiking activity were defined by using a bandwidth of 20 to 40 Hz of the rectified signal, giving an index of spiking power, and therefore a clear representation on when the seizure occurred and the magnitude of the spikes.

All correlations were performed with the Pearson correlation coefficient.

All data are presented as mean ± SD.

5.2.4.3.3 Qualitative analysis

The resulting images of the seizure propagation were compared qualitatively with the ECoG/SEEG findings for all focal/focal secondary generalised seizures reconstructed with EIT. As there was no movement artefact on ECoG/SEEG blurring the signal, it was possible to follow the spread of the seizure until it generalised and then decreased. Therefore, a qualitative visual comparison of the reconstructed EIT change with the spread over the ECoG/SEEG contacts was feasible.

5.3 Results

5.3.1 Seizure model

The initial interictal activity started after 3 to 22 minutes (12±7 min) in all five pigs, with the first seizure occurring after 20 to 60 minutes (31±17 min) from the primary BPN bolus in three pigs. In two animals requiring additional BPN dose, the first seizure occurred after 11 and 7 minutes from the final BPN dose. A dose of 6000 IU of procaine benzylpenicillin was the lowest effective for generating spontaneous recurrent epileptiform activity in these animals. In total, 205 seizures were recorded with EIT in five animals, 20 to 82 per animal (Table 5-1).

In three out of five pigs, a substantial increase in heart rate and in blood pressure, of up to 220 bpm and up to 200/130 mm Hg towards the end of the experiment was observed during seizures. The rise in blood pressure was less prominent and progressed slower than the heart rate over the experimental time. This was not related to administering the additional BPN dose.

Epileptiform cycles repeated every 3 to 10 minutes (Figure 5-4). Grade I lasted 2 to 86 seconds (13±9 sec), from the end of the previous seizure. Following this, Grade II and III occurred with increasing interictal spikes (IIS) frequency. Grade IV, seizures, occurred spontaneously and lasted 8 to 70 seconds (25.8±13 sec, n=205 in 5 pigs).

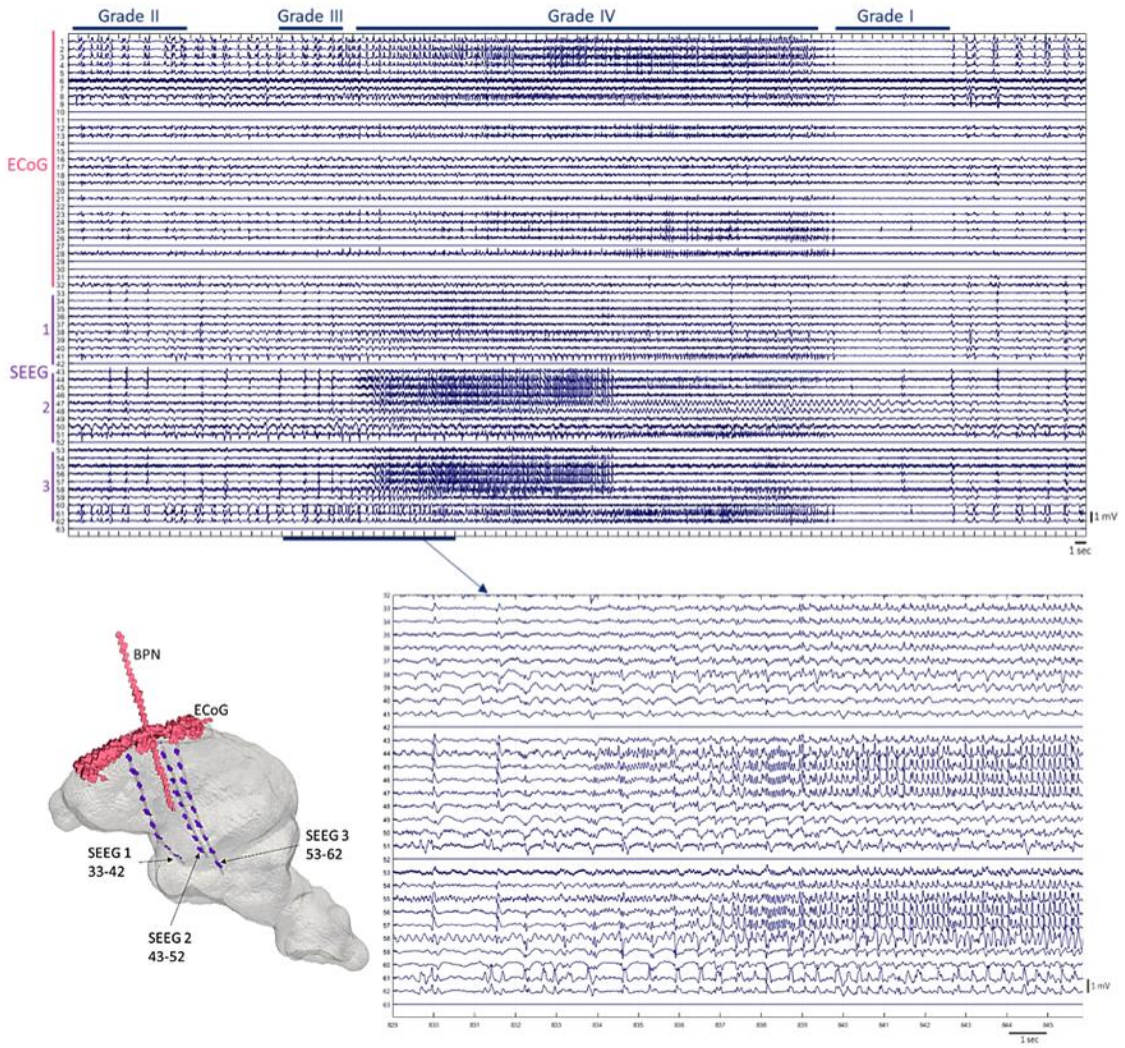

Figure 5-4. Example of seizure epileptiform activity recorded with 32-electrode array ECoG and 3 SEEG 10-contact depth electrodes. Top graph shows the evolution of the four grades over 100 seconds throughout all electrodes, with enlarged seizure onset on SEEG over 15 seconds at bottom graph. Coordinates of the electrodes and the BPN injection cannula obtained from CT are presented on the model on the left. Numbering on SEEG corresponds the deepest contacts having smaller numbers, which the increase towards the surface (i.e. for SEEG 1, contact 33 is the deepest and contact 42 is in the cortex). This numbering configuration is used for all of the figures presented. Focal onset is seen on contacts 44-45, with a quick spread over the adjacent contacts, 46-47 and 55-58 within approximately 4 seconds.

Focal seizures occurred at the beginning of the recordings in three pigs, followed by intermixing of both focal and secondary generalising patterns. If the seizures presented in the third, generalised, form, the focal type did not subsequently reappear in any of the five pigs. The amplitude and spread of the epileptogenic discharges observed in ECoG/SEEG increased with the recording time, without additional BPN injections.

Animal	**Focal**	**Focal, 2˚**	**Generalised**	**Data analysis for EIT**
Pig 1 •	0	0	82	Raw dZ on all sz
Pig 2	6	15	10	Raw dZ on all sz + image on 4 focal and 12 focal 2˚
Pig 3 •	0	0	20	Raw dZ on all sz
Pig 4	11	3	9	Raw dZ on all sz + image on 3 focal and 2 focal 2˚
Pig 5	0	16	33	Raw dZ on all sz + image on 16 focal sz

Table 5-1. Seizures types recorded in each animal. Impedance changes were analysed for all 205 seizures in five animals. Image reconstruction was only attempted for 37 seizures that presented a clear onset on SEEG (the two focal types). 'sz' stands for "seizures", 'dZ' for impedance changes, 'image' for image reconstruction analysis, '2°' for secondary generalised seizures. Animals indicated with • have been given additional dosages of BPN, as described in text.

Pattern I, a focal seizure: 17 focal seizures were recorded in two pigs, with 6 and 11 seizures each. They lasted 13±3 sec and were represented by a clear focal onset seen on adjacent two-three SEEG contacts, which then spread regionally, within 8-10 channels but did not reach the majority of remaining channels (a typical example in Figure 5-5).

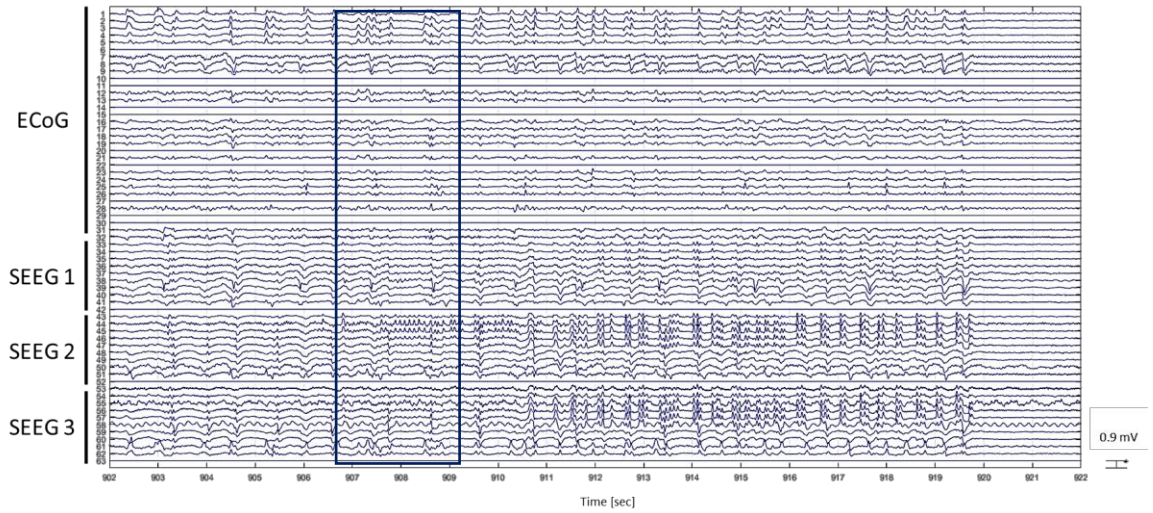

Figure 5-5. Pattern I, a focal seizure. The onset (indicated by a rectangle) is seen on SEEG 2, contacts 44-45 spreads within 4 seconds to the channels nearby, spreading between 44-47 and 55-58 on SEEG 2 and 3. The seizure stops spontaneously within 14 seconds. All channels presented as flat lines were noisy and removed from the analysis.

Pattern II, a focal, secondary generalising seizure: 34 focal, secondary generalised seizures were observed in three animals, with 15, 3 and 16 per pig, lasting 27±4 sec. A focal onset was followed by gradual spread over regional contacts within 1 to 4 seconds and then by a widespread activity over the majority of contacts. Generalisation occurred within 8±4 sec (an example in Figure 5-6).

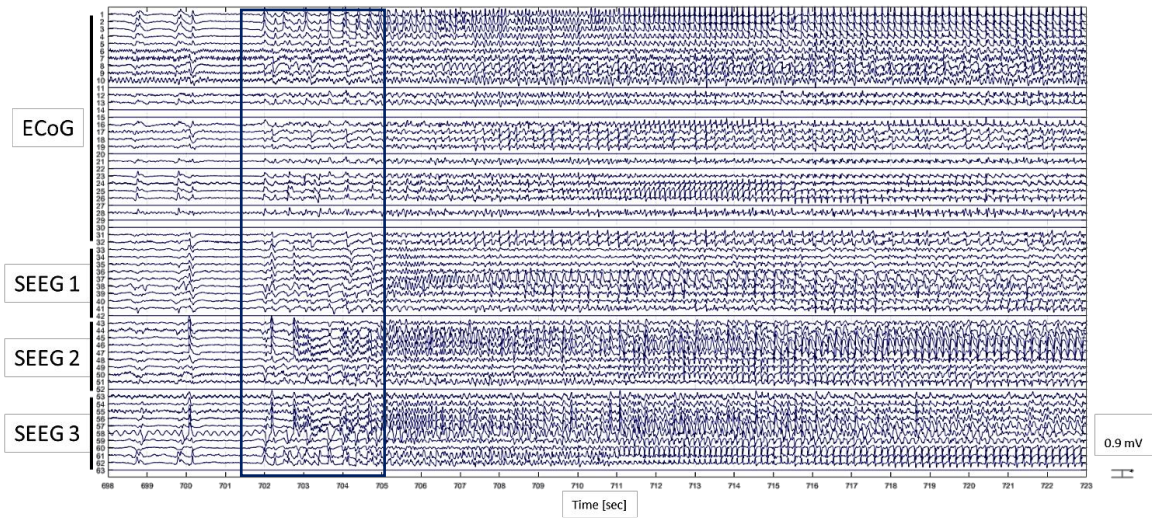

Figure 5-6. Pattern II, a focal with secondary generalisation seizure. The onset (indicated by a rectangle) is seen over the electrodes 44-47 and 55-57, which quickly spreads towards cortical contacts 1-4 and then generalises involving the majority of contacts. The seizure then extends over the cortical contacts, as well as throughout the depth electrodes.

Pattern III, a generalised seizure: this pattern was seen clearly in all five animals, and for two of them this was the only seizure pattern observed throughout the whole recording. The seizures were characterised by widespread epileptogenic discharges seen on most channels; it was not possible to define a clear onset area (example in Figure 5-7). In total, there were 154 generalised seizures recorded, each lasting 34±2 sec.

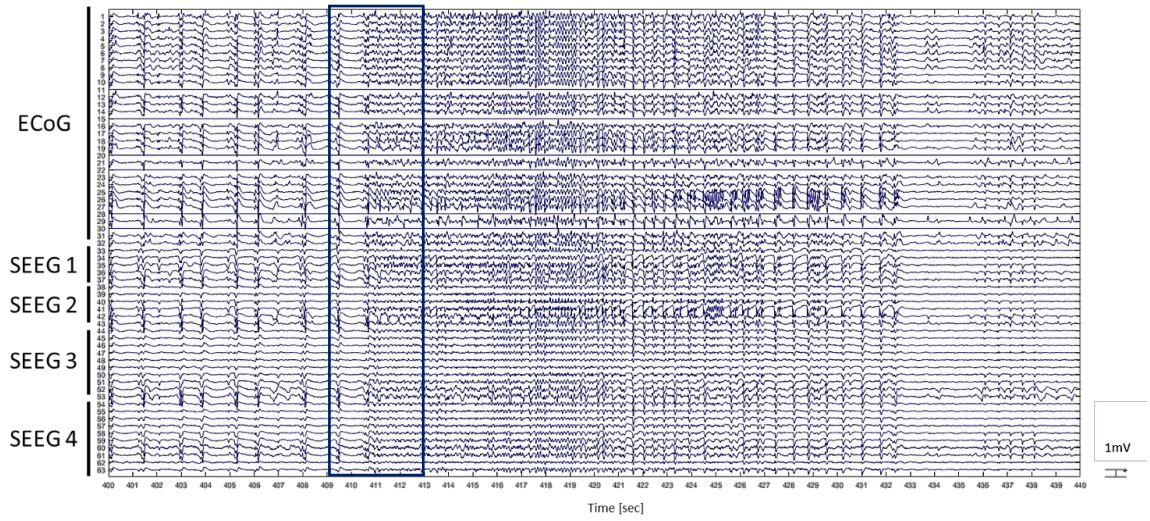

Figure 5-7. Pattern III, a generalised seizure. A seizure is seen over the 40-second page and recorded with 32-electrode array and 4 SEEG contacts. Ictal activity extends over all cortical contacts seen on both, ECoG and cortical contacts of SEEG and the onset is indicated by a rectangle. Grade III is seen at the beginning of the recording, with widespread interictal discharges occurring every 1 to 2 seconds.

5.3.2 Raw impedance responses during all seizures

Each seizure resulted in an impedance increase (Figure 5-8 and Figure 5-9) with a peak of 1.7±0.2 mV (6±2%) in focal (n=17 in two pigs), 2.3±0.4 mV (8±2%) in focal secondary generalised seizures (n=34 in three pigs) and 3.4±1.5 mV (9.5±3%) in generalised seizures (n=154 in five pigs).

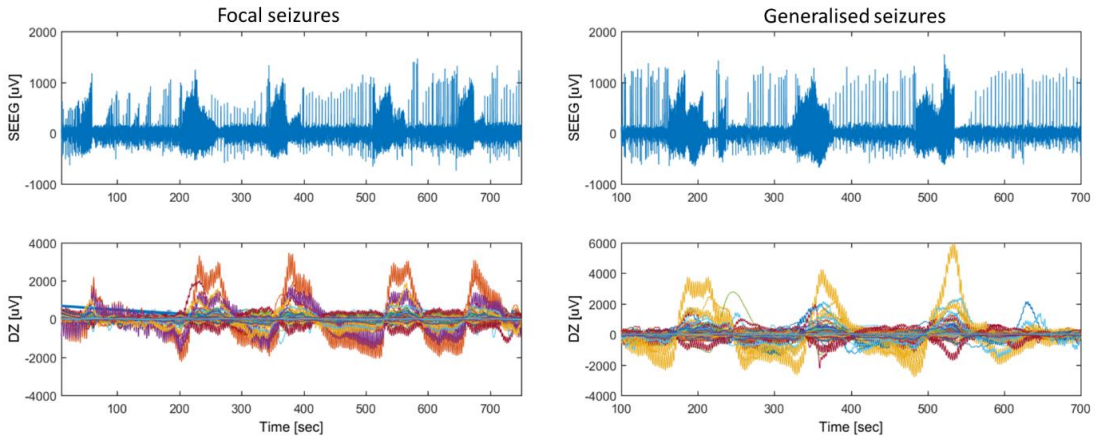

Figure 5-8. Examples of raw impedance increase observed during seizures. Upper graphs show one SEEG channel with interictal and ictal discharges for focal (left) and generalised (right) seizures, while lower graphs show impedance changes on 1450 recording channels during these events over time (different colours). Left, focal seizures: the first seizure was focal, yielding a maximum dZ change of 2 mV, whereas the following four seizures were focal and secondarily generalise, and hence the amplitude of the dZ change was larger. Right, generalised seizures: all three seizures were generalised, causing a larger dZ change, between 4 and 6 mV.

The onset of the impedance increase was delayed from the seizure onset in SEEG by 11±3 seconds for focal seizures (Figure 5-9), by 12±3 seconds for focal secondary generalised and by 15±2 seconds for generalised seizures. The dZ peak was delayed by 29±12 seconds from the seizure onset in SEEG.

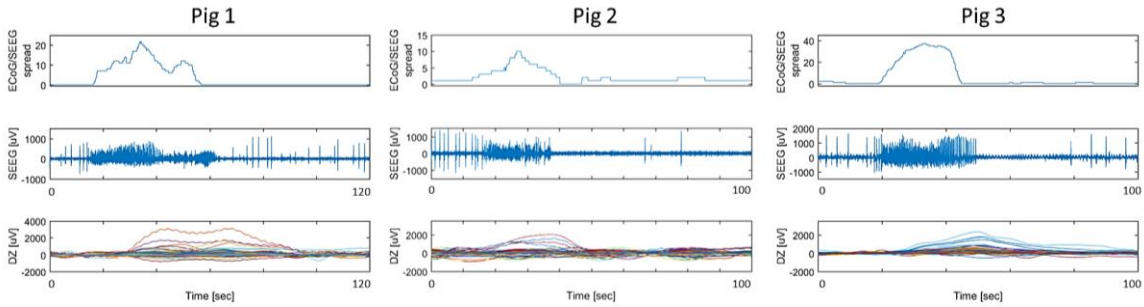

Figure 5-9. Examples of a focal seizure in three pigs that presented this seizure pattern. Top graph indicates the number of ECoG/SEEG contacts recruited during seizure progression, the middle shows activity in the first SEEG channel to show seizure activity, and the bottom graph all the impedance

changes on all 1450 individual channels during the seizure. There is a delay between the onset in SEEG and dZ.

5.3.3 EIT reconstructed images in focal/focal secondarily generalised seizures

The seizures were reconstructed from individual impedance channels. EIT located the initial seizure impedance change to within 10 mm of its apparent onset from the three independent methods: 9±4.5 mm from the tip of the cannula, 9.7±4.3 mm from the mean position of all SEEG electrodes detecting the onset, and 7.5±3.2 mm from the closest SEEG electrode sensitive to the onset (Figure 5-10, Figure 5-12, Figure 5-14 and Table 5-2, n=37).

37 focal and focal, secondarily generalised seizures in three pigs, yielded images of an accurate seizure onset and its propagation to within 8 to 10 mm when compared with ECoG/SEEG distribution when assessed visually (representative example of the onset for each pig on Figure 5-11, Figure 5-13, Figure 5-15, for a focal seizure in one pig Figure 5-16 and for a focal secondary generalised seizure in one pig Figure 5-17). There were observable differences between the animals noted. For the first pig, all reconstructions were repeatable, corresponding to within 7 mm with the SEEG onset and the tip of cannula (6.5±1.7 mm and 6.9±1.9 mm respectively, n=16). For the second pig, the reconstructed onset was localised within the area of 5.5±1.1 mm (n=5) from the active SEEG contacts. However, both SEEG and EIT onsets were almost 2 cm away from the tip of the cannula. In pig 3, EIT impedance onset reconstructed to the area close to the cannula to within 7.8±1.9 mm from the tip of cannula but was more variable with respect to the mean of SEEG contacts active at the onset (14.1±1.9 mm, n=16).

EIT onset reconstruction [mm]				Real location [mm]	
Animal	**Cannula tip**	**Mean SEEG**	**Closest SEEG**	**Cannula to mean SEEG**	**Cannula to closest SEEG**
Pig 1 (n=16)	6.9±1.9	6.5±1.7	4.8±2.5	4.7	3.9
Pig 2 (n=5)	19.1±1.6	5.5±1.1	7.1±2.2	19.5	13.9
Pig 3 (n=16)	7.8±1.9	14.1±1.9	10.1±1.6	11.2	16.8
Overall (n=37)	9±4.5	9.7±4.3	7.5±3.2		

Table 5-2. Detailed accuracy of EIT onset reconstruction. 'EIT onset reconstruction' columns show the n number of all focal seizures reconstructed with EIT for each pig and the distance accuracy of the EIT onset detection with respect to the coordinates of three points, expressed in mm. These points were: 'cannula tip' – the position of the tip of cannula used for benzylpenicillin injection, 'mean SEEG' – the mean position of all SEEG active electrodes at onset, 'closest SEEG' – the closest SEEG electrode detecting seizure onset. The 'Real location' columns show the distance between the tip of the BPN cannula and the mean position of all SEEG active electrodes at the onset ('cannula to mean SEEG') and the closest SEEG electrode detecting the onset ('cannula to closest SEEG').

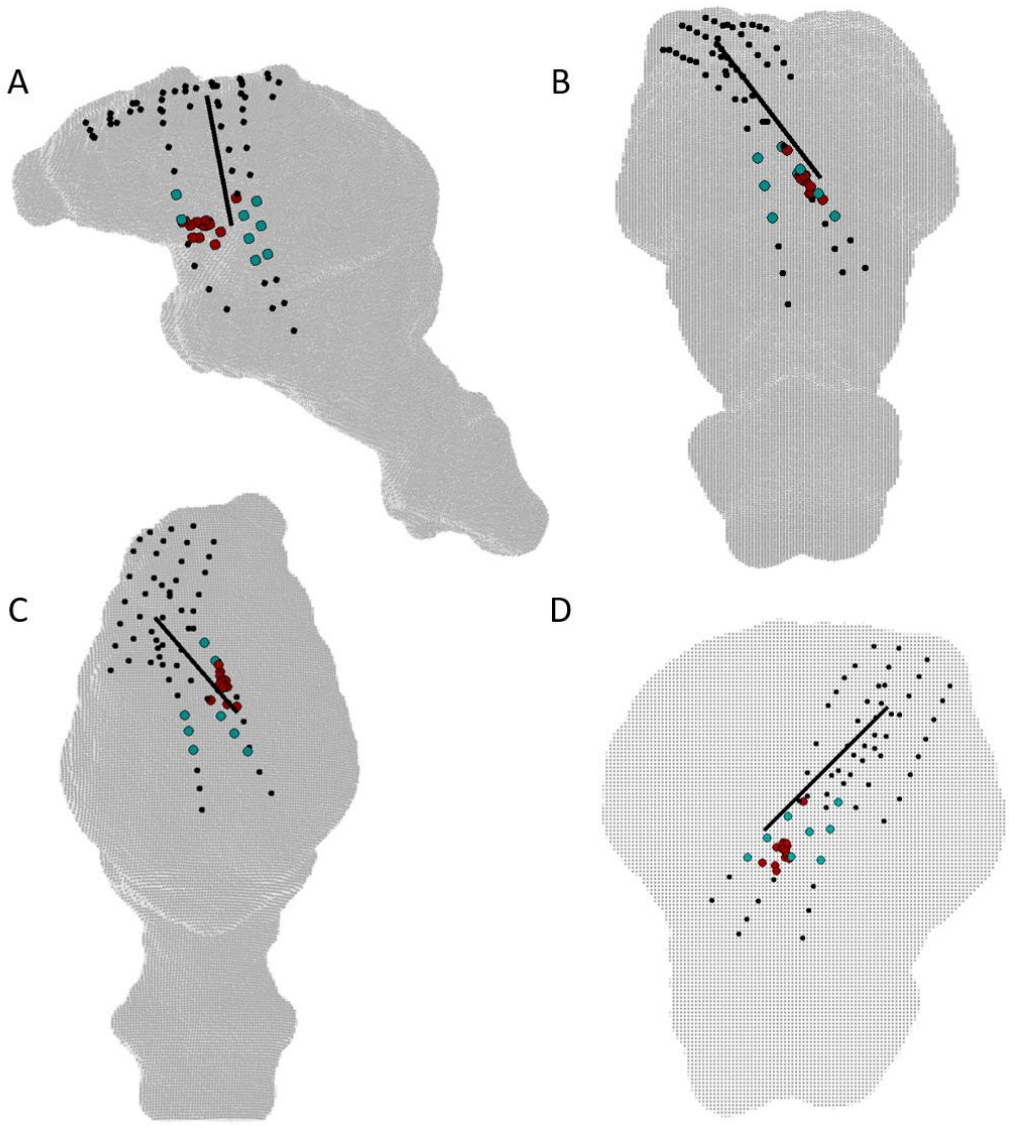

Figure 5-10. Onset reconstruction with EIT (red dots) for 16 focal seizures in pig 1 with respect to SEEG electrodes detecting the onset (green dots) and all ECoG/SEEG electrodes (black dots). The black line represents the cannula for BPN injection. To aid visualisation, four planes are shown: sagittal (A), posterior (B), axial/top (C) and coronal (D). Reconstruction of the onset is repetitive between seizures, corresponding to SEEG electrodes seeing the change (6.5±1.7 mm) as well as to the tip of the cannula (6.9±1.9 mm).

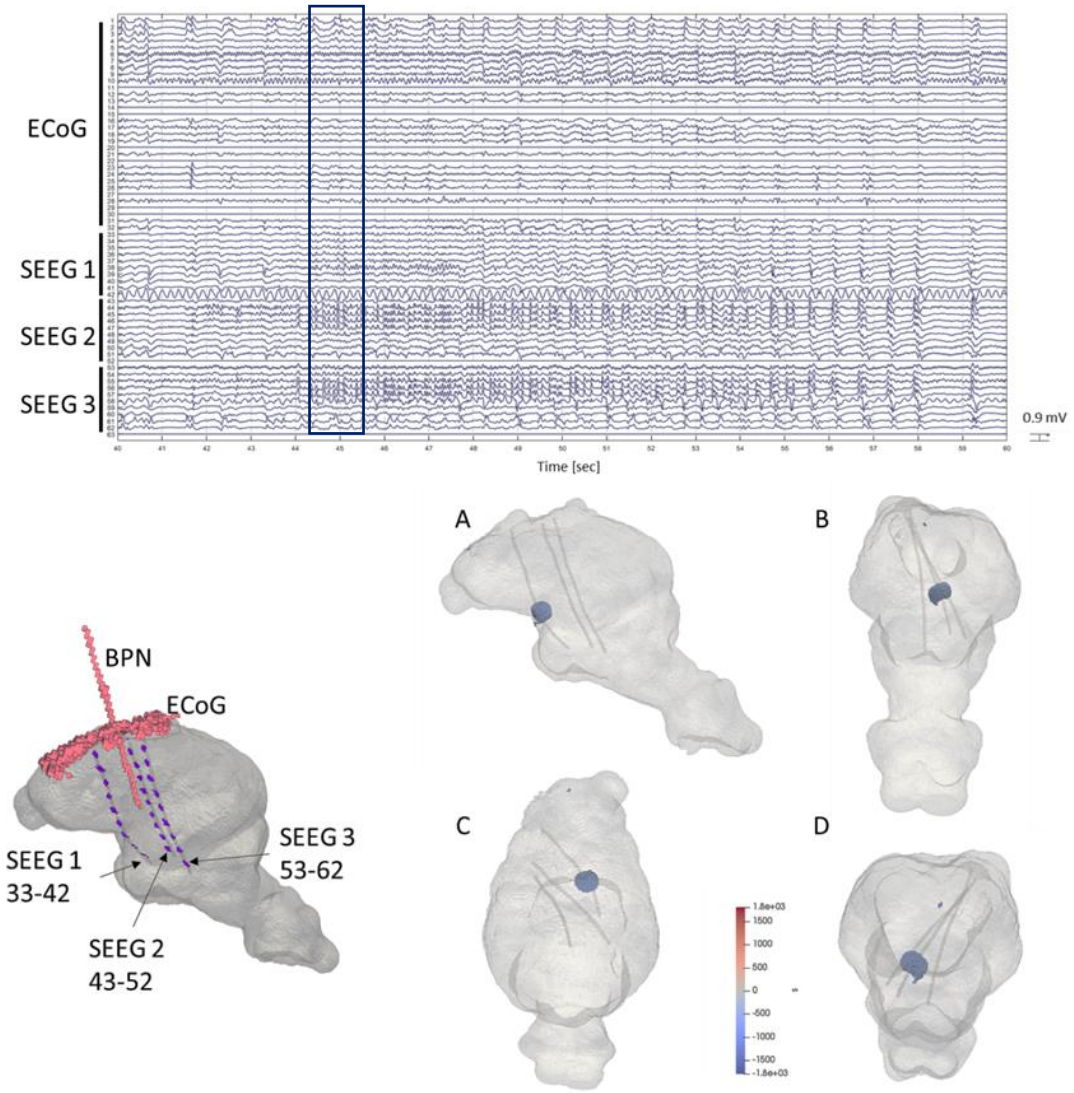

Figure 5-11. Example of focal seizure in pig 1. A model showing the coordinates of ECoG and 3 SEEG electrodes and the BPN cannula is presented on the lower left. The onset of the seizure is indicated by a rectangle on ECoG/SEEG (above). The SEEG electrodes detecting the onset were channels 56-58, 44-47 and 37, 38. The initial EIT reconstruction of the onset started at electrodes 37-38 (bottom right) and later spread towards contacts 56-58 and 44-47 (not shown). The initial EIT change reconstructed 23 seconds after the SEEG onset. The EIT reconstruction is displayed in four planes: sagittal (A), posterior (B), axial (C) and coronal (D), in the same outline as on the previous figure.

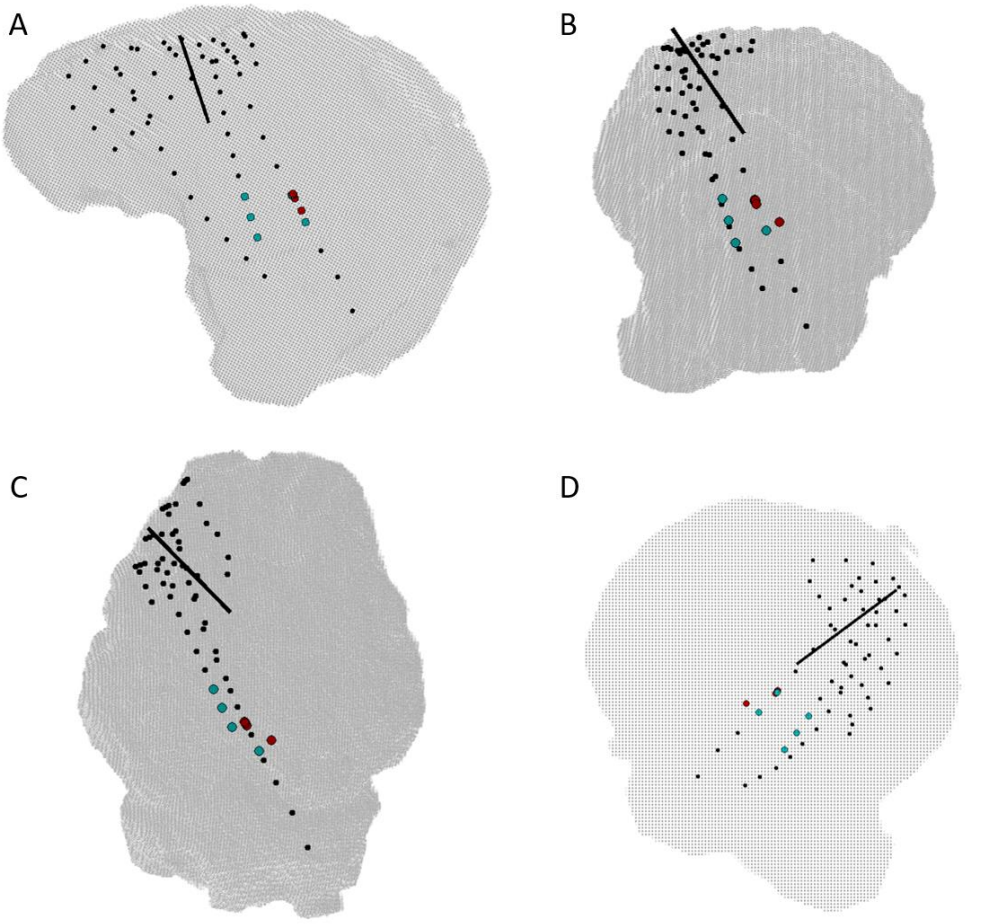

Figure 5-12. Onset reconstruction with EIT for 5 focal seizures in pig 2 with respect to the ECoG/SEEG contacts and cannula. The representations are the same as in the previous figure. EIT localised the seizure onset within 5.5±1.1 mm from the active SEEG contacts at the onset. Both were 19.1±1.6 mm and 19.5 mm from the cannula tip respectively. This may be attributed to dispersion of the injected BPN away from the cannula.

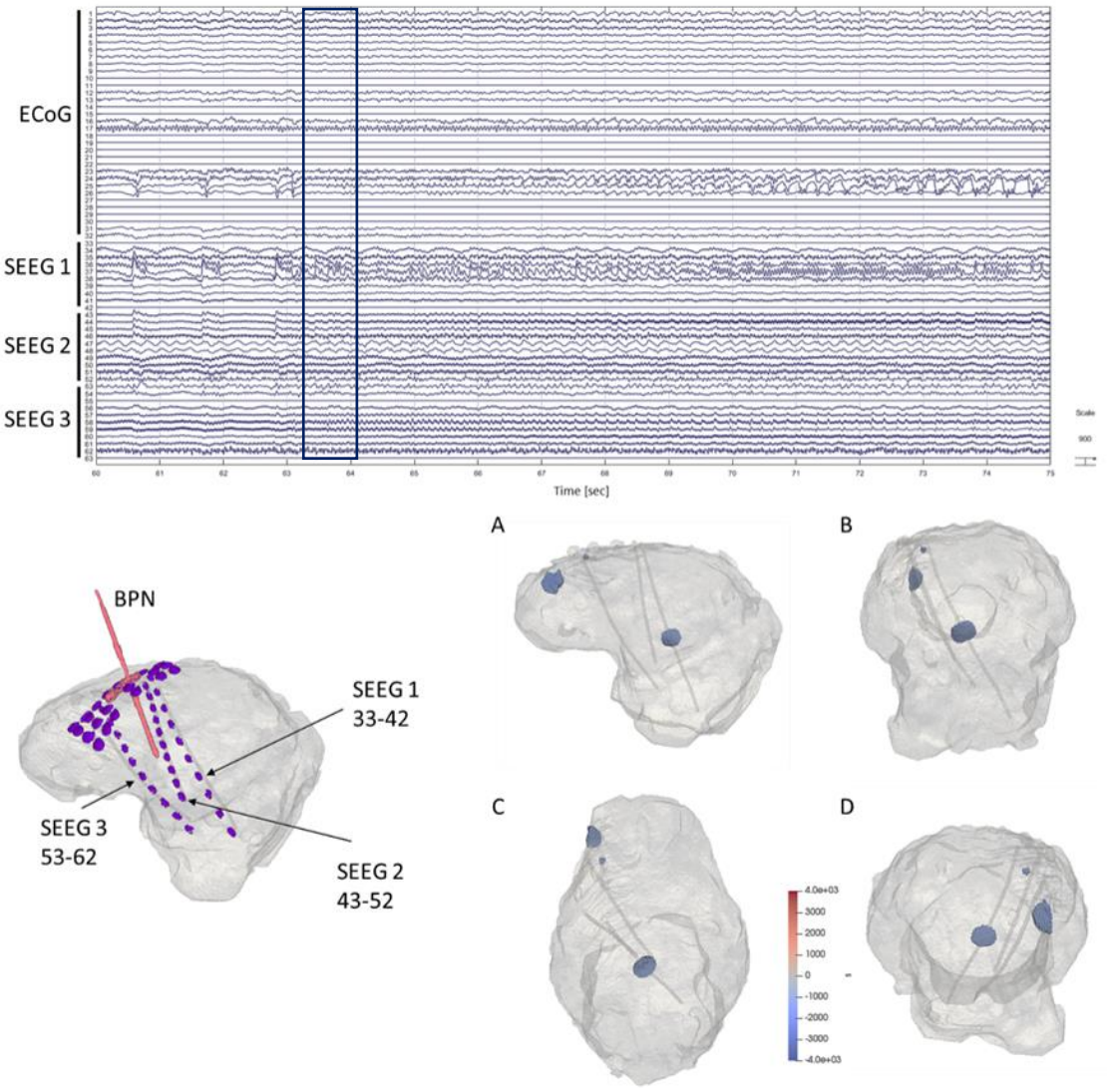

Figure 5-13. Example of the onset reconstruction in pig 2. SEEG (above) shows onset at electrodes 36, 37 and 38, indicated by a rectangle. The EIT reconstruction points to the same area of the brain. Additional change reconstructed on the cortex is associated with the sharp activity seen over the contacts 24, 25 and 26, seen on ECoG. The EIT change occurred 12 seconds after the SEEG onset.

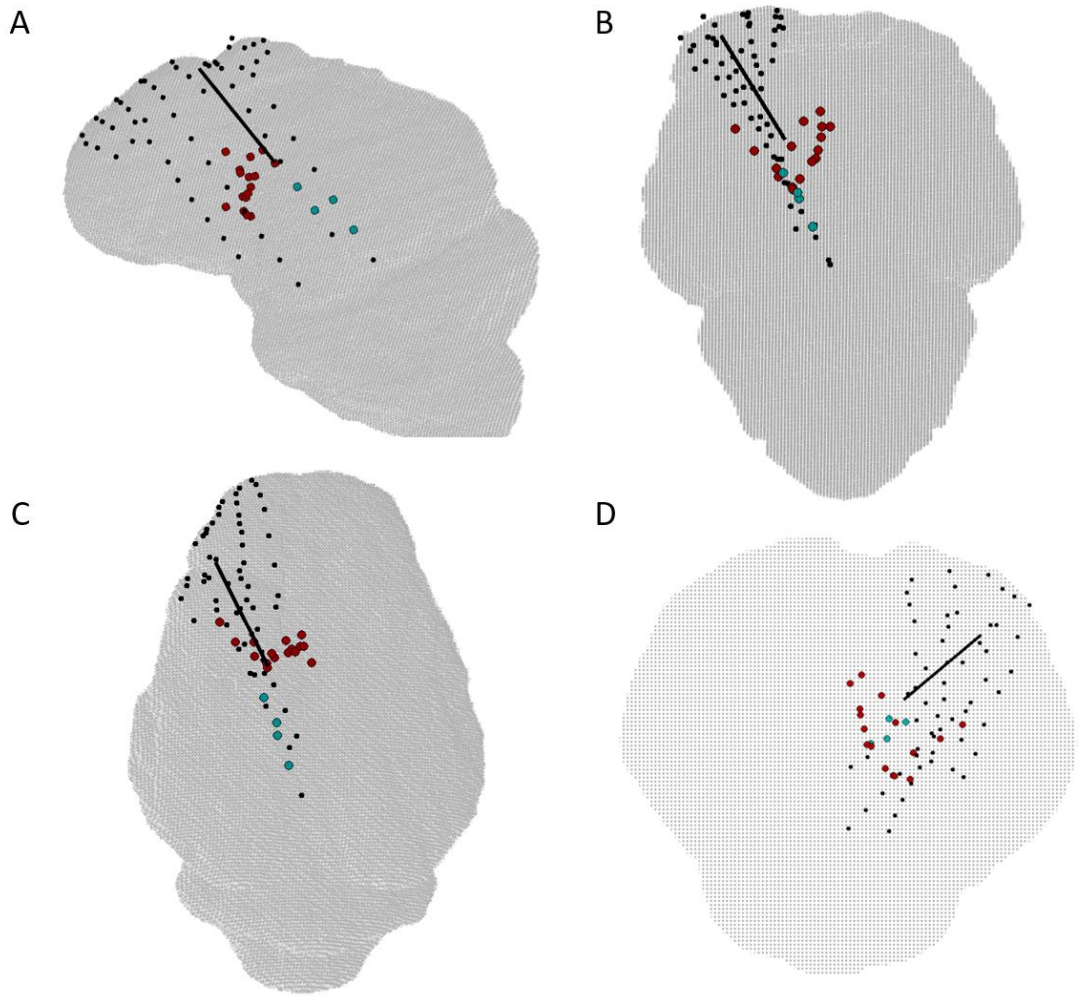

Figure 5-14. Onset reconstruction with EIT for 16 focal seizures in pig 3 with respect to ECoG/SEEG contacts and cannula. The representations are the same as in the previous figure. The seizure onset reconstruction with EIT is within 7.8±1.9 mm from the tip of the cannula. The reconstruction of each onset was more widespread surrounding the tip of the cannula, with a mean distance of 14.1±1.9 mm from the mean position of all SEEG contacts active at the onset.

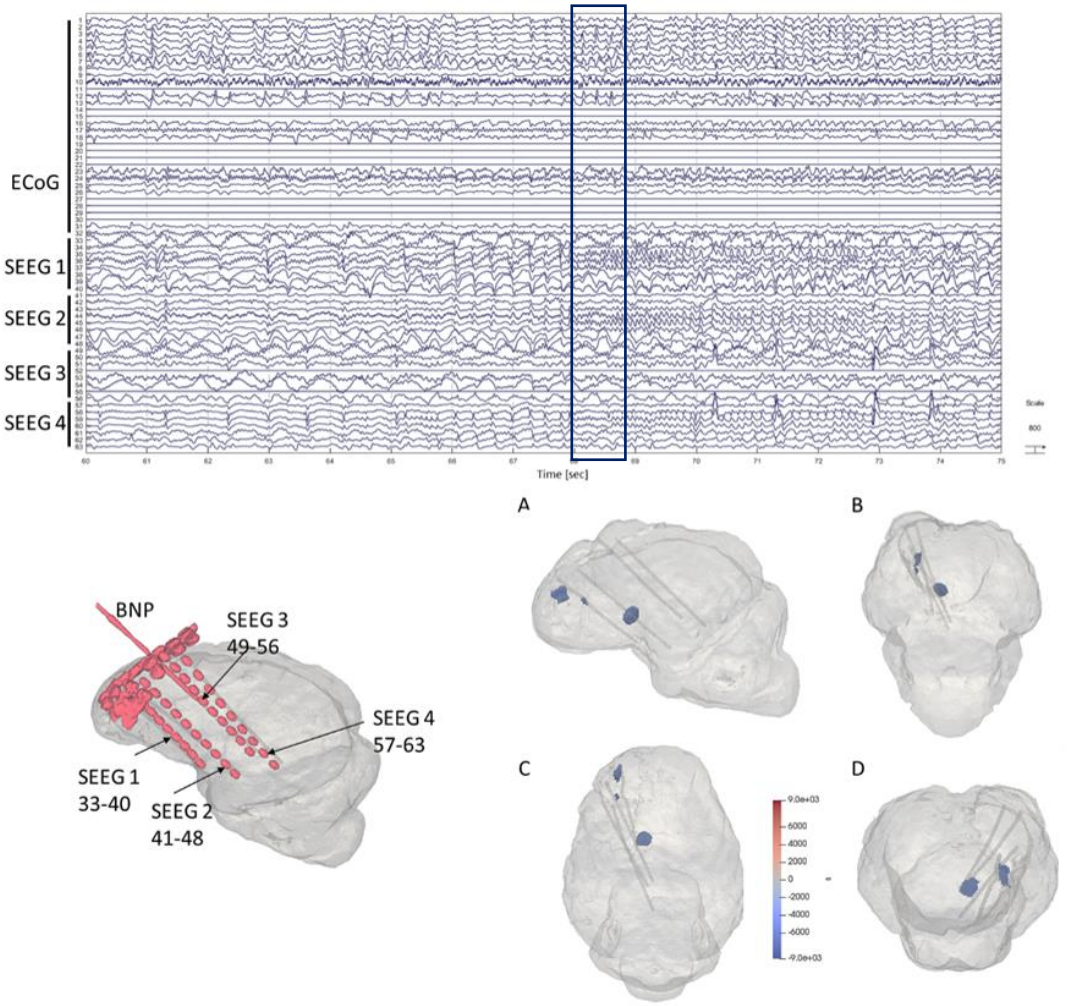

Figure 5-15. Example of focal seizure in pig 3. The onset of the seizure is indicated by a rectangle on ECoG/SEEG. SEEG on the top of the figure shows the onset at electrodes 35, 36, 37, 44, 45, 46, 59 and 60. The EIT reconstruction points towards the contacts 45, 46. There was also cortical activity seen on both, ECoG and EIT. The EIT changes were reconstructed from the signal with a 20-second delay from the SEEG onset.

5.3.4 ECoG/SEEG and EIT signals correlation

In 37 focal and focal secondarily generalising seizures, EIT images appeared to correlate to within 1 cm as seizure activity progressed (Figure 5-16 and Figure 5-17). In focal seizures, the EIT remained localised, whereas in generalising ones, the EIT

impedance changes spread as SEEG contacts showed activity, but with a lag of 11±3 and 12±3 seconds respectively.

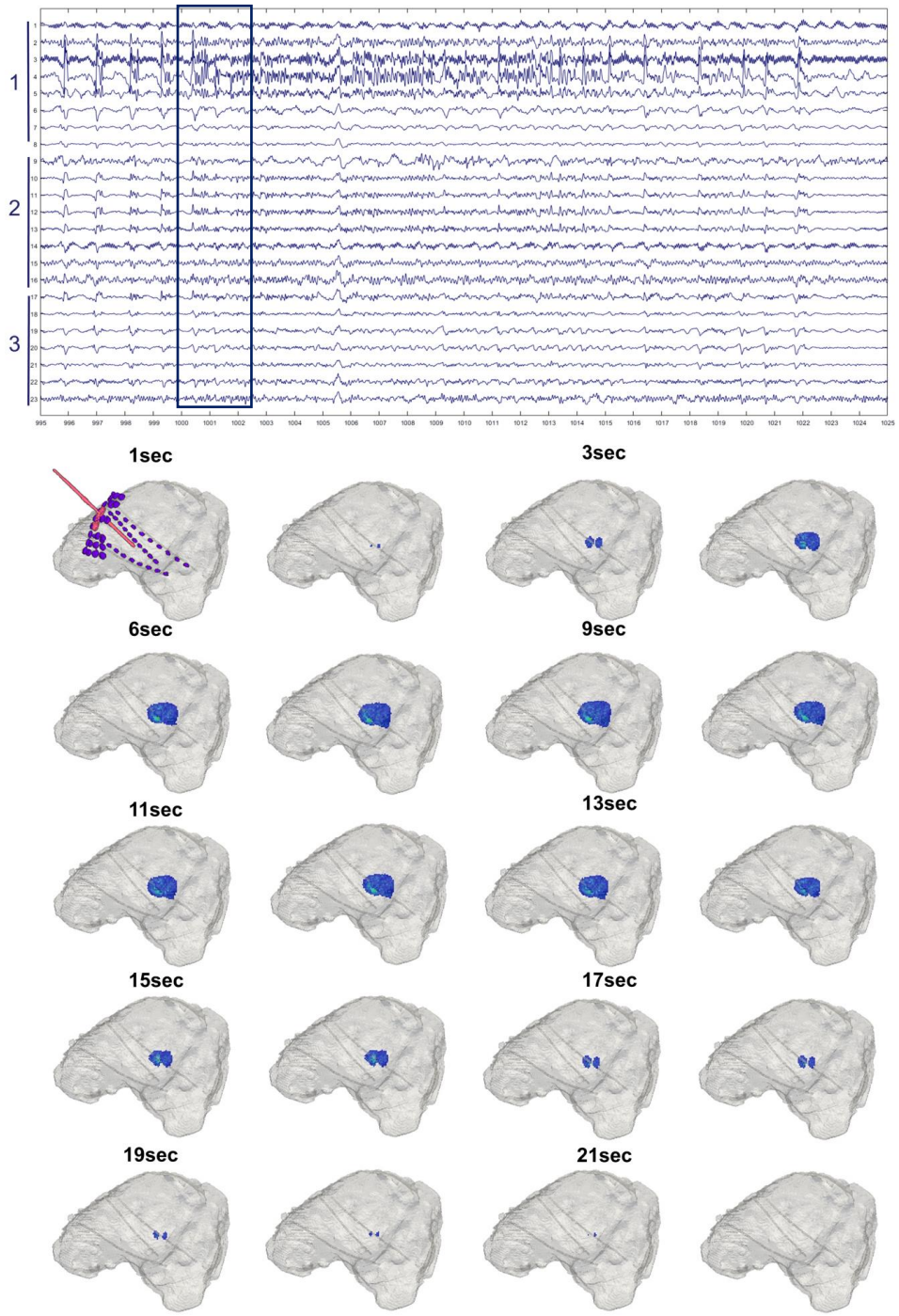

Figure 5-16. Example of progression of focal seizure. The onset of the seizure is indicated by a rectangle on ECoG/SEEG (above). The SEEG electrodes and cannula for BPN injection are shown in Fig 9. The onset of the seizure started at contacts 3-4 on SEEG and is represented by the corresponding location on the EIT reconstruction. The regional spread among the adjacent contacts seen on EIT images correlated with SEEG findings. The dZ change started 12 seconds after the SEEG onset.

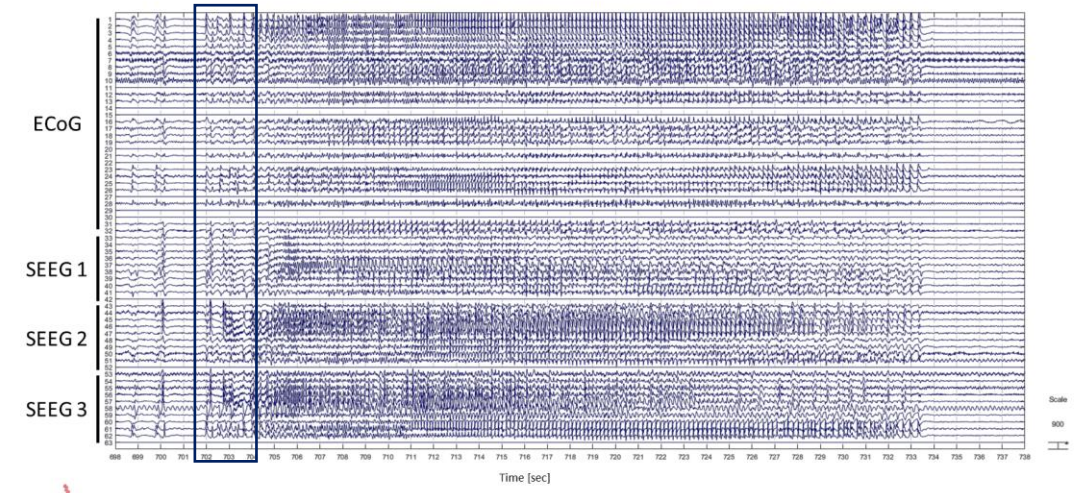
ECoG
SEEG 1
SEEG 2
SEEG 3
Time [sec]

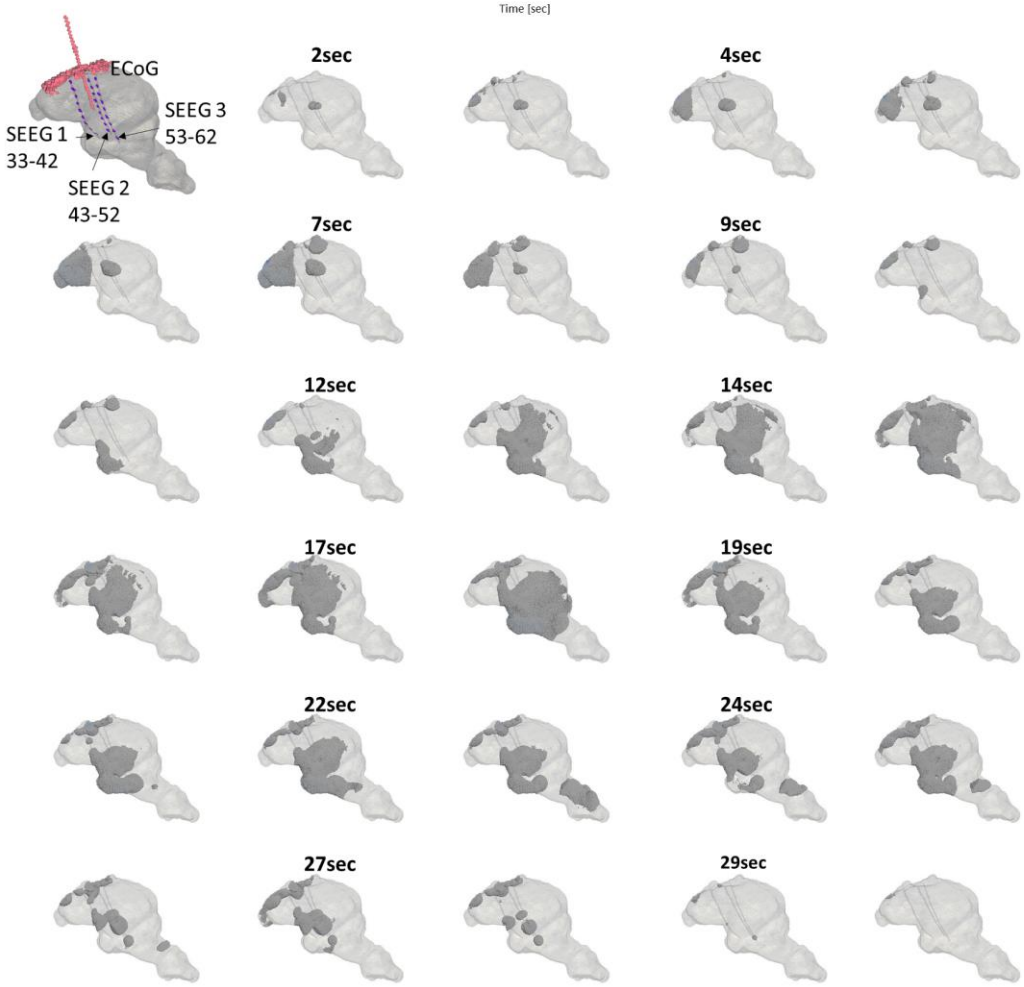
ECoG
SEEG 3
53-62
SEEG 1
33-42
SEEG 2
43-52
2sec
4sec
7sec
9sec
12sec
14sec
17sec
19sec
22sec
24sec
27sec
29sec

Figure 5-17. Example of progression of focal, secondarily generalised seizure. The ECoG/SEEG onset is indicated by a rectangle on top of the figure. The ECoG/SEEG onset corresponds with the deep onset reconstructed with EIT on the lower right. Following the spread of the seizure on cortical channels (ECoG), the reconstruction shows a significant change occurring in the cortex. EIT change was thresholded at 65% of the maximal change. The dZ change started 10 seconds after the SEEG onset.

The amplitude of the impedance change correlated with the number of channels on which the seizure started ($r=0.6$, $p<<0.0001$, Figure 5-18 A) and to which it spread ($r=0.6$, $p<<0.001$, Figure 5-18 B) but not with the spiking activity seen at SEEG ($r=0.03$, $p<0.9$, Figure 5-18 C, n=37 seizures in three pigs).

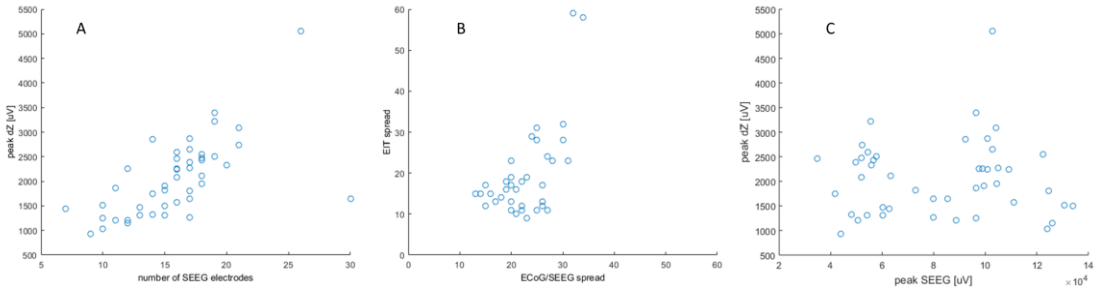

Figure 5-18. Correlation between ECoG/SEEG and EIT signal. (A) correlation between the number of contacts involved in seizure onset on ECoG/SEEG channels (during first four seconds of the onset, x-axis) with the amplitude of the impedance change (peak dZ, y-axis). (B) correlation between the number of contacts involved during the maximal spread of the focal seizure on ECoG/SEEG (x-axis) with the number of ECoG/SEEG contacts to which the seizure spread on EIT reconstruction (y-axis). (C) correlation between the spiking magnitude (peak SEEG, x-axis) with the amplitude of the impedance change (peak dZ, y-axis).

5.4 Discussion

5.4.1 Summary

This study has shown that a single intracranial injection of BPN resulted in focal and generalised seizures in a porcine brain. The epileptic activity could be easily detected with intracranial electrodes, the same as usually used in patients. The activity occurred in a recurrent cyclic pattern, so that it was possible to recognise the seizure from the background normal/interictal activity.

It was also demonstrated that each seizure generated impedance increases that could be recorded on the majority of recording channels and distinguished from the baseline. The impedance increase was always delayed with respect to the electric detection of seizure. The magnitude of the impedance change correlated with the wide spread of the seizure on ECoG/SEEG.

Finally, the onset of focal and focal secondarily seizures produced localised changes in EIT that correlated with the SEEG and/or the position of the tip of the cannula. Also, the spread of the reconstructed change correlated with the spread observed electrophysiologically.

5.4.2 Technical considerations

Several technical issues have been recognised during this study.

First, there was a difference observed in seizure onset as detected by the SEEG electrodes and EIT reconstruction when compared with the location of the tip of the cannula in pig 2. Both SEEG and EIT detected the onset almost 2 cm below the actual injection site. Although very consistent within the animal, it was different from the other pigs. The most likely explanation is that the injected penicillin dispersed away from the cannula. As discussed below, one of the limitations of the study was some variability in defining the onset zone. The BPN injection site was estimated but confirmation with CT was only undertaken at the end of the experiment. Achieving consistency between animals was attempted by using the same volume and size catheter to inject BPN, the same entry point on the epicortical array and trying to keep the similar angle of the cannula when implanting into the brain. However, the size of the brains varied between the animals. It is possible that in this particular pig, the geometry of intracranial electrodes and cannula differed to the other animals (Figure 5-3). Further confirmation on the individual differences between this animal and the others was found in the time latency between the initial injection of BPN and a first seizure recorded. The mean time in all 5 studies was approximately 30 min.

However, for this particular pig, it took 52 minutes to initiate seizures. It is, therefore, possible that the penicillin tracked into deeper structures, which was captured by the SEEG and EIT onset detection.

There was some variation in the placement of the depth electrodes between animals. This was because the electrodes positions were only roughly screened with 2-plane radiographs and accurate CT was only available at the end of each study after euthanising the animal. I attempted to maintain the consistency in placement by defining the craniotomy window with respect to the skull sutures, clearly visible from the surface over the left hemisphere. The same epicortical array was used for all animals and it was placed over the same area of the brain cortex, as exposed with the craniotomy. The array used had pre-defined holes for depth electrodes, with the purpose of maintaining the same entry points for SEEG electrodes between the experiments. This achieved reasonable consistency. Unfortunately, I was unable to use stereotactic placement, as the only available pig stereotaxic atlas (Felix et al. 1997) employs intracranial co-ordinates (*recessus preopticus* and posterior commissure, as opposed to skull sutures) and these were not available to me until after the studies were completed.

A technical challenge was presented by the anatomy of the adult pig skull. The porcine skull size can vary significantly between animals and it is up to 25 mm and even 50 mm thick for middle portion and occipital crest respectively (Sauleau et al. 2009) at 6 months. This variability resulted in a variable number of depth electrodes that could be implanted in each animal. Even though the craniotomy remained similar in the shape and size for all pigs, the variations in skull thickness restricted implantation of either three or four SEEG electrodes, if pre-prepared holes in the epicortical array were used as entry points, depending on the specific anatomy of each brain.

The study was also limited in overall recording time by the availability of the personnel and the CT scanner. Unfortunately, there was no CT available on site, and

the pig had to be transported to a different building for the scan. The scans were only offered until 5 pm and so all the experiments had to be finished, the animal euthanized and transported before this time. Given that the surgery took approximately 2h if no complications occurred, and that the anaesthetic induction could only start at 7:30 am, and also that the first seizures would normally start only one hour after the surgery is finished, the actual productive EIT measurement time from one animal was restricted to only several hours in between the scan and the effective seizure induction. This time-pressure was the main reason for injecting additional doses of BPN in two animals, for which no seizures were detected after an hour of recording.

Similarly to the simulation study described in chapter 3, the overall computational time and memory usage of the reconstruction was quite considerable. Here, it involved up to 5h of CPU time per seizure. However, once the mesh had been created and the sensitivity matrix calculated, they could be reused for all further seizures in the same animal, and so a reconstruction of a single seizure took between 15 and 40 min (depending on the length of the seizure) for 64 injection pairs. This suggested that the method could be feasible to use in clinical settings of telemetry monitoring of epilepsy patients if these necessary initial computations were done at the beginning of the study.

5.4.3 What are the EEG characteristics of this swine model of penicillin-induced seizures, recorded with intracranial electrodes?

The procaine benzylpenicillin model of seizures worked well in the study, as predicted and hoped from the literature, despite our change to the standard protocol with injection into the deep brain structures as opposed to the cerebral cortex (Leaming et al. 1999; Mäkiranta et al. 2005; Opdam et al. 2002; Terndrup et al. 1995; Terndrup et al. 1994; Van Gompel et al. 2011, 2014). The model resulted in repetitive cyclic epileptic activity, for which it was possible to clearly distinguish four phases on raw EEG and all seizures occurred without the trigger. In three pigs, seizures

developed from focal to widespread generalised, whereas in two pigs, only generalised seizures were recorded. The most likely cause was an additional injection of BPN in these two pigs that reacted with generalised seizures only. A typical pattern of increasing amplitude of interictal and ictal discharges over the 3-hour experimental time was also noted in all five animals, unrelated to the amount of BPN injected. The most probable explanation for these observations could be a build-up of the chemoconvulsant effect on GABA receptors and transmission within the regional structures and spontaneous recruitment of adjacent regions into the epileptogenic zone.

There were several anaesthesia setups tested for the BPN seizure model in the past, including isoflurane, fentanyl and morphine (Van Gompel et al. 2011) but not sevoflurane. We used sevoflurane because of its resemblance to isoflurane. It has also been reported to have epileptogenic potential (Constant et al. 2005; Jääskeläinen et al. 2003). The mechanism is unknown, but it has been speculated it is to be linked with the dose-dependent activation of NMDA neuronal receptors (Kreuzer et al. 2014; Iijima et al. 2000; Goo et al. 2017). As the majority of epileptiform activity is observed during the burst suppression or between the burst suppression and isoelectric lines, indicating very deep anaesthesia with a significant decrease in cerebral activity, it has been hypothesised that a window could exist, during which discharges are easier to evoke just before the total brain suppression. However, no further studies have been performed to confirm this mechanism or establish the direct effect of sevoflurane on NMDA receptors. In our case, intracranial EEG was used as additional control of the level of anaesthesia. The aim of the EIT study was to reach deep anaesthesia but not the burst suppression of brain activity. In that way, the animals would be kept under efficient anaesthesia, but the chosen anaesthetic drug would not affect the seizure model and epileptogenic activity in any way and sevoflurane suited this purpose very well. Furthermore, sevoflurane allows maintaining a very stable control of cardiovascular activity, which is crucial while

seizures occur. Overall, it seems that our anaesthetic protocol study was effective for producing seizure activity without affecting the model and served well the purpose of the study.

A limitation of the study was that there was only a little control on where the tip of the cannula for BPN injection pointed. While implanting the cannula, the aim was to point towards the midline and thalamus, and the grey matter of depth structures of hippocampus and amygdala, the most common regions involved in the temporal lobe epilepsies, the most frequent type of epilepsy (Diehl and Lüders 2000; De Tisi et al. 2011; Murphy et al. 2010). However, we could not control stereotaxically or with accurate imaging method where exactly the tip of the cannula reached and was oriented towards. It is thus quite likely that in some cases the tip ended up in white matter fibre tracts, whereas epilepsy is considered a grey matter disease. Most epilepsy studies describe the abnormalities and diffuse atrophy of grey matter that result in seizures, with the impact of white matter in network alterations, rather than triggering the seizure (Concha et al. 2009; Coan et al. 2014; Liu et al. 2016). Consequently, if the BPN was injected into the white matter structures, then no seizures would occur and so an additional dose of the convulsant had to be injected, as it happened in two of the studied pigs. Most likely, the additional bolus of chemoconvulsant created a new focus for seizures and, as the BPN seizure model is dose-dependent; it is likely that the threshold for generalised seizures was exceeded in these two cases even though the focal seizures were not observed. This seems to be the most likely explanation for the fact that in two pigs requiring additional BPN dose, only generalised seizures were seen.

Overall, the seizures observed after triggering with benzylpenicillin resulted in electrophysiological symptoms and their spatiotemporal propagation. Hence, the model seemed accurate and as such can be safely used in further experiments, even though developing means to better control the orientation of the cannula should be also considered.

5.4.4 Does EIT have the ability to image the onset and propagation of the seizures in real-time?

This work shows that it is possible to obtain reliable and repetitive images of the onset as well as the spread of the seizure spatially and temporally for focal seizures. The EIT signal was always delayed from the SEEG onset but it followed very well the pattern of the seizure seen with electroencephalography. The raw impedance changes were very consistent, providing the impedance increase without averaging for every seizure recorded. The magnitude of the dZ correlated with the spread of the seizure on ECoG/SEEG, resulting in the largest impedance changes for generalised seizures. Such changes allow reconstructing each seizure in a real-time mode so that the onset and spread can be followed within a resolution of a second. The ictal images are comparable with the discharges seen over the ECoG/SEEG electrodes for the onset, regardless of the position of the BPN cannula. This was especially striking for the second animal with focal seizures in which the recorded SEEG changes and the apparent onset of the EIT reconstruction both pointed to the very same area almost 2 cm away from the tip of the cannula. For each animal, the onset of the reconstruction with EIT was consistently identifying similar brain structures as the potential foci. Only in the last animal, the EIT onset was slightly more spread over a wider region of around 1.5 cm around the tip of cannula between the 16 focal seizures. In this case, however, the quality of the ECoG/SEEG was significantly worse, as the recording contacts were reused between the experiments and the background recorded on ECoG between the seizures was nosier, with frequent sharp cortical activity. Still, the overall accuracy for the onset of reconstruction in all animals was below 1 cm away from either cannula or the area of activity on SEEG. These results clearly show that EIT can provide real-time imaging of an accurate onset of focal seizures even if only intracranial electrodes are used. These results are extremely promising for further clinical applications, as the

data analysed here were collected with a setup used in the clinic that provides both SEEG and EIT recordings at the same time.

5.4.5 What are the limitations of using EIT for imaging seizures in-vivo?

In its current state, EIT as a method has some limitations. The main drawback is that EIT is currently limited to invasive recordings only. Other imaging methods used in the epilepsy field, such as SPECT, PET or EEG-fMRI do not require intracranial electrodes and they can be used in presurgical evaluation prior to the invasive SEEG implantation. EIT, however, requires intracranial electrodes to obtain enough signal-to-noise ratio allowing detecting changes while injecting safe levels of current. Hence, it cannot be used during routine EEG recordings. Still, however, EIT holds a significant advantage of availability to record in parallel with intracranial monitoring, while using only the SEEG electrodes implanted for clinical reasons. EIT can be used continuously with video telemetry during both interictal and ictal events, which is not possible with PET or fMRI. Also, there is no need for trained personnel to inject tracer at the beginning of a seizure as it is in SPECT.

In this study, EIT has been shown to be capable of providing 3D images of the focal signal spread over the brain that correlates with the spread over the ECoG/SEEG. However, here, the seizure onset was located exactly between the SEEG electrodes; therefore, the majority of current injections, and consequently the highest sensitivity of EIT, were focused around the onset area. This will unlikely be the case in real patients, for whom the electrodes are much more widespread, covering distant areas between the lobes or even the hemispheres. Still, the results for imaging the spread of the focal seizures with EIT in this setup, suggest that EIT could be potentially used to define the margins of the epileptogenic zone. Such a use would be extremely helpful for cases with large lesions diagnosed for the surgery, for whom it is impossible to resect the whole dysplasia. Further work is however required to assess whether EIT can be used to distinguish such zones within the dysplastic region of the cortex and exactly how accurately it can do so.

Only focal seizures were reconstructed in this study, based on the assumption that they would represent the typical clinical scenario most accurately. Focal seizures can be evaluated with EEG, which is currently the gold standard method for seizure assessment. The outcome of EIT could be then compared with the EEG findings, making it the most clinically precise way to justify the results. Focusing the analysis on the focal seizures makes it also more representative for a typical profile of a patient awaiting a potential neurosurgery. In general, only patients with focal refractory epilepsy are further investigated towards the resective surgery. If seizures are generalising rapidly, it is difficult and often impossible to define the epileptogenic zone and, consequently, to decide where to implant the intracranial electrodes and then operate. Hence, we assumed that it would be significantly less likely that we might record such cases with EIT in the hospital even though, we managed to record many generalised seizures in our animal study including the two pigs presenting only generalised seizures throughout the whole experiments. Yet, the EIT imaging accuracy of the onset and spread of generalised seizures was not analysed further, due to its lack of direct clinical relevance and absence of potential application in the clinic as well as the difficulty in comparing any potential results of such analysis with the EEG data.

Finally, slow impedance changes occur due to cell swelling during local intense depolarisation and the shrinkage of the extracellular space drained from water and excess potassium ions (Holder 2005). Such changes arise over seconds and should follow neuronal activity, whereas the EEG has a resolution of milliseconds and detects a summation of postsynaptic activity, either inhibitory or excitatory (Smith 2005). Due to the difference in the resolution and the source of the signal measured between EIT and EEG, EIT could be missing some crucial information on the onset, and therefore on the localisation of a potential surgical target. For instance, in one of the studies examining impedance changes in a rat brain, there was a sudden fast drop in impedance described, occurring at around 5 to 12 milliseconds before the spike is

seen on ECoG, and followed by the slow and steady rise within 120 ms after the spike. (Vongerichten et al. 2016). However, that study was performed on rats with epicortical array serial EIT system, and epileptic activity was triggered with 4-AP or picrotoxin and the impedance changes were detected for interictal spikes, not for the seizures. In our study, the EIT system was not sensitive to the changes occurring within millisecond timeline but still, the results presented here seem to indicate that in the current setup EIT was capable of repetitive and accurate onset localisation that is consistent with the SEEG findings and could aid them in clinic.

5.4.6 Conclusions and future work

Overall, this study has shown that it is possible to obtain reliable images of the onset and spread of the focal seizures with EIT and depth electrodes in the porcine brain during chemically induced seizures. This is the first time that EIT was used in a large folded brain with human intracranial electrodes during ictal events. Seizures induced with procaine benzylpenicillin produced cyclic epileptic activity that could be easily followed and distinguished in ECoG/SEEG. The parallel EIT system provided a reliable method for accurate localisation of the onset of the focal seizures when compared with the ECoG/SEEG outcome. The method produced a promising outcome that may in future improve the localisation of seizure foci in patients. The most important advantage of EIT is that it can be used in parallel with intracranial electroencephalography while recording all ictal and interictal activity. EIT produced functional images showing ictal spread with a temporal resolution of seconds, with a spatial accuracy of less than one-centimetre distance from the onset area defined either by the tip of the cannula or by the active SEEG electrodes. At the moment, the correlation of the seizure spread between ECoG/SEEG and EIT was only performed for a single time point during which a seizure presented the most generalised activity on ECoG/SEEG. This work should be extended further, to compare the volume of the EIT change with the ECoG/SEEG findings over time. These findings could be also extended by parallel studies with fMRI, which was impossible

due to no available scanner during the experiments. Future work should be focused on establishing EIT accuracy if the seizure onset is within further distance from the SEEG electrodes, as well as possibly analysing generalised seizures in a greater detail. There is also a need to better understand the coupling between the interictal spike activity in EEG and the EIT changes localising the primary focus or foci. A further assessment of the impedance changes over the interictal discharges (grade II and III in the described model) would be also desirable. In general, EIT has great potential to help in the clinical diagnosis of the seizure onset zone, to understand epileptic circuits better and thus to obtain improved control over seizures in the future.

Chapter 6

Feasibility of imaging fast impedance changes with depth electrodes occurring during interictal and ictal activity in a large animal model and in patients

Overview

The final and most challenging part of the work presented in this thesis was to detect fast impedance changes happening due to interictal and ictal activity in a gyrated brain. The previously described work showed that it was possible to detect fast and slow impedance changes in simulations on real-patient datasets (chapter 3) and to image ictal-related, slow impedance changes in a large animal brain (chapter 5) with depth electrodes. Taking these studies together with those described in literature, in which fast and slow impedance changes could be recorded in a rat brain with an epicortical array, the most desirable next step appeared to be to try to image fast impedance changes with EIT and depth electrodes for the first time in the human brain. Unfortunately, as described before, it was not possible to record the data on patients during seizures due to clinical obstacles, and so only measurements very limited in time could be collected at the end stage of clinical assessment. The potential options available for collecting such data included focusing on interictal or ictal discharges, and on either fast or slow EIT. In view of the above practical constraints and given that the system used in the animal study described in chapter 5 had not been safety tested for use in the clinic, all the data presented in this chapter were only fast neural changes recorded at 1.7 kHz. In the human recordings analysed here, the data were only interictal. EIT images were reconstructed by back averaging of interictal spikes. EIT images were generated every 2 ms for 200 ms around the spike centre time. In addition to the human study, the same approach was used for spikes produced during ictal activity in one anaesthetised pig. This produced series of EIT images every 2 m over 200 ms of fast impedance changes related to a spike. The spike-related trajectory was analysed using a centre of mass approach on the data collected during seizures in one pig. This was not attempted in humans due to lower signal generated by interictal spikes.

6.1 Introduction

6.1.1 Background

The epileptogenic zone is defined as the minimum area of the brain necessary to generate a seizure. Based on the EEG assessment, the epileptogenic tissue in focal epilepsies can be divided into two main zones generating discharges, the irritative zone and the ictal onset zone that both stay in relationship with the epileptogenic zone. The ictal onset zone is recorded during seizures and the irritative zone generates interictal discharges (interictal epileptiform discharges, IEDs) (Smith 2005; Mcevoy and Harkness 2015; Zijlmanset al. 2019).

An interictal or ictal spike discharge, as recorded with EEG, is a graphic representation of the voltage differences between the two recording electrodes over time. Its frequency, amplitude, distribution and clinical presentation can vary significantly, depending on the affected brain network (de Curtis and Avoli 2008). For example, it has been observed in the interictal EEG-fMRI studies that the spiking activity can be divided into several different populations that modified the brain metabolism on different level, sometimes beyond the identified epileptic focus (Kobayashi et al. 2006, 2005; Federico et al. 2010). The underlying process causing a spike component, either ictal or interictal, is a high-frequency, intense, synchronised neuronal firing, often followed by a slow wave of the hyperpolarisation phase, when the neuronal networks become relatively quiet (Blumenfeld, 2005). However, detailed processes underlying the discharges are still not well understood. It is currently assumed that the sources of interictal and ictal activity may be different but localising the source of IEDs can be helpful in locating the epileptogenic region and defining the prognosis and treatment (Fisher et al. 2017; Karoly et al. 2016). The correlation of interictal discharges in the irritative zone with the ictal onset zone depends on several factors. IEDs are rarely seen in a healthy brain, with a prevalence of 0.2-0.5% among healthy adults and 1.9-3.5% in children, although they are seen commonly on neurological wards, even in patients with non-epileptic

diagnosis (Guerrini 2006; Moshé et al. 2015; Pillai and Sperling 2006). Their association with epilepsy varies depending on their location: anterior temporal or mid-temporal spikes give a high likelihood (of above 85%) of respective regions epilepsy diagnosis, while lower chances of below 75% are associated with discharges arising over the frontal, central and/or occipital regions (Moshé et al. 2015; Pillai and Sperling 2006). Furthermore, however, the exact trajectory of the spikes through the brain networks remains to date unknown. This is due to a lack of a method capable of recording neuronal activity with millimetre and millisecond spatiotemporal resolution, necessary to capture neuronal depolarisation.

Electrical Impedance Tomography has been recently proposed as a method potentially capable to approach this problem. In recent studies, already described in greater detail in chapter 1, EIT has been used to image fast impedance changes related to ictal activity in a rat brain with an epicortical array (Hannan et al. 2018). The authors reported that it was possible to image the trajectory of the ictal spike-and-wave discharges with EIT and an epicortical array. The spikes were triggered with electrical epicortical stimuli. Repeatable impedance changes were recorded during the initial spike phase in the whisker barrel cortex as an early onset, which then spread posteriorly, laterally and ventrally over 20 ms in a rat brain. These findings suggested that EIT could be potentially helpful in neuroimaging of epileptic phenomena and in improving understanding of epilepsy circuits.

6.1.2 Rationale

As described before (chapter 4), it was not possible over the time-course of our studies to fully overcome the technical difficulties due to the artefacts introduced by EIT in the clinical EEG recording system. Thus, we were only granted access to patients for a limited time. It was only possible to measure interictal activity, in subjects who were receiving a full dosage of antiepileptic medications prior to the discharge. Unfortunately, interictal activity has a lower signal-to-noise ratio than ictal discharges and its occurrence varies. In order to maximise the likelihood of

detecting any impedance changes, I recorded fast neural impedance changes and increased the SNR by back averaging of many spike discharges.

Therefore, a serial current injection EIT system was used as opposed to a parallel one, as fast neural recording can only be undertaken at a single frequency (1.7±0.2 kHz). The frequency used in these recordings was a compromise between the optimal 1.355 kHz frequency found for rat epilepsy experiments (Hannan et al. 2018), the requirement from the medical engineer working at the NHNN hospital to inject above the 1.5 kHz band (as described in chapter 4) and the previous experiments, during which 1.7 kHz was successfully employed (Vongerichten et al. 2016; Hannan et al. 2018). This serial EIT system contained a multiplexer, which permitted addressing of any electrode combination. This enabled acquisition of an imaging protocol on multiple contacts, whereas the parallel system at the point of recording the data (i.e. before it was further developed for the study described in chapter 5) allowed injecting only five pairs.

The patients recruited for the study were selected to have continuous or relatively frequent focal interictal activity of a very similar electrophysiological representations, so that back averaging of many spikes was achievable in a reasonable short time. The study was followed by preliminary recordings in one pig during chemically induced seizures to compare the results obtained from interictal discharges in patients and ictal activity in an animal.

6.1.3 Purpose

The main aim of this work was to test whether it is possible to detect fast impedance changes with EIT and depth electrodes related to interictal activity in human epilepsy patients or ictal activity in a chemical model of epilepsy in the pig. The specific questions to be answered with this work were:

Could EIT be used to detect fast impedance changes in human subjects?

Can fast impedance changes occurring due to chemically induced ictal activity be detected and imaged with EIT and depth electrodes?

6.1.4 Experimental design

EIT recordings were performed in four epilepsy patients at Telemetry Ward of the National Hospital of Neurology and Neurosurgery, Queen Square in London. All patients were diagnosed with refractory focal epilepsies and were considered for epilepsy surgery. Hence, they were undergoing intracranial video-EEG telemetry monitoring with multiple depth electrodes implanted stereotaxically (SEEG). At the point of writing this thesis, none of them has yet undergone resective surgery. In addition, only one of them was offered a resection and, therefore, put on a waiting list for neurosurgery. As described in detail in chapter 4, EIT injection current was still affecting the signal collected for clinical purposes, so it was only possible to record EIT for periods of an hour or two towards the end of each patient's stay at the ward when all clinical SEEG had been completed and patients were restarted on a full dosage of antiepileptic treatment and just awaiting surgical removal of the SEEG electrodes. Consequently, only interictal activity was expected. Unfortunately, the recording from one patient could not be analysed, due to an initial technical problem with the EIT equipment, which was later fixed, and very limited time to record the EIT signal from that patient. Therefore, all data presented in this chapter came from the three remaining patients.

The EIT recordings on patients took between 1 to 2 hours. All patients were implanted with 9 to 12 depth electrodes with up to 10 recording channels on each. Out of all contacts available, 64 were selected in advance based on previous neurophysiological and clinical findings and the injection protocol was prepared to aim to cover "the most active" contacts, i.e. those with the highest frequency of interictal discharges, around the irritative zone. The recordings were performed using the parallel EIT system, which recorded both SEEG and the impedance signal but which, however, was set to work in a conventional, sequential (serial) way,

switching between the pairs of electrodes on a regular basis, as the full imaging protocol was programmed.

As none of the patients had seizures during the short periods for EIT recordings, a preliminary study was performed in one pig during seizures. The experimental set-up was as described in chapter 5 but the measurement protocol used mirrored the recordings in humans: fast impedance measurements were performed for 40 minutes on an anaesthetised pig with chemically induced seizures with procaine benzylpenicillin. The animal reacted with a very regular cyclic activity with seizures repeating every 2-3 minutes, so it was possible to set up a serial EIT protocol to perform the EIT measurements during each seizure, so that one seizure was recorded per an injection pair. This approach was similar to the previously described fast neural EIT with an epicortical array in rats (Hannan et al. 2018). During the recordings on the pig, there were 12 injection pairs during which 11 seizures were captured. Due to limited time and resources as well as the highly regular seizure activity required for such measurements, these recordings could not be repeated in more animals and so the findings should be treated as preliminary.

The expected impedance change due to neuronal depolarisation is approximately 0.1 to 0.3% (Aristovich et al. 2016; Vongerichten et al. 2016; Hannan et al. 2018). Hence, averaging the impedance changes related to interictal or ictal spikes is necessary to achieve acceptable SNR for imaging. Assuming that the electrophysiological findings seen during the interictal (patients) or ictal (pig) activity remained consistent throughout the whole EIT recording, an independent current injection pair could be used at every couple of minutes or per seizure respectively. Therefore, an EIT image of an averaged spike could be reconstructed for a patient dataset across all interictal spikes arising from a particular SEEG channel or for an animal from the data combined from 11 seizures.

6.2 Methods

6.2.1 Human Study

The measurements were collected on three epilepsy patients, who were implanted with multiple intracranial depth electrodes and monitored at the Telemetry Ward at NHNN (Figure 6-1 and Table 6-1). All patients had given informed consent to participate. They were approached at least 24 hours prior to recordings to introduce the study, and a written consent was collected just before the EIT measurements. The local ethics committee (London-Harrow Research Ethics Committee, 15/LO/0092) approved the study. The recordings were performed at the end of clinical SEEG monitoring, during which all patients were on full dosage of previously taken AEDs so that only interictal activity was expected. During the recordings on patient 3, the patient reported feeling "like having a seizure" but there was no correlative SEEG change seen and, as this patient was diagnosed with non-epileptic attacks in addition to focal epilepsy, such an attack was accepted as a likely explanation of patient's sensation. The recordings took place in hospital rooms on the ward with the participants lying in bed. An initial preparation procedure to connect the EIT system to intracranial electrodes took around 30 minutes for each patient. The EIT system was used to record both SEEG and EIT and there was no simultaneous EEG monitoring with MicroMed.

6.2.1.1 Patient 1

A 31-year old male, with focal epilepsy since the age of seven that had become difficult to control over the last 5 years. Currently, he experienced up to fifty seizure episodes daily, with frequent nocturnal events. A region of cortical dysplasia in the left frontal lobe was identified in the imaging and video-telemetry confirmed it as the most likely epileptic focus. The patient had been offered surgery for the dysplastic region; however, due to the relative proximity to primary language areas, intracranial electrodes were implanted first to further delineate the epileptogenic

zone more accurately. He was implanted with 12 depth electrodes covering the areas around the left frontal lobe and the lesion (Figure 6-1 and Table 6-1).

6.2.1.2 Patient 2

A 21-year old male, with 9 years of seizure history. Seizures with a loss of awareness currently occurred once a month and they tended to cluster and generalise into clonic seizures. Right occipital cortical damage of aetiology attributable to perinatal ischaemia was found on MRI. The EEG onset matched the location of the lesion. The patient was offered further diagnostics with intracranial electrodes to sample the signal from around the lesion, as well as right parietal, frontal and temporal regions. Overall, he had 11 depth electrodes implanted (Figure 6-1 and Table 6-1).

6.2.1.3 Patient 3

A 33-year old woman, with 5 years of chronic seizure history, but with an additional episode of acute seizures due to a head injury at the age of 15 months. Initially diagnosed with non-epileptic attacks, which still occurred. On scalp EEG, her seizures were localised to the left anterior temporal region. Interictal PET and ictal SPECT supported that localisation. MRI showed only minor hippocampal asymmetry, with smaller hippocampal volume on the right but with preservation of the signal. After an MDT discussion, she was offered implantation of intracranial electrodes to determine if the epilepsy was neocortical, temporal, or extratemporal. She was implanted with 9 depth electrodes covering the regions of the left medial and lateral temporal lobe, temporal pole, insula, orbitofrontal and cingulate cortex, temporo-occipital and parietal junction (Figure 6-1 and Table 6-1).

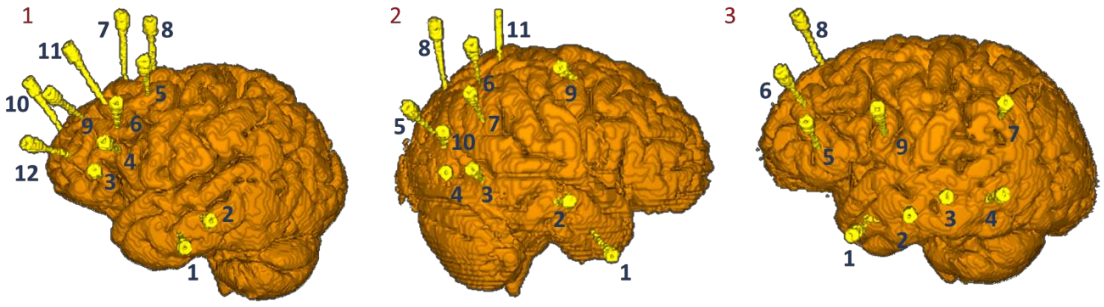

Figure 6-1. Schematics of depth electrode implantations for each of the patients recorded with EIT. The details on the sampling area of each electrode and which contacts were used for EIT recordings are specified in the table below.

	Patient 1		**Patient 2**		**Patient 3**	
	SEEG	**EIT**	**SEEG**	**EIT**	**SEEG**	**EIT**
1	Amygdala (AM)	1-6	Amygdala (AM)	1-5	Amygdala (AM)	1-6
2	Anterior Hippocampus (aH)	1-6	Hippocampus (H)	1-5	Anterior Hippocampus (aH)	1-6
3	Orbitofrontal (OF)	G+R	Fusiform gyrus (TOJ)	1-5	Posterior Hippocampus (pH)	1-6
4	Anterior Insula (IFG)	1-6	Infracalcarine (iCl)	2-7	Fusiform gyrus (TOJ)	1-8
5	Middle Cingulate (mCi)	1-6	Supracalcarine (sCl)	1-5	Orbitofrontal (OF)	1-9
6	Anterior Cingulate (pLes)	1-10	Precuneus (prC)	1-8	Anterior Cingulate (aCi)	1-8

7	Supplementary Motor Area (SMA)	-	Posterior Cingulate (pCi)	1-9 G+R	Posterior Cingulate (pCi)	1-10 G+R
8	Anterior Supplementary Motor Area (aSMA)	-	Superior Parietal Lobule (SPL)	1-5	Superior Frontal Gyrus (SFG)	1-5
9	Anterior to lesion (aLes)	1-7	Mesial Frontal Gyrus (MFG)	1-5	Anterior Insula (aI)	1-6
10	Superior Frontal Gyrus (SFG)	1-7	Lesion (Les)	1-5		
11	Lesion (Les)	1-6	Medial Parietal (mPl)	1-6		
12	Inferior to lesion (iLes)	1-6				

Table 6-1. Sampling area of each depth electrode during the telemetry ("SEEG" column) with the number of contacts connected to EIT ("EIT" column). On each electrode, the lower numbers correspond to more mesial contacts, increasing towards the lateral surface.

6.2.1.4 Animal study

One pig from those participating in the study described in chapter 5 was additionally recorded with a serial EIT system. The animal preparation, anaesthesia, surgery and seizure induction as well as the details of the EIT system used all were as described in detail in chapter 5. Briefly, the pig was implanted with four SEEG electrodes and a 32-contact epicortical array pointing midline, towards the thalamus and seizures were triggered with 30 µl (9000 IU) of procaine benzylpenicillin. This animal exhibited multiple seizures, cycling in the pattern described in chapter 5. The cycle

repeated every 2 to 3 minutes, which allowed preparing an accurate imaging protocol for serial EIT. The protocol was combined with 12 injection pairs, selecting the depth contacts surrounding the tip the BPN cannula only. 11 seizures were recorded in total.

6.2.2 Data acquisition

6.2.2.1 Human study

The preparations and data collection took approximately 1-2.5 h (depending on a patient), as the recording time was limited by the clinical team. The parallel EIT system (chapter 4) was adjusted to work as a serial EIT system so that only one current source was used to inject current, and additional switching board controlled the protocol. 60 μA at 1.7 kHz was injected for 120 sec. The injection protocol comprised 20, 23 and 17 lines for patients 1 to 3 respectively, giving in total 1240, 1426 and 1054 electrode combinations. 62 SEEG contacts were used in total. The signal was averaged for 40 min, 46 min and 34 min respectively for patients 1 to 3.

The SEEG was collected with the ActiCHamp EEG amplifier in the EIT system on 62 contacts. The MicroMed system used for clinical EEG recording was disconnected. Any additional electrodes not connected to EIT were not monitored. Patients were sleeping or relaxing throughout the recordings. None of the patients reported any side effects from the EIT recording.

6.2.2.2 Animal study

Serial EIT data were collected in a very similar way to that described for patients. The recordings took 40 minutes. There were 12 injections of 60 μA at 1.7 kHz current, lasting 200 sec each and resulting in 756 measurement lines. 63 SEEG channels were connected in total. As seizures occurred spontaneously at every 2 to 3 min, the length of one injection in the protocol was adjusted to aim to capture a seizure per each injection. All 11 seizures captured during these recordings presented consistent electrophysiological appearances, hence an EIT image of an

averaged spike was reconstructed from all of the seizures recorded in this animal. The interictal activity recorded between the seizures showed different characteristics and therefore were not taken into the imaging reconstruction.

6.2.3 Data analysis

The same data analysis method was used for both human and animal measurements.

The data were analysed offline in Matlab software to extract both SEEG and impedance signals measured as voltage and percentage changes from the mean of the baseline. The SEEG signal was filtered with a 1 Hz and 200 Hz bandpass filter (6^{th} order). For human recordings, an additional step of re-referencing the SEEG signal to the bipolar montage was performed to visually compare the SEEG signal recorded clinically on MicroMed before EIT recordings to the signal in ActiCHamp. The fast impedance change was extracted using a 200 Hz bandpass filter around the carrier frequency (30^{th} order Butterworth) and demodulated using Hilbert transform.

The channel with the highest amplitude discharges seen in SEEG was selected as the trigger signal for averaging the spikes (either interictal or ictal) and spike-related impedance changes. Markers for the triggers were set manually at the peak of each spike component. The criteria for including spikes into EIT imaging were as follows. In humans, all spikes occurring at one SEEG channel, which was then set as a trigger channel, formed one population of a typical and consistent pattern, allowing averaging them for EIT imaging. The spike pattern observed in the pig was defined as a single spike of a below-50-ms duration and a minimum of 1 mV peak-to-peak amplitude (Figure 6-11). For all spikes detected on the trigger channels, only those spikes that were within ±3 standard deviations of the mean trace of all detected spikes were used for averaging for both humans and the animal. The demodulated EIT signal from all channels was aligned with the triggers. Current-injecting and excessively noisy channels were rejected from the analysis. The latter were defined as having a standard deviation of the baseline above 5 μV. A 100 ms (150 ms for one

patient) epoch window around each triggering spike was used for averaging. The mean of the baseline, during initial 30 ms, was subtracted from each epoch to express the signal as an impedance change. The epochs were then averaged together producing a mean impedance change. All remaining channels with impedance measurements were collected across all interictal (humans) or ictal (pig) activity to produce an averaged impedance response and then used to produce an image of the spike-related change. A significant change was identified by comparing the impedance value at each time point across all channels to the signal at baseline using the paired t-test at 0.01 significance level. The employed statistical analyses are consistent with the approach currently used in the brain EIT (Hannan et al. 2018; Faulkner et al. 2018; Vongerichten et al. 2016; Aristovich et al. 2016). All values are presented as mean ± standard deviation (SD).

6.2.4 Image reconstruction

A similar method for image reconstruction was used for both, human and animal recordings.

In the human study, realistic and subject-specific meshes were created from T1-MRI imaging data for each of the patients. The tissue layer parcellation used for mesh creation for EIT was generated in EpiNav™ software (Epilepsy Navigator) for clinical planning of intracranial electrode implantation. The parcellation required minor additional adjustments in order to create reliable meshes for EIT (Mesher, CGAL http://www.cgal.org/, 2015). These modifications included mapping the electrodes used for EIT, changing their order to match the actual recordings, checking the generated layers and converting the file into a format that could be read by the Mesher software. The total combined process of mesh creation for three patients took less than two hours. The segmentation included CSF with veins, grey matter, white matter and electrodes. The conductivities of the segmented layers were set to 0.3 S/m for grey matter, 0.15 S/m for white matter, 1.79 S/m for CSF, as specified in the literature (Malone et al. 2014; Romsauerova et al. 2006; Horesh et al. 2006). All

meshes were made of 0.7 mm size tetrahedral elements, refined to 0.3 mm in proximity to electrodes. The resulting meshes were 3.5, 3 and 3.1 million tetrahedral elements for patients 1 to 3 respectively. For the reconstructions, coarser, 0.7 mm hexahedral meshes of 2.7, 2.2 and 2.2 million elements were used for patients 1 to 3 respectively. The actual geometry of intracranial electrodes was available from the parcellation. The forward solution was calculated using PEITS on the fine tetrahedral meshes (Jehl et al. 2014). Reconstructions were calculated on the hexahedral meshes with zeroth-order Tikhonov and noise-based image post-processing (Aristovich et al. 2014).

The detailed procedure for image reconstruction performed on the data collected from one pig has been same as described in chapter 5. The animal-specific mesh was created from a CT scan, and hence, no differentiation between grey and white matter could be performed. The conductivity of tissues was modelled as a homogenous section of 0.22 S/m conductivity for the whole brain (Horesh 2006). A 7-million-element tetrahedral mesh was formed from 0.3 mm size elements, whereas a coarser uniform 0.7-million hexahedral mesh used for reconstruction was created from 0.5 mm elements.

The images were reconstructed every 2 ms for both human and animal recordings. For displaying images, the reconstructions were thresholded at 65% of the maximum reconstructed value at every time point. The reconstructed images were assessed qualitatively for three patients, comparing the findings with SEEG and imaging data. The centre of mass of the maximum change was calculated only for the pig, and the distance was calculated with respect to the location of the tip of the cannula.

6.3 Results

6.3.1 SEEG

SEEG measurements recorded during the EIT data collection were consistent with the clinical findings over video-telemetry for all three patients, as assessed visually, in the same way as it is usually reviewed by clinicians in the telemetry.

6.3.1.1 Patient 1

Background SEEG showed continuous spiking activity arising from the contacts around the known cortical dysplasia (maximum signal at pLes7-8, pLes8-9 >Les2-3, Les3-4), with a frequency of 1 per 2 to 5 seconds, occasionally forming polyspikes (Figure 6-2). Spikes recorded from contacts pLes7-8/8-9 lasted up to approximately 50 ms and had an amplitude of up to 0.8-1 mV. Due to their consistency in shape, amplitude and frequency, spikes occurring at this region were later used as reference trigger points for back averaging (Figure 6-11). At a frequency of approximately every 10-25 seconds, the observed interictal discharges presented more widespread distribution over the other channels around the lesion but with the maximum of the signal again around the lesion (Figure 6-3).

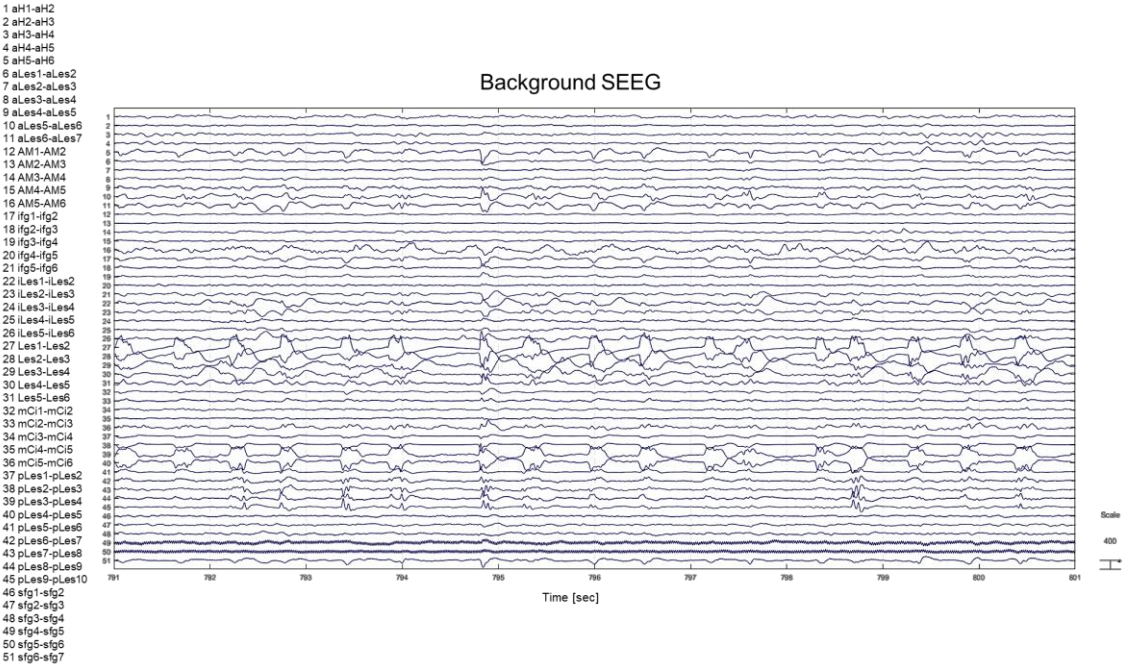

Figure 6-2. Background SEEG from patient 1, bipolar montage, 10-second page. The abbreviations for electrodes correspond to contacts previously described (Table 6-1). Continuous slow with superimposed interictal activity is seen around the cortical dysplasia, with a maximum on contacts pLes7-8/8-9 (43/44) and Les1-2/3-4 (27/28). Contacts OF5-OF6 (not shown) were used for the ground and reference, shared with clinically collected SEEG.

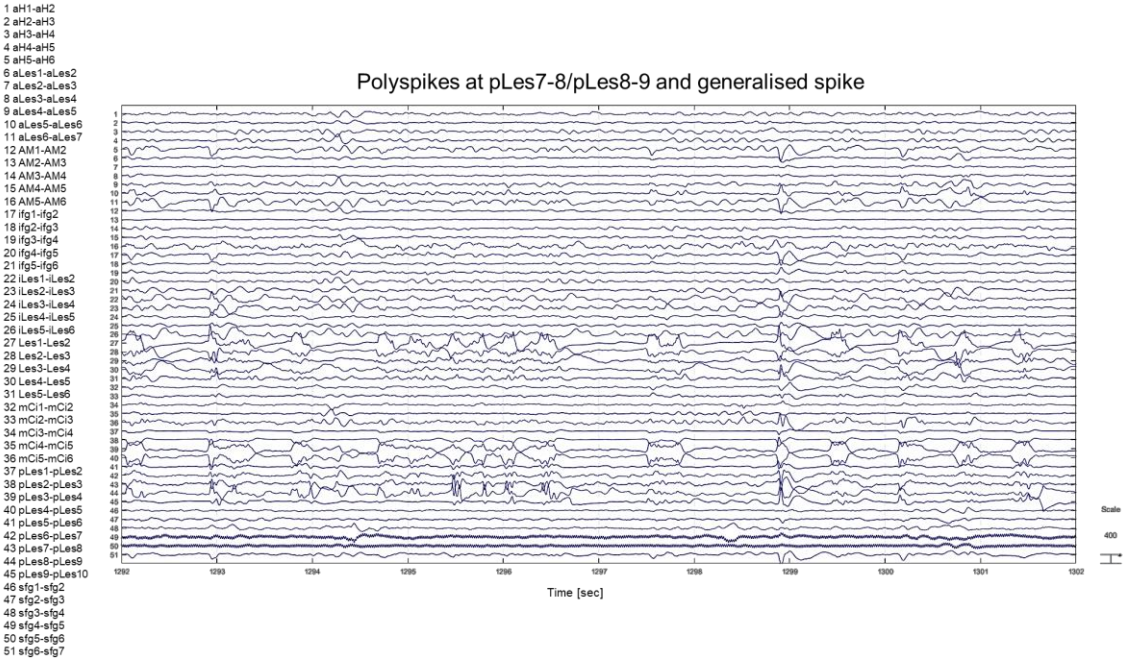

Figure 6-3. Focal and generalised interictal discharges arising from the region around the lesion over 10 seconds, bipolar montage. Contacts sampling the area posteriorly to the lesion (pLes6-7/7-8/8-9) recorded spikes occurring every 1 to 2 seconds, lasting approximately 50 msec, with occasional tendency to form polyspikes (e.g. between 1295 sec and 1297 sec). Infrequently, at every 10-30 sec, spikes presented more generalised activity (e.g. just before 1299 sec). These spikes arousing posteriorly to the lesion, as the most frequent were used as triggers for impedance changes.

6.3.1.2 Patient 2

Background SEEG showed a continuous slowing over the contacts placed in the hippocampus with occasional superimposed spikes (H1-2/3-4, Figure 6-4). Several brain areas generated independent interictal discharges of a variable frequency of between 10 to 60 seconds. The most consistent activity arose from the region of the precuneus, followed by the medial parietal and the occipital lesion (Figure 6-5). The amplitude of the SEEG and the interictal activity was lower than in other patients (background within 100-500 μV). The majority of the discharges had characteristics of sharp waves, rather than spikes, lasting 80-100 msec, with approximately 100-200 μV amplitude. Sharp waves from the precuneus region were set as a reference starting point for back averaging due to their high frequency (Figure 6-11, Figure 6-10).

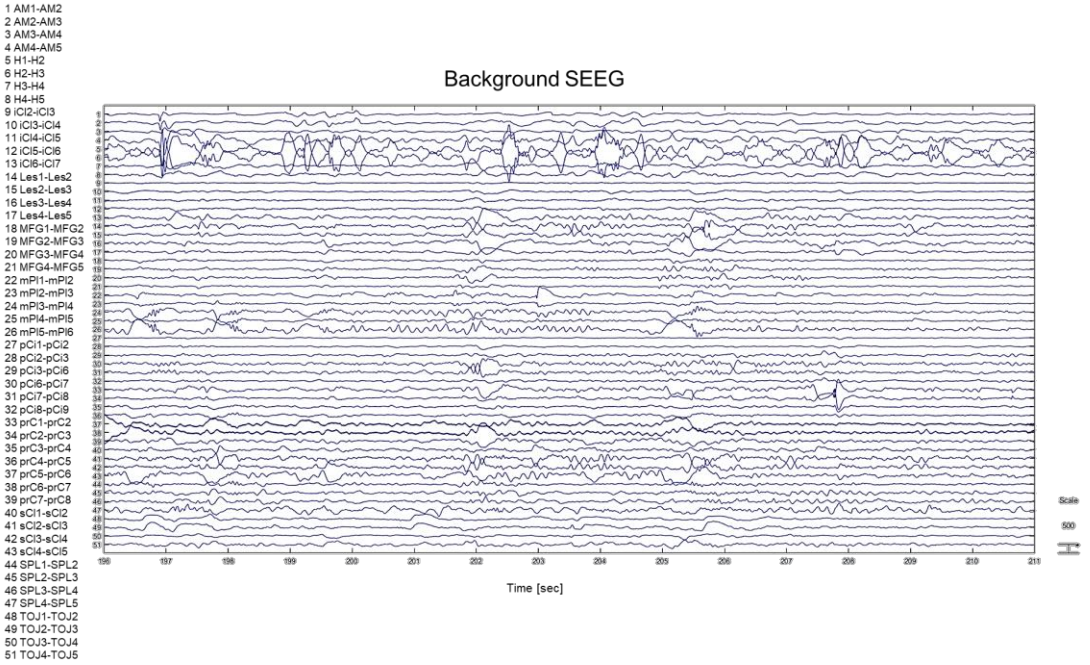

Figure 6-4. Background SEEG recorded from patient 2, 15-second page, bipolar montage, abbreviations correspond with depth contacts. Ground and reference were set on pCi4-pCi5 (not presented), shared with those used clinically. Continuous slowing is seen over H1-2/H3-4 (5/6) throughout the whole page. Superimposed spikes over the slow wave activity in the hippocampus are independent to spikes at prC1-2/prC2-3 (33/34).

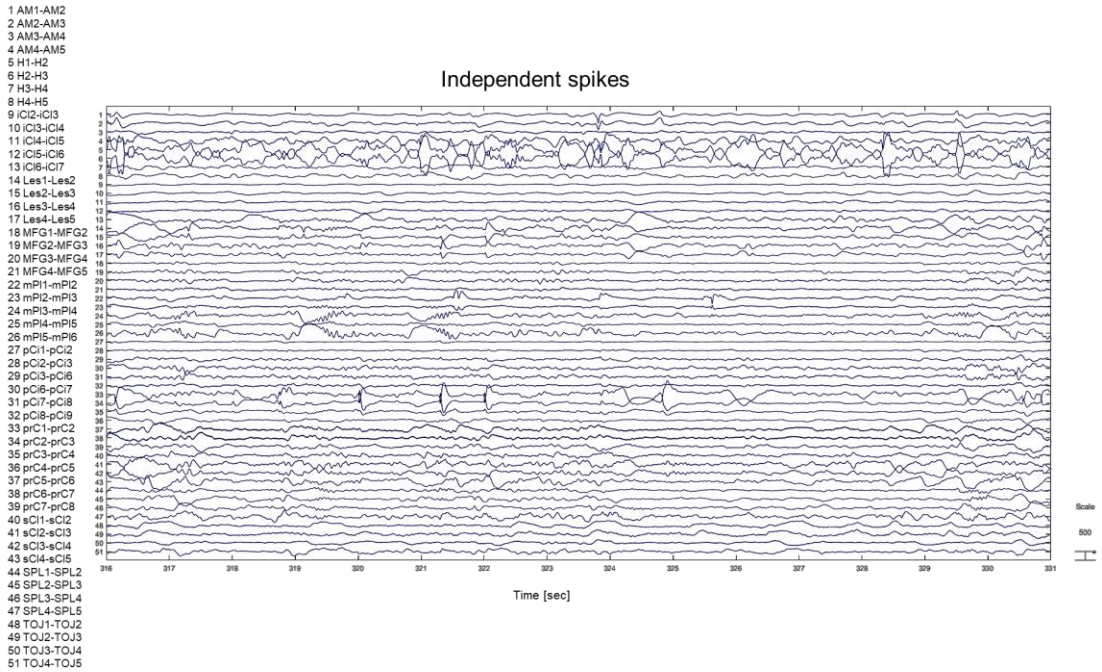

Figure 6-5. Independent interictal activity arising from precuneus and the lesion. The maximum occurs at prC1-2/2-3 (33-34)>Les3-4/4-5 (16-17), independent on Les1-2/2-3 (14-15) and mPl1-2/2-3 (22-23). The region prC1-2/2-3 was used to trigger impedance changes.

6.3.1.3 Patient 3

The background SEEG showed a continuous slow rhythm over the posterior hippocampal contacts with superimposed irregular interictal discharges (Figure 6-6). The maximum of the interictal activity was recorded over the amygdala and posterior part of the hippocampus, spreading towards the anterior hippocampal and posterior cingulate contacts. Interictal spikes occurred independently over the posterior hippocampal and amygdala contacts at maximal frequency of one per 10-20 sec, with the amplitude of around 500 μV (Figure 6-7).

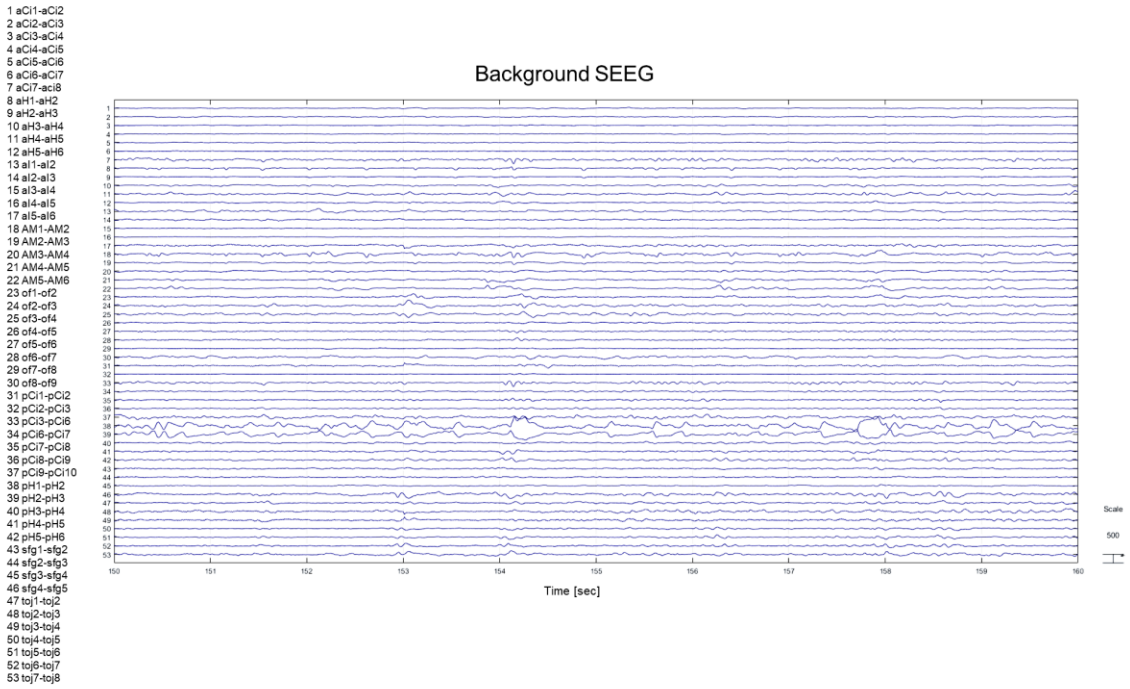

Figure 6-6. Background SEEG recorded from patient 3 over 10 seconds, bipolar montage. Abbreviations correspond to contacts described in the table. Ground and reference were set on contacts pCi4-pCi5.

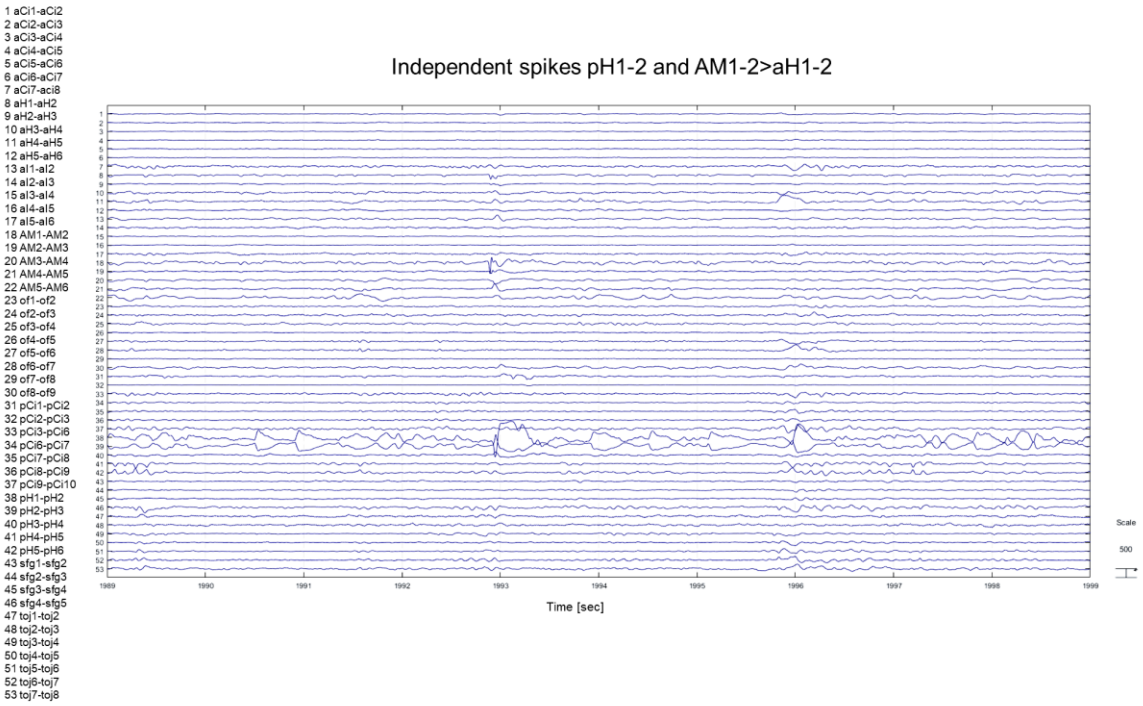

Figure 6-7. Typical representation of interictal activity seen during recording on a 10-second screenshot. The spike just before the 1993rd second of the recording had a maximum on contact pH2 (38-39), with an independent spike seen slightly earlier at AM1-2 (18)>aH1-2 (8).

In addition, in this patient there were three brief events recorded during the EIT study, lasting 113, 98 and 92 seconds respectively (Figure 6-8). The first event started with regular activity with a maximum at the amygdala contacts (AM1-2>aH1-2) that was followed within the next 30 s by spikes with a maximum at the posterior hippocampal contacts (pH1-2>pH2-3). During the second and third event, both electrodes, the amygdala and posterior hippocampus, recorded high amplitude (up to 5 mV) and high frequency (up to 10 spikes per second) regular activity at the same time (contacts pH1-2>pH2-3 and AM1-2>aH1-2). The maximum amplitude for all three events was seen on the posterior hippocampal contacts (pH1-2>pH2-3, up to 5 mV) that spread over the amygdala and anterior hippocampus (AM1-2>AM2-3, aH1-2>aH2-3, up to 0.5 mV and 0.7 mV respectively). During the first event, the patient reported a sudden hot flush, but it did not repeat during the subsequent

events. The patient stated that she usually experienced such a feeling after having a seizure and she also described that she had multiple seizures over the previous 24h of telemetry. Overall, she explained her feelings as a typical post-seizure body reaction. These spikes, arousing from the posterior hippocampal contacts, were used to trigger impedance changes. However, only the spikes occurring during these three events were used to form EIT images. Interictal activity occurring between these events had significantly lower amplitude and longer duration, and therefore were treated as not consistent enough to use for EIT imaging (Figure 6-10).

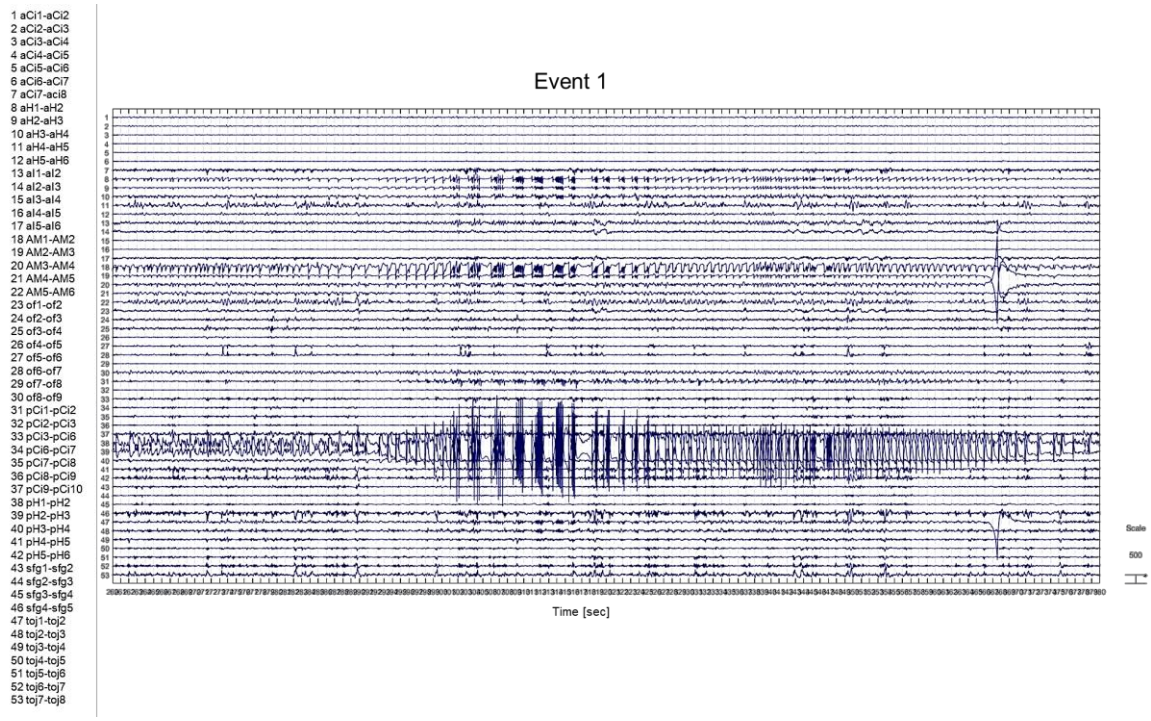

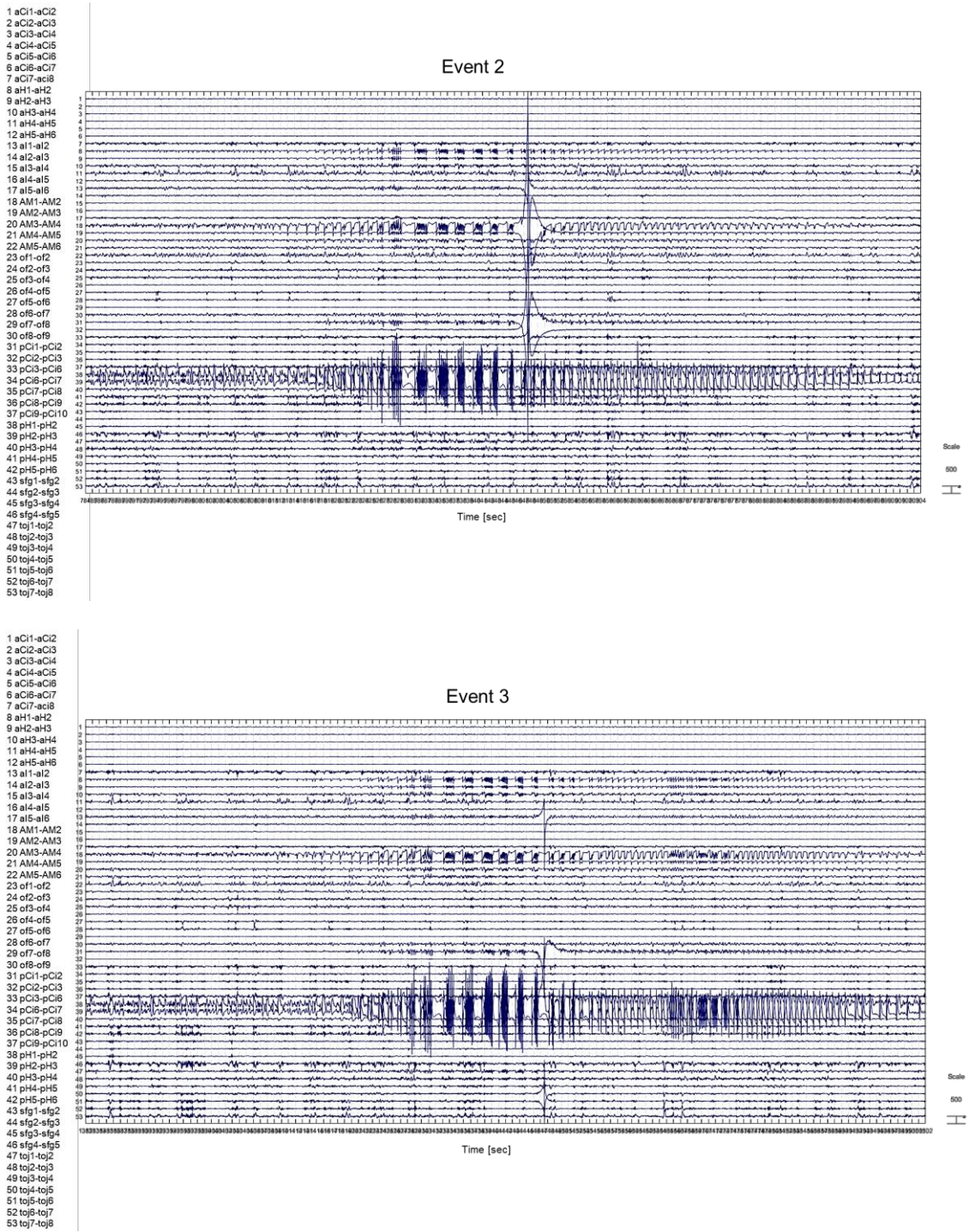

Figure 6-8. Three events captured during EIT measurements seen on a 120-second page. The signal of maximum amplitude was over posterior hippocampus (pH1-2>pH2-3, contacts 38>39), with lower amplitude on the amygdala (AM1-2>AM2-3, contacts 18>19) and much lower on anterior

hippocampus (aH1-2>aH2-3, contacts 8>9). Also, in all three events, a clear switching artefact coming from EIT can be distinguished (the most evident on event 2), which does not significantly affect the quality of recorded SEEG.

6.3.1.4 Switching artefact from EIT

The artefact coming from a switch between the electrode pairs injecting current can be clearly distinguished on SEEG (Figure 6-8 and Figure 6-9). It masked approximately 1.5 seconds of the data over the injecting channel but did not critically affect the SEEG signal.

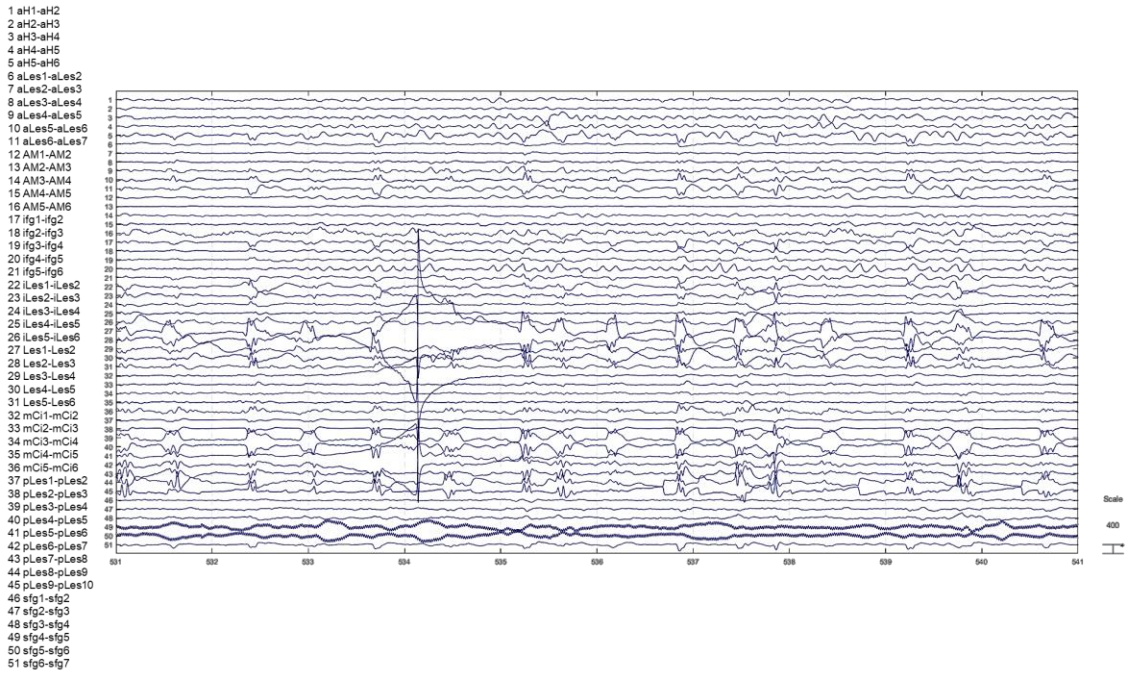

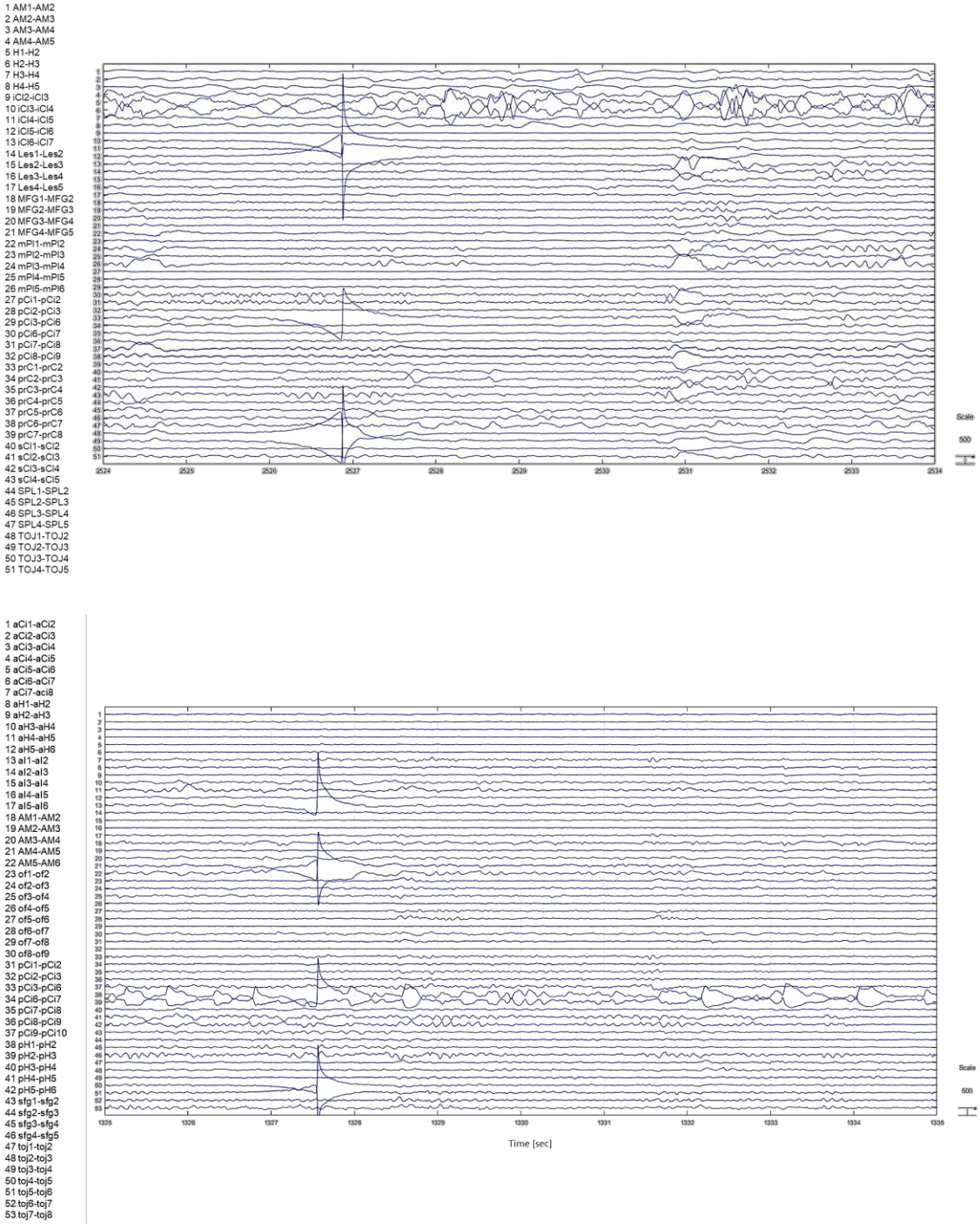

Figure 6-9. Representative examples of the switching artefact coming from EIT in three patients respectively. The artefacts are seen on contacts: (1) Les1-2/2-3 (27/28), pLes5-6/6-7 (41/42), (2) iCl3-4/4-5/5-6 (10/11/12), prC1-2 (33), TOJ1-2/TOJ2-3 (48/49) and (3) aI1-2 (13), AM4-5/5-6

(21/22), pH1-2 (38), TOJ4-5/5-6 (50/51). In all cases, the artefact was followed by a completely recovered SEEG signal.

6.3.1.5 SEEG during animal recordings

There were 11 seizures recorded in ECoG/SEEG during the animal study. All seizures were generalised and widespread, lasting 25±9 sec (Figure 6-10). Their electrophysiological characteristics were very similar, and a representative example is shown below (Figure 6-10). One channel with the highest amplitude was used to trigger the impedance changes (channel 31 on Figure 6-10 and Figure 6-11).

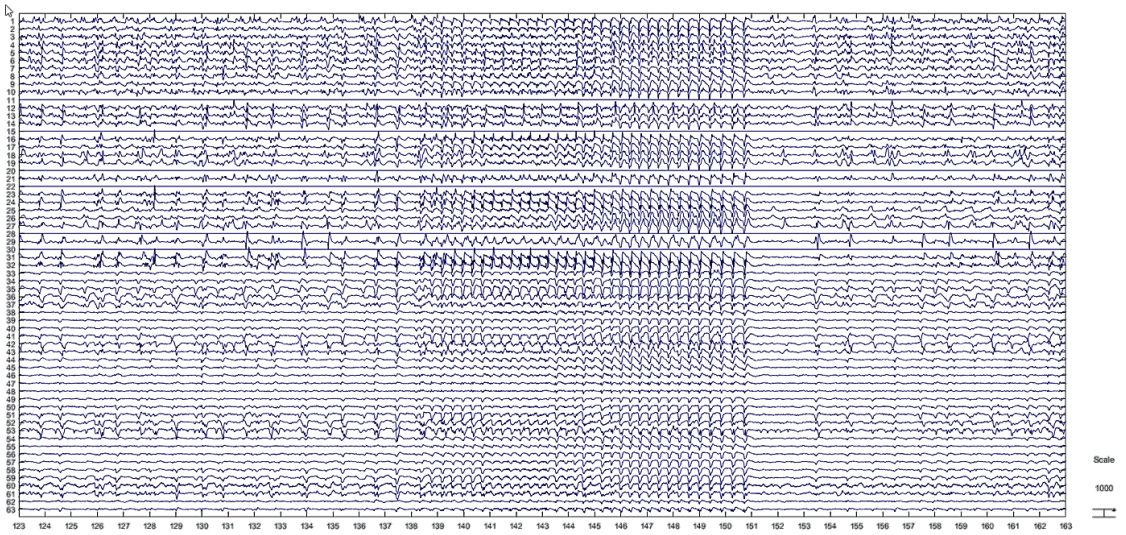

Figure 6-10. A representative example of seizure recorded from the pig over 40 seconds. Contacts 1 to 32 were epicortical and 33-63 were depth electrodes (SEEG 1 contacts 33-38 and 62, SEEG 2 contacts 39-44, SEEG 3 contacts 45-54, SEEG 4 contacts 55-61 and 63). The seizure is widespread and generalised.

6.3.1.6 Interictal and ictal activity averaged for EIT

Consistent interictal and ictal discharges occurring on a single channel were used as triggers for averaging the related impedance changes (Figure 6-11).

For patient 1, 356 regular spikes were averaged together. They occurred at contacts located posteriorly to the lesion, with approximately 17 spikes per injection pair, lasting up to 50 msec and up to 1 mV amplitude (Figure 6-11 top row).

In patient 2, the interictal activity was less sharp, when compared with other patients, as it lasted longer (up to 100 msec) and had on average lower amplitude (around 100 μV), forming sharp waves. The most frequent activity was seen on the contact in the region of precuneus, occurring at approximately 5 sharp waves per injection pair frequency, giving 115 events in total to average (Figure 6-11 second row).

In patient 3, only the spikes occurring during the three events described above were averaged together, as they presented significantly higher amplitude (up to 5 mV) and high frequency (Figure 6-11, third row) when compared with other activity seen on the same channel. 293 spikes occurred at the posterior hippocampal contact during six injection pairs, with approximately 40 spikes per an injection pair.

In the pig, there were 11 seizures recorded during 12 injection pairs. On average, there were 138 spikes per an injection pair and 1518 spikes in total (Figure 6-11 bottom row). As only interictal spikes occurred during one injection, they were not taken into the final EIT image reconstruction.

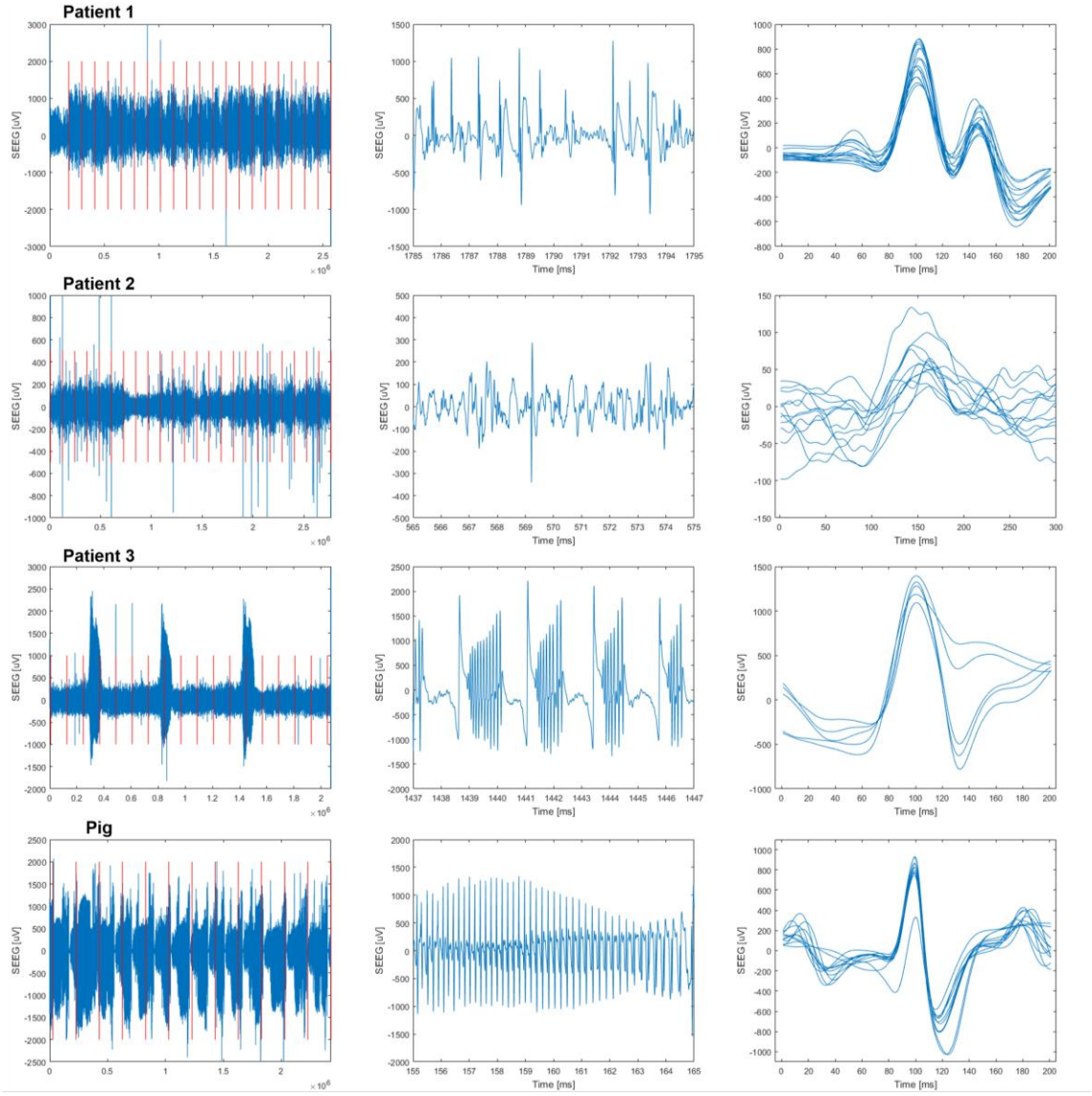

Figure 6-11 Interictal and ictal activity seen in patients 1 to 3 and in the pig. The first (left) column shows the whole channel recorded and used to trigger the impedance changes with superimposed vertical lines for EIT switches between injecting pairs. The second (middle) column presents 10 seconds of representative activity. The third (right) column illustrates an averaged spike for an EIT injection pair. Clearly, the highest variability and the lowest amplitude were seen in patient 2, suggestive of the lower expected signal generated for EIT.

6.3.2 Raw impedance signal change

6.3.2.1 Human study

Impedance changes of a maximum of -0.04%, -0.2% and -0.05% were detected in three patients respectively (Table 6-2 and Figure 6-12). However, significant impedance changes were only recorded on a minority of all channels (Table 6-2).

Patient	Epileptic activity	Averaged spikes	dZ ± SD [%]	dZ ± SD [µV]	Channels with dZ (*)
1	IIS	356	-0.04±0.05	-1.3±0.2	10
2	IIS	115	-0.2±0.4	-4.4±0.5	5
3	3 events	293	-0.05±0.02	-3.2±0.2	13

Table 6-2. Impedance changes detected due to interictal spikes (IIS) occurring in patients. In the last patient, only the spikes occurring during 3 events were averaged. (*) means number of channels with significant impedance change ($p<0.01$).

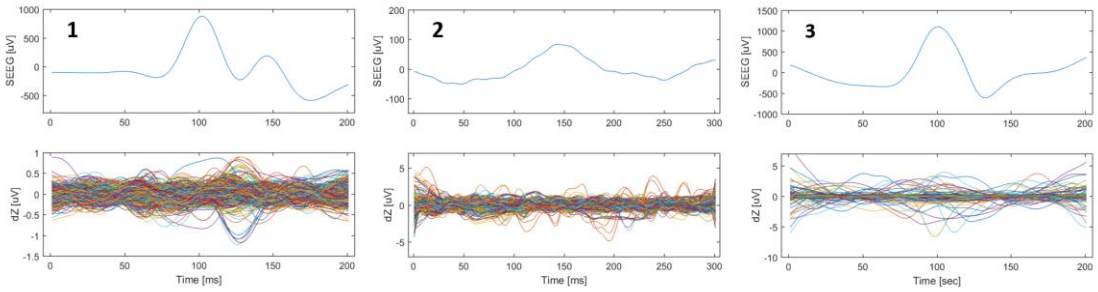

Figure 6-12. Spike (top, SEEG) and impedance response (bottom, dZ, complete imaging dataset) from the 62-channel EIT recording averaged across all interictal spikes detected in three patients respectively. An impedance change corresponding to the spike could be only seen over several channels, with the least pronounced response in both SEEG and EIT recorded in patient 2.

6.3.2.2 Animal study

A change of -4.9±0.5 μV or -0.02±0.01% was recorded after averaging 1518 ictal spikes during 11 seizures (Figure 6-13).

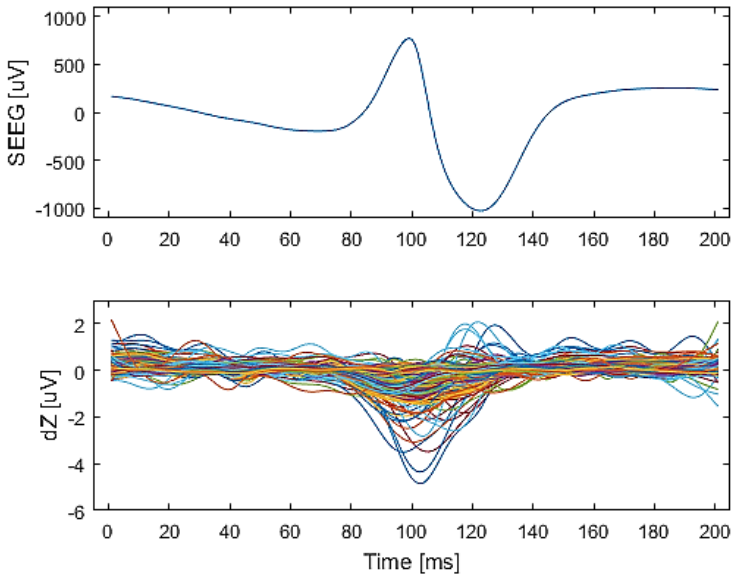

Figure 6-13. Spike (top, SEEG) and impedance response (bottom, dZ) averaged over 11 seizures recorded from an anaesthetised pig. Only significant impedance traces are plotted ($p<0.01$, $n=605$).

6.3.3 Reconstructed images

6.3.3.1 Human study

Due to the low number of the channels recording a significant impedance change, a complete imaging dataset included all avaliable dZ channels. Therefore, the images were only asssessed visually and qualitatively with respect to the SEEG findings.

The impedance change was reconstructed within the area of the cortical lesion and SEEG activity for patient 1 (Figure 6-14 and Figure 6-15). Also, the impedance change for patient 3 reconstructed within the region active on SEEG during the events (Figure 6-18 and Figure 6-19). In the data from patient 2, the reconstructed change started within the precuneus region, which was consistent with the most frequent interrictal activity recorded, however it was then seen over the midline and

frontally, which was not consistent with the interictal discharges and the location of the lesion in this patient (Figure 6-16 and Figure 6-17).

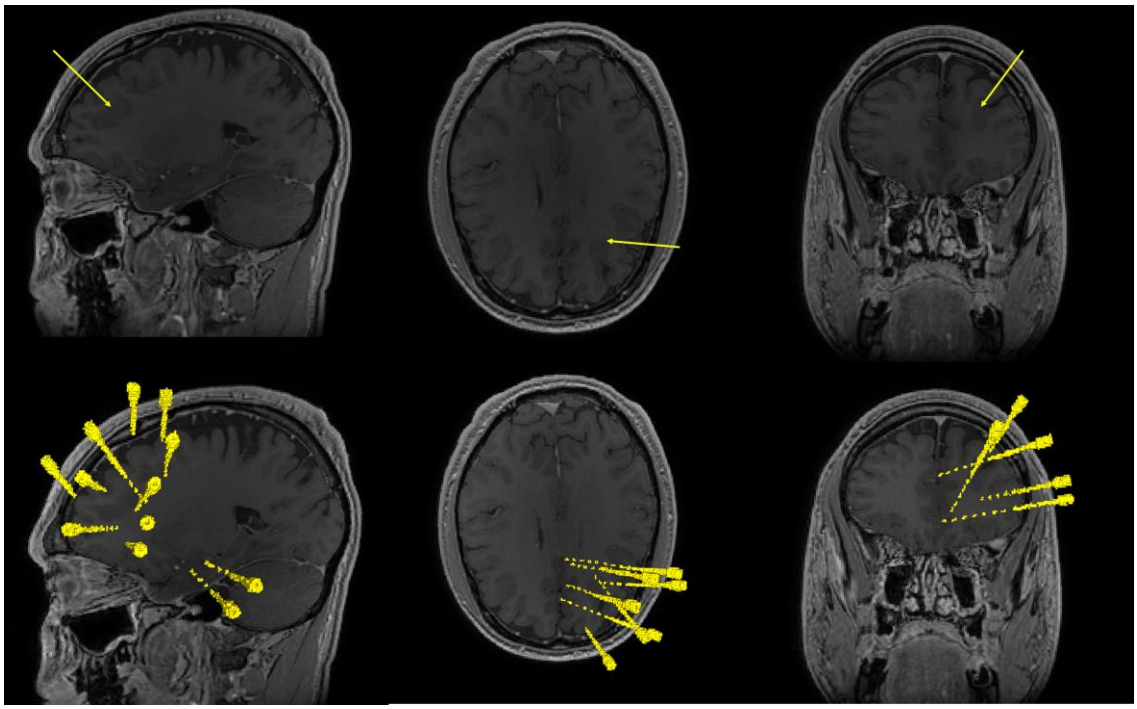

Figure 6-14. T1-MRI of patient 1. Cortical dysplasia between the middle and inferior frontal gyri (confirmed with FLAIR MRI) is indicated with arrows in the upper row. The electrode arrangement is shown in the lower row.

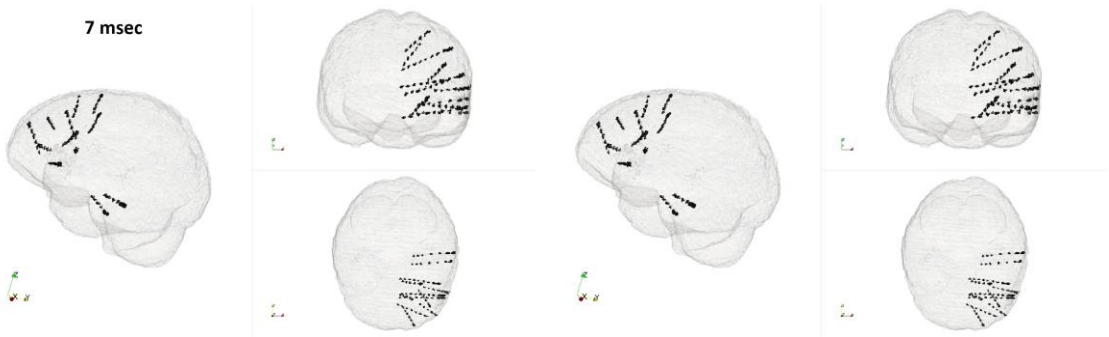

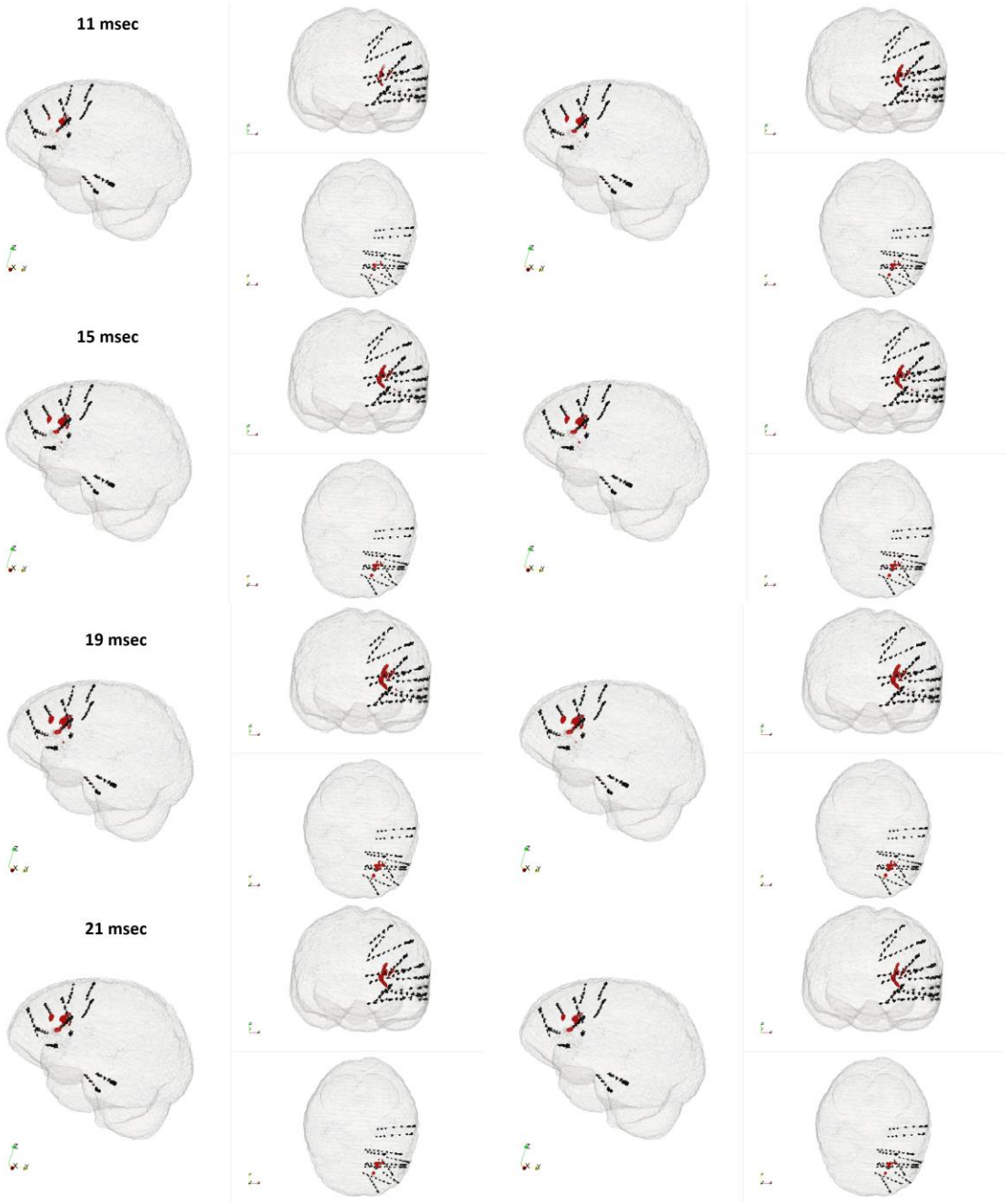
11 msec
15 msec
19 msec
21 msec

Figure 6-15. EIT image sequence of averaged interictal spikes in patient 1. For each frame, the whole brain is shown on sagittal (main), coronal (upper) and axial (lower) planes. Black dotted lines represent SEEG electrodes. The impedance change starts and spreads over the dysplastic region, when compared with the imaging findings seen on the previous figure and EEG.

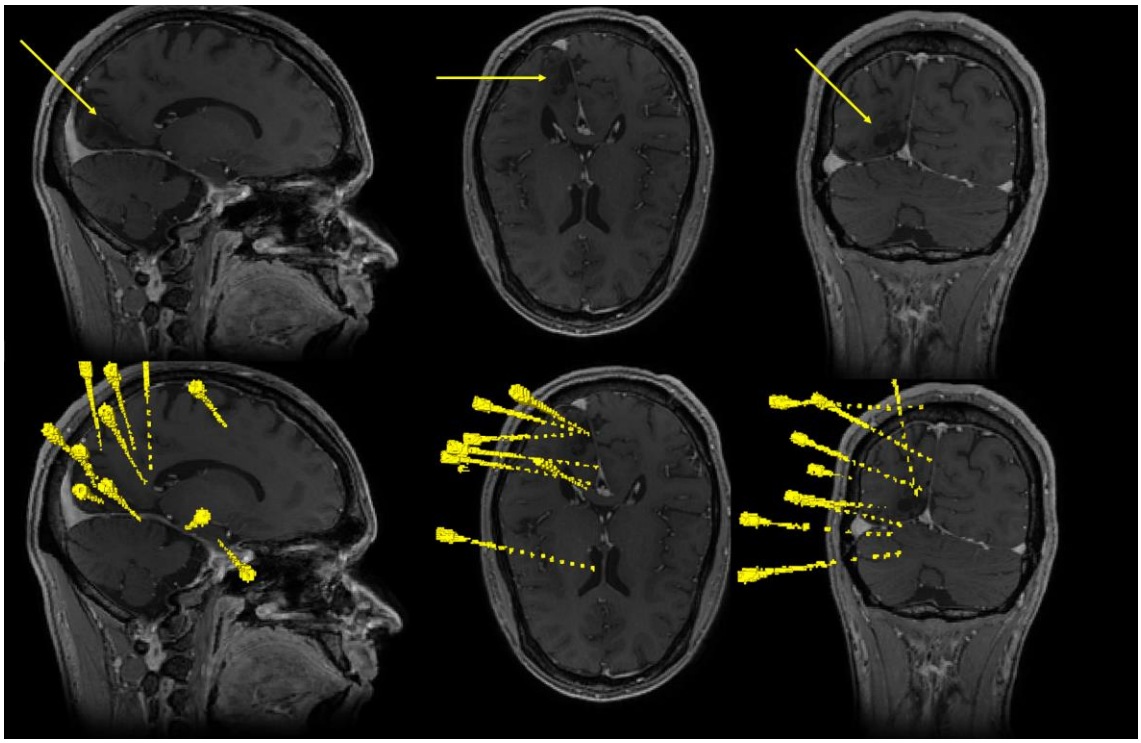

Figure 6-16. MRI of the second patient. Arrows point to cortical dysplasia in the right occipital lobe in the upper row. Depth electrodes arrangements are shown on corresponding planes in the lower row.

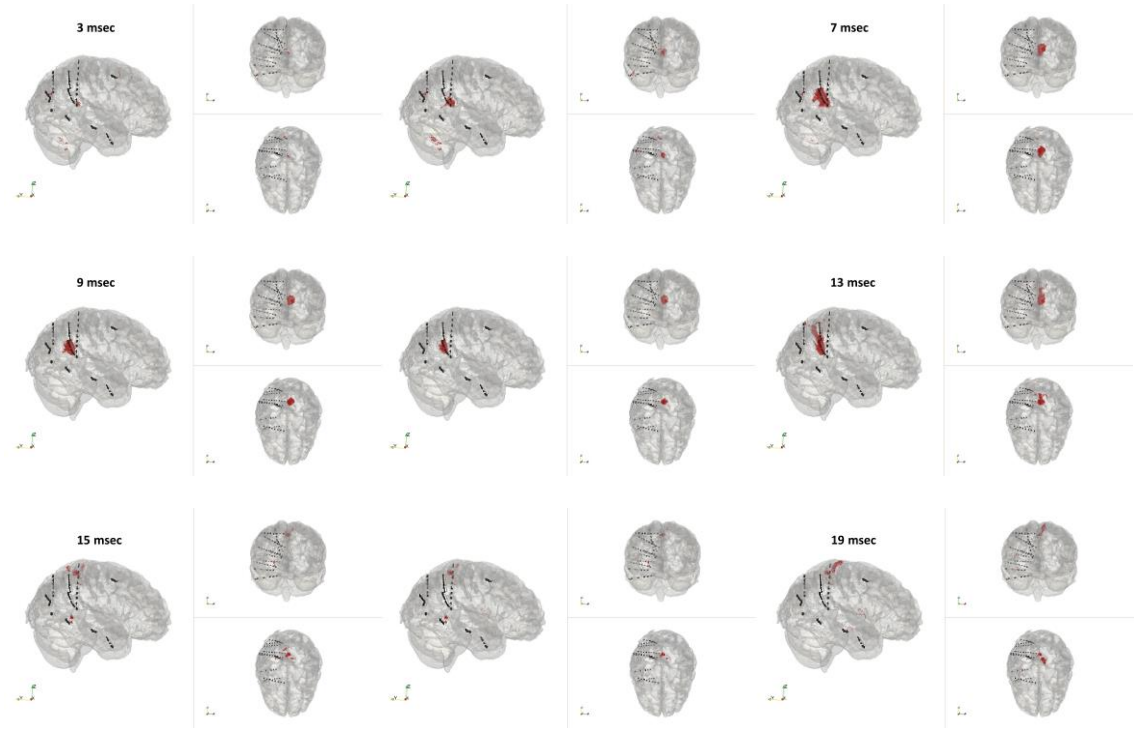

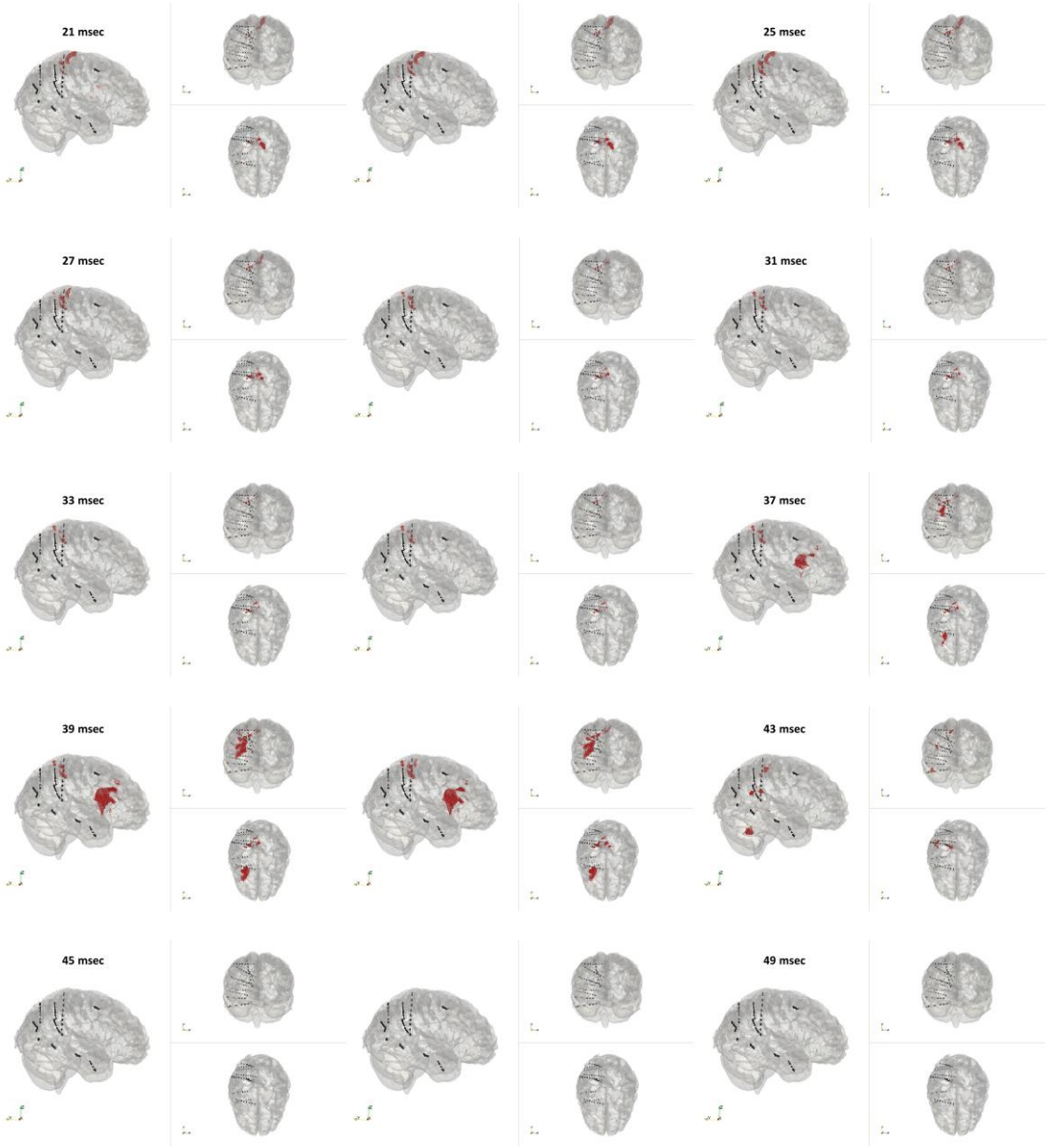

Figure 6-17. Reconstructed impedance changes in patient 2. The orientation as described above. Significant change starts posteriorly over the left hemisphere, indicating the region of the precuneus, where interictal activity was seen the most frequently. Then it spreads towards the central sulcus region of the left hemisphere, accompanied later by the large change seen within the right frontal lobe. The later changes seen over central and prefrontal regions were not consistent with the SEEG activity or with the right occipital brain lesion.

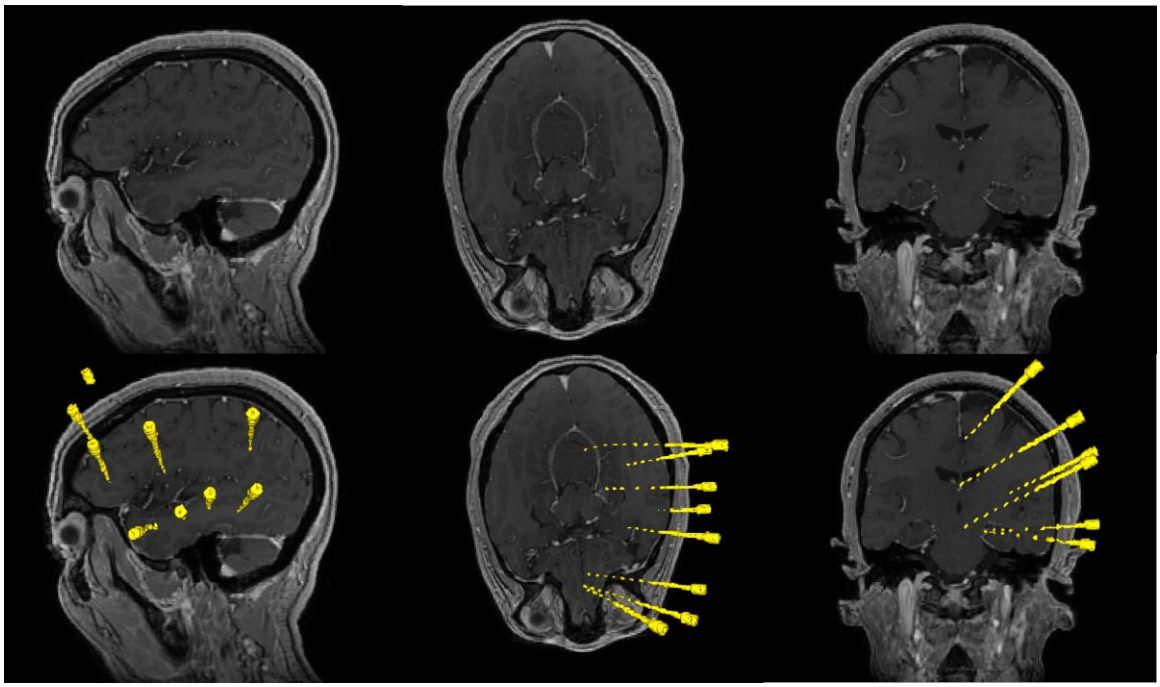

Figure 6-18. Non-lesional MRI of the third patient. The bottom row shows the arrangements of depth electrodes.

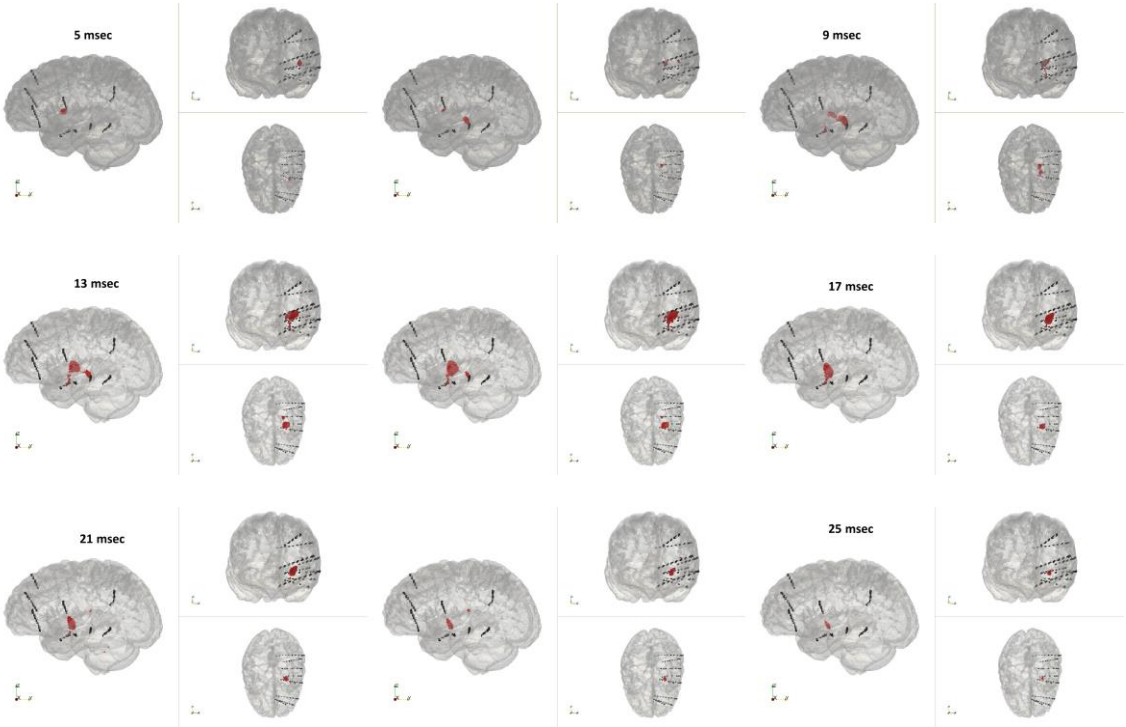

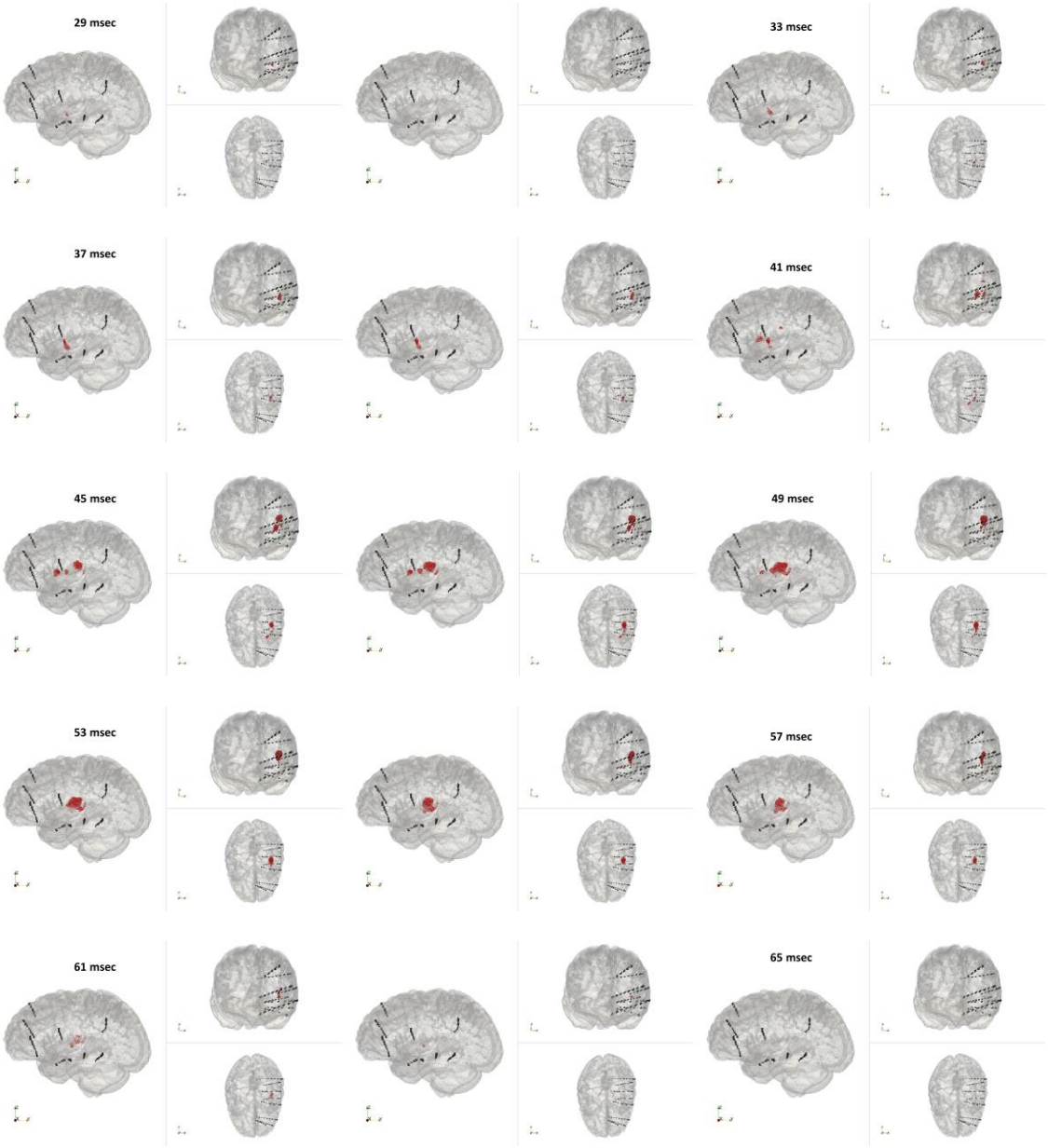

Figure 6-19. EIT reconstruction of the impedance change recorded during the events in the third patient. The orientation of the pictures as described above. The change is seen over the region of hippocampus and amygdala, which agrees with the SEEG findings.

6.3.3.2 Animal study

The significant raw impedance change was detected on 90% of the channels allowing reconstructing and following the pathway of the spike-related fast impedance

change deep in the brain. The onset of the impedance change started 3.3 mm from the BPN cannula tip 10 ms before the peak of the SEEG spike, the peak impedance change was localised 4.5 mm from the BPN cannula tip 4 ms after the peak of the SEEG spike (Figure 6-20 and Figure 6-21).

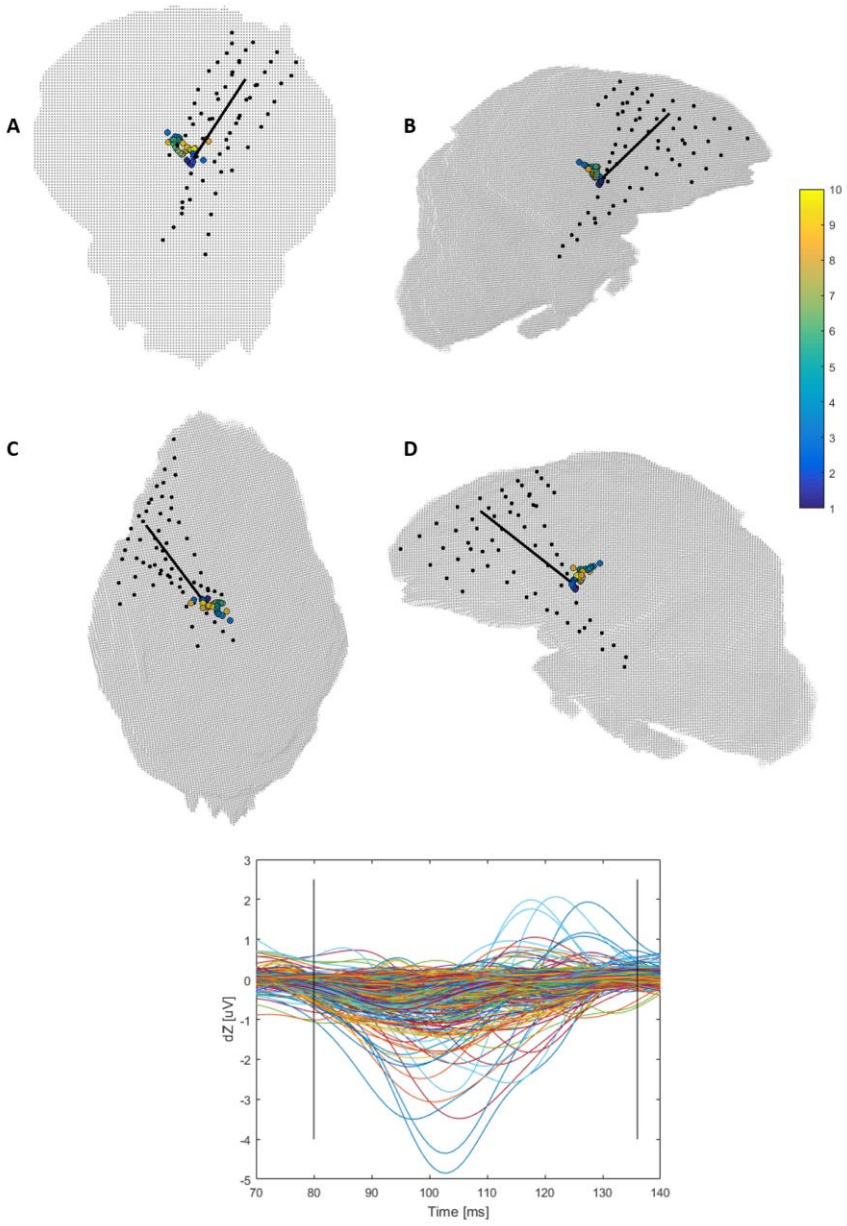

Figure 6-20. The centre of mass of the reconstructed change at every 5 msec starting from 80 msec (dark blue on the scale) to 135 msec (towards yellow on the scale) as represented by the vertical lines on the dZ graph at the bottom of the figure. The signal starts within the close proximity of the tip of the cannula (4.5 mm) and circulates towards it with the peak dZ change at 3.3 mm from the cannula tip as seen on coronal (A), axial (C) and lateral (both sides B and D) projections of the pig brain.

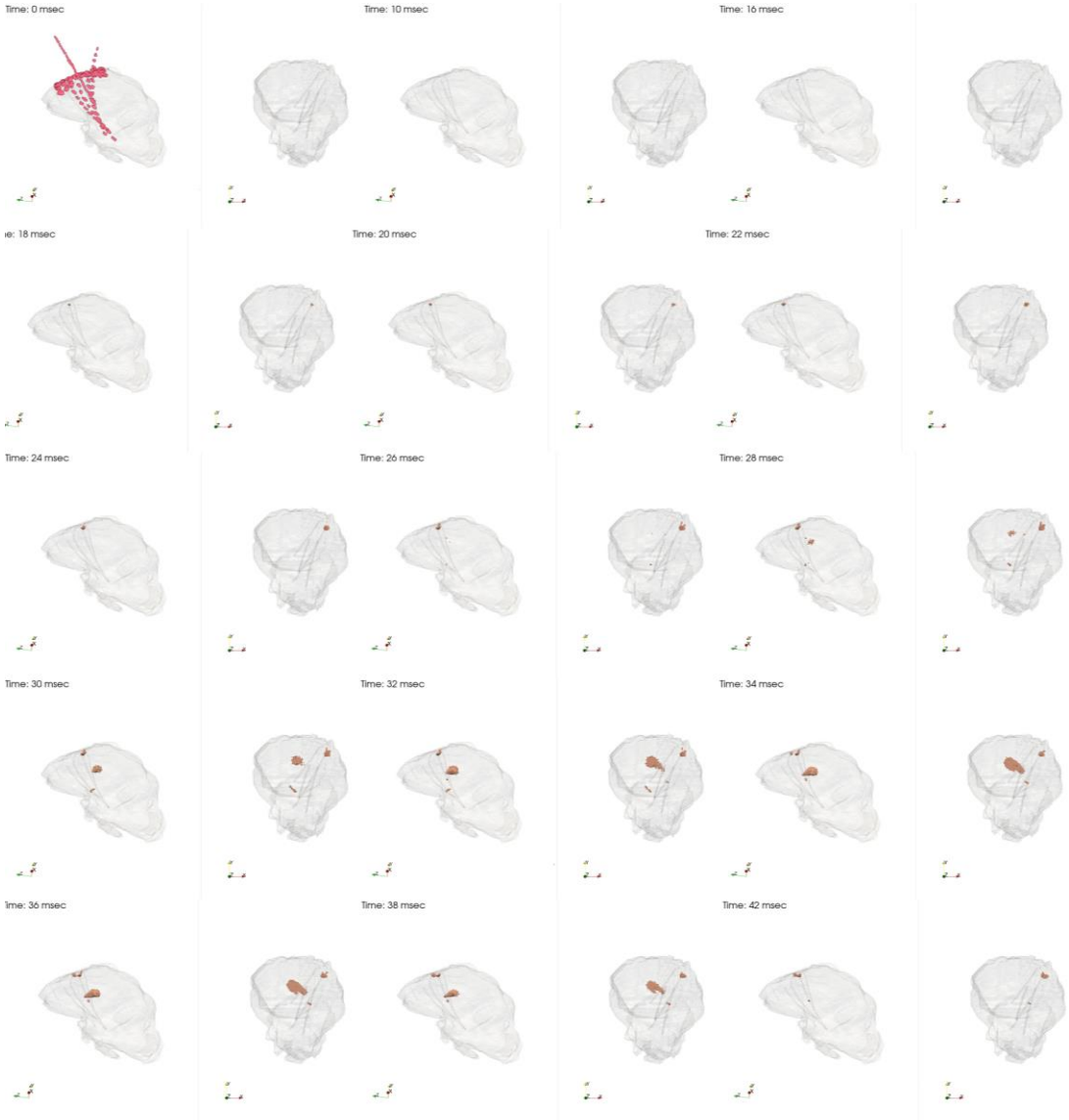

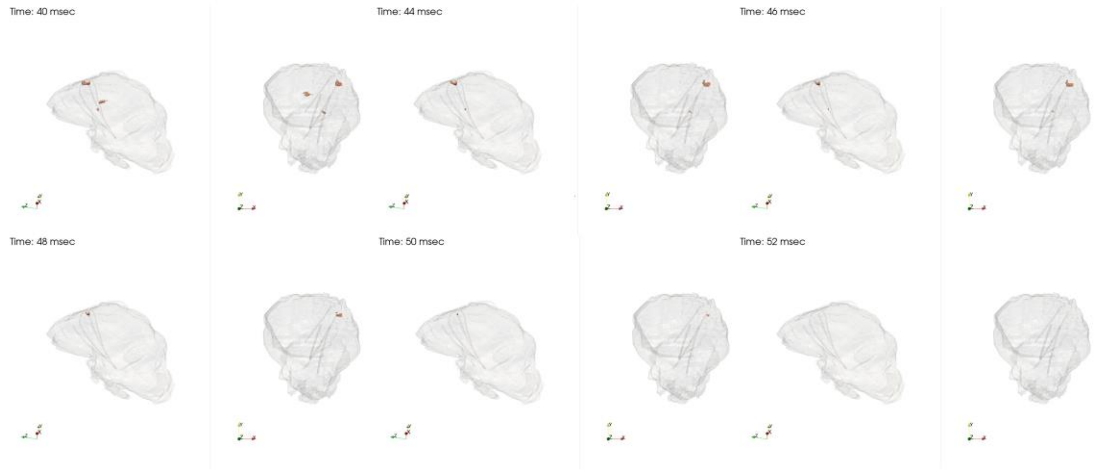

Figure 6-21. Reconstruction of impedance signal in the whole porcine brain. For each time point (specified in the left corner of each two-image panel) the brain is shown in two planes separated by a vertical line: lateral (left) and coronal (right). The first picture at 0 ms displays the positions of ECoG/SEEG electrodes and BPN cannula. The electrodes are then shadowed to simplify the view. 0 ms here corresponds to 70 ms on the graph above. Apart from the main change within the close proximity to the cannula, there is a corresponding change seen in the cortex, most likely caused by the presence of the cannula or a BPN leakage from it.

6.4 Discussion

Overall, this early work shows that it is possible to detect fast impedance changes with depth electrodes and EIT in a gyrated brain. Also, the preliminary results of analysing interictal activity from epilepsy patients suggest that such changes could be reconstructed into images. When assessed visually, in two out of three patients the change localises to the accurate areas as detected by SEEG and imaging. The initial change seen in the second patient is also consistent with the region generating the most frequent interictal activity, which later propagates anteriorly in EIT, not posteriorly where the epileptogenic in SEEG dysplasia was. However, there are several factors that might influence the results and that could potentially be the reason for unsuccessful reconstruction in this one patient. Furthermore, the preliminary recordings during seizures in one animal pointed to the change occurring within the close proximity of the tip of the cannula that injected BPN.

These results could not be compared with ECoG/SEEG, as all seizures were generalised with no onset to be detected, however, the apparent source location at the tip of the cannula seemed quite reasonable.

6.4.1 Clinical considerations

The expected amount of data collected from intracranial patients was significantly limited due to several reasons. These included time constraints imposed by the clinical team, difficulty in getting access to patients, and a very limited overall number of patients that could fit into the study profile.

The human study was drastically limited in time available to record the data. Due to the previously described MicroMed SEEG signal contamination (chapter 4), the data could only be recorded while patients were waiting for the depth electrodes removal, once all medical procedures were completed and for a very limited period lasting only until the physiologists started presurgical preparations. In addition, at that point, all patients were on 100% AEDs to prepare them for a safe discharge. Thus, the predicted likelihood of recording ictal events was very low. Also, as the procedure of the electrode removal is relatively simple, awaiting patients are usually arranged as emergency cases and as such, they might get called to the surgical theatre at any point of the day, whenever the surgeons are free. If that happens during the EIT study, while the total imaging acquisition protocol has not been yet finished, the recording needs to stop regardless, resulting in an incomplete dataset. This indeed happened during the study further limiting the amount of useful data we were able to collect.

Furthermore, as EIT recordings happened at the end of the clinical study, some patients refused to participate despite the initial interest. This was likely because patients were simply tired after a long stay at the hospital, constant video-monitoring, clinical procedures and being bed-ridden due to the length and weight of the connecting cabling. Also, they have usually participated in various research

studies throughout the stay and so appeared less keen on joining further ones later during their stay. Overall, on the last day of the telemetry, all patients were undoubtedly very keen to get disconnected from the EEG system, and to get the electrodes removed as soon as possible. In addition to the patients' personal considerations there were clinical ones too. If there had been any symptoms that could suggest a potential infection, the electrodes have been removed promptly. That was indeed a case for one patient recruited for the study and already prepared to record with EIT. All these factors made our research activity very difficult when scheduled at the end of the telemetry.

6.4.2 Technical considerations

The use of EpiNav software for electrode planning at NHNN resulted in a significant decrease in time required to prepare individual head meshes for EIT image reconstruction and, hence, speeded up the pre-imaging preparations. As described in chapter 3, the previously used method, with which the segmentation was made semi-manually from CT/T1-MRI in Seg3D software, was far from optimal. It required a lot of manual work and masks corrections, despite the high resolution and quality of the scans. With EpiNav, the parcellation is made automatically, which is a very efficient process. The created layers were very accurate and could be distinguished in detail for subcortical structures or basal ganglia, etc. This could be extremely helpful in future to create more accurate meshes, potentially improving the resolution of EIT imaging.

In the animal study, the main limitation was the number of animals available for testing. It was only possible to record one pig as a preliminary data collection case. This individual recording expressed a repetitive epileptogenic pattern occurring very often and repeating every 2 to 3 minutes on a regular basis. This allowed for not only the clinical situation to be imitated but also the seizures to be recorded in an almost 'on-demand' pattern, which is optimal for EIT recordings. Such a pattern was

however not reproduced in any other animal studied, thus limiting the number of potential subjects available for more thorough analysis.

6.4.3 Could EIT be used to detect fast impedance changes in human subjects?

Overall, it seems that it is indeed possible to detect fast impedance changes in human subjects; however, the results of this study suggest that several criteria must be met to be able to record them with EIT and reconstruct images.

First, the characteristics of the averaged spike, as seen on SEEG, are crucial. It is particularly apparent if comparing the interictal activity recorded from patient 2 with the others. In this patient, the averaged discharge has pronounced features, i.e. its shape, duration of just above 100ms, and amplitude of around 100μV, of a sharp wave, rather than a spike. Such activity, even though known to be equally representative for interictal discharges as the spike (Curtis and Avanzini 2001; Pillai and Sperling 2006), was not robust enough to generate an impedance change detectable with our current EIT setup. This impression was further supported by the findings from other EIT studies in rats performed with epicortical arrays (Vongerichten et al. 2016; Faulkner et al. 2018b; Hannan et al. 2018). In all of these experiments, the source of the signal, either physiological evoked activity or epileptic ictal/interictal discharges, was always within several millivolt magnitudes, so microvolt spikes could not generate enough SNR. Finally, the total number of interictal discharges averaged in this patient was the lowest of all three cases. Averaging is used to increase the amplitude of the recorded change so that the signal can stand out from the background neuronal activity. The SNR improves in proportion to the square root of the number of trials, hence the best way to improve collected signal is to record more repetitions. Yet, it was not possible to extend the duration of the recording in this patient due to aforementioned, clinically imposed, time limitations. This could mean the recorded dataset for this patient contains

simply too little signal rather than present an inherent problem of averaging a sharp wave in EIT, although it is impossible to conclude for certain either way.

As for patients 1 and 3, the remarkably larger spiking activity seen on SEEG could be reconstructed into the region of the cortical dysplasia and/or SEEG activity respectively. It is important to emphasize that the conductivity values for image reconstruction were unified for all tissues, without taking into account possible differences that could characterise the dysplastic regions. Hence, while reconstructing the EIT signal, there were no prior assumptions on where the epileptogenic activity could come from. This suggests that EIT is indeed capable of detecting fast impedance changes and even of reconstructing them into most likely meaningful images. Unfortunately, though these could be only assessed qualitatively, as the SNR of the interictal activity was too low to provide statistical analysis.

This study is the first time fast impedance changes arising from interictal activity have been recorded and imaged. The previous studies on rats aimed at recording interictal activity (Vongerichten et al. 2016) substantially differ from the real patient scenario, as not only they aimed to record slow impedance changes with an epicortical array, but also the seizures were generated with multiple cortical injections of chemoconvulsants into the rat brain. In our recordings, we managed to measure the real interictal activity, as it arises from the epilepsy patient's brain rather than an artificial seizure model. This might be the reason why, due to the sheer nature of the spontaneous interictal activity, the generated impedance change we measured is relatively smaller and more difficult to detect than in any model studied previously. Also, both the size and the geometry of the sampled space in the human brain with depth electrodes and the rat brain with an epicortical array differ significantly. It is likely that the change of a similar magnitude to that recorded in the rat is much more difficult to detect in a big volume of a gyrated human brain, so the fact it was possible to record visible changes in the signal can be regarded as a success.

6.4.4 Can fast impedance changes occurring due to ictal activity be detected and imaged with EIT and depth electrodes?

The preliminary results recorded from one animal, clearly showed that it was possible to detect and reconstruct fast impedance changes into the images. If similar changes were recorded in human subjects, the obtained signal was apparent but difficult to objectively assess, although it did result in a reconstruction within the same area as SEEG detected in two subjects. The main limitation of the study is that it lacked in both the time of measurements, which could increase the SNR and provide a signal that could be analysed quantitatively, and the number of individuals studied that would allow more thorough statistical analysis, and so further work is required to confirm the findings.

There are several factors of physiological and technical nature that affect spike-related impedance detection. As described above, the source of the signal and thus the physiological features of the spike itself are crucial for EIT detection. During a seizure, repeatable high-amplitude and high-frequency spikes produce enough SNR for EIT detection as seen in the animal part of this study and described before in numerous other animal studies (Faulkner et al. 2018; Hannan et al. 2018). However, the example of patient 3 demonstrated that the size of the ictal-generating region, as well as the distance between that area and injecting current electrodes, are also essential for detection. In this case, we unexpectedly managed to record series of three brief and very focal events, involving only several adjacent contacts. However, the impedance change was only seen on a few channels, and hence, the data could only be assessed qualitatively even though it produced a reconstruction that seemed to have matched the SEEG findings. The most likely reason why the recorded change was the distance between the contacts detecting the onset and channels injecting EIT current. Most of the time during these three events, the EIT injecting electrodes were approximately 40 to 50 mm away, which is obviously not optimal as the maximum current density can be only obtained within the regions

adjacent to the injecting electrodes. Given that the serial EIT system was used in order to maximise the signal within the irritative zone, the selection of contacts for the EIT protocol had to be compromised between recording enough interictal activity over a limited time available, and reasonably covering areas of the brain, from where the majority of interictal activity arises, to obtain enough data for a full imaging acquisition protocol. For these reasons, in patient 3, the injection protocol involved contacts on five relatively distant electrodes, so that the current travelled between the orbitofrontal cortex, fusiform gyrus, posterior part of cingulate, amygdala, hippocampus and insula. Unfortunately, at the time of the events, the injections were at a distant zone around the orbitofrontal/fusiform and insular regions and hence, did not reach the hippocampal contact before the brief event finished. This observation highlights the need to record patients over longer periods than those made available to us in this study. Given that even such a modest recording of epileptic activity provided a reasonable reconstruction, one can easily imagine EIT would be well capable of accurately imaging the changes arising from the epileptic activity if enough time is secured for the recordings.

In contrast, in the animal study, the BPN seizure focus was placed exactly between four SEEG electrodes used for EIT injections, so that the electrodes simply surrounded the focus zone within 20 mm around the cannula. In addition, the characteristics of the event itself were significantly different from those in the patient. In the latter, it was a brief and very localised event, extremely limited in spread over the SEEG contacts. In the pig, the seizures were widespread and generalising in SEEG in the smaller brain volume resulting in a significantly stronger signal. What is more, the seizures also repeated frequently yielding more measurements that could be averaged. All these factors made the experimental setup in the pig almost ideal and very different to the human case. It allowed us to show for the first time that recording ictal spike-related fast impedance changes can be

recorded with depth electrodes in a gyrencephalic brain and reconstructed into images.

A detailed analysis of the reconstructed images from the pig showed that the spike-related fast impedance change reconstruction is focused within the area very close to the BPN cannula. Over time, the maximal change spreads regionally and disappears (Figure 6-20). A detailed comparison of the anatomical structures as seen in the MRI atlas and the obtained CT of the pig suggested that the tip of the cannula was placed close to the thalamus. It is therefore probable that the observed impedance signal during the spike was actually the signal transmission between the thalamic nuclei. Thalamic nuclei have been reported as having an important role in primary seizure circuits but also in a spread of the seizure activity to the other brain regions (Bertram et al. 2008), as observed in the generalised seizures in our study. Further work is however required to validate this theory.

It is also interesting to compare the pathway reconstruction in the pig with the whole brain images over time (Figure 6-21). There is a clear activity seen in the cortex that preceded the deep source by several milliseconds. One of the more likely explanations could be that it represents additional cortical focus due to a small BPN leakage from the cannula, as this area is close to the cannula entry point. It is, however, also possible that it could represent the actual cortical engagement in the cortico-thalamic loop of the seizure. In order to explain the findings more accurately, further confirmation with more experiments on animals is necessary.

6.4.5 Conclusion and future work

This preliminary work shows the results of detecting and imaging fast impedance changes due to ictal or interictal activity measured with depth electrodes in large and gyrencephalic brains of humans and pigs. There are many challenges when assessing the outcome of this study; however, the initial results are encouraging for pursuing the work further. Meaningful data were recorded in both the human and

animal studies, during interictal and ictal activity respectively, and they both reconstructed into seemingly reasonable images. At the moment, the most important step would be to prove whether the detected changes are repeatable and consistent. In order to achieve that, more recordings on both animals and humans should be performed, ideally over longer periods allowing measuring ictal discharges in human subjects. As performing further studies on humans requires significant engineering work and faces many clinical obstacles, further confirmation of our findings in an extended animal study is desirable. It would be also valuable to use more accurate meshes of pigs' brains in future, allowing to differentiate between the brain tissues and potentially improving the resolution of the method.

Our findings also clearly show the difference in the strength of a signal generator, whether it is ictal or interictal. However, it is not possible to make any strong statements out of such a limited study. Ideally, a swine model of interictal discharges should be developed that would allow an accurate comparison with the human recordings. Such a model could be potentially obtained by injecting a smaller dose of BPN than that described in our studies, but it is impossible to predict, whether it could work efficiently without further tests.

Overall, this preliminary work presents encouraging results for future work. It shows a significant development of the method towards its clinical use and towards improving the diagnostic yield and providing a greater understanding of epilepsy in future.

Chapter 7

Conclusions and future work

Overview

This work extended the use of EIT to a large and gyrencephalic brain such as human or porcine. It showed that it is feasible and possible to use EIT to image epileptogenic activity with depth electrodes normally used for presurgical evaluation of focal refractory epilepsy. Despite these developments, this work is only a step forward towards the routine use of brain EIT in humans and there are many possible future developments worth further exploration.

7.1 Summary of work

The work presented in chapter 2 aimed to investigate whether the recent technical improvements could enable EIT to be used for imaging slow impedance changes occurring during visual evoked activity in healthy human volunteers using scalp electrodes, so that non-invasively only. This was largely unsuccessful, as the technical improvements were unable to help to overcome the blurring effect of the CSF, skull and scalp on impedance measurements. For these reasons, all the following studies were undertaken on intracranial recordings either in human subjects, in whom intracranial electrodes were used for presurgical evaluation in epilepsy, or in a large animal model developed specifically for the purpose of this study.

Chapter 3 summarised a computer modelling study using imaging data from three patients with intracranial electrodes implanted for presurgical evaluation of epilepsy. For simulated seizure onset perturbations EIT improved the accuracy and coverage of foci localisation compared to stereotactic electroencephalography (SEEG) detection or EEG inverse-source modelling for both fast and slow impedance changes. This suggested that EIT would be beneficial in surgical management of epilepsy by helping in localising and assessing the epileptogenic zone. However, the EIT system primarily used in our group had been known to produce switching

artefacts in EEG collected for clinical purposes, and therefore a new parallel EIT system had to be developed for use in the hospital.

In chapter 4, the developments, refinements and tests of this new portable EIT system were described. This system could be safely used on patients in a hospital environment with EIT running in parallel to video-EEG telemetry. The system was able to inject current continuously at multiple frequencies in parallel; it did not require averaging and post-hoc signal processing to remove switching artefacts, which was the case for the previous fast neural serial EIT system. The injection current protocol for intracranial recordings was optimised and the performance of the new EIT system assessed in resistor phantoms and with scalp EEG on volunteers. This showed that the EEG signal could be collected simultaneously with EIT. The new system was then employed to measure EIT in two patients with intracranial electrodes. Unfortunately, preliminary measurements showed that the clinical EEG system used in the hospital we collaborated with had hardware limitations, including its input range, so that EIT affected the EEG signal on the channels injecting current. This was overcome to some extent in recordings on the second patient using an external filter box. The filter box was not able to fix the EIT influence problem completely though and so, the clinical team at the hospital decided EIT could be only recorded on patients during the interictal activity at the end of the clinical monitoring but not during the seizures.

This decision moved the studies into two directions as described in chapters 5 and 6. First, a clinical scenario was reproduced by developing an animal model of seizures, in which slow impedance changes were measured with the newly developed parallel EIT system. However, it was not optimal to record slow impedance changes occurring due to interictal activity from patients because of the low SNR. Hence, secondly, a serial EIT system was used to record fast impedance changes related to the averaged interictal spikes on patients at the end of their clinical monitoring at the Telemetry ward.

The work presented in chapter 5 aimed at developing a method to chemically induce focal seizures in an anaesthetised pig implanted with depth electrodes (identical to those normally used in patients) and measure slow impedance changes associated with ictal activity. This showed, for the first time, that EIT is able to produce reproducible images of the onset and spread of slow impedance changes related to focal seizures in real-time and without averaging. The images correlated with the findings observed with the current gold-standard method, intracranial EEG. These results were extremely encouraging, especially in light of the difficulties in getting access to patients.

Finally, chapter 6 described a final study on imaging fast impedance changes during ictal and interictal activity in an animal and, for the first time, in patients implanted with depth electrodes. Preliminary recordings from patients and one pig showed that it was possible to record such challenging changes in the brain with only intracranial electrodes used and reconstruct them into images. Despite these encouraging results, the signal was very difficult to record, and the sample was very small, so a follow-up study with more patients and animals is desirable.

7.2 Conclusions and future work

The work presented in this thesis suggests that EIT could be safely and ethically performed in parallel to complement SEEG and image impedance changes arising during seizures with intracranial electrodes in human subjects and in large animals. It is a significant step forward towards EIT use in patients, as now a platform has been created for a further clinical trial. Our results indicate EIT use in combination with EEG on patients implanted with depth electrodes has the potential to improve the diagnostic yield in epilepsy, especially for focal epilepsy cases. However, the encouraging results from this thesis are only a small step forward, and future work should be concentrated on trying to optimise the method for forthcoming clinical studies.

The most important part of the future work would be to further improve the EIT system so that it can be used in the clinical environment. This is a complex and time-consuming part of the developments, requiring deep engineering and technical knowledge. However, if successful, EIT could be potentially used for long-term intracranial recordings on epilepsy patients for the first time. As described in chapter 4, the current EIT design still requires development in order to record the signal in parallel to clinically collected SEEG. This step involves not only overcoming the problem of EIT-related artefacts in clinical SEEG but also finding the optimal way of connecting the EIT system to a patient if the majority of SEEG contacts are shared with EIT. It is necessary that all connections between EIT and SEEG are not uncomfortable for the patient during a daily routine in the hospital, they stay in place throughout the monitoring, including the seizures, and they are simple to disconnect if required. Furthermore, once the long-term recordings take place, it will be necessary to face the issue of data storage and analysis. EIT samples the signal at 50-100 kHz, in contrast to clinical EEG, which is usually at 1-2 kHz. The intracranial EEG signal is often collected with at least 60 contacts but usually more. Hence, the amount of data collected with EIT, if recording the signal constantly for as long as EEG video telemetry, will be enormous and could be problematic to store, especially in the clinical setting, or process. Hence, finding an optimal way to collect the data in chunks and automatically store them either locally or in a data cloud for analysis seems like an essential problem to address in order to progress EIT further. Splitting the data into parts would be also helpful to decrease the calculation time for the optimal EIT image reconstruction of each seizure. Finally, for the safety reasons, the current EIT system is fully battery-powered, so that it requires daily checks and changes of the batteries for ActiCHamp, laptop and the system itself. Addressing this issue would also help to make the EIT recordings more routine.

An important follow-up question that arose after obtaining the results described in chapter 5, was whether they could be repeated in patients. We have not been able to

test this during the time course of our studies, as the bespoke parallel system we developed for the animal study was not safety tested for human use. This time-consuming procedure was beyond the scope of this thesis; however, it is certainly possible in future as further studies recording ictal-related EIT slow impedance changes on patients are necessary. The results from the animal study are encouraging but the human brain is not only larger and with intracranial electrodes usually implanted so they are spread much more inside it, but also the EIT signal would not be a result of an artificially created seizure but due to real ictal activity in the epileptic brain. It is impossible to predict how well EIT will deal with these difficulties, but the future work should first aim to improve and test the parallel EIT system so that the animal study could be repeated on epilepsy patients.

Undoubtedly, the work presented in chapter 6, i.e. recording fast impedance changes in humans due to interictal activity and in one pig due to ictal activity, has been preliminary. It was extremely difficult to get access to patients and, therefore, the samples are too small to allow one to make statistically sound general conclusions. The results of this study should be thus only considered as initial, orienting findings and future work should be concentrated on increasing the number of subjects in both groups and on testing, whether the method works on a bigger sample and, if so, what are its limitations.

It would be also interesting to find out if it is possible to reconstruct the onset for the generalised seizures in animals. The problem with this task is that none of the currently used diagnostic methods can precisely detect the onset of such seizures,, therefore, there is no objective way to quantify the reconstructed EIT changes. It should be, however, possible to study the internal consistency of the imaging findings for a given animal, assuming that all seizures start within the same area. Hence, future work could be also dedicated to analysing the generalised seizures data that are already collected from the animals, as described in chapter 5.

A visual inspection of the preliminary results from the human subjects suggests that the results of the animal study could have been potentially improved if more accurate meshes had been used. The meshes that were implemented in the study described in chapter 5 were produced from CT and therefore were uniform to have precise positions of the depth electrodes and the cannula. It is likely that the accuracy of the structures reconstructed with EIT could have been improved if more detailed meshes, which would differentiate CSF, grey and white matter, had been used. At the moment of the experiments, it was unfortunately, impossible to obtain an MRI scan of each pig but, if similar studies are to be repeated in future, this should be an important consideration in their design.

Even if EIT works only for focal seizures, the results for slow changes in animals, as well as the preliminary findings for the fast impedance changes are very promising. If confirmed in future studies outlined above, they can open opportunities for using EIT as a tool complementary to those already used in clinics. For example, EIT could be used to try to minimise the number of depth electrodes implanted, as well as to better understand epilepsy and seizures by providing real imaging data. At present, a typical patient undergoing depth electrodes implantation has at least 8 but often 12-13 probes implanted. They are used not only for the onset localisation but also for mapping the adjacent cortex and, hence, allow predicting the potential consequences of the resective surgery. However, if EIT was able to help in localising the epileptogenic activity, it could potentially be used to obtain a better seizure control in different ways alternative to the open brain surgery. Such methods could include, for example, deep brain or vagus nerve stimulations. Future work is however required to explore these opportunities further.

Finally, but also interestingly, would be to investigate, whether EIT could be ever used as a non-invasive method to image the brain. As showed in chapter 2, currently the SNR is not large enough to obtain reliable images of physiological activity. However, it is, in theory, possible that EIT could be paired with other imaging

techniques to obtain better SNR. One possibility would be to couple EIT with MRI, MEG or wearable OPM, as the skull does not significantly affect a magnetic field. However, a lot of future work will be necessary to explore these topics in any depth.

In conclusion, the work described in this thesis suggests that EIT has the potential to image epileptogenic activity in a gyrated brain if used with depth electrodes. The signal can be collected in parallel with SEEG and recorded seizures could be reconstructed into images. Future work is required to confirm the initial findings and proceed with a clinical study on human subjects.

Bibliography

Adey, W. R., Kado, R. T., & Didio, J. (1962). Impedance measurements in brain tissue of animals using microvolt signals. *Experimental Neurology*, *5*(1), 47–66. https://doi.org/10.1016/0014-4886(62)90069-9

Akdogan, I., Adiguzel, E., Yilmaz, I., Ozdemir, M. B., Sahiner, M., & Tufan, A. C. (2008). Penicillin-induced epilepsy model in rats: Dose-dependant effect on hippocampal volume and neuron number. *Brain Research Bulletin*, *77*(4), 172–177. https://doi.org/10.1016/j.brainresbull.2008.08.001

Alarcon, G. (1996). Electrophysiological aspects of interictal and ictal activity in human partial epilepsy. *Seizure*, *5*(1), 7–33. https://doi.org/10.1016/S1059-1311(96)80014-8

Alarcon, G., Guy, C., Binnie, C. D., Walker, S. R., Elwes, R. D. C., & Polkey, C. E. (1994). Intracerebral propagation of interictal activity in partial epilepsy: Implications for source localisation. *Journal of Neurology, Neurosurgery and Psychiatry*, *57*(4), 435–449. https://doi.org/10.1136/jnnp.57.4.435

American Clinical Neurophysiology Society. (2006). *Recommended standards for visual system evoked potentials*. *Journal of Clinical Neurophysiology* (Vol. 23). https://doi.org/10.1097/00004691-198610001-00014

Aristovich, K. Y., dos Santos, G. S., Packham, B. C., & Holder, D. S. (2014). A method for reconstructing tomographic images of evoked neural activity with electrical impedance tomography using intracranial planar arrays. *Physiological Measurement*, *35*(6), 1095–1109. https://doi.org/10.1088/0967-3334/35/6/1095

Aristovich, K. Y., Packham, B. C., Koo, H., Santos, G. S. dos, McEvoy, A., & Holder, D. S. (2016). Imaging fast electrical activity in the brain with electrical impedance tomography. *NeuroImage*, *124*, 204–213. https://doi.org/10.1016/j.neuroimage.2015.08.071

Avery, J., Dowrick, T., Faulkner, M., Goren, N., & Holder, D. (2017). A versatile and reproducible multi-frequency electrical impedance tomography system. *Sensors*, *17*(2). https://doi.org/10.3390/s17020280

Avery, J., Dowrick, T., Witkowska-Wrobel, A., Faulkner, M., Aristovich, K., & Holder, D. (2019). Simultaneous EIT and EEG using frequency division multiplexing. *Physiological Measurement*, *40*(3), 034007. https://doi.org/10.1088/1361-6579/ab0bbc

Bagshaw, A. P., Liston, A. D., Bayford, R. H., Tizzard, A., Gibson, A. P., Tidswell, A. T., … Holder, D. S. (2003). Electrical impedance tomography of human brain function using reconstruction algorithms based on the finite element method. *NeuroImage*, *20*(2), 752–764. https://doi.org/10.1016/S1053-8119(03)00301-X

Beghi, E., Giussani, G., Abd-Allah, F., Abdela, J., Abdelalim, A., Abraha, H. N., … Murray, C. J. L. (2019). Global, regional, and national burden of epilepsy, 1990–2016: a systematic analysis for the Global Burden of Disease Study 2016. *The Lancet Neurology*, *18*(4), 357–375. https://doi.org/10.1016/S1474-4422(18)30454-X

Bell, G. S., De Tisi, J., Gonzalez-Fraile, J. C., Peacock, J. L., McEvoy, A. W., Harkness, W. F. J., … Duncan, J. S. (2017). Factors affecting seizure outcome after epilepsy surgery: An observational series. *Journal of Neurology, Neurosurgery and Psychiatry*, *88*(11), 933–940.

https://doi.org/10.1136/jnnp-2017-316211

Bell, G. S., Neligan, A., & Sander, J. W. (2014). An unknown quantity - The worldwide prevalence of epilepsy. *Epilepsia*, *55*(7), 958–962. https://doi.org/10.1111/epi.12605

Belliveau, Kennedy, McKinstry, Buchbinder, Weisskoff, Cohen, … Rosen. (1991). Functional Mapping of the Human Visual Cortex by Magnetic Resonance Imaging. *Science (New York, N.Y.)*, *254*, 716–719.

Benbadis, S. R., & Lin, K. (2008). Errors in EEG interpretation and misdiagnosis of epilepsy. Which EEG patterns are overread? *Eur Neurol*, *59*(5), 267–271. https://doi.org/10.1159/000115641

Benbadis, S., Wyllie, E., & Bingaman, W. (2005). Intracranial Electroencephalography and Localization Studies (pp. 1059–1068).

Bertram, E. H., Zhang, D. X., & Williamson, J. M. (2008). Multiple roles of midline dorsal thalamic nuclei in induction and spread of limbic seizures. *Epilepsia*, *49*(2), 256–268. https://doi.org/10.1111/j.1528-1167.2007.01408.x

Blumenfeld, H. (2005). Cellular and network mechanisms of spike-wave seizures. Epilepsia, 46 (Suppl. 9), 21-33. https://doi.org/10.1017/S1472928807000209

Boto, E., Holmes, N., Leggett, J., Roberts, G., Shah, V., Meyer, S. S., … Brookes, M. J. (2018). Moving magnetoencephalography towards real-world applications with a wearable system. *Nature*, *555*(7698), 657–661. https://doi.org/10.1038/nature26147

Burle, B., Spieser, L., Roger, C., Casini, L., Hasbroucq, T., & Vidal, F. (2015). Spatial and temporal resolutions of EEG: Is it really black and white? A scalp current density view. *International Journal of Psychophysiology*, *97*(3), 210–220. https://doi.org/10.1016/j.ijpsycho.2015.05.004

Brigell, M., Bach, M., Barber, C., Kawasaki, K., & Kooijman, A. (1998). Guidelines for calibration of stimulus and recording parameters used in clinical electrophysiology of vision. *Documenta Ophthalmologica*, *95*(1), 1–14. https://doi.org/10.1023/A:1001724411607

Buckmaster, P. S. (2004). Laboratory animal models of temporal lobe epilepsy. *Comp Med.*, *54*(5), 473–485.

Cendes, F., Theodore, W. H., Brinkmann, B. H., Sulc, V., & Cascino, G. D. (2016). *Neuroimaging of epilepsy*. *Handbook of Clinical Neurology* (Vol. 136). https://doi.org/10.1016/B978-0-444-53486-6.00051-X

Coan, A. C., Campos, B. M., Yasuda, C. L., Kubota, B. Y., Bergo, F. P. G., Guerreiro, C. A. M., & Cendes, F. (2014). Frequent seizures are associated with a network of gray matter atrophy in temporal lobe epilepsy with or without hippocampal sclerosis. *PLoS ONE*, *9*(1). https://doi.org/10.1371/journal.pone.0085843

Cohen, D., Cuffin, B. N., Yunokuchi, K., Maniewski, R., Purcell, C., Cosgrove, G. R., … Schomer, D. L. (1990). MEG versus EEG localization test using implanted sources in the human brain. *Annals of Neurology*, *28*(6), 811–817. https://doi.org/10.1002/ana.410280613

Concha, L., Beaulieu, C., Collins, D. L., & Gross, D. W. (2009). White-matter diffusion abnormalities in temporal-lobe epilepsy with and without mesial temporal sclerosis. *J Neurol Neurosurg Psychiatry*, *80*(3), 312–319. https://doi.org/10.1136/jnnp.2007.139287

Constant, I., Seeman, R., & Murat, I. (2005). Sevoflurane and epileptiform EEG changes. *Paediatric Anaesthesia*, *15*(4), 266–274. https://doi.org/10.1111/j.1460-9592.2004.01538.x

Cooper, R., Winter, A. ., Crow, H. ., & Walter, W. G. (1965). Comparison of subcortical, cortical and scalp activity using chronically indwelling electrodes in man. *Electroencephalography and Clinical Neurophysiology*, *18*(3), 217–228. https://doi.org/10.1016/0013-4694(65)90088-X

Craner, S. L., & Ray, R. H. (1991). Somatosensory cortex of the neonatal pig: I. Topographic organization of the primary somatosensory cortex (SI). *Journal of Comparative Neurology*, *306*(1), 24–38. https://doi.org/10.1002/cne.903060103

Cuffin, B. N., Cohen, D., Yunokuchi, K., Maniewski, R., Purcell, C., Cosgrove, G. R., … Kennedy, J. (1991). Tests of EEG Locahzation Accuracy Using Implanted Sources in the Human Brain. *Annals of Neurology*.

Curtis, M. , & Avanzini, G. (2001). Interictal spikes in focal epileptogenesis, *63*, 541–567.

Curtis, M., & Avoli, M. (2008). Initiation, Propagation and Termination of Partial (Focal) Seizures. *Disabil Rehabil.*, *49*(2), 743–750. https://doi.org/10.1167/iovs.07-1072.Complement-Associated

De Tisi, J., Bell, G. S., Peacock, J. L., McEvoy, A. W., Harkness, W. F., Sander, J. W., & Duncan, J. S. (2011). The long-term outcome of adult epilepsy surgery, patterns of seizure remission, and relapse: A cohort study. *The Lancet*, *378*(9800), 1388–1395. https://doi.org/10.1016/S0140-6736(11)60890-8

Diehl, B., & Lüders, H. O. (2000). Temporal lobe epilepsy: when are invasive recordings needed? *Epilepsia*, *41 Suppl 3*(5), S61–S74.

Diehl, B., Sisodiya, S., & Manford, M. (2015). Frontal lobe epilepsy. In *ILAE Teaching Weekend Lectures. The Fifteenth Teaching Weekend on Epilepsy* (p. Chapter 14). https://doi.org/10.1159/000127778

Dowrick, T., & Holder, D. (2018). Phase division multiplexed EIT for enhanced temporal resolution. *Physiological Measurement*, *39*(3), 034005. https://doi.org/10.1088/1361-6579/aaad59

Dowrick, T, Blochet, C., & Holder, D. (2015). *In vivo* bioimpedance measurement of healthy and ischaemic rat brain: implications for stroke imaging using electrical impedance tomography. *Physiological Measurement*, *36*(6), 1273–1282. https://doi.org/10.1088/0967-3334/36/6/1273

Dowrick, T., Sato Dos Santos, G., Vongerichten, A., & Holder, D. (2015). Parallel, multi frequency EIT measurement, suitable for recording impedance changes during epilepsy. *Journal of Electrical Bioimpedance*, *6*(1), 37–43. https://doi.org/10.5617/jeb.2573

Dowrick, Thomas, Blochet, C., Chaulet, N., & Holder, D. (2014). A Custom EIT System Based On Off-The-Shelf Equipment. In *15th International Conference on Biomedical Applications of Electrical Impedanec Tomography* (p. 17).

Duncan, J. S. (2011). Selecting patients for epilepsy surgery: Synthesis of data. *Epilepsy and Behavior*, *20*(2), 230–232. https://doi.org/10.1016/j.yebeh.2010.06.040

Duncan, J. S., Sander, J. W., Sisodiya, S. M., & Walker, M. C. (2006). Adult epilepsy. *Lancet*, *367*(9516), 1087–1100. https://doi.org/10.1016/S0140-6736(06)68477-8

Duncan, J. (2017). Occipital and parietal lobe epilepsies. *Epilepsy 2017: From Benchside to Bedside. A Practical Guide to Epilepsy. Lecture Notes from the Sixteenth Epilepsy Teaching Weekend*, 189–192.

Ebersole, J. S. (1991). EEG dipole modeling in complex partial epilepsy. *Brain Topography*, *4*(2), 113–123. https://doi.org/10.1007/BF01132768

Elger, C. E., & Schmidt, D. (2008). Modern management of epilepsy: A practical approach. *Epilepsy and Behavior*, *12*(4), 501–539. https://doi.org/10.1016/j.yebeh.2008.01.003

Engel Jr, J. (1996). Surgery for seizures. *New England Journal of Medicine*, *334*(10), 647–652.

Fabrizi, L., McEwan, A., Oh, T., Woo, E. J., & Holder, D. S. (2009). A comparison of two EIT systems suitable for imaging impedance changes in epilepsy. *Physiological Measurement*, *30*(6), S103–S120. https://doi.org/10.1088/0967-3334/30/6/S07

Fabrizi, L., Sparkes, M., Horesh, L., Perez-Juste Abascal, J. F., McEwan, a, Bayford, R. H., … Holder, D. S. (2006). Factors limiting the application of electrical impedance tomography for identification of regional conductivity changes using scalp electrodes during epileptic seizures in humans. *Physiological Measurement*, *27*(5), S163–S174. https://doi.org/10.1088/0967-3334/27/5/S14

Fabrizi, L., Yerworth, R., McEwan, A., Gilad, O., Bayford, R., & Holder, D. S. (2010). A method for removing artefacts from continuous EEG recordings during functional electrical impedance tomography for the detection of epileptic seizures. *Physiological Measurement*, *31*(8). https://doi.org/10.1088/0967-3334/31/8/S05

Faulkner, M., Jehl, M., Aristovich, K., Avery, J., Witkowska-Wrobel, A., & Holder, D. (2017). Optimisation of current injection protocol based on a region of interest. *Physiological Measurement*, *38*(6), 1158–1175. https://doi.org/10.1088/1361-6579/aa69d7

Faulkner, M., Hannan, S., Aristovich, K., Avery, J., & Holder, D. (2018). Characterising the frequency response of impedance changes during evoked physiological activity in the rat brain. *Physiological Measurement*, *39*(3), 034007. https://doi.org/10.1088/1361-6579/aab01f

Faulkner, M., Hannan, S., Aristovich, K., Avery, J., & Holder, D. (2018). Feasibility of imaging evoked activity throughout the rat brain using electrical impedance tomography. *NeuroImage*, *178*(April), 1–10. https://doi.org/10.1016/j.neuroimage.2018.05.022

Federico, P., Archer, J. S., Abbott, D. F., & Jackson, G. D. (2010). Cortical / subcortical BOLD changes An EEG-fMRI study at 3 T. https://doi.org/10.1212/01.WNL.0000156358.72670.AD

Felix, Leger, Albe-Fessard, Marcilloux, Rampin, Laplace, … Duclos. (1997). Stereotaxic Atlas of the Pig Brain. *Brain Research Bulletin*, *49*, 1–138. https://doi.org/10.1017/S0022215100111879

Fisher, R. S. (1989). Animal models of the epilepsies. *Brain Research Reviews*, *14*(3), 245–278. https://doi.org/10.1016/0165-0173(89)90003-9

Fisher, R. S. (2015). Redefining epilepsy. *Current Opinion in Neurology*, *28*(2), 130–135.

https://doi.org/10.1097/WCO.0000000000000174

Fisher, R. S., Cross, J. H., D'Souza, C., French, J. A., Haut, S. R., Higurashi, N., … Zuberi, S. M. (2017). Instruction manual for the ILAE 2017 operational classification of seizure types. *Epilepsia*, 1–12. https://doi.org/10.1111/epi.13671

Fox, P. T., Mintun, M. a, Raichle, M. E., Miezin, F. M., Allman, J. M., & Van Essen, D. C. (1986). Mapping human visual cortex with positron emission tomography. *Nature*, *323*(6091), 806–809. https://doi.org/10.1038/323806a0

Gaitatzis, A., Carroll, K., Majeed, A., & Sander, J. W. (2004). The epidemiology of the comorbidity of epilepsy in the general population. *Epilepsia*, *45*(12), 1613–1622. https://doi.org/10.1111/j.0013-9580.2004.17504.x

Gilad, O., & Holder, D. S. (2009). Impedance changes recorded with scalp electrodes during visual evoked responses: Implications for Electrical Impedance Tomography of fast neural activity. *NeuroImage*, *47*(2), 514–522. https://doi.org/10.1016/j.neuroimage.2009.04.085

Goren, N., Avery, J., Dowrick, T., Mackle, E., Witkowska-Wrobel, A., Werring, D., & Holder, D. (2018). Data Descriptor: Multi-frequency electrical impedance tomography and neuroimaging data in stroke patients. *Scientific Data*, *5*, 1–10. https://doi.org/10.1038/sdata.2018.112

Goren, N., Avery, J., & Holder, D. S. (2013). intracranial bleeding monitoring Excerpted from : of the 15th International Conference on Biomedical Applications of ELECTRICAL IMPEDANCE, 3–5.

Goren, N., Avery, J., Dowrick, T., Mackle, E., Witkowska-Wrobel, A., Werring, D., & Holder, D. (2018). Data Descriptor: Multi-frequency electrical impedance tomography and neuroimaging data in stroke patients. *Scientific Data*, *5*, 1–10. https://doi.org/10.1038/sdata.2018.112

Goo, E. K., Lee, J. S., & Koh, J. C. (2017). The optimal exhaled concentration of sevoflurane for intubation without neuromuscular blockade using clinical bolus doses of remifentanil: A randomized controlled trial. *Medicine (United States)*, *96*(9), 1–5. https://doi.org/10.1097/MD.0000000000006235

Grech, R., Cassar, T., Muscat, J., Camilleri, K., Fabri, S., Zervakis, M., … Vanrumste, B. (2008). Review on solving the inverse problem in EEG source analysis. *Journal of NeuroEngineering and Rehabilitation*, *5*(1), 25. https://doi.org/10.1186/1743-0003-5-25

Guerrini, R. (2006). Seminar Epilepsy in children. *Www.Thelancet.Com*, *367*, 499. Retrieved from www.thelancet.com

Hannan, S., Faulkner, M., Aristovich, K., Avery, J., & Holder, D. (2018). Frequency-dependent characterisation of impedance changes during epileptiform activity in a rat model of epilepsy. *Physiological Measurement*, *39*(8). https://doi.org/10.1088/1361-6579/aad5f4

Hannan, S., Faulkner, M., Aristovich, K., Avery, J., Walker, M., & Holder, D. (2018). Imaging fast electrical activity in the brain during ictal epileptiform discharges with electrical impedance tomography. *NeuroImage: Clinical*, *20*(July), 674–684. https://doi.org/10.1016/j.nicl.2018.09.004

Harreveld, a Van, & Schade, J. (1962). Changes in the electrical conductivity of cerebral cortex

during seizure activity. *Experimental Neurology*, *400*, 383–400. Retrieved from http://www.sciencedirect.com/science/article/pii/0014488662900511

Hashimoto, T., Kashii, S., Kikuchi, M., Honda, Y., Nagamine, T., & Shibasaki, H. (1999). Temporal profile of visual evoked responses to pattern-reversal stimulation analyzed with a whole-head magnetometer. *Experimental Brain Research*, *125*(3), 375–382. https://doi.org/10.1007/s002210050693

Holder. (2005). *Electrical Impedance Tomography*. *Series in Medical Physics and Biomedical Engineering*.

Holder, D. S., Rao, a, & Hanquan, Y. (1996). Imaging of physiologically evoked responses by electrical impedance tomography with cortical electrodes in the anaesthetized rabbit. *Physiological Measurement*, *17 Suppl 4*, A179–A186. https://doi.org/10.1088/0967-3334/17/4A/022

Holder, David. (1992). Electrical impedance tomography of brain function. *Brain Topography*, *5*(2), 127–166. https://doi.org/10.3389/conf.fnins.2010.05.00003

Horak, P., Meisenhelter, S., Song, Y., Testorf, M., Kahana, M., Viles, W., … Jobst, B. (2017). Interictal epileptiform discharges impair word recall in multiple brain areas. *Epilepsia*, *58*(3), 373–380. https://doi.org/10.1002/cncr.27633.Percutaneous

Horesh, L., Schweiger, M., Bollhöfer, M., Holder, D. S., & Arridge, S. R. (2006). Multilevel preconditioning for 3D large-scale soft-field medical applications modelling. *International Journal of Information and Systems Sciences*, *2*(4), 532–556.

Horesh, L. (2006). *Some novel approaches large scale algorithms for multi-frequency electrical impedance tomography of the human head Some Novel Approaches in Modelling and Image Reconstruction for Multi-Frequency Electrical Impedance Tomography of the Human Brain Lior Hore*. PhD thesis.

IEC 60601. (2012). *International standard*.

Iijima, T., Nakamura, Z., Iwao, Y., & Sankawa, H. (2000). The epileptogenic properties of the volatile anesthetics sevoflurane and isoflurane in patients with epilepsy. *Anesthesia and Analgesia*, *91*(4), 989–995. https://doi.org/10.1097/00000539-200010000-00041

Ito, H., Takahashi, K., Hatazawa, J., Kim, S.-G., & Kanno, I. (2001). Changes in human regional cerebral blood flow and cerebral blood volume during visual stimulation measured by positron emission tomography. *Journal of Cerebral Blood Flow & Metabolism*, *21*(5), 608–612. https://doi.org/10.1097/00004647-200105000-00015

Jääskeläinen, S. K., Kaisti, K., Suni, L., Hinkka, S., & Scheinin, H. (2003). Sevoflurane is epileptogenic in healthy subjects at surgical levels of anesthesia. *Neurology*, *61*(8), 1073–1078. https://doi.org/10.1212/01.WNL.0000090565.15739.8D

Jackson, G. D., & Badawy, R. a B. (2011). Selecting patients for epilepsy surgery: Identifying a structural lesion. *Epilepsy and Behavior*, *20*(2), 182–189. https://doi.org/10.1016/j.yebeh.2010.09.019

Jehi, L. E., O'Dwyer, R., Najm, I., Alexopoulos, A., & Bingaman, W. (2009). A longitudinal study of surgical outcome and its determinants following posterior cortex epilepsy surgery. *Epilepsia*, *50*(9), 2040–2052. https://doi.org/10.1111/j.1528-1167.2009.02070.x

Jehl, M., Aristovich, K., Faulkner, M., & Holder, D. (2016). Are patient specific meshes required for EIT head imaging? *Physiological Measurement*, *37*(6), 879–892. https://doi.org/10.1088/0967-3334/37/6/879

Jehl, M., Dedner, A., Betcke, T., Aristovich, K., Klofkorn, R., & Holder, D. (2014). A Fast Parallel Solver for the Forward Problem in Electrical Impedance Tomography. *IEEE Transactions on Bio-Medical Engineering*, *PP*(99), 1. https://doi.org/10.1109/TBME.2014.2342280

Jensen, M. S., & Yaari, Y. (1988). The relationship between interictal and ictal paroxysms in an in vitro model of focal hippocampal epilepsy. *Annals of Neurology*, *24*(5), 591–598. https://doi.org/10.1002/ana.410240502

Jiménez-Jiménez, D., Nekkare, R., Flores, L., Chatzidimou, K., Bodi, I., Honavar, M., … Alarcón, G. (2015). Prognostic value of intracranial seizure onset patterns for surgical outcome of the treatment of epilepsy. *Clinical Neurophysiology*, *126*(2), 257–267. https://doi.org/10.1016/j.clinph.2014.06.005

Kandratavicius, L., Alves Balista, P., Lopes-Aguiar, C., Ruggiero, R. N., Umeoka, H., Garcia-Cairasco, N., … Pereira Leite, J. (2014). Animal Models of Epilepsy: Utility and Limitations. *Neuropsychiatric Disease and Treatment*, *10*, 1693–1705. https://doi.org/10.2147/NDT.S50371

Karoly, P. J., Freestone, D. R., Boston, R., Grayden, D. B., Himes, D., Leyde, K., … Cook, M. J. (2016). Interictal spikes and epileptic seizures: Their relationship and underlying rhythmicity. *Brain*, *139*(4), 1066–1078. https://doi.org/10.1093/brain/aww019

Kelley, K., & Theodore, W. H. (2005). Prognosis 30 years after temporal lobectomy. *Neurology*, *64*(11), 1974–1976. https://doi.org/10.1212/01.WNL.0000163998.01543.CF

Klivington, K. a, & Galambos, R. (1967). Resistance shifts accompanying the evoked cortical response in the cat. *Science (New York, N.Y.)*, *157*(3785), 211–213. https://doi.org/10.1126/science.157.3785.211

Kobayashi, E., Bagshaw, A., Jansen, A., Andermann, F., Andermann, E., Gotman, J., & Dubeau, F. (2005). epileptogenicity in Intrinsic epileptogenicity in polymicrogyric cortex suggested by EEG-fMRI BOLD responses. *Neurology Apr*, *64*(7), 1263–1266.

Kobayashi, E., Bagshaw, A. P., Bénar, C. G., Aghakhani, Y., Andermann, F., Dubeau, F., & Gotman, J. (2006). Temporal and extratemporal BOLD responses to temporal lobe interictal spikes. *Epilepsia*, *47*(2), 343–354. https://doi.org/10.1111/j.1528-1167.2006.00427.x

Koretsky, A. P. (2004). New developments in magnetic resonance imaging of the brain. *NeuroRx : The Journal of the American Society for Experimental NeuroTherapeutics*, *1*(1), 155–164. https://doi.org/10.1602/neurorx.1.1.155

Kreuzer, I., Osthaus, W. A., Schultz, A., & Schultz, B. (2014). Influence of the sevoflurane concentration on the occurrence of epileptiform EEG patterns. *PLoS ONE*, *9*(2), 0–6. https://doi.org/10.1371/journal.pone.0089191

Kuzniecky, R., de la Sayette, V., Ethier, R., Melanson, D., Andermann, F., Berkovic, S., … Feindel, W. (1987). Magnetic Resonance Imaging in Temporal Lobe Epilepsy Magnetic Resonance Imaging in Temporal Lobe Epilepsy. *Annals of Neurology*, *22*(3), 341–347.

Kwong, K., Kwong, K., Belliveau, J., Chesler, D., Goldberg, I., Weisskoff, R., … Turner, R. (1992).

Dynamic magnetic resonance imaging of human brain activity during primary sensory stimulation. *Proc Natl Acad Sci U S A*, *89*(12), 5675–5679. https://doi.org/10.1073/pnas.89.12.5675

Lachaux, J. P., Rudrauf, D., & Kahane, P. (2003). Intracranial EEG and human brain mapping. *Journal of Physiology Paris*, *97*(4–6), 613–628. https://doi.org/10.1016/j.jphysparis.2004.01.018

Leaming, J. M., Terndrup, T. E., & Ognibene, S. (1999). Glottal patency during experimental cortical seizures in piglets. *Academic Emergency Medicine*, *6*(7), 682–687. https://doi.org/10.1111/j.1553-2712.1999.tb00435.x

Lesser, R. P., Crone, N. E., & Webber, W. R. S. (2010). Subdural electrodes. *Clinical Neurophysiology*, *121*(9), 1376–1392. https://doi.org/10.1016/j.clinph.2010.04.037

Lesser, R. P., Crone, N. E., & Webber, W. R. S. (2011). Using subdural electrodes to assess the safety of resections. *Epilepsy and Behavior*, *20*(2), 223–229. https://doi.org/10.1016/j.yebeh.2010.08.022

Lind, N. M., Moustgaard, A., Jelsing, J., Vajta, G., Cumming, P., & Hansen, A. K. (2007). The use of pigs in neuroscience: Modeling brain disorders. *Neuroscience and Biobehavioral Reviews*, *31*(5), 728–751. https://doi.org/10.1016/j.neubiorev.2007.02.003

Liu, M., Bernhardt, B. C., Hong, S. J., Caldairou, B., Bernasconi, A., & Bernasconi, N. (2016). The superficial white matter in temporal lobe epilepsy: A key link between structural and functional network disruptions. *Brain*, *139*(9), 2431–2440. https://doi.org/10.1093/brain/aww167

Liston, A., Bayford, R., & Holder, D. (2012). A cable theory based biophysical model of resistance change in crab peripheral nerve and human cerebral cortex during neuronal depolarisation: Implications for electrical impedance tomography of fast neural activity in the brain. *Medical and Biological Engineering and Computing*, *50*(5), 425–437. https://doi.org/10.1007/s11517-012-0901-0

MacDonald, R. L., & Barker, J. L. (1977). Pentylenetetrazol and penicillin are selective antagonists of GABA-mediated post-synaptic inhibition in cultured mammalian neurones [25]. *Nature*, *267*(5613), 720–721. https://doi.org/10.1038/267720a0

Malone, E., Jehl, M., Arridge, S., Betcke, T., & Holder, D. (2014). Stroke type differentiation using spectrally constrained multifrequency EIT: evaluation of feasibility in a realistic head model. *Physiological Measurement*, *35*(6), 1051–1066. https://doi.org/10.1088/0967-3334/35/6/1051

Mäkiranta, M., Ruohonen, J., Suominen, K., Niinimäki, J., Sonkajärvi, E., Kiviniemi, V., … Tervonen, O. (2005). BOLD signal increase preceeds EEG spike activity - A dynamic penicillin induced focal epilepsy in deep anesthesia. *NeuroImage*, *27*(4), 715–724. https://doi.org/10.1016/j.neuroimage.2005.05.025

McElligott, J. G.; Melzack, R. . (1967). Localized by Thermal Visual Changes and Auditory Evoked in the Brain. *Experimental Neurology*, *17*, 293–312.

Mcevoy, A. W., & Harkness, W. J. F. (2015). Methods of epilepsy surgery. In *ILAE Teaching Weekend Lectures. The Fifteenth Teaching Weekend on Epilepsy* (p. Chapter 47).

McEwan, a, Romsauerova, a, Yerworth, R., Horesh, L., Bayford, R., & Holder, D. (2006). Design and calibration of a compact multi-frequency EIT system for acute stroke imaging. *Physiological Measurement*, *27*(5), S199–S210. https://doi.org/10.1088/0967-3334/27/5/S17

McIntosh, A. M., Averill, C. A., Kalnins, R. M., Mitchell, L. A., Fabinyi, G. C. A., Jackson, G. D., & Berkovic, S. F. (2012). Long-term seizure outcome and risk factors for recurrence after extratemporal epilepsy surgery. *Epilepsia*, *53*(6), 970–978. https://doi.org/10.1111/j.1528-1167.2012.03430.x

McNamara, J. O. (1984). Kindling: an animal model of complex partial epilepsy. *Annals of Neurology*, *16 Suppl*, S72–S76. https://doi.org/10.1002/ana.410160712

Merlet, I., & Gotman, J. (1999). Reliability of dipole models of epileptic spikes. *Clinical Neurophysiology*, *110*(6), 1013–1028. https://doi.org/10.1016/S1388-2457(98)00062-5

Mosewich, R. K., So, E. L., O'Brien, T. J., Cascino, G. D., Sharbrough, F. W., Marsh, W. R., … O'Brien, P. C. (2000). Factors predictive of the outcome of frontal lobe epilepsy surgery. *Epilepsia*, *41*(7), 843–849. https://doi.org/10.1111/j.1528-1157.2000.tb00251.x

Moshé, S. L., Perucca, E., Ryvlin, P., & Tomson, T. (2015). Epilepsy: New advances. *The Lancet*, *385*(9971), 884–898. https://doi.org/10.1016/S0140-6736(14)60456-6

Mullin, J. P., Shriver, M., Alomar, S., Najm, I., Bulacio, J., Chauvel, P., & Gonzalez-martinez, J. (2016). Is SEEG safe ? A systematic review and meta-analysis of stereo-electroencephalography – related complications, 386–401. https://doi.org/10.1111/epi.13298

Murphy, M., Smith, P. D., Wood, M., Bowden, S., O'Brien, T. J., Bulluss, K. J., & Cook, M. J. (2010). Surgery for temporal lobe epilepsy associated with mesial temporal sclerosis in the older patient: A long-term follow-up. *Epilepsia*, *51*(6), 1024–1029. https://doi.org/10.1111/j.1528-1167.2009.02430.x

Nakao, S., Takahira, K., Tsushima, K., Ikeda, S., Shingu, K., & Murao, K. (2004). The Anticonvulsant Effects of Volatile Anesthetics on Lidocaine-Induced Seizures in Cats. *Anesthesia & Analgesia*, *90*(1), 148. https://doi.org/10.1097/00000539-200001000-00032

Neligan, A., Hauser, W. A., & Sander, J. W. (2012). *The epidemiology of the epilepsies*. *Handbook of Clinical Neurology* (1st ed., Vol. 107). Elsevier B.V. https://doi.org/10.1016/B978-0-444-52898-8.00006-9

Ngugi, A. K., Bottomley, C., Kleinschmidt, I., Sander, J. W., & Newton, C. R. (2010). Estimation of the burden of active and life-time epilepsy: A meta-analytic approach. *Epilepsia*, *51*(5), 883–890. https://doi.org/10.1111/j.1528-1167.2009.02481.x

Noachtar, S., & Borggraefe, I. (2009). Epilepsy surgery: a critical review. *Epilepsy & Behavior : E&B*, *15*(1), 66–72. https://doi.org/10.1016/j.yebeh.2009.02.028

Nowell, M., Miserocchi, A., McEvoy, A. W., & Duncan, J. S. (2014). Advances in epilepsy surgery. *Journal of Neurology, Neurosurgery, and Psychiatry*, *85*(11), 1273–1279. https://doi.org/10.1136/jnnp-2013-307069

Nowell, M., Rodionov, R., Diehl, B., Wehner, T., Zombori, G., Kinghorn, J., … McEvoy, A. (2014). A novel method for implementation of frameless stereoeeg in epilepsy surgery.

Neurosurgery, *10*(4), 525–534. https://doi.org/10.1227/NEU.0000000000000544

Nowell, M., Sparks, R., Zombori, G., Miserocchi, A., Rodionov, R., Diehl, B., … Duncan, J. (2015). Comparison of computer-assisted planning and manual planning for depth electrode implantations in epilepsy. *Journal of Neurosurgery*, 1–3. https://doi.org/10.3171/2015.6.JNS15487.

Odom, Bach, Barber, Brigell, Marmor, Tormene, … Vaegan. (2004). Visual evoked potentials standard. *Documenta Ophthalmologica*, *108(2)*, 115–123. https://doi.org/10:1167/3.10.1

Odom, Bach, Brigell, Holder, McCulloch, Tormene, & Vaegan. (2010). ISCEV standard for clinical visual evoked potentials (2009 update). *Documenta Ophthalmologica*, *120*(1), 111–119. https://doi.org/10.1007/s10633-009-9195-4

Ogawa, S., & Lee, T. (1990). Brain magnetic resonance imaging with contrast dependent on blood oxygenation. *Proceedings of the …*, *87*(24), 9868–9872. https://doi.org/10.1073/pnas.87.24.9868

Oh, T., Gilad, O., Ghosh, a., Schuettler, M., & Holder, D. S. (2011). A novel method for recording neuronal depolarization with recording at 125-825 Hz: Implications for imaging fast neural activity in the brain with electrical impedance tomography. *Medical and Biological Engineering and Computing*, *49*(5), 593–604. https://doi.org/10.1007/s11517-011-0761-z

Oostenveld, R., & Praamstra, P. (2001). The five percent electrode system for high-resolution EEG and ERP measurements. *Clinical Neurophysiology*, *112*(4), 713–719. https://doi.org/10.1016/S1388-2457(00)00527-7

Opdam, H. I. H., Federico, P., Jackson, G. D. G., Buchanan, J., Abbott, D. F., Fabinyi, G. C. a, … Bellomo, R. (2002). A sheep model for the study of focal epilepsy with concurrent intracranial EEG and functional MRI. *Epilepsia*, *43*(8), 779–787. https://doi.org/10.1046/j.1528-1157.2002.04202.x

Pant, S., Te, T., Tucker, A., & Sadleir, R. J. (2011). The conductivity of neonatal piglet skulls. *Physiological Measurement*, *32*(8), 1275–1283. https://doi.org/10.1088/0967-3334/32/8/017

Parkes, L. M., Fries, P., Kerskens, C. M., & Norris, D. G. (2004). Reduced BOLD response to periodic visual stimulation. *NeuroImage*, *21*(1), 236–243. https://doi.org/10.1016/j.neuroimage.2003.08.025

Pillai, J., & Sperling, M. R. (2006). Interictal EEG and the diagnosis of epilepsy. *Epilepsia*, *47*(SUPPL. 1), 14–22. https://doi.org/10.1111/j.1528-1167.2006.00654.x

Ramantani, G., Cosandier-Rimélé, D., Schulze-Bonhage, A., Maillard, L., Zentner, J., & Dümpelmann, M. (2013). Source reconstruction based on subdural EEG recordings adds to the presurgical evaluation in refractory frontal lobe epilepsy. *Clinical Neurophysiology*, *124*(3), 481–491. https://doi.org/10.1016/j.clinph.2012.09.001

Regesta, G., & Tanganelli, P. (1999). Clinical aspects and biological bases of drug-resistant epilepsies. *Epilepsy Research*, *34*(2–3), 109–122. https://doi.org/10.1016/S0920-1211(98)00106-5

Ren, L., Kucewicz, M. T., Cimbalnik, J., Matsumoto, J. Y., Brinkmann, B. H., Hu, W., … Worrell, G. A. (2015). Gamma oscillations precede interictal epileptiform spikes in the seizure onset

zone. *Neurology*, *84*(6), 602–608. https://doi.org/10.1212/WNL.0000000000001234

Romsauerova, a, McEwan, a, Horesh, L., Yerworth, R., Bayford, R. H., & Holder, D. S. (2006). Multi-frequency electrical impedance tomography (EIT) of the adult human head: initial findings in brain tumours, arteriovenous malformations and chronic stroke, development of an analysis method and calibration. *Physiological Measurement*, *27*(5), S147–S161. https://doi.org/10.1088/0967-3334/27/5/S13

Ryan Wagner, H., Feeney, D. M., Gullotta, F. P., & Cote, I. L. (1975). Suppression of cortical epileptiform activity by generalized and localized ECoG desynchronization. *Electroencephalography and Clinical Neurophysiology*, *39*(5), 499–506. https://doi.org/10.1016/0013-4694(75)90051-6

Ryvlin, P., & Rheims, S. (2016). Predicting epilepsy surgery outcome. *Current Opinion in Neurology*, *29*(2), 182–188. https://doi.org/10.1097/WCO.0000000000000306

Salek-Haddadi, A., Diehl, B., Hamandi, K., Merschhemke, M., Liston, A., Friston, K., … Lemieux, L. (2006). Hemodynamic correlates of epileptiform discharges: An EEG-fMRI study of 63 patients with focal epilepsy. *Brain Research*, *1088*(1), 148–166. https://doi.org/10.1016/j.brainres.2006.02.098

SAFETY, HEALTH AND WELFARE AT WORK (GENERAL APPLICATION) REGULATIONS 2007 REVISED Updated to 1 January 2018. (2018), (299).

Sauleau, P., Lapouble, E., Val-Laillet, D., & Malbert, C. H. (2009). The pig model in brain imaging and neurosurgery. *Animal*, *3*(8), 1138–1151. https://doi.org/10.1017/S1751731109004649

Scheffer, I. E., Berkovic, S., Capovilla, G., Connolly, M. B., French, J., Guilhoto, L., … Zuberi, S. M. (2017). ILAE classification of the epilepsies: Position paper of the ILAE Commission for Classification and Terminology. *Epilepsia*, 1–10. https://doi.org/10.1111/epi.13709

Scherg, M. (1990). Fundamentals of dipole source potential analysis. *Auditory Evoked Magnetic Fields and Electric Potentials, Advances in Audiology*.

Schindler, K., Zubler, F., Steimer, A., Gast, H., Rummel, C., Abela, E., … Pollo, C. (2016). Ictal time-irreversible intracranial EEG signals as markers of the epileptogenic zone. *Clinical Neurophysiology*, *127*(9), 3051–3058. https://doi.org/10.1016/j.clinph.2016.07.001

Schmidt, D., & Löscher, W. (2003). How effective is surgery to cure seizures in drug-resistant temporal lobe epilepsy? *Epilepsy Research*, *56*(2–3), 85–91. https://doi.org/10.1016/j.eplepsyres.2003.10.004

Schuele, S. U., & Lüders, H. O. (2008). Intractable epilepsy: management and therapeutic alternatives. *The Lancet Neurology*, *7*(6), 514–524. https://doi.org/10.1016/S1474-4422(08)70108-X

Smith, S. J. M. (2005). EEG in the diagnosis, classification, and management of patients with epilepsy. *Journal of Neurology, Neurosurgery, and Psychiatry*, *76 Suppl 2*, ii2-7. https://doi.org/10.1136/jnnp.2005.069245

Stypulkowski, P. H., Giftakis, J. E., & Billstrom, T. M. (2011). Development of a large animal model for investigation of deep brain stimulation for epilepsy. *Stereotactic and Functional Neurosurgery*, *89*(2), 111–122. https://doi.org/10.1159/000323343

Tao, J. X., Baldwin, M., Hawes-Ebersole, S., & Ebersole, J. S. (2007). Cortical substrates of scalp EEG epileptiform discharges. *Journal of Clinical Neurophysiology : Official Publication of the American Electroencephalographic Society*, *24*(2), 96–100. https://doi.org/10.1097/WNP.0b013e31803ecdaf

Tao, J. X., Ray, A., Hawes-Ebersole, S., & Ebersole, J. S. (2005). Intracranial EEG substrates of scalp EEG interictal spikes. *Epilepsia*, *46*(5), 669–676. https://doi.org/10.1111/j.1528-1167.2005.11404.x

Tatum, W., Husain, A., & Benbadis, S. (2008). *Handbook of EEG interpretation*. (R. Percy & R. Johnson, Eds.). Demos Medical Publishing.

Teplan, M. (2002). Fundamentals of EEG measurement. *Measurement Science Review*, *2*, 1–11. https://doi.org/10.1021/pr070350l

Terndrup, T.E., Kadison, A., & Woo, P. (1995). Glottal patency during experimental cortical seizures in piglets. *Pediatric Research*, *6*(7), 932–937. https://doi.org/10.1111/j.1553-2712.1999.tb00435.x

Terndrup, T E, Darnall, R., Knuth, S. L., & Bartlett, D. (1999). Effects of experimental cortical seizures on respiratory motor nerve activities in piglets. *Journal of Applied Physiology*, *86*(6), 2052–2058.

Terndrup, Thomas E., Starr, F., & Fordyce, W. E. (1994). A piglet model of status epilepticus: Comparison of cardiorespiratory and metabolic changes with two methods of pentylenetetrazol administration. *Annals of Emergency Medicine*, *23*(3), 470–479. https://doi.org/10.1016/S0196-0644(94)70065-6

Tidswell, T., Gibson, A., Bayford, R. H., & Holder, D. S. (2001). Three-dimensional electrical impedance tomography of human brain activity. *NeuroImage*, *13*(2), 283–294. https://doi.org/10.1006/nimg.2000.0698

Tidswell, T., Holder, D. S., Yerworth, R. J., Eadie, L., Murray, S., Morgan, L., & Bayford, R. H. (2003). A comparison of headnet electrode arrays for electrical impedance tomography of the human head. *Physiological Measurement*, *24*(2), 527–544. https://doi.org/10.1088/0967-3334/24/2/363

Tizzard, A., Horesh, L., Yerworth, R. J., Holder, D. S., & Bayford, R. H. (2005). Generating accurate finite element meshes for the forward model of the human head in EIT. *Physiological Measurement*, *26*(2), S251–S261. https://doi.org/10.1088/0967-3334/26/2/024

Tootell, R. B. H., Dale, a M., Sereno, M. I., & Malach, R. (1996). New images from human visual cortex. *Trends in Neuroscience*, *19*, 481–489.

Uludag, K., Dubowitz, D. J., Yoder, E. J., Restom, K., Liu, T. T., & Buxton, R. B. (2004). Coupling of cerebral blood flow and oxygen consumption during physiological activation and deactivation measured with fMRI. *NeuroImage*, *23*(1), 148–155. https://doi.org/10.1016/j.neuroimage.2004.05.013

Ung H, Cazares C, Nanivadekar A, Kini L, Wagenaar J, Becker D, … Davis Ka. (2017). Interictal Epileptiform Activity Outside the Seizure Onset Zone Impacts Cognition. *Brain*, *18*(140), 2157–2168. https://doi.org/10.1093/awx178

Urigüen, J. A., & Garcia-Zapirain, B. (2015). EEG artifact removal-state-of-the-art and guidelines.

Journal of Neural Engineering, *12*(3), 31001. https://doi.org/10.1088/1741-2560/12/3/031001

Van Gompel, J. J., Bower, M. R., Worrell, G. A., Stead, M., Chang, S. Y., Goerss, S. J., … Lee, K. H. (2014). Increased cortical extracellular adenosine correlates with seizure termination. *Epilepsia*, *55*(2), 233–244. https://doi.org/10.1111/epi.12511

Van Gompel, J. J., Bower, M. R., Worrell, G. A., Stead, M., Meier, T. R., Goerss, S. J., … Lee, K. H. (2011). Swine model for translational research of invasive intracranial monitoring. *Epilepsia*, *52*(6), 49–53. https://doi.org/10.1111/j.1528-1167.2011.03096.x

Vongerichten, A. N., Santos, G. S. dos, Aristovich, K., Avery, J., McEvoy, A., Walker, M., & Holder, D. S. (2016). Characterisation and imaging of cortical impedance changes during interictal and ictal activity in the anaesthetised rat. *NeuroImage*, *124*, 813–823. https://doi.org/10.1016/j.neuroimage.2015.09.015

von Ellenrieder, N., Beltrachini, L., & Muravchik, C. H. (2012). Electrode and brain modeling in stereo-EEG. *Clinical Neurophysiology*, *123*(9), 1745–1754. https://doi.org/10.1016/j.clinph.2012.01.019

Vollmer-Haase, J., Folkerts, H. W., Haase, C. G., Deppe, M., & Ringelstein, E. B. (1998). Cerebral hemodynamics during electrically induced seizures. *NeuroReport*, *9*(3), 407–410.

Witkowska-Wrobel, A., Aristovich, K., Faulkner, M., Avery, J., & Holder, D. (2018). Feasibility of imaging epileptic seizure onset with EIT and depth electrodes. *NeuroImage*, *173*(February), 311–321. https://doi.org/10.1016/j.neuroimage.2018.02.056

Wellmer, J., Von Der Groeben, F., Klarmann, U., Weber, C., Elger, C. E., Urbach, H., … Von Lehe, M. (2012). Risks and benefits of invasive epilepsy surgery workup with implanted subdural and depth electrodes. *Epilepsia*, *53*(8), 1322–1332. https://doi.org/10.1111/j.1528-1167.2012.03545.x

Wrench, J. M., Matsumoto, R., Inoue, Y., & Wilson, S. J. (2011). Current challenges in the practice of epilepsy surgery. *Epilepsy and Behavior*, *22*(1), 23–31. https://doi.org/10.1016/j.yebeh.2011.02.011

Wolf, G. K., Gómez-Laberge, C., Rettig, J. S., Vargas, S. O., Smallwood, C. D., Prabhu, S. P., … Arnold, J. H. (2013). Mechanical ventilation guided by electrical impedance tomography in experimental acute lung injury. *Critical Care Medicine*, *41*(5), 1296–1304. https://doi.org/10.1097/CCM.0b013e3182771516

Yablonskiy, D. A., Ackerman, J. J. H., & Raichle, M. E. (2000). Coupling between changes in human brain temperature and oxidative metabolism during prolonged visual stimulation. *Pnas*, *97*(13), 7603–7608.

Yvert, B., Bertrand, O., Thevenet, M., Echallier, J. F., & Pernier, J. (1997). A systematic evaluation of the spherical model accuracy in dipole model localization. *Electroencephalography and Clinical Neurophysiology* , *102*(97), 452–459.

Zeki, S., Watson, J. D., Lueck, C. J., Friston, K. J., Kennard, C., & Frackowiak, R. S. (1991). A direct demonstration of functional specialization in human visual cortex. *The Journal of Neuroscience : The Official Journal of the Society for Neuroscience*, *11*(3), 641–649. https://doi.org/10.1.1.211.5726

Zijlmans, M., Zweiphenning, W., & van Klink, N. (2019). Changing concepts in presurgical assessment for epilepsy surgery. *Nature Reviews Neurology*. https://doi.org/10.1038/s41582-019-0224-y

Zuluaga, M. A., Rodionov, R., Nowell, M., Achhala, S., Zombori, G., Cardoso, M. J., … Ourselin, S. (2014). SEEG trajectory planning: Combining stability, structure and scale in vessel extraction. *Lecture Notes in Computer Science (Including Subseries Lecture Notes in Artificial Intelligence and Lecture Notes in Bioinformatics)*, *8674 LNCS*(PART 2), 651–658. https://doi.org/10.1007/978-3-319-10470-6_81

Software

https://github.com/EIT-team/PEITS

https://github.com/EITteam

https://github.com/EIT-team/Parallel_CS_Altium